MIMI Tech GmbH
Preusweg 98, D-52074 Aachen
friedrich@mimi-tech.com

MIMI Tech GmbH, Preusweg 98, D-52074 Aachen
www.mimi-tech.com, friedrich@mimi-tech.com

MIMI Tech
Metallurgical Innovations and Materials for Industrial Technology Improvement

Mapping Study on Aluminium Melt Purification from Post Consumer Scrap

Order dated Jan. 2023

Im Auftrag der European Aluminium Association und

International Aluminium Institute

Prof. Dr.-Ing. Dr. h.c. Bernd Friedrich

unter Zuarbeit von Cong Li, Dr. Ing. Danilo Curtolo, und Hanwen Chung

October 24, 2023

MIMI Tech GmbH
Preusweg 98, D-52074 Aachen
friedrich@mimi-tech.com

MIMI Tech GmbH
Preusweg 98, D-52074 Aachen
friedrich@mimi-tech.com

1. Executive summary

1.1. Preface

Aluminum recycling is a crucial aspect of sustainability due to its energy-efficient nature, using only 5% of the energy required for primary production and emitting just 0.6 kg of CO_2 per kg of aluminum during remelting. Roughly 75% of all historically produced primary aluminum is still in use, showcasing its potential in a circular economy and GHG emissions reduction. However, recycling rates for aluminum vary across products and alloys, with an average of 35 % and a target of 50 % by 2050. The increasing use of aluminum in vehicles for emissions reduction presents both opportunities and challenges in recycling due to diverse alloys used in this sector, such as the 2XXX, 5XXX, 6XXX, and 7XXX series. The diversity of the alloys makes post-consumer scrap recycling a complex task. Given the scarcity of high-quality scraps and increasing market pressures on reclaiming existing scrap streams, the aluminium industry must address and adapt recycling processes to meet its evolving demands. On the way towards the development of a green, sustainable, and economical recycling route, melt refining plays a critical role.

Since Jan. 2023, MIMI Tech GmbH (http://www.mimi-tech.com) was commissioned by European Aluminium Association (EAA) and International Aluminium Institute (IAI), for conducting a "Mapping Study on Aluminium Melt Purification from Post Consumer Scrap".

For brevity, hereafter in the report, the study is named after "Mapping" study.

The "Mapping" study focuses on evaluating methods for removing impurities from contaminated aluminium melts, understanding the negative effects of concerned impurities in aluminium production process as well as on (semi-)final products. Besides, it pays attention to neutralization approaches as an alternative option of impurity removal techniques.

The study involves a comprehensive literature review and technical evaluation of existing impurity removal technologies. It also covers a catalog of negative impacts of impurities, causing mechanisms, and neutralization approaches. Moreover, the report contains expert views contributed from aluminium companies and invited techniques providers/research centers/leading scientists. Figure 1 gives a study overview as well as execution timeline.

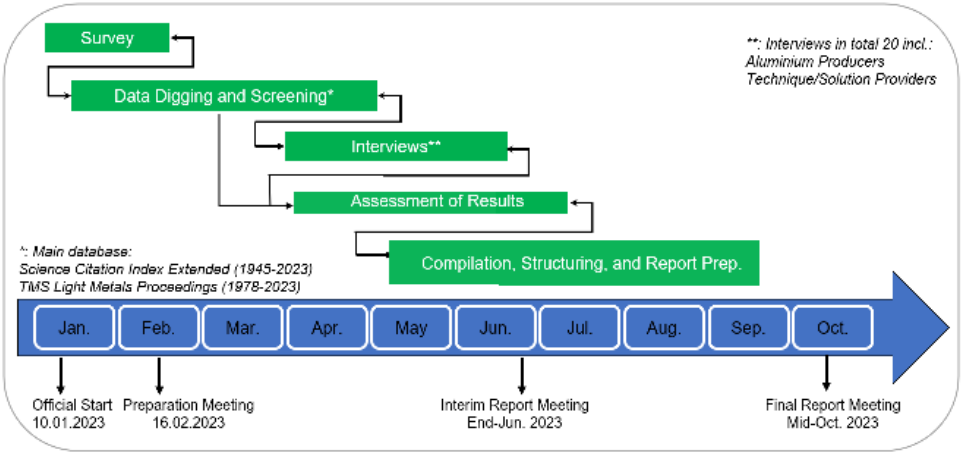

Figure 1: "Mapping" study overview and timeline of execution.

MIMI Tech GmbH
Preusweg 98, D-52074 Aachen
friedrich@mimi-tech.com

1.2. Methodology

The works of "Mapping" study were broken down into 5 work packages (WPs) namely survey, data digging and screening, interviews, assessment of results, and finally compilation, structuring, and report preparation. All WPs are listed in Figure 1.

In total 21 impurities were selected according to survey results as target impurities. They are Fe, Cu, Zi, Si, Mn, Pb, Mg, V, Li, Be, B, Ni, Sc, Ca, Na, Ti, Cr, Ga, Zr, Cd, Hg. The 21 elements were searched in the Web of Science (WoS) core collections and TMS (The Minerals, Metals & Materials Society) Light Metals Proceedings database, with an aim to identify relevant literatures studying corresponding removal techniques. With respect to negative impact and neutralization of impurities, the Table 1 compiled searched items based on impurity and corresponding impact.

Table 1: List of main negative effects categories reported for each selected impurity.

Impurity	Negative Effects and Neutralization Approaches				
Fe	Mechanical properties	Corrosion	Elongation	Fatigue	Large particle formation
Zn	Dilution ratio on 6XXX	Extrudability	Corrosion	Surface finish	
Si	Effect on anodizing	Melting point	Formability	Embrittlement	Large particle formation
V	Conductivity	Dispersoid element	Surface quality		
Cu	Dilution ratio on 6XXX	Corrosion	Alloy spec. limit on 5XXX/8XXX		
Mg	Brazeability	Laser welding performance			
Mn	Alloy spec. limit	Large particle formation			
Ga	Corrosion	Electric resistivity			
Ti	Intermetallic formation	Solidification			
B	Intermetallic formation	Solidification			
Ni	Corrosion				
Cr	Customer specification				
Cd	Bio-Hazard				
Hg	Bio-Hazard				
Pb	Legislation on packaging prod.				
Li	Alloy spec. limit				
Sc	Alloy spec. limit				
Na	Embrittlement				
Ca	Hydrogen absorption				

Alloy properties impacts
Quality impacts
Process impacts
Legislation
Alloy spec / dilution

Found Literatures were screened and meanwhile categorized per removal techniques and negative impacts and neutralization approaches. Figure 2 gives an article distribution for removal group and negative effect group, respectively. In total 315 articles were assessed and the results from 288 articles were compiled in this ca. 200 pages report composed of two major parts: Chapter 4-Part I – Removal Technologies, and Chapter 5-Part II – Negative Effects and Neutralization techniques.

MIMI Tech GmbH
Preusweg 98, D-52074 Aachen
friedrich@mimi-tech.com

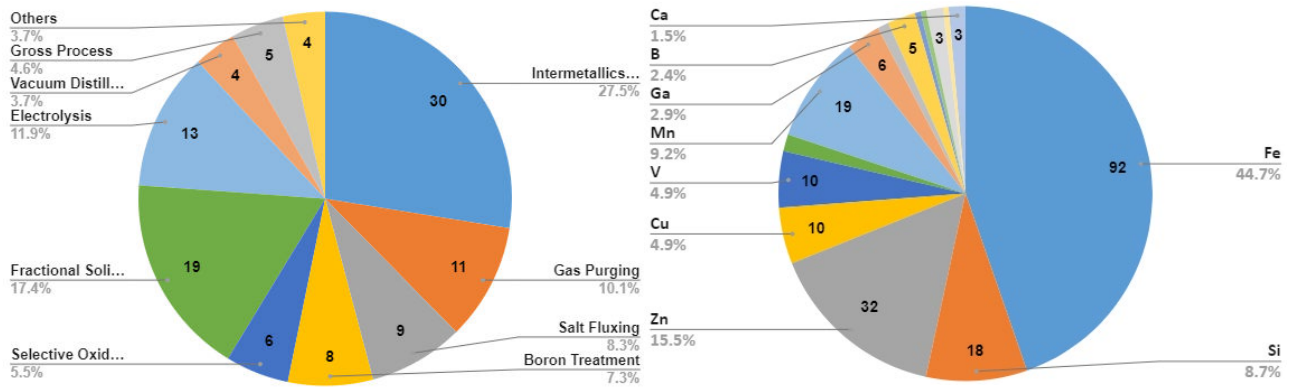

(a) (b)

Figure 2: Literature distribution (available ones) on: (a) removal techniques; (b) negative impact and neutralization of impurities.

In parallel to literature works, interviews were conducted with 11 aluminium companies and 9 invited techniques providers. The affiliations of interviewees are listed in Table 2. The discussions focused mainly on technical evaluation of impurities removal techniques. The comments contributed by interviewees will be presented via "strength-weakness- opportunity-threat (SWOT) diagram and key-take aways in the full report.

Table 2: Affiliation of Interviewees from both aluminium companies (left) and techniques providers (right).

Aluminium Companies
Alcoa
Aludium
Aluminium Duffel
Assan
Gränges
Hydro Deutschland
Mytilineos S.A.
Nippon
Raffmetal
Speira

Techniques Providers
Hoesch
Vesuvius
Pyrotek
Arconic
Dynamic Concept
Christian Doppler Laboratory at Leoben University
Leading Scientist, Dr. Don Doutre
Weiqiao Suzhou R&D
National Vacuum Institute at Kunming Uni. of Science and Technology
/

1.3. Results in a Nutshell

1.3.1. Removal Technologies

MIMI Tech GmbH
Preusweg 98, D-52074 Aachen
friedrich@mimi-tech.com

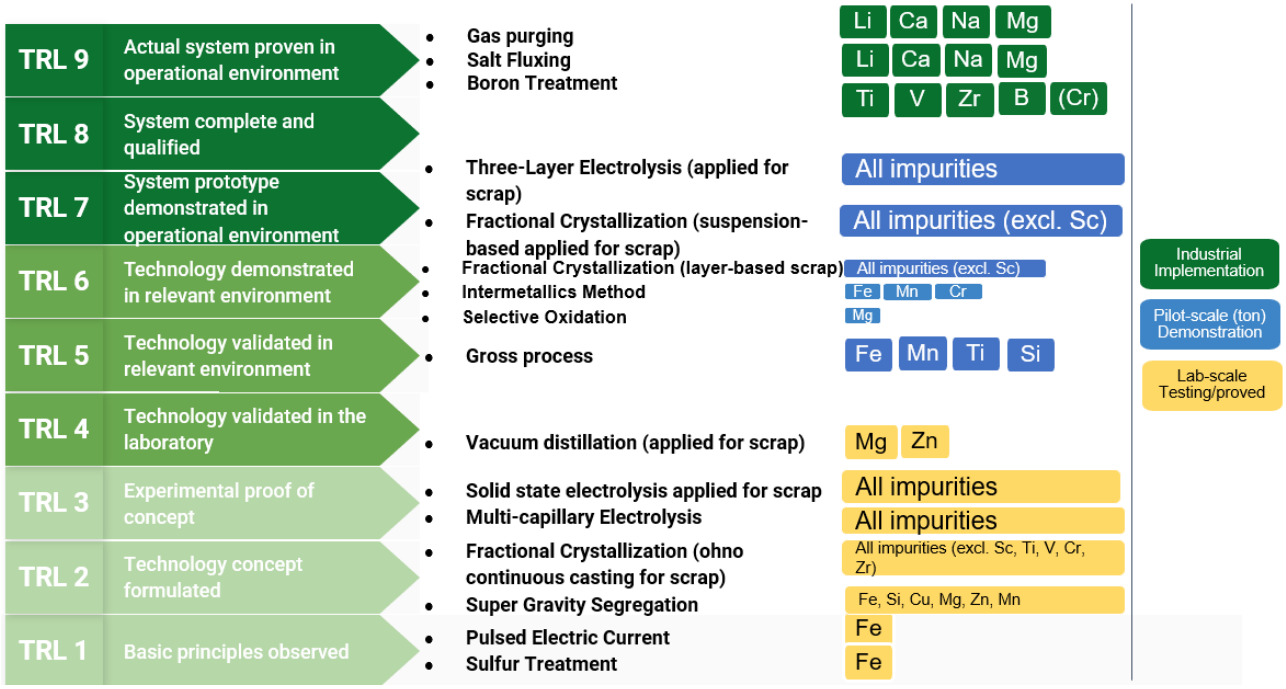

Figure 3: TRL level of impurity removal techniques and their application range, largest scale of implementation.

Based on available literatures, various impurities removal techniques were evaluated. Figure 3 gives a summary diagram which compiles the TRL level of different techniques and their application range along with largest scale of implementation. Salt fluxing, gas purging processes, boron treatment processes are grouped in TRL 9, as they were developed and implemented since long time. Techniques such as the three-layer electrolysis, fractional crystallization, have been widely used for the removal of trace impurities from metals. However, the changes seen in the aluminum sector are driving the industry to re-evaluate these technologies for possible utilization in the recycling of aluminum. The application of both three-layer electrolysis, fractional crystallization for the removal of large quantities of impurities from molten aluminum has been reported with relatively high success within relatively high TRL 6-7. However, the energy cost (for three-layer electrolysis) and the yield (for fractional crystallization) are major issues preventing the wide adoption of both technologies. Selective oxidation and intermetallics precipitation and separation processes were mostly appropriately placed at TRL 6, meaning industrial-scale demonstration is rarely seen. Vacuum distillation, on the other hand, is highly selective and yet can only be used for highly specific applications, mostly for the removal of Mg and Zn from aluminum streams.

Other technologies identified during our investigations are: the Gross process, pulsed current method, sulfur treatment, and super gravity segregation. The Gross process works by creating sub-chlorides of aluminum at high temperatures, separating it from its impurities and later reducing it at low temperatures back to metallic aluminum. All within a closed loop process. However, the energy cost is a major issue, as the chlorination process runs at ca. 1300°C. This process was originally developed as an alternative to the Hall-Héroult process, but it is reported to be possibly used for Al-scrap recycling. The pulsed current method, sulfur treatment, and super gravity segregation are so far only in early laboratory status (TRL 1-2), more tests are needed to validate the fundamental principles and assess their potential on large-scale application. Detailed

MIMI Tech GmbH
Preusweg 98, D-52074 Aachen
friedrich@mimi-tech.com

description about above mentioned other processes can be found in Sub-chapter 4.9 and Sub-chapter 4.10 of the full report.

For most of the techniques listed in Figure 3, comprehensive evaluation work was made with regards to impurity removal efficiency, application range, energy consumption, treatment capacity (when available), etc. An example result is provided in Table 3.

Table 3: Average values obtained from the literature sources on the removal efficiency and energy consumption of three-layer electrolysis.

Category	Impurity Removal Efficiency [Removal rate %]	Impacts on Process [Energy Consumption, kWh/kg]	TRL Range within Literature	Max. Treatment Capacity
Three-Layer electrolysis - Scrap	93.72%	16.0	TRL 4-9	N.A.

1.3.2. Negative Effects and Neutralization Techniques

Table 1 given in Sub-chapter 1.2 illustrates the main categories of negative effects pertaining to each investigated impurity. Based on this list, a literature review was performed to identify the underlying causes of each negative effect on the Al-alloys. The review also covers possible neutralization approaches, i.e., measures that can be utilized to eliminate or reduce the negative effect of each impurity. On the writing front, each negative effect was divided into their impact within the industry, being it a process impact (e.g., workability) or a product quality impact (e.g., mechanical properties).

As an example of the results from Chapter 5-Part II – Negative Effects and Neutralization techniques, Table 4 lists negative effect of Fe in different commercial alloys and possible neutralized approaches. As a critical impurity, Fe induces formation of undesired ß-phases which create all sorts of impacts on mechanical properties, corrosion, etc.

To briefly summarize the negative effect for other elements, Zn and Si are very harmful to some specific alloy applications and processing. Higher Zn content, for instance, results in an increased corrosion behavior, particularly in terms of pitting formation. Si, on the other hand causes the formation of eutectic phases at the grain boundaries due to its solubility in Al and could impede the formation of anodic film. When Cu content is high in the alloys, the susceptibility to corrosion effect is increased. The study on the impact of Ti and B is mostly related with usage of Al-Ti-B grain refiners. The inoculated TiB_2 particles were found to influence the precipitation of intermetallics during solidification process.

Neutralization processes are mostly directly associated with certain negative impacts. Reported such processes include alloy doping, heat treatment, rapid solidification, and external field imposition, as is exemplified in Table 4.

Detailed description of each impurity's negative effect on diverse wrought and cast alloys can be found in the full report. Following the negative effect of certain impurities in specific alloy, the identified techniques employed to neutralize those impurities, decreasing, or even eliminating their effects were discussed as well.

MIMI Tech GmbH
Preusweg 98, D-52074 Aachen
friedrich@mimi-tech.com

Table 4: Negative effect of Fe impurities and neutralization approaches, as an example of the whole summary table.

Imp.	Product	Negative Effect	Neutralization
Fe	1XXX	Corrosion.	Friction stirring process (FSP).
Fe	2XXX	Formation of Iron-rich phase reduce mechanical properties.	Add Mn, Y, Sc, and Gd as Iron-phase modifiers.
Fe	5XXX	Reduce formability and ductility, reduction in mechanical properties	Add Co, Cr, and Mn as Iron-phase modifiers.
Fe	5XXX	Corrosion.	-
Fe	6XXX	Reduce formability and ductility, reduction in mechanical properties.	hetero-deformation-induced (HDI) strengthening and HDI strain hardening.
Fe	7XXX	negatively affect the mechanical properties and performance.	Elevated cooling rates, and add Ca as a neutralizing element.
Fe	7XXX	Corrosion.	Add Mn as Fe modifier.
Fe	8XXX	Reduced ductility, strength, decreased toughness, increased occurrence of recrystallization, and deteriorate the material's properties.	Add Ce, and Y as Fe modifier.
Fe	2XX	Decrease alloy's properties.	Heat treatment (artificial aging)
Fe	3XX	Effect on the overall integrity and mechanical properties, decrease quality of the casting, hot tearing tendency.	T6 heat treatment, Sr, Ni, Mn, Mg, and Al-Ti-B as Iron-phase modifier, intensive stirring, the increasing in the mold temperature.
Fe	3XX	Increase in the corrosion.	-
Fe	4XX	negatively impacts the mechanical properties.	Add Mn, Cr, Be, Co, Mo, Ni, V, W, Cu, Sr, or rare earth elements as Iron-phase modifier, increased fluid flow, rapid solidification, ultrasonic vibration, Process Parameters Optimization (cooling rate), Melt Heat Treatment and Solid Solution Heat Treatment.
Fe	5XX	Deterioration of ductility and fatigue properties.	Heat treatment T6.
Fe	8XX	Deteriorated mechanical properties of the material, leading to reduced lifetime or durability.	Add Zr, and Er as Fe modifier.

1.4. Deliverables

The following files have been sent as deliverables of the “Mapping” Study

1. Queries for Data Digging (Excel);
2. PDF Lists for Found Articles (Excel);
3. Full Text PDFs of Evaluated Literatures (to EAA), in total 315 PDFs;
4. Full Report (PDF, including an Executive Summary), in total ca. 200 pages;
5. Presentations from Intermediate Meeting and Final Report Meeting, in total two PDFs.

1.5. Acknowledgements

MIMI Tech GmbH
Preusweg 98, D-52074 Aachen
friedrich@mimi-tech.com

The MIMI Tech team would like to express heartfelt thanks to the individuals interviewed from aluminum companies and technology providers (refer to the list in Table 2). Without their active engagement and valuable contributions, the "Mapping" study could not have been successfully completed.

1.6. Table of Content

MIMI Tech GmbH
Preusweg 98, D-52074 Aachen
friedrich@mimi-tech.com

MIMI Tech GmbH
Preusweg 98, D-52074 Aachen
friedrich@mimi-tech.com

MIMI Tech GmbH
Preusweg 98, D-52074 Aachen
friedrich@mimi-tech.com

MIMI Tech GmbH
Preusweg 98, D-52074 Aachen
friedrich@mimi-tech.com

2. Introduction

Aluminium recycling is critical due to its notable characteristics: infinite recyclability and low energy required during scrap remelting (2.8 kWh/kg Al) compared to primary route [1], [2], [3]. Notably, 75% of all historically produced primary aluminium remains in use [4]. These factors position aluminium as an essential element in the circular economy of raw materials and a potent material for reducing greenhouse gas emissions. However, recycling rates vary widely (20% to 80%) across different aluminium products and alloys, with an overall average of 35%. This figure is set to reach 50% by 2050 [5].

Existing recycling strategies are primarily based on alloy classes, with limited interchangeability between distinct groups of products [4]. Challenges are seen for recycling especially in the automotive sector where aluminium's adoption has surged due to stringent efficiency regulations. While aluminium use in vehicles reduces GHG emissions through weight reduction and increased scrap utilization [6], the complex mix of aluminium alloys with other materials complicates recycling, especially in the transportation sector where diverse alloys like 2XXX series (Al-Cu), 5XXX series (Al-Mg), 6XXX series (Al-Mg-Si), and 7XXX series (Al-Zn-Mg-Cu), are primarily for body sheets, frames, and structural components. Additionally, cast Al-Si alloy is used for engine blocks [7], [8].

The incompatibility of theses alloys makes the usage of the post-consumer scrap coming from this sector into different product classes and alloys a challenge. The current recycling practices frequently necessitate dilution with primary metal to conform to the rigorous quality and performance criteria of various alloys and product requirements of many alloy classes. Specialized alloys required such stringent impurity controls that recycled metal becomes very difficult to be utilized. Consequently, post-consumer scrap is often primarily employed for producing lower-grade casting alloys and products in numerous instances. However, the push for greener products and low CO_2 footprint pushes many clients, especially automotive manufacturers, to request a high percentage of scrap content into their products.

To counter the negative effect of impurities, the first option is melt refining. While less noble and reactive elements or gases can be removed using methods like gas purging and salt addition, the presence of certain noble alloying elements above specification typically requires dilution with primary aluminium or low-alloyed scraps (1XXX series). Alternative methods for removing such elements, including segregation (fractional crystallization), electrolytic refining, and distillation, have been explored. However, these processes often come with high costs or low yields.

When removal techniques aren't economically viable for certain elements, an alternative option is neutralization. To address this, a comprehensive literature review identified the causes of negative effects on Al-alloys and potential neutralization methods to mitigate each impurity's impact. These negative effects were categorized based on their influence on industry processes, quality, product performance, or compliance with legislation and specifications.

Given the scarcity of high-quality scrap and increasing market pressures on existing scrap streams, the aluminium industry must address and adapt recycling processes to meet its evolving demands.

This "Mapping study" financed by European Aluminium Association (EAA) and International Aluminium Institute (IAI), focuses on reviewing the state-of-the-art processes for impurities removal from contaminated aluminium melts, as well as the mapping of the negative effects of the main

MIMI Tech GmbH
Preusweg 98, D-52074 Aachen
friedrich@mimi-tech.com

impurities present in the aluminium products along with the available possibilities for their effective neutralization.

The study aimed at a broad and structured literature review and technical assessment of existing technologies. To enable it, a series of interview sections with several aluminium companies, technology providers, and technical specialists were conducted to assess the selected technologies and their feasibility within the operations in cast-houses and recycling centres.

The report is structured in two major parts. The first part (Part I) present impurities removal techniques namely: gas purging (Sub-chapter 4.1), salt fluxing (Sub-chapter 4.2), boron treatment (Sub-chapter 4.3), three-layer electrolytic refining (Sub-chapter 4.4), fractional solidification (Sub-chapter 4.5), selective oxidation (Sub-chapter 4.6), Intermetallics precipitation and separation (Sub-chapter 4.7), vacuum refining (Subchapter 4.8), etc. The contents for each of the chapters spans from fundamental mechanisms, purification results, to views from both aluminium companies and techniques providers.

With regard to negative impact of impurities and neutralization approaches, the content was clustered in Sub-chapter 5.1 to 5.15. Literature evaluation results were grouped following a hierarchy of “impurity-alloy-negative impact & neutralization”.

MIMI Tech GmbH
Preusweg 98, D-52074 Aachen
friedrich@mimi-tech.com

3. Methodology

The works of the "Mapping" study were broken down into 5 work packages (WPs), all of which have been completed within a time frame of 9 months. Figure 4 gives an overview of all WPs and execution timeline. The methodologies adopted for each WP will be introduced separately in the current chapter.

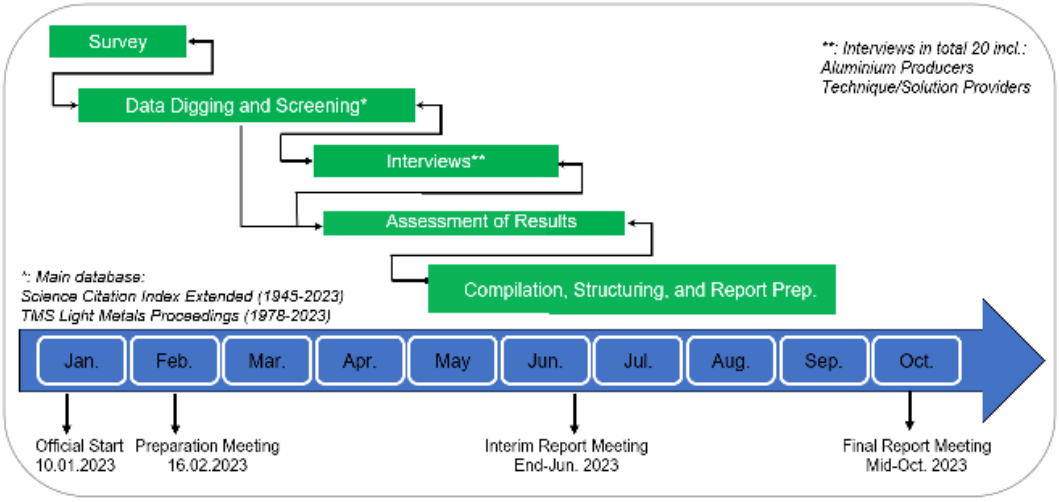

Figure 4: Timeline and overview of "Mapping" Study.

3.1. Survey

At the beginning of the study, an online survey was launched to gain a first impression on focal points of the study on interests of partners. The most important outcomes of the survey are shown in Figure 5 and Figure 6.

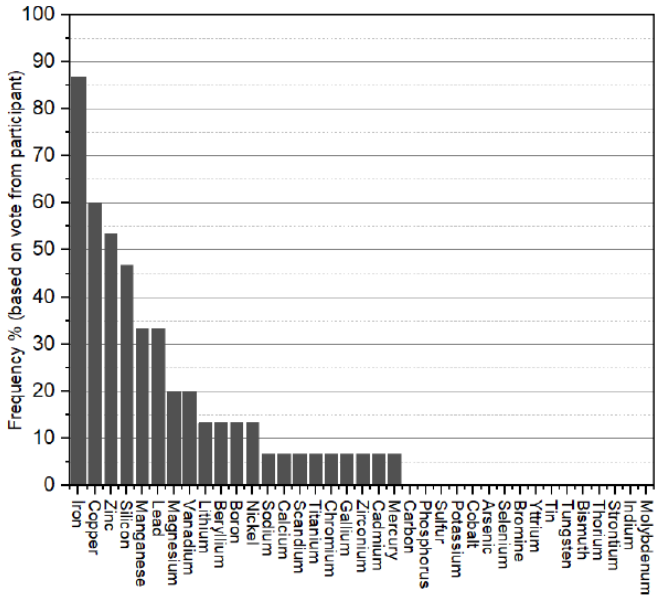

Figure 5: Impurities of interest for removal in the "Mapping" study.

MIMI Tech GmbH
Preusweg 98, D-52074 Aachen
friedrich@mimi-tech.com

Impurity	Negative Impact and Neutralization (to be Searched)				
Fe	Mechanical properties	Corrosion	Elongation	Fatigue	Large particle formatior
Si	Effect on anodising	Melting point	Formability	Embrittlement	Large particle formatior
Zn	Dilution ratio on 6XXX	Extrudability	Corrosion	Surface finish	
Cu	Dilution ratio on 6XXX	Alloy spec. limit on 5XXX/8XXX		Corrosion	
V	Conductivity	Dispersoid element	Surface finish		
Mg	Brazeability & Laser welding performance				
Mn	Alloy spec. limit	Large particle formation			
Ga	Corrosion	Eletric resistivity			
Ti	Intermetallic formation	solidification			
B	Intermetallic formation	solidification			
Ni	Corrosion				
Cr	Customer spec.				
Cd	Bio-Hazard			Legend:	
Hg	Bio-Hazard			Alloy properties	
Pb	Legislation on packaging.			Quality impacts	
Li	Alloy spec. limit			Process impacts	
Sc	Alloy spec. limit			Legislation / Bio-Hazard	
Na	Embrittlement			Alloy spec / dilution	
Ca	Hydrogen absorbtion				

Figure 6: Target of impurities for searching the negative effect and neutralization approaches.

It can be seen from Figure 5 that in total 21 impurities were voted, namely, Fe, Cu, Zi, Si, Mn, Pb, Mg, V, Li, Be, B, Ni, Sc, Ca, Na, Ti, Cr, Ga, Zr, Cd, Hg (ranked by voting fraction). All voted 21 elements listed in Figure 5 were assessed, in terms of available removal techniques. With respect to negative impact of impurities and corresponding neutralization measures, the compilation diagram shown in Figure 6 guided our search work.

3.2. Data Digging and Screening

The data digging work was conducted with employment two databases: 1) Web of Science (WoS) Core Collection (www.webofscience.com) and TMS Light Metals Proceedings. The first database contains two major sub-databases namely: Science Citation Index Expanded (SCIE) from 1945 to present and Conference Proceeding Citation Index-Science (CPCI-S) from 1990 to Present. The TMS Light Metals database contains title of articles published in 1978-1988, 1991, 2013, 2014, 2015, 2023, all of which has not yet entered WoS Core Collection.

Table 5: Example search query composed for Fe removal[1].

Search Query
1#: TI=(al OR alumin$um)
2#: TS=(flux* OR salt*OR agent* OR powder* OR reagent* OR addit* OR treat* OR compound* OR inject* OR granul* OR (gas*) OR (degas*) OR ("gas flux*") OR (barbotag*) OR (intermetallic*))
3#: TS=((fe OR iron) NEAR/3 (remov* OR eliminat* OR purif* OR reduc* OR decre*)) OR TS=(de-fe OR deiron* OR de-iron*)
4#: TS=(water OR waste-water OR si-al OR aqueous* OR composite* OR cataly* OR film* OR layer*)

[1] AND, OR, NEAR, $, *, TI, TS are search operators, instruction of operator functions can be found in http://webofscience.help.clarivate.com/en-us/Content/advanced-search.html

MIMI Tech GmbH
Preusweg 98, D-52074 Aachen
friedrich@mimi-tech.com

5#: #2 AND #3 AND #1
#6: #5 NOT #4

The search work in WoS was performed using "Advanced Search" function. A series of queries were composed to ensure a precise identification of relevant publications. An example query used for searching "Fe Removal via the Intermetallics Method" is given in Table 5. All queries used for searching work were compiled in a separate excel table which has been sent as one of the deliverables of the "Mapping Study" (Sub-chapter 1.4).

With respect to the complementary search made using a title catalog of TMS Light Metals Proceedings. The following Table 6 lists keywords were used individually:

Table 6: List of key words used within the search in the TMS Light Metals Proceedings database.

Bio-Hazard or Hazard or Biological Hazard	Surface finish or surface finishing	Removal or Remove or refine or refining
Embrittlement or Brittle	Legislation or packaging	Conductivity or Electric
Hydrogen or Absorption or Hydrogen Absorption	Recycling	particle(s) or particle formation or particle forming
Elongation or Lengthening or Stretching	Solidification	elimination or eliminating
Fatigue or Limit or stress or break or failure	Crystallisation or Crystallization	mechanical or mechanical properties

Preliminary screening work was conducted by reading abstract the found articles. Full text of articles which fall in the scope of current study were downloaded/scanned wherever accessible. Note that relevant literatures (incl. patents) from citations of assessed literatures were also reviewed wherever accessible. Relevant literatures from own literature base, wherever relevant, were collected and reviewed.

In parallel to the screening work, papers were categorized per removal techniques and negative impacts. Table 7 gives number of relevant articles and available ones. The unavailable article PDFs composed of inaccessible conference papers, non-English language publications etc.

Table 7: Number of Found-Screened Literatures and Available Ones.

Section	Screened	PDF Available
Removal Techniques	122	109
Negative Impact & Neutralization	283	206
TOTAL	405	315

Among the available articles, Figure 7(a) and (b) gives a distribution of articles in pie chart form for removal techniques and negative impact, respectively. It can be seen from Figure 7(a) that intermetallics method and fractional solidification process attract most research interest, whilst much less attention was paid on vacuum distillation. The other methods in Figure 7(a) refers to pulsed current, sulfur treatment, and super gravity segregation. With respect to negative impact of

MIMI Tech GmbH
Preusweg 98, D-52074 Aachen
friedrich@mimi-tech.com

impurities, Fe, Zn, Si, Mn, Cu appear to be the most unwelcome impurities, reflected by the number of literatures shown in Figure 7(b).

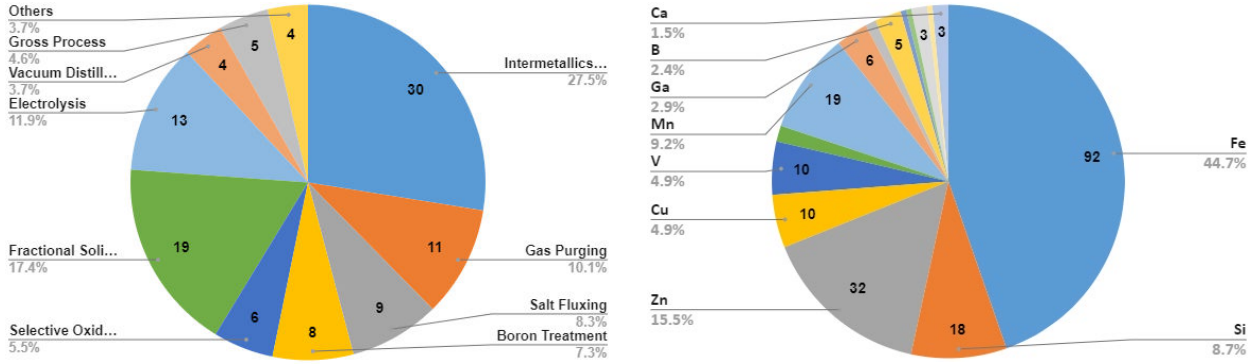

(a) (b)

Figure 7: Literature distribution on: (a) removal techniques; (b) negative impact of impurities.

A Microsoft Excel inventory was built up which encompassing titles of all found literatures (including available and not available ones). The inventory has been sent as one of the deliverables of the "Mapping" study (Sub-chapter 1.4). Besides, available articles in full text PDF form have been sent to EAA as one of the deliverables of the study (Sub-chapter 1.4).

3.3. Interviews

Interview works were conducted with 11 aluminium companies and 9 invited techniques providers, the latter of which includes research and development (R&D) centre, academic institutes, leading scientist etc. List of interviewee affiliations is provided in Table 8.

Table 8: Affiliation of Interviewees from both aluminium companies (left) and techniques providers (right).

Aluminium Companies
Alcoa
Aludium
Aluminium Duffel
Assan
Gränges
Hydro Deutschland
Mytilineos S.A.
Nippon
Raffmetal
Speira
CBA

Techniques Providers
Hoesch
Vesuvius
Pyrotek
Arconic
Dynamic Concept
Christian Doppler Laboratory at Leoben University
Leading Scientist, Dr. Don Doutre
Weiqiao Suzhou R&D
National Vacuum Institute at Kunming Uni. of Science and Technology
/
/

The conversation with aluminium companies focused on evaluation of techniques dug out from databases. The talks with techniques providers started later than the interviews with aluminium companies. During the open discussion with techniques providers, more time was devoted for discussing possible solutions to the issues summarized from interviews with aluminium companies.

MIMI Tech GmbH
Preusweg 98, D-52074 Aachen
friedrich@mimi-tech.com

3.4. Assessment of Results

Articles concerning impurity removal techniques were evaluated with respect to principle, impurity removal efficiency, energy consumption/CO_2 (qualitatively), cost (qualitatively), technology readiness level (TRL). With regard to articles about negative impact of impurities and corresponding neutralization measures, the main evaluation aspects are the mechanisms and neutralization possibilities.

The comments contributed from aluminium companies were categorized into strength, weakness, opportunity, threat (SWOT) points. The frequency-count of categorized comments were plotted into SWOT diagrams, as will be presented in each sub-chapter related with removal techniques. The comments contributed by techniques providers were compiled as key take-aways placed following the interview results of aluminium companies.

A qualitative and quantitative (when available) comparison of the key characteristics of each assessed removal technologies (efficiency, capacity, cost, TRL level, energy consumption) were done in a “radar plot” format. This enables a straightforward comparison of each technology in regard to its strengths and weaknesses. Evidently, details about investment costs, energy consumption, capacity, etc. were not readily available to all technologies, especially the ones at low TRL levels. For those, a qualitative estimation was made based on available information in literature and experiences from the MIMI-Tech Team.

The methodology for creating a bubble plot to illustrate SWOT (Strengths, Weaknesses, Opportunities, Threats) results involves representing data in a visually informative manner. In this plot, the vertical axis measures the total number of comments received, while the horizontal axis segments the comments into four categories: strengths, weaknesses, opportunities, and threats, indicating the total comments within each category. Bubble sizes within the plot are proportional to the ratio of comments within each category relative to the total number of comments. This approach allows for a clear and intuitive visualization of the distribution and significance of SWOT analysis comments, helping to identify key areas of focus and concern based on the relative sizes of the bubbles.

3.5. Compilation, Structuring, and Report Preparation

The report was finally prepared by compiling and structuring the assessment results of literature and interviews. The entire report was structured into two major parts, namely impurity removal techniques and negative impact of impurities and neutralization approaches.

Content with respect to impurities removal techniques can be found in Chapter 4-Part I – Removal Technologies. Within each sub-chapter, technique principle and purification results were reviewed firstly, following which the interview results were presented. At the end the challenges towards a higher TRL were summarized based on preceding evaluations.

With regard to negative impact of impurities and neutralization approaches, the content was clustered in Chapter 5-Part II – Negative Effects and Neutralization techniques. Literature evaluation results were grouped following a hierarchy of “impurity-alloy-negative impact & neutralization”. On the writing front, found articles related to large particle and intermetallic formation, solidification

MIMI Tech GmbH
Preusweg 98, D-52074 Aachen
friedrich@mimi-tech.com

etc. were redirected to their impact on either product properties (e.g., mechanical properties) or process impacts (e.g., workability).

MIMI Tech GmbH
Preusweg 98, D-52074 Aachen
friedrich@mimi-tech.com

4. Part I – Removal Technologies

4.1. Gas Purging (Ca, Mg, Na, Li, Zn)

4.1.1. Literature Results

4.1.1.1. Fundamentals and Principles

Gas purging treatment is a widely applied process in cast houses or foundries for melt refining purpose. Depending on refining purpose and target impurities, different gases may be employed.

Alkali and Alkaline Earth Metals

When removal of Na, Ca, Mg, Li is concerned, reactive gas mixtures composed of Cl_2/SF_6/-N_2/Ar/He may be injected into the melt and the removal of impurities is made available by chemical reactions [9], [10]. Elements that are more affinitive to the reactive gas than aluminium react preferentially with the gas and form impurity-bearing compounds. One exemplifying reaction is given in Equation 1 for illustrating Mg removal mechanism, assuming a 760 °C process temperature [11]. At end of the process, the formed halides are partitioned to melt surface due to density difference. Melt skimming operation is then conducted to ensure impurities-borne halide compounds are removed.

$Mg+Cl_2 \rightarrow MgCl_2$, ΔG= -481.7 kJ/mol Cl_2 Equation 1

Figure 8 gives the standard Gibbs energy of formation of oxides, chlorides, and fluorides, calculated at 723 °C [12]. According to thermodynamics laws, the calculation results shown in Figure 8 suggests, in theory, Cl_2 may be used to remove Ca, Ba, Li, Sr, Mg, Na, K. The removal feasibility of Si, Mn, Zn, Fe, Cu is however precluded by the diagram.

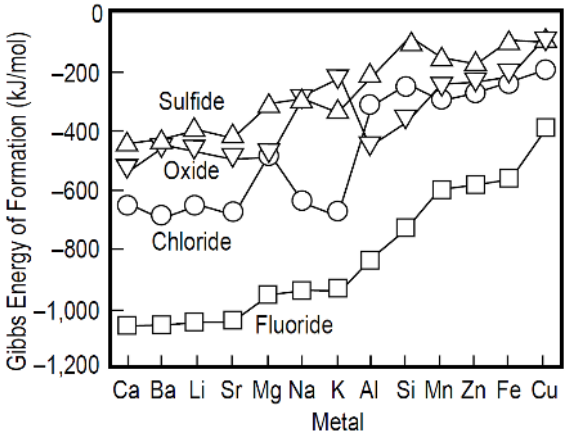

Figure 8: Standard Gibbs energy of formation of several sulfides, oxides, chlorides, and fluorides. The data are given at 723 °C per mole of S, O_2, Cl_2, and F_2, respectively. Reproduced from [12].

Various commercial set-ups are available to implement gas purging treatment. The relevant equipment includes simple lance, porous plug, rotary impeller, treatment station, and in-line degasser. Different equipment is deployed according to production route and plant layout. Figure 9 shows snapshot of rotary gas injector (RGI), aluminium compact degasser (ACD).

MIMI Tech GmbH
Preusweg 98, D-52074 Aachen
friedrich@mimi-tech.com

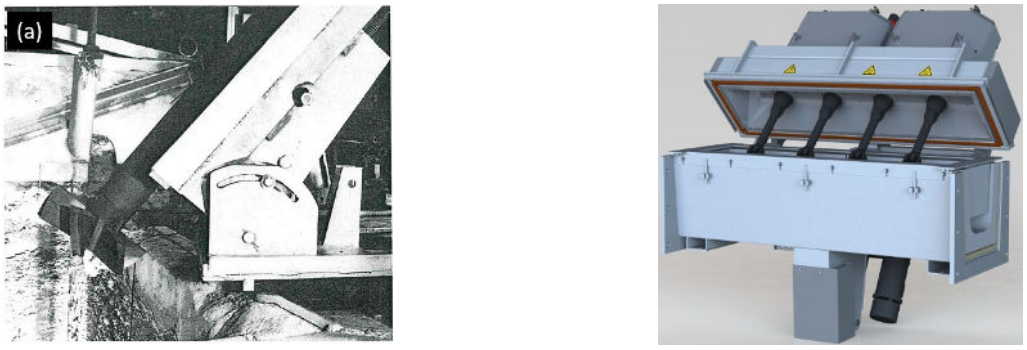

(a) (b)

Figure 9: Commercial set-ups for gas purging treatment: (a) rotary gas injector; (b) in-line degasser. Reproduced from [13], [14].

Zinc

Gas purging process was also reported being able to remove Zn [15]. For this purpose, the usage of reactive component in the gas mixture becomes not necessary. Boeree [15] tried to use Ar to remove Zn from scraps and it was proposed the Zn removal was driven by partial pressure difference. According to the author, at elevated melt temperatures (near Zn boiling point), liquid Zn evaporates to gas bubbles which has a lower Zn partial pressure. Because of buoyance, the bubble moves upwards, and Zn is carried into the atmosphere where condensation takes place. In the same study, it was mentioned that scraps remelting and holding process also contribute to Zn removal in addition to gas purging process.

4.1.1.2. Purification Results

Alkali and Alkaline Earth Metals

For Na, Ca, Mg, Li removal, both N_2-Cl_2 and Ar-Cl_2 were reported to be used in the industry, with the latter one being more frequently mentioned. The operational parameters for gas purging process are summarized in Table 9 [10], [16]–[19].

Table 9: Operation parameters used for impurity removal during gas purging process applied in industrial trials. Summarized based on [10], [16]–[19].

Gas Type	Cl_2 concentration	Flow Rate (Overall)	Treatment Time
Ar-Cl_2, N2-Cl_2	4-38%	44-276 L/min	20-60 (batch data only)

The removal efficiency of alkali and alkaline earth metals is usually as high as 80-99 % depending on operational parameters (incl. treatment time), alloy type. The removal kinetics can be appropriately described by two classic models namely zero-order model and first-order model. Figure 10 shows Ca removal result using an Alcoa A622 batch-unit [20]. From 0-60 min, the Ca removal follows the zero-order model, and from 60 min to 80 min it follows the first order model.

MIMI Tech GmbH
Preusweg 98, D-52074 Aachen
friedrich@mimi-tech.com

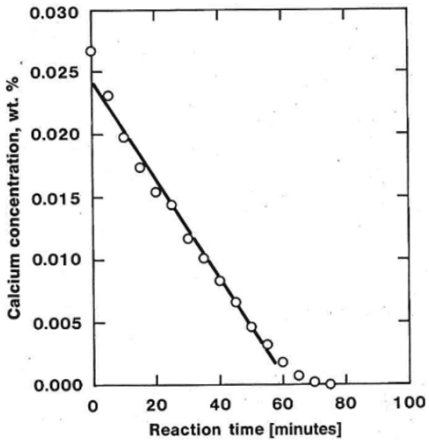

Figure 10: Ca content variation as a function of gas purging time. Reproduced from [20].

Which model prevails during gas purging is decided by mass transfer rate of impurity element to the melt-bubble interface [11]. When the mass transfer is sufficiently high, the rate at which impurity is removed is governed by supply rate of Cl_2 to the bubble-melt interface. At a constant Cl_2 injection rate, the removal rate of impurities remains invariable hence one can observe the linear decrease of Ca concentration as a function of elapsed time, an example of which is shown in Figure 10 (0-60 min). When mass transfer rate of impurity to the melt-bubble interface is not enough to consume injected Cl_2, the impurity removal rate is dictated by mass transfer rate of impurity. As mass transfer rate is a function of real time impurity concentration [11], one may expect a timely decay of impurity removal rate. Such trend is also exemplified also in Figure 10 (60-80 min).

The validity of the above two models has been demonstrated by industrial trials, the application scope of respective model depends on operational parameters and real-time impurity concentration in the melt. At trace range of impurities, the first-order removal model finds its prevalent application [19] [20].

Studies have shown that the removal rate of elements is a function of impurity type, operational parameters including rotor speed, gas flow rate, Cl_2 concentration. Based on impurities types, evaporation [21] and preferential oxidation [17], [18] are other possible mechanisms which can enhance the removal rate. Moreover, studies from Kulunk et al. [21]and Celik et al. [13] suggest alloying/impurity elements may interact with each other during gas purging process which may hinder or accelerate certain impurity's removal process.

Zinc

With respect to Zn removal, Boeree et al. [15] purged Ar into Al-2.42Zn alloy melt for 30 min at melt temperature 900 °C, 20 % Zn removal efficiency was realized. It should be mentioned in the reference trial when no Ar was used, 13 % of Zn decrease was also observed. To make robust conclusion on effectiveness of gas purging on Zn removal, more trials are needed in the future.

All literature results reviewed in this section suggest the lower boundary for removal of Na, Li, and Ca by application of gas purging process is less than 10 ppm, for Mg the boundary value is between 10-100 ppm, for Zn the boundary value is above 1 wt. %.

4.1.1.3. Disadvantages

MIMI Tech GmbH
Preusweg 98, D-52074 Aachen
friedrich@mimi-tech.com

The main disadvantage of gas purging process is related with the usage of Cl_2 gas. The Cl_2 gas may lead to hostile working environment and pollutants emitted to the atmosphere. The released pollutants may contain $AlCl_3$, HCl, Al_2O_3, in addition to Cl_2 [11], [13], [18]. One of the reasons responsible for the emission issue is excessive Cl_2 supply, which may take place particularly at low impurity level of the melt [11]. Stage-wise gas flow rate control may provide a solution for avoidance of excessive Cl_2 supply. The strategy may be realized through in-line degassers with multi-compartments. For batch process, Fu et al. [11] proposed to integrate $Cl_2/AlCl_3$ sensor into the furnace system and adjust the Cl_2 supply rate according to feedback of the sensor.

4.1.1.4. Summary of Literature Assessment

Table 10: Summary of literature assessment concerning gas purging.

Category	Impurity Removal Efficiency [Removal rate %][1)]	Lower Removal Limit (Mg, Na, Li, Ca, Zn)	TRL Range within Literature	Max. Treatment Capacity
Gas Purging	76.09	Mg: 10-100 ppm; Na, Li, Ca: < 10 ppm; Zn: > 1 %	TRL 2-9	65 ton

1) Collective impurities, averaged value from all assessed literatures.

4.1.2. Interview Section Analysis

During the interview talk and the follow-up analysis work, gas purging and salt fluxing techniques were assessed together. For the sake of simplicity, the result corresponding to gas purging technique concerning interview results will be presented alongside with salt fluxing in section 4.2.2.

MIMI Tech GmbH
Preusweg 98, D-52074 Aachen
friedrich@mimi-tech.com

4.2. Salt Fluxing (Ca, Mg, Na, Li)

4.2.1. Literature Results

4.2.1.1. Fundamentals and Principles

The development of salt fluxing process was driven by the pursuing of Cl_2-free melt purification techniques. By injecting salt compounds composed of chlorides and/or fluorides, impurities such as Na, Li, Ca, Mg can be removed [12], [22], [23]. Attempts were reported for removal of Fe using borates salt fluxing method [24], yet the positive results have not been validated by other independent laboratories.

During the process of salt fluxing, halides compounds are injected into the melt or dumped onto the melt surface. The charging of salts is often accompanied by melt stirring operations to provide a good kinetics condition for impurity removal. Take the usage of $MgCl_2$-based salt for example, after introduction of salt fluxes, spontaneous exchange reactions take place between impurities and the salt, as is suggested in Equation 2-Equation 4. The Gibbs energy change is calculated assuming reaction temperature 727 °C [22]. The formed impurity-borne salt compounds (e.g., NaCl, $CaCl_2$) are separated to the slag layer on top of the melt surface, due to their lower density relative to aluminium melt. Followed by melt skimming operations, impurities can be removed in form of slag.

$MgCl_2$ (l) + 2Na (l)→ Mg (l) + 2NaCl (s) (ΔG= -155.2 kJ/mol) Equation 2
$MgCl_2$ (l) + Ca (l)→ Mg (l) + $CaCl_2$ (s) (ΔG= -160.7 kJ/mol) Equation 3
$MgCl_2$ (l) + 2Li (l)→ Mg (l) + 2LiCl (s) (ΔG= -176.6 kJ/mol) Equation 4

Analogously to chlorination process, the removability of certain type of impurity through salt fluxing process is regulated by thermodynamics laws [12]. Figure 8 in the preceding sub-chapter already gives the standard Gibbs energy of formation for fluorides and chlorides compounds of common impurities. Theoretical consideration suggests $MgCl_2$ is an effective ingredient not only for removal of Li, Na, and Ca but also Ba, and Sr. Analogously to chlorination and chlorides fluxing process, Ca, Ba, Li, Sr, Mg, Na, and K may also be removed by using AlF_3.

(a) (b)

Figure 11: Commercial set-ups for salt Fluxing: (a) rotary flux injector (RFI); (b) treatment of aluminium in crucible (TAC) Station. Reproduced from [25], [26].

MIMI Tech GmbH
Preusweg 98, D-52074 Aachen
friedrich@mimi-tech.com

Abundant salt flux suppliers can be found worldwide. The selection of salt flux types for alkali and alkaline earth metal removal depends on impurity type as well as alloy types. For potline aluminium, AlF_3 is commonly used for removal of Ca, Na, and Li [23], [27], [28]. For Al-Mg alloys, $MgCl_2$-based salt is a popular option [22]. Cautions need to be taken to avoid removal of alloying elements and introduction unwanted impurities during salt fluxing process [12], [22].

Industrially, salt fluxing process is implemented via equipment such as rotary flux injector (RFI, for furnace process), crucible/ladle treatment station (e.g., "TAC"-Treatment of Aluminium in Crucible), and in-line degasser (e.g., ACD-Alcan Compact Degasser) [23], [25], [26], [29], [30]. Figure 11(a) and (b) shows snapshots/schematic of a RFI and a TAC set up, respectively.

4.2.1.2. Purification Results

Reported studies related to salt fluxing are mostly with ton-scale. Table 11 summarizes the operational parameters compiled from available literatures. The removal efficiency of alkali and alkaline earth metals through salt fluxing is usually as high as 80-90 % level depending on operational parameters, alloy types and treatment time.

Table 11: Operation parameters used for impurity removal during salt fluxing process applied in industrial trials. Summarized based on [22], [23], [27], [29], [31]–[33].

Salts Composition	Salt Addition Rate (kg/ton)	Carrier Gas Flow Rate (L/min)	Treatment Time (min)	Operating Temp. (°C)	Temp. Drop (°C)
$MgCl_2$-KCl, NaCl-KCl-AlF_3, AlF_3, NaCl-KCl-NaCl	0.35-2 (in one exceptional case 8)	20-45	6-30 (batch) < 1 (in line)	715-850	40-50

The impurity removal kinetics during salt fluxing process mostly follow a first-order model, meaning that a time-dependent fading removal rate with decrease of impurity content in the melt. Figure 8 shows as an example when salt fluxing process was applied to remove Na and Ca from an 5182 alloy. The salt was dumped on the melt surface and the melt surface was truck-stirred.

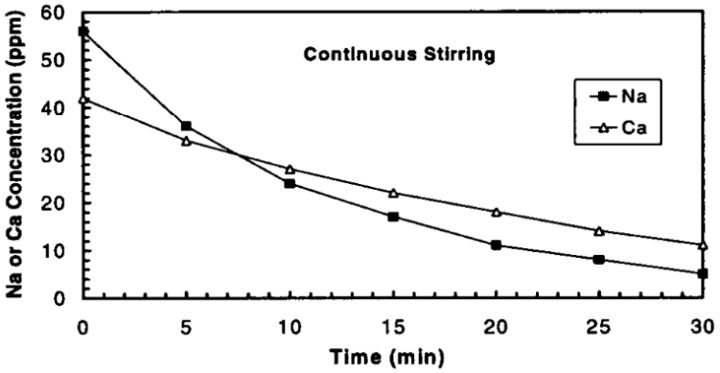

Figure 12: Removal of Na and Ca from AA5182 alloy by salt fluxing process. Reproduced from [22].

The influence of operational parameters on removal kinetics of impurities is suggested by different case studies. For a given type of impurity, melt stirring intensity, salt flux addition rate, and temperature were suggested to positively affect the removal kinetics [22], [23]. Removal kinetics

MIMI Tech GmbH
Preusweg 98, D-52074 Aachen
friedrich@mimi-tech.com

may vary from element from to element. For example, Na was found to be removed at a faster kinetics than Ca [22], [28].

Literature results suggest the lower boundary for removal of Na, Li, and Ca, by application of gas purging process in less than 10 ppm, whilst for Mg this value between is 0.1 -1 wt. %.

4.2.1.3. Summary of Literature Assessment

Table 12 summarizes the overall assessments made based on all literatures assessed in the current sub-chapter.

Table 12: Summary of literature assessment concerning salt fluxing.

Category	Impurity Removal Efficiency [Removal rate %][1)]	Lower Removal Limit (Mg, Na, Li, Ca, Zn)	TRL Range within Literature	Max. Treatment Capacity
Salt Fluxing	83.75	Mg: 0.1-1 %; Na, Li, Ca: < 10 ppm;	TRL 3-9	12 ton (Batch) 1 ton/min (in-line)

1) collective removal efficiency averaged from all assessed literatures.

4.2.2. Interview Section Analysis

The below section presents interview results from both gas purging and salt fluxing techniques.

4.2.2.1. Aluminium Companies

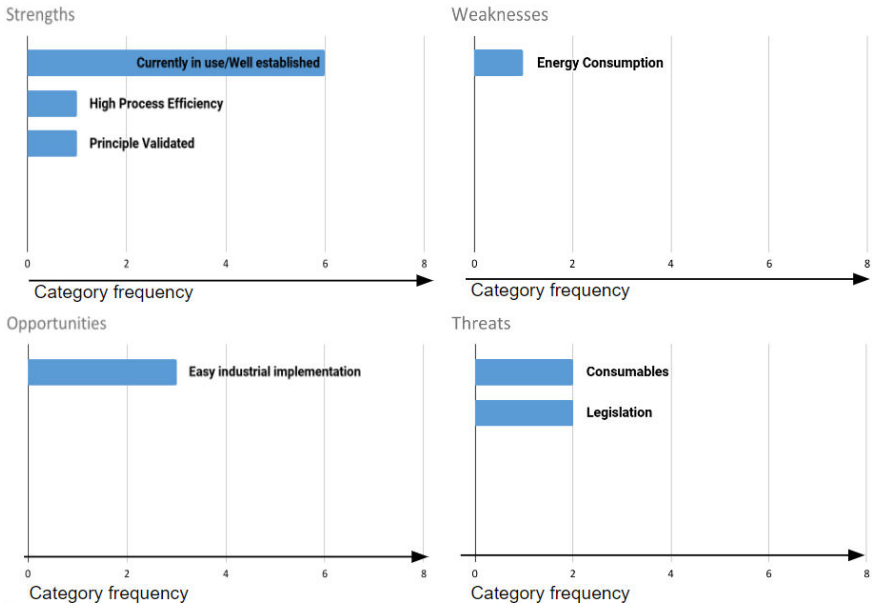

Figure 13: SWOT analysis for gas purging and salt fluxing.

MIMI Tech GmbH
Preusweg 98, D-52074 Aachen
friedrich@mimi-tech.com

Figure 13 shows interview result with respect to assessment of gas purging and salt fluxing process.

Both gas purging and salt fluxing processes operate under validated thermodynamics principle and are acknowledged for having good efficiencies. Should new species or compounds be identified in the future for removal of noble elements (with respect to aluminium) through a reaction driven mechanism, there is an opportunity to use the already industrially established gas/salt fluxing process and only exchange the gas/salt types. In such a case, the capital cost related to new technology deployment can be reduced to a large extent.

The one comment falling into weakness category is the heat loss during gas/salt fluxing since sometimes the furnace has to be opened during the fluxing process. Consumables, particularly the price of salt fluxes was mentioned as one of the threats when the addition rate of salt shall be high for melt with high content of impurities (e.g., Mg). Depending on countries and regions, legislation issue exists for the application of Cl_2 gas.

4.2.2.2. Techniques Providers

In terms of potential of application of gas/salt fluxing process on removal of noble elements (e.g., Fe, Mn, Si, Cu), few positive feedback was received. Most interviewees from techniques provider were not optimistic on identifying a new substance/compound which can remove noble elements. The main reasons are given from the thermodynamic laws' perspective. It was also commented that so far there have been not enough quantity of requests received from customers to kick-off the new fluxes development. It is worth noting there was on interviewee mentioned that Si removal through a fluxing process is now in serious discussion. The under-development/developed method is intended to bring Si down to ppm level and may be applied for alloys containing dilute amount of Si. In terms of Fe removal through a fluxing process, there has been no straightforward methods indicated by interviewees.

The consumable issue shown in Figure 13 was also touched during the interviews and it was indicated there is a certain threshold level of impurities, beyond which using flux becomes not economically favorable comparing with primary metal dilution strategy.

MIMI Tech GmbH
Preusweg 98, D-52074 Aachen
friedrich@mimi-tech.com

4.3. Boron Treatment (Ti, V, Zr)

4.3.1. Literature Results

4.3.1.1. Fundamentals and Principles

Boron (B) treatment is an industrial process for upgrading ordinary pure aluminium (99.6 wt. %) to electrical-conductor (EC) grade aluminium, the latter of which has a strict requirement on transition metals content [34]. The process was demonstrated to be effective for removal of vanadium (V), titanium (Ti), and zirconium (Zr) [35]–[37]. Whilst for Chromium (Cr), uncertainty remains [38].

During boron treatment process, B is added into the melt via master alloys in form of ingot, waffle, or rod [35], [37]. The added B borne in AlB_2/AlB_{12} particles reacts with transition metal to form relevant impurity-borne compounds as is given in Equation 5 [39],

$$M+AlB_2(s)=MB_2(s)+Al(l) \qquad \text{Equation 5}$$

The thermodynamic driven force of impurity removal stems from the different Gibbs energy of formation between AlB_2 and MB_2 phases, which is demonstrated in Figure 14 [39].

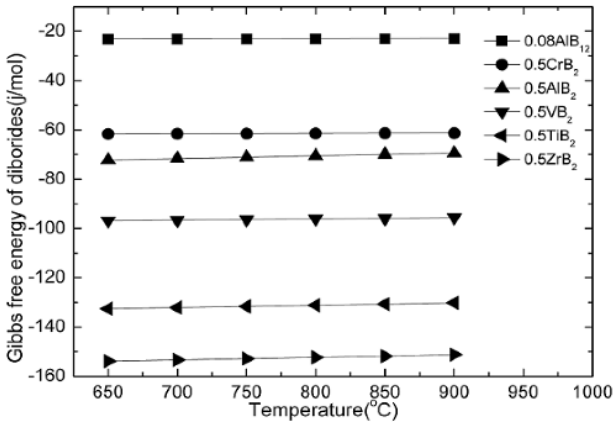

Figure 14: Gibbs free energy of formation of metal borides as a function of process temperature. Reproduced from [38].

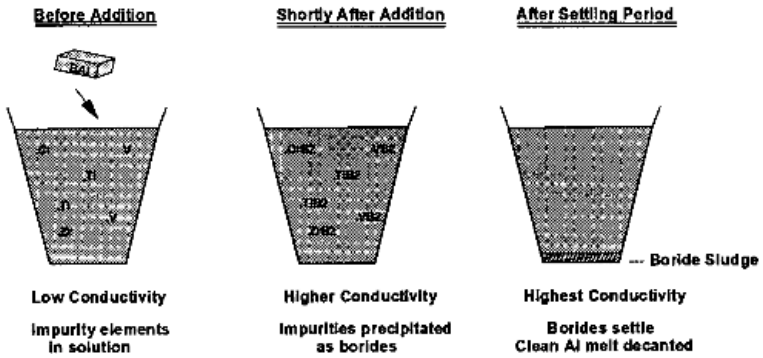

Figure 15: Illustration of transition metal removal by boron treatment. Reproduced from [35].

Upon addition of B, the melt is set dwell for certain period of time. The holding operation may be conducted in transfer ladle or holding furnace, during which period the formed particles settles to the bottom of the melt [36], [37]. As a result, impurity content in the bulk melt decreases. Figure 15 shows schematically the purification process [35]. Figure 16 shows micrographs of settled diborides

MIMI Tech GmbH
Preusweg 98, D-52074 Aachen
friedrich@mimi-tech.com

which are formed upon charging Al5B (AlB_2 phase contained) and Al4B (AlB_{12} phase contained) master alloys [36].

Boron addition rate is an important factor which can determine the removal efficiency. An optimum boron addition rate means a rapid impurities removal process and, in the meantime, the remained boron content in the melt after treatment is minimized. In practical cases, boron is added in a 20-75 % excess amount with respect to stoichiometric requirement [35], [36].

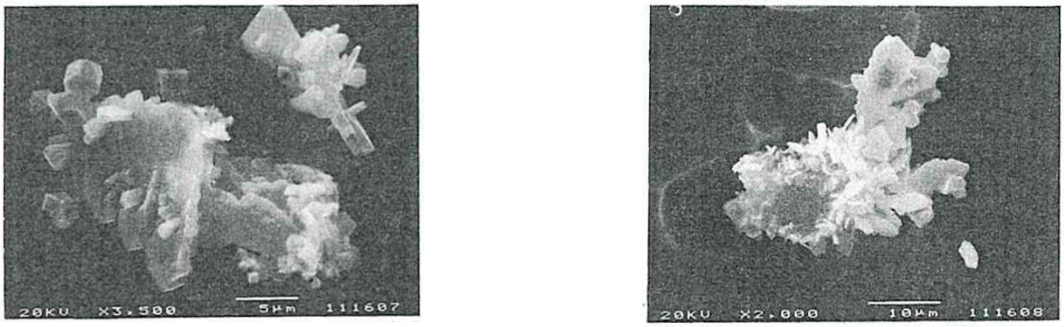

(a) (b)

Figure 16: Morphology of diborides precipitated by addition of: (a) AlB_2; (b) AlB_{12}. Reproduced from [36].

4.3.1.2. Removal Kinetics

The rate of impurity removal during boron treatment is governed by the rate at which reaction between impurities and AlB_2/AlB_{12} phase as well as settling rate of impurity bearing borides. At several hundreds of ppm initial impurity level, the reactions between AlB_2/AlB_{12} phase and impurities were indicated to take place within a very short period [35]. Figure 17 shows results from trials conducted using 99.7 aluminium with 100 ppm Ti and 100 ppm V, added boron equivalent to 50 % stoichiometric excess assuming TiB_2 and VB_2 are formed, process temperature is 730 °C [35]. The sharp increase in conductivity of samples in the beginning of treatment process can reasonably be attributed to rapid formation of borides which fixed Ti/V impurities [35] dissolved in the melt. The plateaued section of the curve was proposed to be a result a gravitational sedimentation of formed borides at elapsed melt holding time.

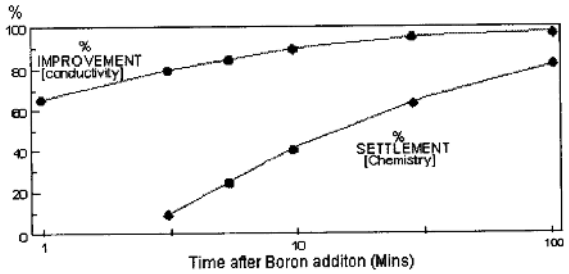

Figure 17: Variation of conductivity and sediments amount as a function of boron treatment time. Reproduced from [35].

When melt holding time needs to be minimized, addition rate of Al-B master alloy may be adjusted higher so as to enhance mass transfer rate of impurity elements [35]. Another way to enhance mass transfer rate was reported by Khalliq et al. [40]. The authors stirred the melt intermittently by gas

MIMI Tech GmbH
Preusweg 98, D-52074 Aachen
friedrich@mimi-tech.com

purging upon charging of an Al-B master alloy. Results shows a significantly enhanced V removal rate.

Table 13: Al-B phase characteristics. Reproduced from [35].

Nominal Comp. of Master Alloy	Al-B Phase	Predominant boride phase	Size	Morphology
Al4B/Al5B	AlB_2	3.19	20-40 µm	Angular
Al4B/Al5B	AlB_{12}	2.55	60-100 µm	Rounded

The selection of Al-B master alloys can also affect impurities removal rate. Two phases namely AlB_2 and AlB_{12} are available in different Al-B master alloys [35], [36]. The two phases can act as carrier of B specie. Table 13 lists the critical characteristics of the two types of Al-B phase [35]. The large difference in size between both types of borides will lead to on one hand the different rate at which the mass transfer of impurities takes place. On the other hand, it will lead to a different settling velocity of the formed borides. As according to Stokes' law, coarser particles always settles faster than fine ones. Trial result from Setzer et al. [36] suggests a faster removal rate of impurities when AlB_{12} was employed, as is evident in Figure 18.

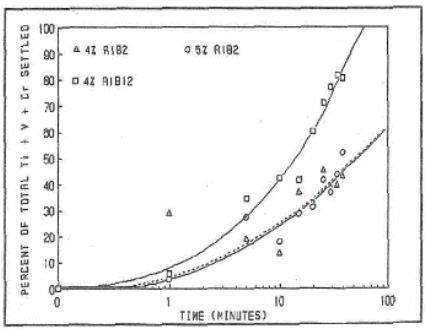

Figure 18: Settled Ti/V/Cr borides as a function of time upon introduction of different Al-B phases by using different master alloys. Reproduced from [36].

For melt with identical initial concentration of different impurities, literature results indicate removal rate can be ranked as Ti/Zr > V > Cr [37], [38], [41], [42].

4.3.1.3. Purification Results

Figure 19 shows impurity variation as a function of time for 12 kg 99.7 % aluminium with 100 ppm Ti and 100 ppm V. Al5B master alloy (AlB_2 phase contained) was used and the added boron equivalent to 50 % stoichiometric excess assuming TiB_2 and VB_2 were formed, process temperature was 730 °C. It can be seen that within 100 min melt holding time, 60-70 % Ti and V was removed respectively [35].

MIMI Tech GmbH
Preusweg 98, D-52074 Aachen
friedrich@mimi-tech.com

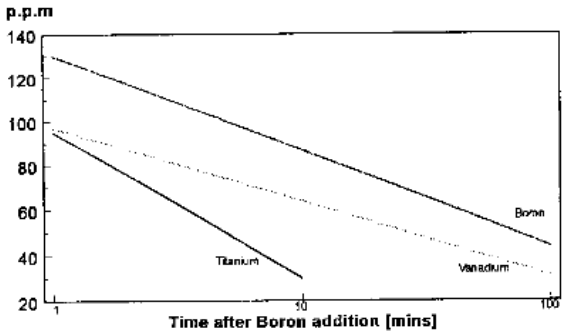

Figure 19: Variation of transition metal amount [ppm] in the melt as a function of boron treatment time. Reproduced from [35].

Similar results were obtained by Setzer et al. [36] who conducted boron treatment in a 3500 kg transfer crucible. Boron was added into the melt via AlB_2 phase in 145 % excess amount with respect to stoichiometric demands. The initial impurity content of Ti, V, Cr was respectively 45, 138, and 4 ppm. The collective removal efficiency of Ti, V, and Cr after 100 min melt holding, is 60 %. The result is similar to lab-scale trials shown in Figure 19.

In a larger scale of trials, boron was added into a 50-ton furnace with melt containing 62.7 ppm V, 30.7 ppm Ti, 3.9 ppm Zr, and 4.9 ppm Cr. Al8B master alloy (AlB_{12} phase contained) was used to introduce 168 ppm B into the melt, the charging was made in 3 separate times and the melt holding temperature was controlled at 750 °C. The time dependent decrease of impurity content is given in Figure 20(a) and (b). Over 50 % V and Ti was respectively removed in the first 100 min. Upon 300 min treatment time, the removal efficiency for both V and Ti was respectively ca. 76 and 87 wt. %. The removal of Cr and Zr was not as significant as Ti and V, due to their very low initial concentration [37].

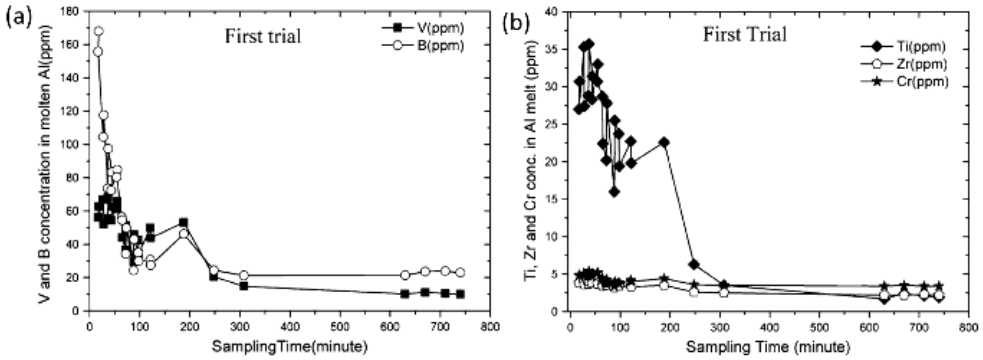

(a) (b)

Figure 20: The change in concentration of transition metals as a function of elapsed time after boron treatment: (a) V and B; (b) Ti, Zr, and Cr. Reproduced from [37].

All literatures which have been assessed in this sub-chapter suggest the lower boundary for removal of V, Ti, Zr by application of boron treatment process is respectively less than 10 ppm.

4.3.1.4. Disadvantages

The main disadvantage of boron treatment is the sediments in the floor of the holding furnace/ladles. For melts where boron treatment needs to be frequently conducted, impurity

MIMI Tech GmbH
Preusweg 98, D-52074 Aachen
friedrich@mimi-tech.com

bearing borides particles, termed also as sludges can accumulate in the floor of the furnace, causing possible damages of furnace lining.

4.3.1.5. Summary of Literature Assessment

Table 14 summarizes the overall assessments made based on all literatures assessed in the current sub-chapter.

Table 14: Summary of literature assessment concerning boron treatment.

Category	Impurity Removal Efficiency [Removal rate %][1)]	Lower Removal Limit (V, Ti, Zr)	TRL Range within Literature	Max. Treatment Capacity
Boron Treatment	62.4	Respectively less than 10 ppm	TRL 4-9	50 ton

1) averaged value from all assessed literatures.

4.3.2. Interview Section Analysis

4.3.2.1. Aluminum Companies

During the interviews with aluminium companies all comments in relation to boron treatment were protocoled. The interpretation result of the corresponding protocol is compiled into a SWOT analysis diagram which is shown in Figure 21.

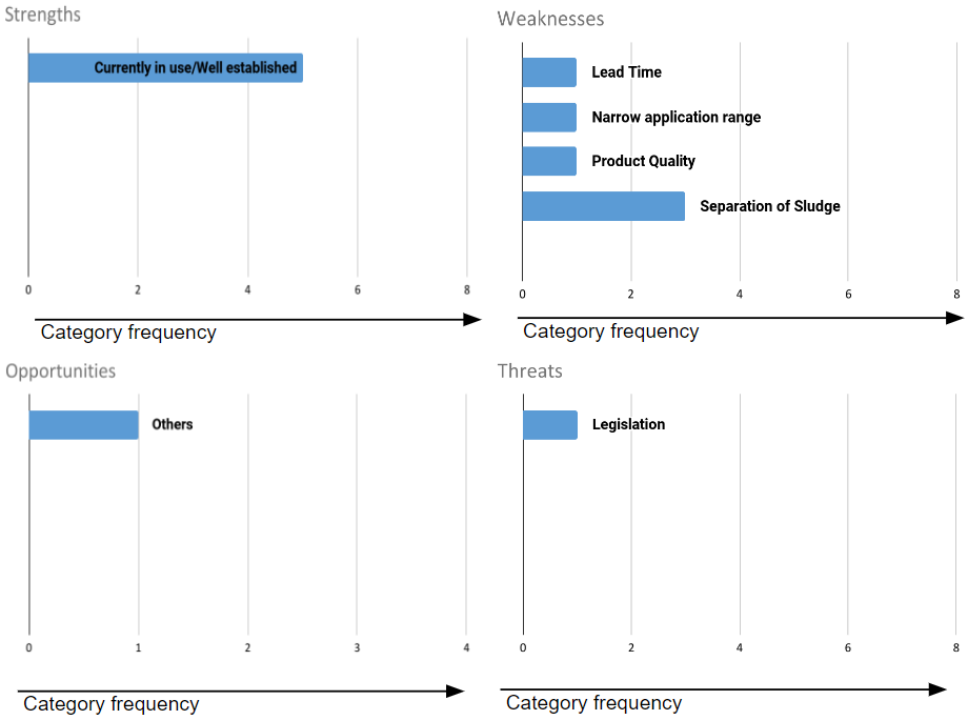

Figure 21: SWOT Analysis for Boron Treatment.

MIMI Tech GmbH
Preusweg 98, D-52074 Aachen
friedrich@mimi-tech.com

The boron treatment process is already an industrially established process. Nevertheless, there is still much room and requirements for process optimization. During boron treatment, separation of the sludge particles (i.e., impurity-bearing borides) is conducted by melt holding process. The holding operation increases process lead time and meanwhile make frequent furnace hygiene operations necessary. To optimize the separation step in the boron treatment process, one of the suggestions is to search for innovative ways which are capable of separating the sludge particles rapidly and in the meantime can prevent the sludge particles from partitioning in the furnace floor.

Intrinsic shortcomings of the boron treatment were also mentioned during the interview. These includes firstly narrow application range, which refers to low removal efficiency of Cr impurity. Furthermore, the boron treatment process leads to formation of coarse borides particles which may deteriorate product quality if the particles cannot be controlled before casting. Moreover, it was commented by one of the interviewees that in his country, the usage of boron is restricted for legislative reasons.

4.3.2.2. Techniques Providers

The low removal efficiency of Cr was attributed by one technique provider to the preferable reactions between Ti/V and Al-B phase in the melt the melt where there are abundant Ti/V impurities relatively to Cr.

With respect to alternative sludge separation techniques other than natural sedimentation, both filtration and degasser were nominated as potential in-line processes. Cartridge, ceramic foam filter (CFF), tube filters were specifically mentioned, quote from an interviewee worth a try for removal boride sludge particles.

One technique indicated the formed Ti bearing borides particles can be utilized as grain refining agents. In other words, they may be kept in the melt through casting process instead of being removed. To do so, Al-B master alloy is recommended to be added in the launder before degasser so that the big boride particles can be removed selectively through degasser and filter. Those fine TiB_2 boride particles may remain in the melt upon degassing and filtration process, and act as grain nucleates during alloy solidification.

One technique provider advocated proper dosage of grain refining master alloys so as to prevent excessive Ti amount in the scrap materials. Cleaning flux was suggested by one technique provider quoting helpful in easing removal of the boride sludge deposited at furnace floor.

MIMI Tech GmbH
Preusweg 98, D-52074 Aachen
friedrich@mimi-tech.com

4.4. Three-layer electrolytic refining (All elements, not well suited for high Mg, Na, Ca, and Zn)

4.4.1. Fundamentals and Principles

A process for electrolytic refining with three layers (also known as Hoopes Cell) was first created by W. Hoopes in collaboration with F. Frary and later commercialized by Alcoa in the early 1920s (see Figure 22). The process has been continuously enhanced and fine-tuned since then to achieve higher efficiency and purity as well as lower costs [43], [44].

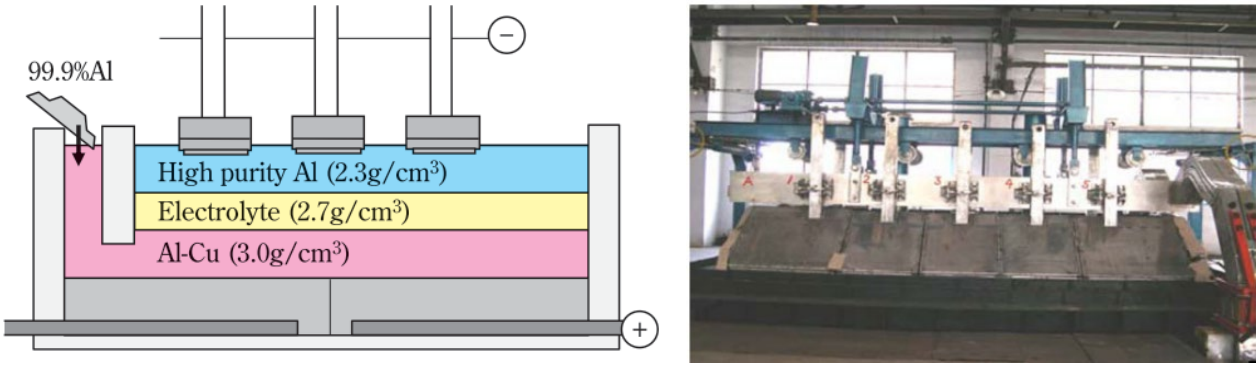

Figure 22: (Left) Schematic diagram of three-layer electrolytic refining process, and (right) an 85kA three-layer electrolytic refining cell [44], [45].

The method relies on molten salt electrolysis, which involves three distinct layers in the electrolytic cell. The bottom layer is an Al-Cu alloy (3.0-3.3 grams.cm^{-3}) that serves as the anode, the middle layer is a molten salt mixture (2.5-2.7 grams.cm^{-3}) that acts as the electrolyte, and the top layer is the refined molten aluminum (2.3 grams.cm^{-3}) that forms the cathode. The layers are separated by their density differences. The aluminum in the anode dissolves into the electrolyte and deposits on the cathode, while the impurities remain in the anode [44], [46].

The process of purifying aluminum by electrolysis depends on the fact that most of the impurities in aluminum (such as Cu, Fe, and Si) have higher standard electrode potentials (E0) than Al (see Figure 23). Some other impurities, such as Na, Ca, Mg, have lower standard electrode potentials than Al and are electrolytically transported to the electrolyte. However, these impurities do not deposit on the cathode as long as the electrolyte has enough Al^{3+}-ions, because they have more negative deposition potential than Al. Instead, they accumulate in the electrolyte over time [47].

MIMI Tech GmbH
Preusweg 98, D-52074 Aachen
friedrich@mimi-tech.com

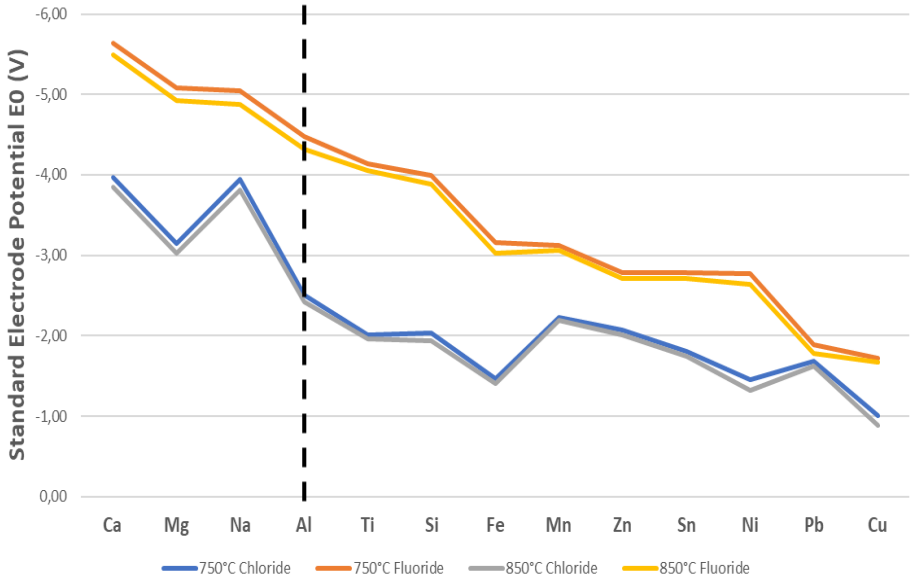

Figure 23: Standard electrode potentials E0 (V) at the cell temperatures of 750°C and 850°C calculated via FactSage, using FTLite and FactPS databases.

The process of obtaining pure aluminum involves transferring it from the top layer to a side-well chamber as more aluminum is added to the alloy layer at the bottom (see Figure 22). It is crucial to maintain a higher density in the bottom layer than in the electrolyte to prevent cross-contamination. If too much aluminum is added to the anode layer, the density can become too close to the electrolyte and cause cross-contamination. The acceptable density range is between 3.0 and 3.3 grams.cm-3, which corresponds to a copper content of 25 to 35 wt.%. The addition of copper to the impure aluminum lowers its melting point from 660°C to around 560°C and increases its density to about 3.0, ensuring that the bottom layer consists only of the anode alloy [48], [49], [46], [45].

4.4.1.1. Anode layer

In the Al-Cu anode, aluminum is electrolytically transferred to the cathode layer via the electrolyte layer. The anode layer retains copper and impurities until too much residual impurity is accumulated, and then it has to be replaced [48], [46], [45]. During electrolysis, all elements more noble than aluminum (see Figure 23, right of dashed line) stay in the anode, forming a multicomponent system that is gradually enriched with mainly iron and silicon (as the main impurities in primary aluminum), while the aluminum content reduces.

The elements that are more positive than aluminum remain in the anode and start to crystallize firstly in the side-well, used for feeding new anode material, as the temperature is about 30 to 40 °C lower than in the electrolyte [47]. When the anodic alloy has about 5-10 wt.-% iron and 10 wt.-% silicon, a solid phase separates out [50] (see Figure 24), with two different shapes: one is needle-like with high Fe and Mn content (Figure 24a) and the other is round-like with less Fe and Mn (Figure 24b).

These crystals can be removed from the side-well, which helps to reduce the impurities in the anode alloy [47]. The thickness of the anode layer affects the rate of impurity accumulation and removal. A thin layer leads to faster saturation and more frequent removal of crystals. A thick layer requires a deeper melting zone in the cell, which increases the costs and the amount of aluminum in the

MIMI Tech GmbH
Preusweg 98, D-52074 Aachen
friedrich@mimi-tech.com

metal stock. Based on practical experience, a thickness of 20 to 25 centimeters for the anode layer is optimal.

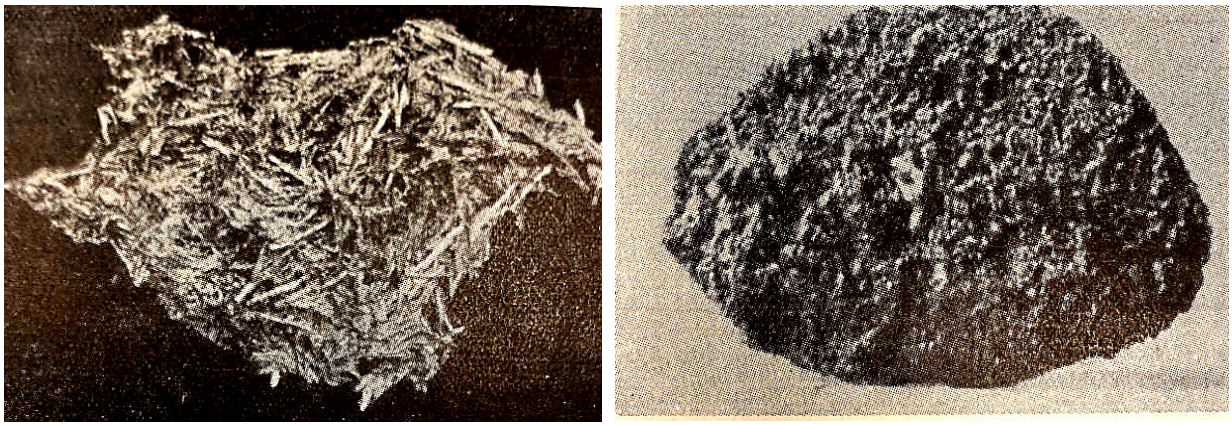

(a) (b)

Figure 24: a) Needle-form Crystal (12.72 % Cu; 5.26 % Zn; 6.23 % Si; 18.5 % Fe; 5.18 % Mn), and b) Round Crystal (15.18 % Cu; 5.1 % Zn; 5.16 % Si; 9.6 % Fe; 1.95 % Mn) [47].

4.4.1.2. Electrolyte layer

The electrolyte is composed of fluorides, chlorides, and a mixture of salts of Na, Ba, Al, Ca, and Mg, being Ba mainly used to increase the electrolyte density [44]. The all fluoride-high temperature electrolyte (Original from Hoope's process) was subsequently replaced by low temperature chloride- fluoride electrolyte (Pechiney process). This modification allowed the process temperature to reduce from 1000°C down to 740-750°C. Several other major modifications in automatization, process control, and raw material quality were conducted along the years to improve the process efficiency and end-purity of the product [49].

In the electrolyte, the current passes through all cations such as Al^{3+}, Ba^{2+} or Na^{+} towards the cathode, but because aluminum has the highest deposition potential among these elements, it is primarily deposited at the cathode. The Ba^{2+} and Na^{+}-ions are enriched at the cathodic layer of the electrolyte. At the anode, the ionization of aluminum is the predominant process, since it has the most negative potential among all other possible reactions, therefore, as long as there is enough Al^{3+} within the electrolyte, the Ba and Na will not be transported to the cathode [47].

Considering the thermodynamics, to extract one gram of aluminum from alloy and transferring it to the molten super pure aluminum layer, only 37pprox.. 0.005 volts is required, according to the Nernst equation (Equation 6):

$$E = -\frac{R\ x\ T}{z\ x\ F} x\ ln\frac{a_{Al}^{a}}{a_{Al}^{c}} = \frac{-8.314\ x\ 1023}{3\ x\ 96485} x\ ln\ (0.85) \approx 0.0047\ V \qquad \text{Equation 6}$$

, where R is the universal gas constant: R = 8.314 $J.K^{-1}.mol^{-1}$, T is the temperature in kelvins, z is the number of electrons transferred in the cell reaction or half-reaction, F is the Faraday constant (F = 96485 $C.mol^{-1}$), a_{Al}^{a} is the activity of the reduced form, and a_{Al}^{c} is the activity of the oxidized form.

MIMI Tech GmbH
Preusweg 98, D-52074 Aachen
friedrich@mimi-tech.com

According to Srinivasan et. Al [49], the relation between both activities is 0.85 for Al in an Al-Cu alloy.

The above equation shows that, theoretically, very little energy is needed to transfer aluminum from a 70% solution in copper at the anode to a pure-metal cathode [51]. When the results from Nernst equation is used to calculate the amount of energy needed via the Gibbs free energy change (ΔG = -n x F x E) , it indicates a theoretical value of nearly 1385 J/mol i.e. 0.0147 kWh/Kg of pure aluminum for an isothermal transfer from the alloy to the cathode [52]. However, in practice, commercial cells such as the ones using the all-fluoride electrolyte, operate at about 5.5V resulting in an energy consumption of ~18 kWh/kg of super pure aluminum. This is due because a major portion of the excess energy is needed for overcoming the ohmic resistance of the bath as well as in maintaining the thermal balance of the cell [49].

Since a minimum thickness of the electrolyte layer is also indispensable for an appropriate ultra-purification effect and preventing cross contamination with the anode, its thickness is usually kept between 12 and 15 centimeters. However, it is preferable to keep the thickness of the layer as small as possible because an increased thickness is accompanied by larger energy consumption [47].

4.4.1.3. Cathode layer

As for the cathode, its thickness is kept typically in the range of 10 to 15 centimeters to put the graphite electrodes easily in the melt as well as to keep a minimum layer on top after the removal of the refined metal [47].

4.4.1.4. Behavior of Impurities and typical anode alloy composition

The metals, which are more noble than aluminum (see Table 12), are not electrolytically transported from the anode layer. This holds true as long as there are sufficient Al^{3+} ions in the electrolyte, i.e., the content of aluminum in the anode layer is high enough (~ca. 45%), and any over voltage is not allowed so it does not reach a threshold to start ionizing other more elements. In theory, if the voltage is carefully controlled, Calcium, Magnesium, Sodium, and Aluminium will be transported to the electrolyte, as the first three are more ignoble as the Aluminium, and during the deposition, only Aluminium will be transported towards the cathode, as the other three impurities would have a higher deposition potential than Aluminium [51].

In praxis, Aluminium, together with Calcium, Magnesium, and Sodium passes into the electrolyte. Calcium is harmless to the electrolyte, but an excess of Magnesium can change the electrolyte properties and, being near to aluminum in the standard electrode potential series, may appear in the refined metal [51]. Magnesium in the feed metal must therefore be reduced to a safe level of 0.1 wt.% by e.g., a preliminary fluxing process. Zinc behaves abnormally; although more noble than aluminum, it can appear in the cathode metal when its concentration exceeds a few per cent in the anode, owing to its high vapor pressure [51].

The selectivity of the process depends mostly on the proper operation of the cell, rather than the composition of input materials. If the operation is stable and the cell conditions are optimum, a purity of 4N8 can be achieved even with highly alloyed scrap as feed material. The Table 15 illustrates typical input materials for the anode alloy, classified either as primary Al input or scrap

MIMI Tech GmbH
Preusweg 98, D-52074 Aachen
friedrich@mimi-tech.com

alloy addition. The major impurities (Fe and Si) will be accumulated in the anode alloy, while minor impurities such as Ca, Mg, and Na will be accumulated in the electrolyte and cell walls [51].

Table 15: Some typical analyses of anode alloys for prime and scrap alloy feed.

Element /wt.%	Virgin-Metal feed		Scrap-Alloy feed	
	Example 1	Example 2	Example 1	Example 2
Cu	30.4	25.5	32.1	24.1
Al	64.8	68.4	46.6	55.7
Si	1.3	2.	10.0	7.7
Fe	2.5	3.3	3.4	4.5
Zn	0.5	0.3	4.5	5.5
Mn	0.1	0.2	1.1	0.7
Mg	0.1	0.1	0.15	0.12
Ni	0.3	0.2	1.4	1.0
Pb	-	-	0.6	0.4
Sn	-	-	0.15	0.3
Ti	0.04	0.05	0.04	0.08

4.4.2. Results from the literature review

4.4.2.1. Treatment of primary aluminum

As seen in the fundamental section above, the research done in three-layer electrolysis was largely focused on finding an optimum electrolyte composition for the process. Other researchers also reported the obtained purification of individual elements and the overall energy consumption, which will be the focus of this section.

A small scale experiment was performed by Vasanc et al. [53] in his paper from 1986, where he reported an overall removal of 83.7% of all impurities within primary aluminum. In his works, he emphasized the importance of the electrolyte in obtaining proper process control, product quality and cost [53].

In a paper written by Kondo at al. [54], in 1990, about the production of high-purity aluminum in Japan, they shared some of the key process and economic figures about the three-layer electrolysis process for the upgrade of primary aluminum towards high purity. It is reported that over 98.8% of all impurities present in the initial primary aluminum could be removed, at an energy cost ranging between 14-18 kWh/kg of purified aluminum [54].

In a more recent paper, from 2008, Zhao et al. [55] have designed an 85 kA cell for the production of high-purity aluminum. Their work showed a removal efficiency of 98.67%, consistent with the other studies. They also reported an energy consumption of 14 kWh/kg of purified aluminum, emphasizing that the electrolyte engineering plays a direct role on costs [55].

All literatures which have been assessed suggest the lower boundary for removal of impurities to be less than 1 ppm.

The Table 16 below summarizes the results and other assessments made for all literature found for the three-layer electrolysis of aluminum, starting from primary aluminum.

MIMI Tech GmbH
Preusweg 98, D-52074 Aachen
friedrich@mimi-tech.com

Table 16: Average values obtained from the literature sources on the removal efficiency and energy consumption [53], [54], [55].

Category	Impurity Removal Efficiency [Removal rate %]	Impacts on process [Energy consumption, kWh/kg]	TRL Range within Literature	Max. treatment capacity
Three-Layer Electrolysis – Primary	98.83%	15.7	TRL 9	N.A.

4.4.2.2. Treatment of aluminum scrap

The use of three-layer electrolysis process has been intensively researched, as it does not differ technically from the refining process applied for primary- and high-purity aluminum. It becomes clear that the advances in process control, electrolyte composition, cell design, etc. have a direct effect on energy consumption. Early studies reported several times higher energy consumption than the current ones. A few examples will be shown below.

The earliest report found was from 1957, from Beljajew et al. [47], where a classical three-layer electrolysis was used to refine heavily contaminated aluminum scrap, reaching 98.92% impurity removal efficiency. Despite its purification success, the low scale of the process coupled with the very large electrolyte layer height used, made the tried process very energy intensive, at an energy consumption of 39 kWh/kg of purified aluminum [47].

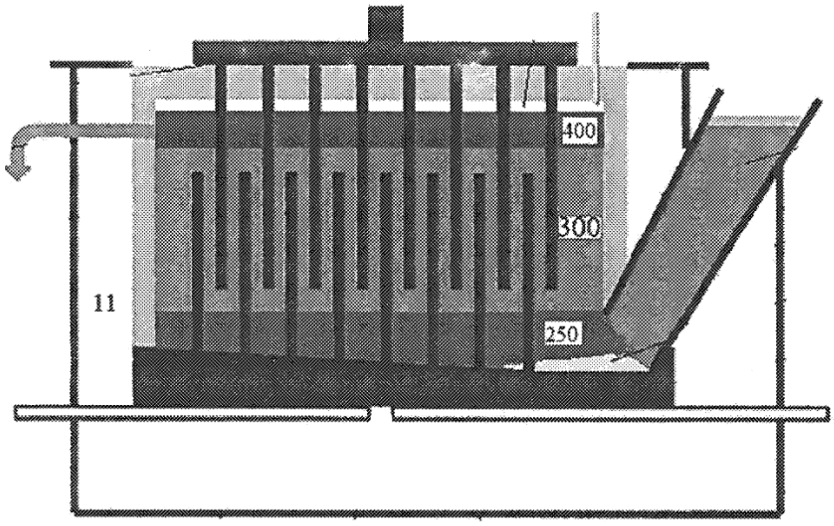

Figure 25: Sketch of three-layer electrolysis process with overlapped electrodes, as shown in De Young et al. [56]

In the same year, Pearson et al. [51] also explored this concept for purified contaminated aluminum sources, reporting an energy consumption between 18 and 23 kWh/kg of purified aluminum. He stated that the purity of metal attainable depends more on the steady operation and condition of the cell than on the composition of the anode alloy (input material). Under good conditions,

MIMI Tech GmbH
Preusweg 98, D-52074 Aachen
friedrich@mimi-tech.com

aluminum with a purity of 99.998% can be obtained. The major impurities present in the product are Cu, Fe, and Si from the anode alloy, along with small quantities of Ca, Mg, Na, and Ba from the electrolyte. If the cell is not properly operated, the Cu, Si, and Fe may increase in proportion to their presence in the anode alloy [51].

The most recent report of utilizing the three-layer electrolysis for the purification of highly contaminated aluminum scrap sources comes from De Young et al. [56], in his patent for the company Alcoa (see Figure 25). His studies, still in low TRL, showed promising results to remove impurities from the aluminum using a fraction of the energy usually required by a traditional three-layer electrolysis process. His innovation lies in the electrode design, where the overlapping electrode configuration greatly decreases the distance between electrodes. This effectively reduces the voltage drop, directly reducing the energy requirements for the process. It is claimed to have an energy consumption of between 2 and 6 kWh/kg of purified aluminum. Other embodiments of his patent claim an energy consumption from 1 – 15 kWh/kg [56].

Other alternative electrolysis approaches for upgrading aluminum scrap found in the literature were solid-state electrolysis and capillary electrolysis. In low TRL laboratory investigation, Solheim et al. [57] utilized a side-by-side geometry cell for the refining of 7XXX series alloy, reaching an impurity removal efficiency of 99.75%, at an energy consumption of 7 kWh/kg of purified aluminum [57].

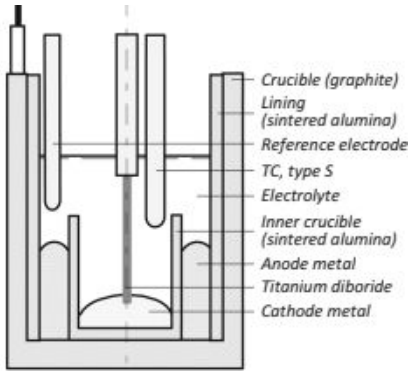

Figure 26: Laboratory cell for the separation of Al [57].

Other investigations from Lu et al. [58] and Oya et al. [59] utilized low temperature molten salt electrolysis to refine Al, depositing it over a cathode plate. It was reported 97.83% and 99.00% removal efficiency with an energy consumption of 7 and 17 kWh/kg of purified aluminum, respectively. Both studies are still in low TRL level 4 and show promising results for further industrialization [58], [59].

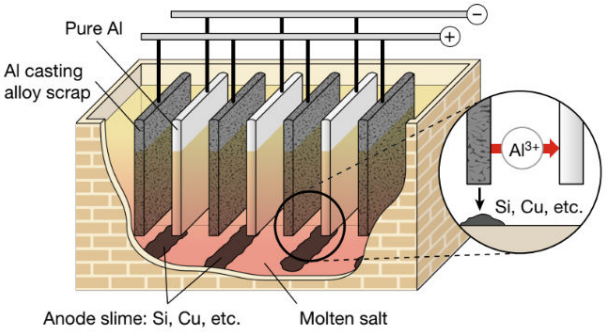

Figure 27: Schematic of the solid state electrolysis process proposed by Lu et al. [58].

MIMI Tech GmbH
Preusweg 98, D-52074 Aachen
friedrich@mimi-tech.com

Another approach was introduced by Yasinskiy et al. [60] where he proposed an alternative to three-layer process, this approach was used for purifying and extracting aluminum from scrap using a thin-layer multiple-capillary molten salt electrochemical system. This research is still in low TRL 4 and no information regarding energy consumption was given. However, due to the very low proximity between anode alloy and cathode (separated by capillaries within a ceramic plate), it is expected that the energy consumption will be much smaller than traditional three-layer electrolysis process [60].

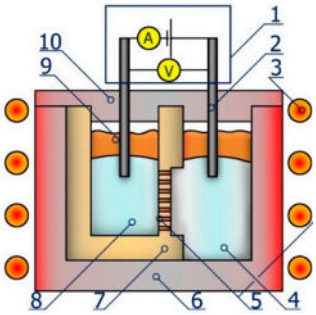

Figure 28: Schematic representation of a multi-capillary cell [60]

All literatures which have been assessed suggest the lower boundary for removal of impurities to be less than 100 ppm.

The Table 17 below summarizes the results and other assessments made for all literature found for the three-layer electrolysis of aluminum scrap or highly contaminated aluminum.

Table 17: Average values obtained from the literature sources on the removal efficiency and energy consumption [47], [51], [56], [57], [58], [59].

Category	Impurity Removal Efficiency [Removal rate %]	Impacts on process [Energy consumption, kWh/kg]	TRL Range within Literature	Max. treatment capacity
Three-Layer electrolysis – Scrap	93.72%	16.0	TRL 4-9	N.A.

4.4.3. Interview Section Analysis

4.4.3.1. Aluminum companies

Three-layer electrolysis is an already established technology among a few of the companies interviewed for this study. It is, however, currently utilized only for the production of high-purity aluminum (4N8-5N) from the input of primary grade aluminum (3N). Its utilization as a means of upgrading contaminated scrap has been researched in the past, showing good technical results but very high energy consumption. More recently, Alcoa explored this technology, at lower TRL, with an innovation aimed at reducing its operational costs, with promising preliminary results.

MIMI Tech GmbH
Preusweg 98, D-52074 Aachen
friedrich@mimi-tech.com

SWOT Analysis

The SWOT Analysis (Figure 29) shows that the interviewed Aluminum companies see the clear strengths behind this technology and many opportunities to implement it for the scrap refining. However, there were also many weaknesses and threats identified. In the sections below, the main discussion points will be addressed for each category.

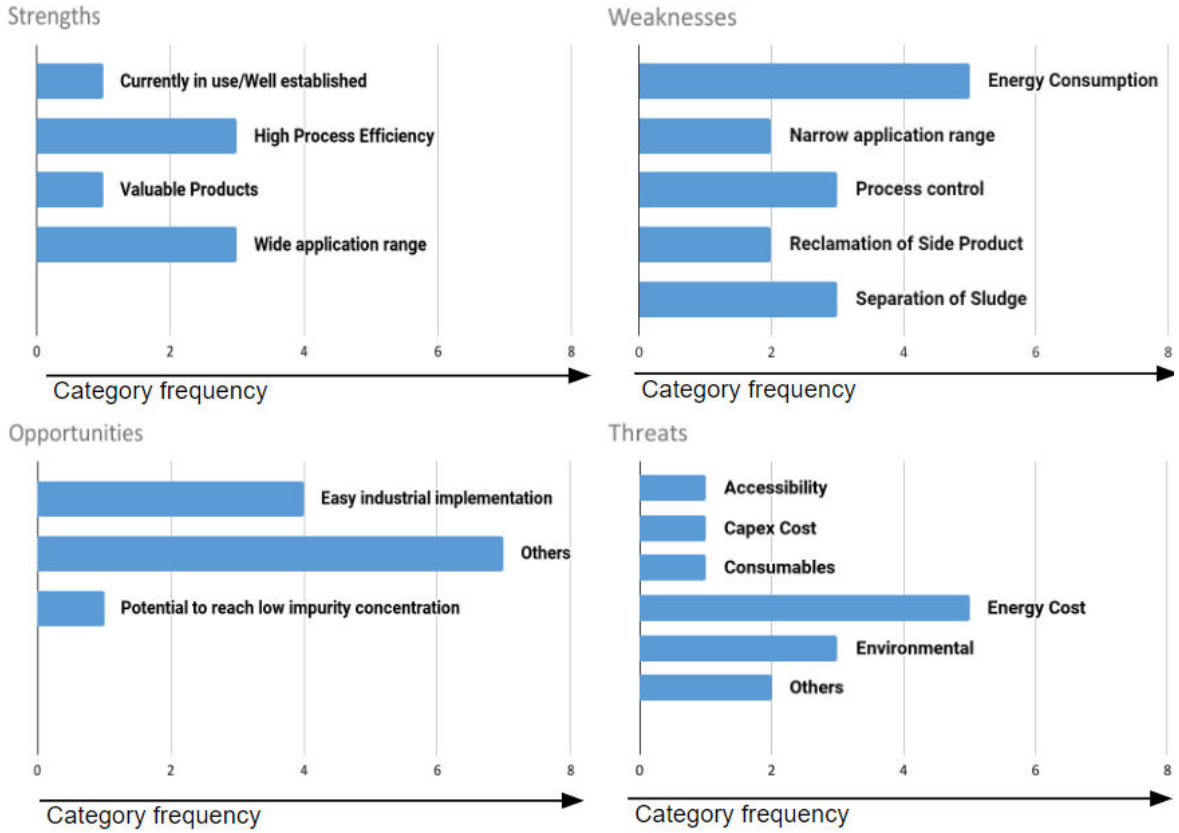

Figure 29: SWOT Analysis for the three-layer electrolysis process, applied to scrap purification.

Strengths and Opportunities

The main strengths identified are related to the robustness of the process, as it can treat almost any kind of aluminum scrap at very high contamination level, resulting in a very clean, primary-like aluminum. Moreover, the current industrial utilization and know-how built by using this technology for the production of high-purity aluminum were seen as a strength.

The opportunities identified within this technology are mostly related to the recent technological advancements that help to minimize the high energy costs associated with the three-layer electrolysis. Some examples are the works done by Alcoa in reducing the electrode distance, and the innovative cell design from Yasinskiy et al. in replacing the electrolyte layer by a porous ceramic layer impregnated with electrolyte. Additionally, the maturity of this technology and the possibility of treating very high contaminated scraps makes it a very promising solution to the upgrade of certain classes of aluminum scraps.

MIMI Tech GmbH
Preusweg 98, D-52074 Aachen
friedrich@mimi-tech.com

Weakness and Threats

The biggest concern within weakness is, by far, the energy consumption required to upgrade the scrap towards primary grade aluminum. This energy consumption is, currently, similar to the energy required to produce primary aluminum. This high energy consumption is mostly related to the voltage drop induced by the electrolyte layer, and the thermal losses within the cell. There are a few research, both in industry and in academia, aiming at reducing this energy loss. Once successful, it can make viable the adoption of this technology for the upgrade of highly contaminated scrap.

The residue material, i.e., the Al-Cu anode alloy enriched with impurities, presents the biggest identified Threat for this technology. The proper destination of this material – maybe to other industries– is very important to enable the adoption of the three-layer electrolysis and to promote the circularity of its by-products.

4.4.3.2. Technology providers and industry experts interviewed

4.4.3.3. Alcoa

The company Alcoa was interviewed regarding their experience with many of the removal technologies identified in this study. In this section, we will focus on the discussion regarding the development of the three-layer electrolysis for scrap refining. It was pointed out that, due to the strategic nature of their technological development, not many details could be openly discussed at this moment. However, few information about the process, especially regarding the possible utilization paths and destination of residues, was discussed.

Despite its clear robustness in treating almost any type of scrap, Alcoa pointed out that this technology may be first utilized in special products segments, e.g., for the automotive industry, which has very strict demands in both purity and recyclable content targets. It was also discussed that the removal of the accumulated impurities in the anode alloy can happen by skimming or siphoning any precipitate formed (e.g., Fe and Si precipitates when concentration reaches ~ 5-10%).

4.4.4. Challenges Towards a higher TRL

The three-layer electrolysis technology has reached maturity and is widely implemented for the production of high purity aluminum. The utilization of this technology for scrap refining has no technical barrier. However, the high energy cost is the main blocking point for the adoption of this process in upgrading scraps. This can only be achieved if the energy costs drop down to suitable levels and/or there is a niche market request for high recycled content in specialty products usually made with high-purity constituents, such as for some products in aerospace and automotive industries.

To reduce the high energy consumption, the approaches identified in the literature are all related to reducing the energy losses occurring within the electrolyte layer. The patent from Alcoa brought closer both electrodes to reduce the voltage drop within the process, claiming to reduce the energy consumption. While the works from Yasinskiy et al. utilized an impregnated porous ceramic barrier to substitute the molten electrolyte layer, hence reducing the energy consumption. This later study is still in the early stages and requires further development in pilot scale, etc. Other low TRL studies utilized solid layer electrolysis as a way to purify scrap, showing good perspectives. Moreover, a suitable utilization or destination of the contaminated anode alloy needs to be developed to reduce

MIMI Tech GmbH
Preusweg 98, D-52074 Aachen
friedrich@mimi-tech.com

its economic impact on the refined aluminum product. So far, only one small study, from Wei et al. was found addressing this issue for Iron specifically [61].

MIMI Tech GmbH
Preusweg 98, D-52074 Aachen
friedrich@mimi-tech.com

4.5. Fractional crystallization (All elements, not well suited for Sc, Ti, V, Cr, Zr)

4.5.1. Fundamentals and Principles

As an alternative to cost and investment-intensive three-layer electrolysis, ultrapure aluminium has been produced for decades by segregation (also known as fractional crystallization). The segregation process is driven by the fractional crystallization mechanism, which promotes the expelling of impurities from the crystallizing interface. In fractional crystallization, the difference in solubility of impurity elements in the solid and liquid phases of the base metal is explored in order to crystallize solids with lower impurity levels than the initial melt phase [62], [63].

The ratio of the concentration of impurity elements in the solid (C_S) and liquid (C_L) phases is called the distribution coefficient ($k=C_S/C_L$). This coefficient represents the theoretical maximum impurity removal that can be achieved in one purification step. Table 18 summarizes the literature values for k coefficient for most impurities present in aluminium [64]–[68].

The smaller the k coefficient is from unity, the higher the removal efficiency of fractional crystallization. On the other hand, impurities with k greater than 1 tend to remain in the solid phase and become partially incorporated into the crystallized material. If the distribution coefficient of the impurity is close to 1, fractional crystallization cannot be performed efficiently [69]. The previously purified solids can be continuously subjected to a further fractional crystallization step to increase their purity by removing the solute-rich portion [70].

Table 18: Literature values of distribution coefficients of impurities in aluminium [64]–[68].

Elements	Distribution coefficient k	Elements	Distribution coefficient k
Fe	0.018–0.053	Ti	7–11
Cu	0.15–0.153	Si	0.082–0.12
Ag	0.2–0.3	K	0.56
Au	0.18	Zr	2.3–3
Zn	0.35–0.47	Pb	0.0007–0.093
Ni	0.004–0.09	P	<0.01
Mn	0.55–0.9	Sc	0.9
Mg	0.29–0.5	Sb	0.09
Ca	0.006–0.08	V	3.3–4.3
Cr	1.8	Na	0.013

4.5.1.1. Differences between Layer- and Suspension based segregation method

Over the past few decades, several segregation methods have been developed in both industry and academia, all of which are based on the same principles of fractional crystallization described above. However, they can be distinguished according to the crystallization technique used. If the crystals formed during crystallization grow freely in the melt, this is referred to as a “suspension-based” process. When the formed crystals grows as a solid layer on a cooled surface, this can be defined as a “layer-based” process (see Figure 30) [71].

MIMI Tech GmbH
Preusweg 98, D-52074 Aachen
friedrich@mimi-tech.com

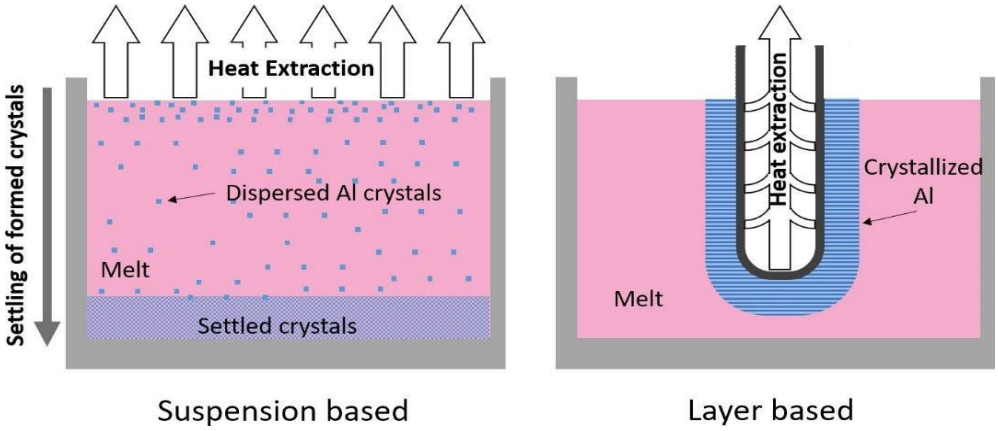

Figure 30: Sketch of a suspension-based (left) and a layer-based (right) segregation methods [71].

When comparing the two techniques, the suspension-based process has the advantage of a larger solid/liquid interface area, with each nucleated crystal having its own fractional crystallization interface. Compared to the suspension technique, the layer technique has the advantage that no additional process is required to separate the formed crystals from the bulk melt. Not only does this benefit the process, but it also avoids the entrapment of a solute-rich melt in the purified product. However, both processes have been reported to achieve similar cleaning results and can be operated as a batch or continuous process [71].

4.5.1.2. Theoretical impurity segregation according to Scheil-Gulliver model

When diffusion in the solid phase is ignored and complete mixing of the expelled impurities in the liquid phase is considered, the variation in impurity content along a crystallized solid can be described by the Scheil-Gulliver equation [72], [73].

$$C_S = k \cdot C_0 \cdot (1 - f_S)^{k-1} \qquad \text{Equation 7}$$

, where f_S is the solidified fraction of the melt, k is the distribution coefficient, and C_0 is the initial solute concentration.

Figure 31 shows the impurity distribution for some common impurities found in aluminium according to the Scheil's model (Equation 7), considering an initial concentration of 0.01 wt.% and the distribution coefficients in Table 18. Notably, for impurities with k > In 1, solute enrichment is present at the beginning of the crystallization. In fact, it was observed that this model, although giving a good indication of the expected curve, could not be used to fully predict the behavior of the impurities and the purification obtained in fractional crystallization. This is because of the kinetic aspects of the crystallization process, which Scheil's model does not fully consider.

MIMI Tech GmbH
Preusweg 98, D-52074 Aachen
friedrich@mimi-tech.com

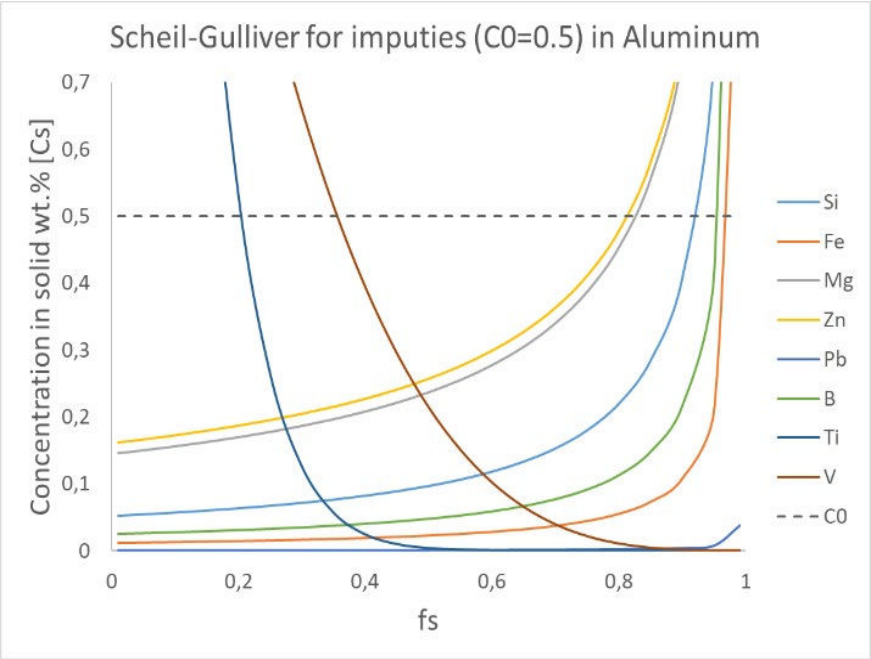

Figure 31: Distribution of some common impurities in aluminium according to Scheil-Gulliver model, considering the initial concentration of all impurities (C0) as 0.5 wt.%.

The Scheil-Gulliver model offers only a general estimate of the anticipated outcomes, as it solely accounts for the full diffusion of the solid expelled into the liquid phase. For a more comprehensive perspective, it is advisable to consider the Burton, Prim, and Slichter (BPS) model, as presented in Equation 8 [74].

$$k_{eff} = \frac{k_0}{k_0 + (1 - k_0) \cdot e^{[-V\delta_{bps}/D]}}$$ Equation 8

A planar growth morphology is possible under specific conditions, including low supercooling, low solute concentration, and a slow growth rate. These conditions are typically present in processes like crystal growth and fractional solidification. On the other hand, at the boundaries of developing crystals (where solutes with k<1 segregate), the melting point is lower compared to the crystal's central region. Consequently, these regions exhibit more pronounced growth at their centers, resulting in the formation of solute-rich channels along their boundaries. This growth pattern is named cellular growth. Another growth morphology, dendritic growth, is highly undesirable for refining purposes and should be carefully avoided. Dendritic growth occurs, for example, when the growth rate is excessive or when solute concentration is excessively high [75].

Cellular and dendritic structures are undesirable in the context of refining because they tend to trap solutes during crystallization, impeding their separation into the melt phase. To ensure a planar growth interface, it is essential for the growth rate to remain below the threshold defined in Equation 10. Additionally, factors such as the type and initial concentration of impurities play a significant role in determining the morphology of the growth interface.

MIMI Tech GmbH
Preusweg 98, D-52074 Aachen
friedrich@mimi-tech.com

$$G \leq \frac{D \cdot \Delta T \cdot k}{m \cdot C_0 \cdot (1-k)}$$ Equation 9

,where G is the growth rate, ΔT is the temperature gradient in the liquid interface, m is the slope of liquidus line in the binary phase diagram, k is the distribution coefficient (CS/CL), D is the solute diffusion coefficient in the melt and C0 is the initial concentration of solute.

4.5.2. Results from the literature review

4.5.2.1. Treatment of primary and high-purity aluminum

The first mentioned literature found about the large scale suspension-based fractional crystallization for the purification of aluminum was from Jacobs et al. [76] in 1967. In his patent for Alcoa, he claimed that he was able to obtain aluminum with 4N3 purity starting from primary (2N7) aluminum, at a 30% yield. The main impurities present in the input materials were 0.028% Fe, 0.042% Si, 0.013% Ga, and 0.007% peritetic (V, Zr, Ti, Cr). This process consisted of a 680 kg batch process, with a chamber preheated at 700°C. The furnace had a metal-air surface interface of 0.8 m2, where the melt was cooled. The crystallization time took 99 minutes, at a rate of 33 kg/m2. The process ran until 70% of metal was crystallized. To compact the crystal bed and expel the molten aluminum between the crystals towards the bulk melt, a heated graphite tamper (645 cm2) pressed the crystal bed at a defined interval [76].

Dawless et al. [77] wrote a patent in 1988 for Alcoa demonstrating a two-stage suspension-based fractional crystallization. The patent claims that this process is already being used commercially for the production of 6N purity aluminum, starting from 4N3 grade Al input (obtained from three-layer electrolysis). The residue from the first stage is returned to the three-layer electrolytical refining to upgrade it back to 4N3. The residue from the second stage is fed back to the first stage for subsequent refining [77].

Hashimoto et al. [64] went even further, and he was able to purify aluminum to 7N purity, starting from 6N aluminum obtained via a combination of three-layer electrolysis and fractional crystallization. To reach this purity, he employed the zone melting process, a classical low-scale batch layer-based fractional crystallization. His technique employed a cropping procedure, where the end of the zone refined bar (where impurities are accumulated) was discarded and its first half joined with another first half from a second zone-refined bar. This approach was effective in preventing Sc back diffusion and also for Ti, V, Zr, and Cr removal [64]. Another layer-based approach was done by Mikubo et al. [78], where he utilized the Pechiney process to produce 4N+ aluminum starting from primary [78].

Another non-conventional suspension-based approach was patented in 2004 by De Vries et al. [79], where a continuous process was developed using molten salt to remove the formed crystals. In his patent, it was claimed that the process was running at a production rate of 20 tons/day with 90% yield, starting with 2N7 primary purity, upgrading it to 3N8 [79].

Several other authors explored fractional crystallization to obtain high- and ultra-purity aluminum. More recent studies includes the work of the Pure Metals group from the IME Institute of RWTH Aachen University [80], [81], [82], [83] and other investigations from Chinese research groups [84], [85]. All these authors explored different techniques and methodologies to ultra-purify aluminum,

MIMI Tech GmbH
Preusweg 98, D-52074 Aachen
friedrich@mimi-tech.com

starting from ranges between 2N7 – 4N5. Another very low-scale trial from Zhao et al. [86] aimed at promoting the fractional crystallization of aluminum under supergravity conditions of up to 1000 "G's". The author successfully improved the separation of the crystals from the melt.

All literatures which have been assessed suggest the lower boundary for removal of major eutectic impurities ($k < 1$) to be less than 10 ppm.

The Table 19 below summarizes the results and other assessments made for all literature found for the fractional crystallization of aluminum, starting from primary or high-purity grade.

Table 19: Average values obtained from the literature sources on the removal efficiency and energy consumption [87], [77], [88], [78], [80], [81], [82], [79], [84], [85], [86].

Category	Impurity Removal Efficiency [Removal rate %]	Impacts on process [Energy consumption [1], kWh/kg]	TRL Range within Literature	Max. treatment capacity
F.C. – High Purity	98.57%	0.8	TRL 3 – 9	Up to 22tons/day
F.C. – Primary	73.45%	1.8	TRL 3 – 9	

[1)] when not available, it was estimated based on the additional information available in the source, such as holding time, temperature, etc. The estimations were based on a simplified heat balance using specific heat capacity and latent heat of fusion for Al as well as correction coefficients to compensate for the heat losses occurring during the process through the furnace wall and melt surface.

4.5.2.2. Treatment of aluminum scrap

Just like the examples seen above, fractional crystallization can be– and has already been- utilized for the upgrade of scrap aluminum towards primary grade aluminum. These applications ranged from TRL 2 up to TRL 7.

In a patent for the company Alcoa (Figure 32), Kahveci et al. [89] used the already developed suspension-based fractional crystallization process of Alcoa for the upgrade of 5XXX aluminum scrap.

As with any fractional crystallization process, this process follows the mass conservation law, and the achieved purification is directly related to the yield of removed purified fraction. For a yield of 81.6%, the process reduced the silicon level from 290 ppm down to 167 ppm, and the Fe levels dropped from 610 ppm down to 399 ppm. Other elements were also reduced according to the yield and their distribution coefficient in Al. Cr, for instance, was enriched in the product as it has a distribution coefficient higher than one [89].

MIMI Tech GmbH
Preusweg 98, D-52074 Aachen
friedrich@mimi-tech.com

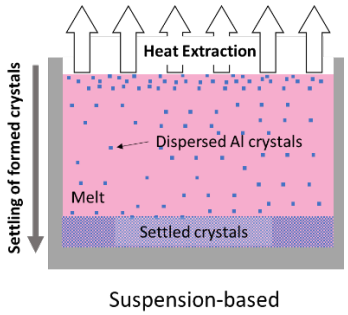

Figure 32: Alcoa suspension-based fractional crystallization process, figure adapted from [89].

The Alcoa's method described above is characterized as a batch process, which means that after the crystals are formed and settled down the furnace ladle, and the residual melt with impurities are tapped out of the furnace, the purified aluminum crystals need to be melted again and tapped out of the furnace, effectively separating both purified and impure aluminum phases.

To solve this issue and transform this process from a batch process towards a continuous process, Wouters et al. [90] (Figure 33) patented for the company Aleris a modification in which he added another element (e.g. 3.5 wt.% Cu) to increase the overall initial melt density. The formed purified crystals (now with lower density than the initial melt) can float to the melt surface and be efficiently separated from the melt. This characteristic enabled the continuity of this process, as with the removal of purified aluminum crystal, more molten aluminum scrap and copper can be added to the melt.

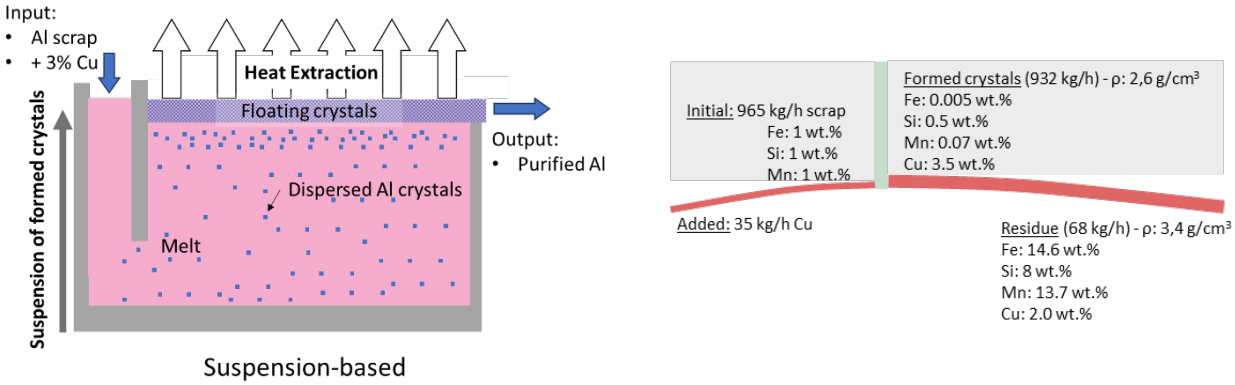

(a) (b)

Figure 33: Adapted from [90], where (a) shows the modified Alcoa's process; (b) Mass flow and chemical composition of the input material, products, and residues.

In his patent, it was claimed that when the process ran with an aluminum scrap containing 1% Fe, 1% Si, and 1% Mn, the product was upgraded reaching a removal of 81% (0.005% Fe, 0.5% Si, 0.07 % Mn). In this claim, 3.5% Cu was added for density increase, however other materials like Zn can be added to increase the melt density. These elements will partially contaminate the purified aluminum phase, however, depending on the destination of it (2XXX or 7XXX alloys), these elements can be incorporated within the alloy [90].

Several other research are also reported in literature, where the authors also employed fractional crystallization for the upgrade of aluminum scrap. Their novel techniques aimed for example at increasing the separation efficiency by, for example, the isothermal squeezing of the semi-solid

MIMI Tech GmbH
Preusweg 98, D-52074 Aachen
friedrich@mimi-tech.com

formed phase (Venditti et al. [91]), or with aid of electromagnetic stirring (Murakami et al. [92]). Other research done by Xu et al. [93] investigated numerically, the feasibility of the OCC (Ohno Continuous Crystallizer) process in upgrading aluminum scrap, showing good potential for this technique. Other numerical studies on the OCC method were done by Fashu et al. [94] as well.

All literatures which have been assessed suggest the lower boundary for removal of major eutectic impurities ($k < 1$) to be less than 0.1 wt.%. However, this lower limit was achieved only when low-contaminated scrap (less than 3 wt.% total initial impurity content) was treated.

The Table 20 below summarizes the results and other assessments made for all literature found for the fractional crystallization of aluminum, starting from either scrap or scrap-like aluminum.

Table 20: Average values obtained from the literature sources on the removal efficiency and energy consumption [89], [91], [92], [90], [83], [93].

Category	Impurity Removal Efficiency [Removal rate %]	Impacts on process [Energy consumption [1], kWh/kg]	TRL Range within Literature	Max. treatment capacity
F.C. – Scrap	55.65%	0.7	TRL 2 -7	Up to 24tons/day

[1] when not available, it was calculated based on the additional information available in the source.

4.5.3. Interview Section Analysis

4.5.3.1. Aluminum companies

Some of the interviewed companies are already exploring, at low scale, the utilization of fractional crystallization for the upgrade of scrap. However, no detailed information was given on which scraps are being treated nor any other performance metrics.

SWOT Analysis

The SWOT Analysis (Figure 34) shows that while there are clear strengths and opportunities for this technology, the weakness and threats were the categories that most companies commented on. In the sections below, the main discussion points will be addressed for each category.

MIMI Tech GmbH
Preusweg 98, D-52074 Aachen
friedrich@mimi-tech.com

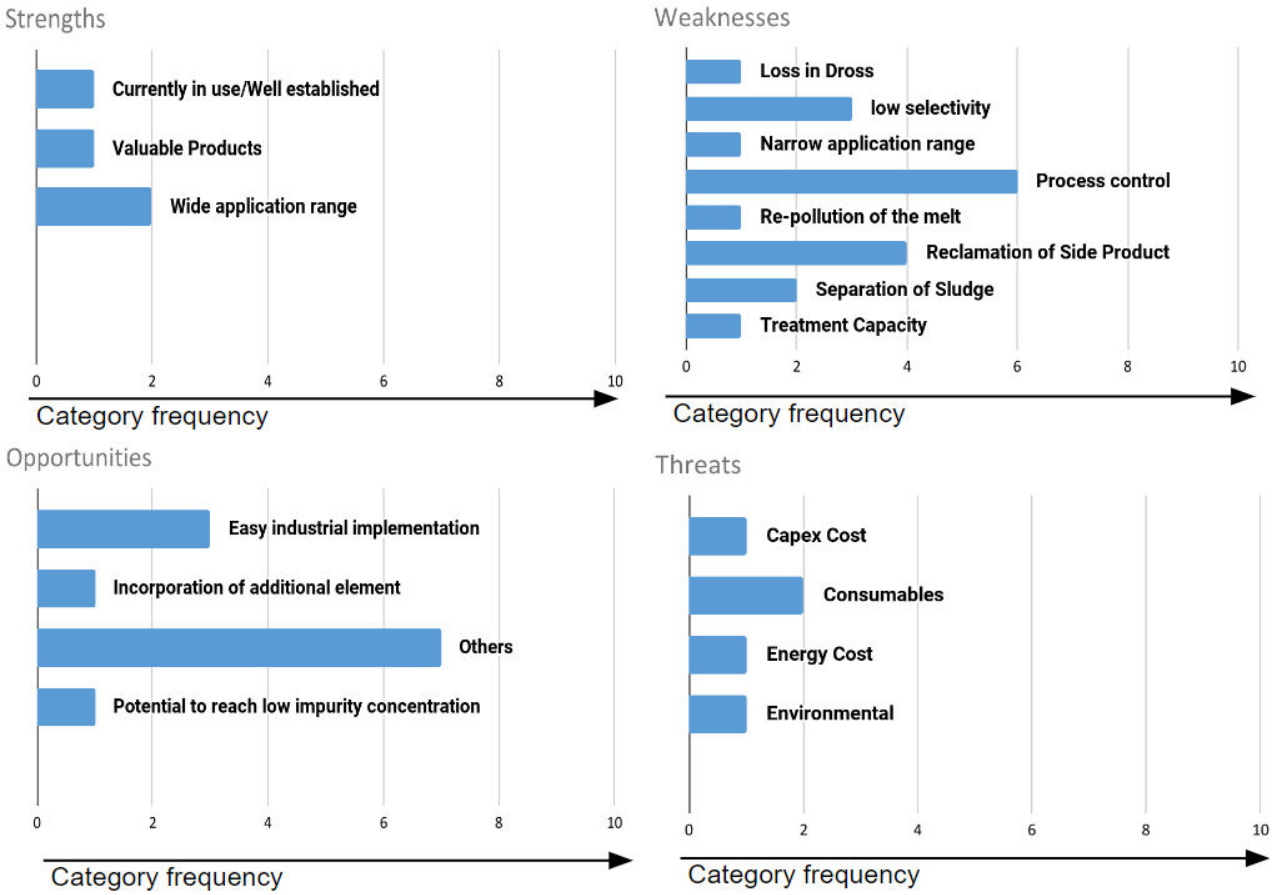

Figure 34 :SWOT Analysis for the fractional crystallization process, applied to scrap purification.

Strengths and Opportunities

This process has been utilized for decades to produce high- and ultra-pure aluminum. Therefore, its implementation, process conditions, etc. are already widely studied and established. Moreover, most common impurities found in aluminum and most of major alloying elements presents in the scraps can be removed from aluminum via the fractional crystallization, having the potential to reduce substantially the impurity concentration of the melt.

In specific examples, such as the one from the Aleris patent [90], it was pointed out that the utilization of copper or zinc-containing scrap as a source of copper or zinc, respectively, could be a way to valorize the purified fraction, offsetting the process cost. This naturally applies only for a very specific product and application range.

Another advantage pointed out by a company that has already used this technology for high purity aluminum production is the low energy required in the process. Since the proper process control requires a very well insulation within the crystallization chamber, very little energy loss occurs. Also, during crystallization, latent heat is released to the melt, further reducing the need for extra energy input.

MIMI Tech GmbH
Preusweg 98, D-52074 Aachen
friedrich@mimi-tech.com

Weakness and Threats

The most concerns expressed during the interviews relates to the residual fraction of metal after the treatment process. The identified weakness of this process concerns the suitable destination and utilization of the impurity-enriched phase and its overall economic impact on the process technical and economic feasibility. Moreover, the low impurity selectivity and the demanding fine process control were also pointed out as weaknesses of this process. Some companies also expressed concerns about the low scalability of this process and losses associated with dross formation during the process.

Following the same direction of the weaknesses, the identified threats were mostly related to the whole process costs, CAPEX, energy consumption, and consumables. The destination of the impurity-rich residual melt was also an identified issue and possible environmental threat.

4.5.4.Technology providers and industry experts interviewed

4.5.4.1. Supplier of metallurgical equipments

One of our interviewees is a Canadian-based company that provides a broad range of cast house equipment. Among them, they have developed a fractional crystallization technology that is used to produce diverse grades of high-purity aluminum, from 3N8 up to 5N2.

Figure 35 : Modular design fractional crystallization equipment.

It consists of a modular batch configuration, in which several units can be run in parallel. Its tailored design provides good flexibility to adapt to the client's volume and purification requirements, being able to treat several tons of aluminum per day. These characteristics make it compatible for the majority of cast houses. According to the company's CEO, the use of their fractional crystallization technology towards recycling is being developed.

In the discussion with another world-renowned supplier of cast-house equipment, the usage of a deep bed filter to filter out the formed pure aluminum crystals was explored. In this concept, the filtered purified crystals would then be heated again after the filtration, letting the purified melt flow out of the furnace.

MIMI Tech GmbH
Preusweg 98, D-52074 Aachen
friedrich@mimi-tech.com

The use of a vortex system to push the particles against the filter was also discussed as a possible option, although it would pose a very challenging control of the melt temperature.

4.5.4.2. Nippon Light Metal Holdings

Nippon Light Metal Holdings shared that it has already developed large experience with the process of fractional crystallization, towards production of high-purity aluminum. The company is also experimenting with the application of fractional crystallization towards upgrading aluminum scrap.

It was pointed out that the utilization of the remaining concentrated portion after purification will be an economic matter. For certain types of scrap, such as 6XXX series, elements like Zn (high distribution coefficient in Al, hence not very efficiently removed) is likely to be an issue for this process.

4.5.4.3. Interview with Aluminum Industry Expert

We have conducted an interview with a retired industry expert, with large experience in developing molten metal manufacturing processes, having many decades of experience within the industry, leading, and participating in many of its developments.

The interviewee shared with us his previous experience with fractional crystallization for upgrading Al scrap. Early investigations (90s – 2000s) showed that fractional crystallization using layer-based processes did have a certain degree of success in the purification of contaminated aluminum. However, the obtained results were much lower than theoretically predicted by the distribution coefficient and phase diagrams.

At that time, it was reported that, to achieve a successful separation at the time, the process had to be repeated many times. In each time, the energy cost of the overall process increases, and the amount of purified aluminum decreases (due to loss of the impure Al-fraction). This all made the overall cost of the purified aluminum via fractional crystallization very high, approaching the values per kilogram of three-layer electrolysis. The same applied to the investigations done with suspension-based fractional crystallization, where similar results were obtained.

4.5.5. Challenges Towards a higher TRL

The fractional crystallization process is an already employed method within the high purity aluminum production. Its utilization as scrap refining has already been tested, and the main issue is the low efficiency of the process when high amounts of impurities are present in the initial material.

This low efficiency is due to the kinetics of this process, in which during the segregation of impurities, they are accumulated within a diffusion layer region at the interface between the solid and liquid phases, reducing the movement of these segregated impurities towards the melt and causing it to be reabsorbed by the moving crystallization interface during the solidification.

This diffusion layer can be partially reduced with the aid of strong convection, hence improving the movement of impurities towards the melt during the crystallization. Another approach is to promote a very slow crystallization, i.e., reducing the solidification rate, allowing enough time for the impurities to move towards the melt. This, however, has an obvious impact on productivity. To counteract this slow crystallization, one approach utilized in the literature was to increase the

MIMI Tech GmbH
Preusweg 98, D-52074 Aachen
friedrich@mimi-tech.com

crystallization area by promoting a “suspension-based” process, where the crystallization occurs at the surface of suspended crystals within the melt, which are later removed from the residual melt using different techniques.

Furthermore, the proper destination of the impurities enriched residual melt was identified as having large importance to the economic feasibility of the process.

MIMI Tech GmbH
Preusweg 98, D-52074 Aachen
friedrich@mimi-tech.com

4.6. Selective Oxidation (Mg)

4.6.1. Literature Results

4.6.1.1. Fundamentals and Principles

Selective oxidation process was developed to remove Mg from aluminium alloys. The behind motivation is to invent a halides-free Mg removal process. The process works based on the affinity difference between impurity elements against Al to oxygen. Although thermodynamic calculations shown in Figure 8 [12] indicates Ca, Sr, Na, K, Li, Sr, Mg may all be possibly removed by selective oxidation method, the literatures found all focused on Mg removal.

The solid oxidants employed include pure SiO_2 oxide and SiO_2-contained minerals such as zeolite which is cheap by cost [95]–[99]. Table 21 lists the types of reported SiO_2-based oxides used for Mg removal and their composition.

Table 21: SiO_2-based oxides used for selective oxidation and their composition [97], [98], [100].

Used oxides	Composition
Quartz	SiO_2 (98 %), Al_2O_3, CaO, Fe_2O_3
Zeolite	SiO_2 (56.09 %), Al-Fe-Mg-K-Ca-Na-O, H_2O
“Shirasu” Mineral	SiO_2 (74 %), Al_2O_3, K_2O, Na_2O, Fe_2O_3, CaO, MgO, TiO_2

Figure 36(a) shows a micrograph of “Shirasu” mineral used by researchers for Mg removal [100]. During selective oxidation process, SiO_2-contained material in powder form was charged into the melt or directly onto the melt surface [99], [100]. Upon contacting SiO_2 particles, Mg in the melt reacts preferentially with SiO_2. Figure 36(b) shows morphology of a partially reacted SiO_2 particle identified in a SiO_2 treated melt. The spinel oxide was observed to form as a shell enclosing the unreacted SiO_2 particle.

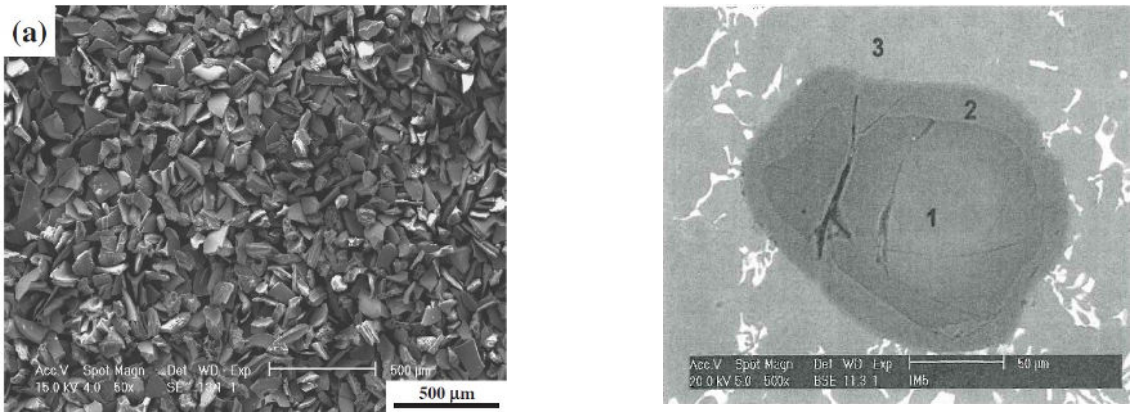

(a) (b)

Figure 36: Micrographs showing: (a) morphology of “Shirasu” mineral; (b) a partially reacted SiO_2, where 1 marks SiO_2, 2 marks $MgAl_2O_4$, 3 marks aluminium alloy matrix. Reproduced from [96], [100].

Different reactive products such as magnesia (MgO) or spinel ($MgAl_2O_4$) can be formed depending on Mg concentration in the melt. The corresponding reactions are given in Equation 10 and Equation 11, [97], [98].

MIMI Tech GmbH
Preusweg 98, D-52074 Aachen
friedrich@mimi-tech.com

$2[Mg]_{Al} + 3Al_{(l)} + 2SiO_{2(s)} \rightarrow MgAl_2O_{4(s)} + 2Si_{(s)}$, ($\Delta G_{750\,°C}$= -424.617 kJ/mol) Equation 10

$2[Mg]_{Al} + 2SiO_{2(s)} \rightarrow 2MgO + [Si]_{Al}$, ($\Delta G_{750\,°C}$= -60.68 kJ/mol) Equation 11

In reported studies, SiO_2 were often incorporated into the melt with the help of inert carrier gas through injection lances [99]. A relevant system is shown in Figure 37. At end of the process, most of the slag particles including reactive products and non-reacted SiO_2-contained particles, due to their poor wettability, are partitioned in the vicinity of the melt surface and bottom of the crucible as dross [97], [100].

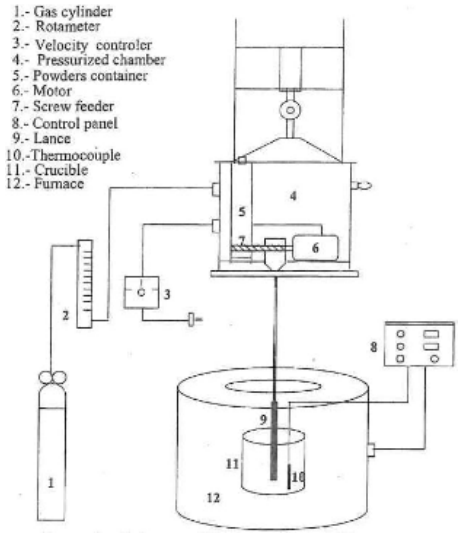

Figure 37: SiO_2 powder injection system. Reproduced from [99].

4.6.1.2. Purification Results

The scale of selective oxidation trials ranges from 8-20 kg and SiO_2 powders were purged together with Ar/N_2 using a lance (Figure 37). The treatment temperature was usually controlled at 750 °C whilst the particle size spans from 63-850 µm. In terms of efficiency, the initial concentration of Mg varied from 1.1-1.6 wt. % and 60 min SiO_2 treatment led to 80-99 % Mg removal [95]–[100]. Figure 38 gives a representative result from Barrera-Méndez et al.[98].

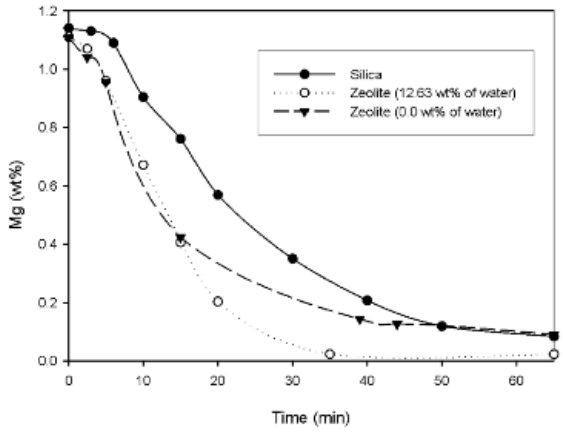

Figure 38: Mg concentration-time curve during application of selective oxidation method in an A322 alloy. Reproduced from [98].

MIMI Tech GmbH
Preusweg 98, D-52074 Aachen
friedrich@mimi-tech.com

There is also one case study where the authors treated Al-5Mg alloy by stirring SiO_2-contained mineral on melt surface. The result is given in Figure 39(a) which shows that within 40 min treatment the Mg content decreased from 4.5 wt. % to ca. 0.1 wt. % [100]. Nevertheless, it is worth noting that Mg removal was realized at the expense of introducing Si into the melt, as is evident in Figure 39(b).

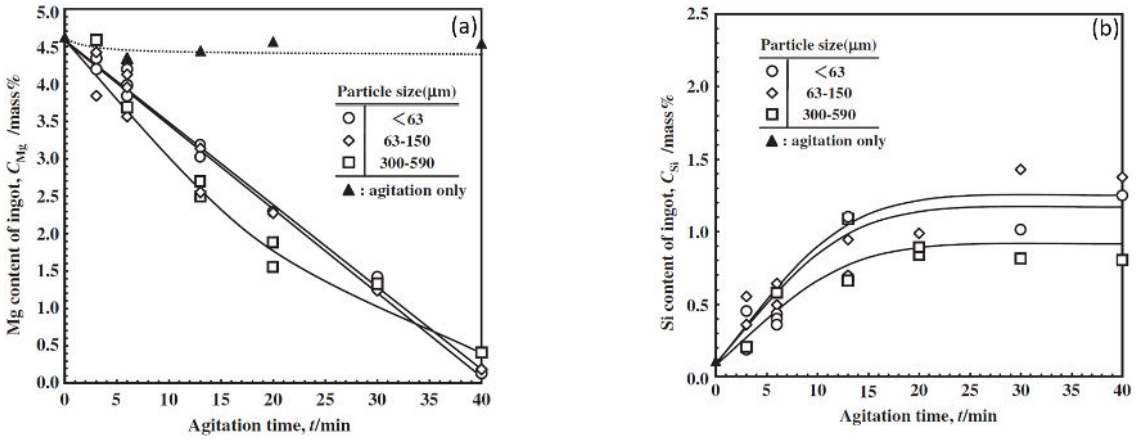

(a) (b)

Figure 39: Variation of Mg/Si content as a function of treatment time during application of selective oxidation method in a 5083 alloy: (a) Mg; (b) Si. Reproduced from [100].

Figure 40 shows result from the only found industrial-scale study. The trials were conducted in a 2500 kg furnace [99]. SiO_2 particles were charged via melt vortex and meanwhile injected into the melt. The removal efficiency was around 60 % within 150 min treatment time. Apparently the removal efficiency and rate was lower than the lab- and demo-scale trials shown in Figure 38 and Figure 39. The reasons may be attributed to insufficient melt stirring which lead to reduced removal kinetics.

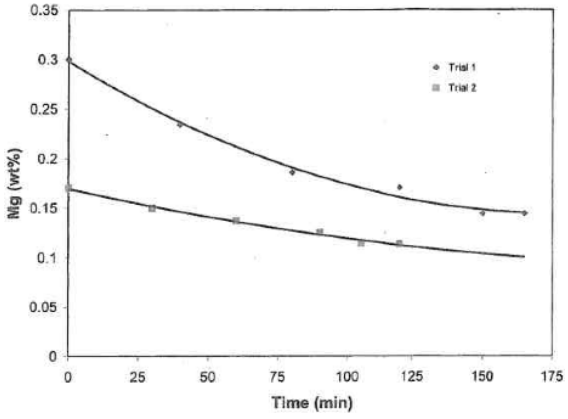

Figure 40: Variation of Mg content as a function of treatment time during application of selective oxidation method. Reproduced from [99].

The Mg removal kinetics were found to be positively related with process temperature and powder injection rate. Fine size powers were favored compared with coarse ones due to high surface to volume ratio. Nevertheless, too fine powders may lead to agglomeration which impedes a high Mg removal rate [96]–[100].

The lower boundary for removal of Mg by application of selective oxidation process is claimed to be less than 10 ppm.

MIMI Tech GmbH
Preusweg 98, D-52074 Aachen
friedrich@mimi-tech.com

4.6.1.3. Side Product and Disadvantages

The main side product of selection oxidation process is dross. Typical phases identified in the dross are $MgAl_2O_4$, MgO, SiO_2, Al, Si. Depending on composition of used SiO_2-contained materials, other phases such as $CaAl_2Si_2O_8$ may also present in the dross [96]–[100].

The disadvantages of selective oxidation include firstly melt contamination. While reducing Mg content in the melt, SiO_2 is reduced to Si which can be dissolved into the treated melt. The Si dissolution may be welcome for cast alloys. However, excessively introduced Si content in wrought alloy melt, can be troublesome [100]. In addition to dissolved impurities, the application of selection oxidation can increase the non-metallic inclusions (NMIs) amount in the melt. Results from Flores et al. [97] suggests up to 2 % inclusions present in the melt after treatment. The high amount of oxides can seriously deteriorate the melt cleanliness quality. Last but not the least, the dross ratio for removal of 1.1 wt. % Mg were reported to be 8 wt. % - 16 wt. % [98]. The high amount of dross generation may make the process economically unfavorable particularly in industrial scale.

4.6.1.4. Summary of Literature Assessment

Table 22: Summary of literature assessment concerning selective oxidation.

Category	Impurity Removal Efficiency [Removal rate %][1)]	Lower Removal Limit	TRL Range within Literature	Max. Treatment Capacity
Selective Oxidation	84.82	< 10 ppm	TRL 4-6	3 ton

1) averaged value from all assessed literatures.

4.6.2. Interview Section Analysis

4.6.2.1. Aluminum Companies

Figure 41 compiles all comments collected from interviews with aluminium companies in a SWOT analysis diagram. The main comments will be presented per two groups, i.e., strength and opportunities group and weakness and threat group.

MIMI Tech GmbH
Preusweg 98, D-52074 Aachen
friedrich@mimi-tech.com

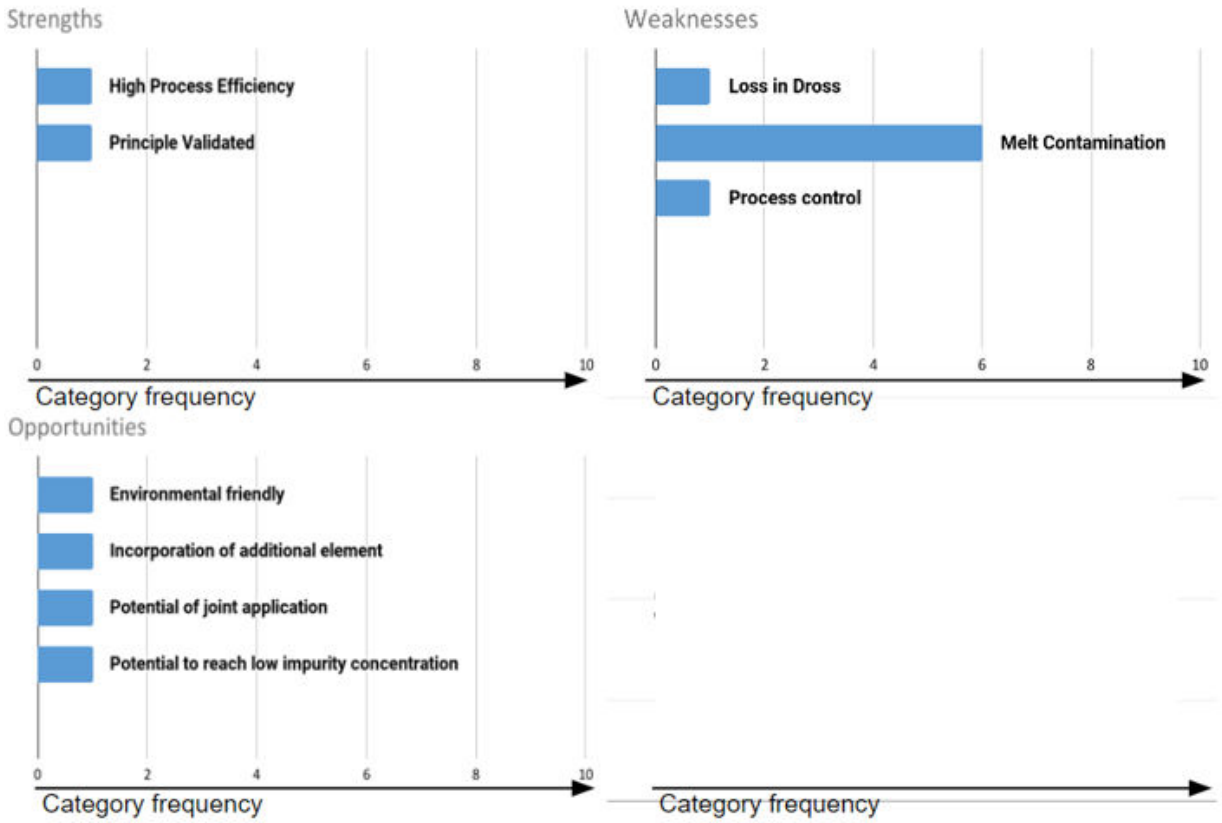

Figure 41: SWOT analysis for the selective oxidation process.

Strengths and Opportunities

The comments on pros of the technique are in general in line with literature findings. The incorporation of additional elements refers to Si hence are related to products (e.g., cast alloys) where Si is an alloying element. It has been commented that the method may find its application jointly with a good inclusion separation method. Besides, it was mentioned that it is worthwhile trying to apply the method in alloys which contain minor amount of Mg impurities in addition to highly Mg contaminated alloys.

Weakness and Threats

The amount of dross was mentioned once by an interviewee who worries about economic feasibility. The most concerned point of the technique was melt contamination with respect to spinel particles and Si element. For wrought alloys, excessive Si amount in the melt may deteriorate product mechanical properties and workability.

4.6.2.2. Techniques Providers

With respect to interviews with techniques providers, few comments were collected, which indicates limited potential seen by technique providers. One of the comments worth mentioning is related to the removal of Mg at a low range. In some aluminium foil products, Mg content needs to be controlled below 70 ppm, often the reduction from 40-20 ppm onwards becomes more and more difficult. Here selective oxidation may find its applications if literature results can be reproduced.

MIMI Tech GmbH
Preusweg 98, D-52074 Aachen
friedrich@mimi-tech.com

Other comments include some plants in China burn off excessive Mg in the melts by holding the melt at elevated temperatures and makes hourly skimming operation. There is also one expert who suggests that instead of removal, it may be wiser to direct alloys scraps with excessive Mg content to the production of alloys where Mg is not an impurity.

4.6.3. Challenges Towards a Higher TRL Process

For alloys with strict restriction of Si content, the application of selection oxidation can be difficult. Therefore, the following consideration is made for alloys whose designation can tolerate Si introduced by silicon oxides.

The main barrier hindering the further development of the selective oxidation process comes not from technical and equipment difficulties. Instead, the main challenge lies in how to control process, i.e., how to minimize introduced inclusions and dross generation ratio. The latter issue can decide the economic feasibility of the process.

MIMI Tech GmbH
Preusweg 98, D-52074 Aachen
friedrich@mimi-tech.com

4.7. Intermetallics Precipitation and Separation (Fe, Mn, Cr, Si, Zn, Mn, Cu, Cr, Ni)

Intermetallics (IMs) precipitation and separation method is one of the most published methods for removal of dissolved impurities, with Fe being the primary focus. Despite cumulative increase of publication numbers in the related field over the last decades, industrial application is rarely seen. The current sub-chapter summarizes the proposed principle of the method and furthermore compiled purification results reported in literatures. In the latter part of this sub-chapter, comments collected through interviews made with aluminium companies and techniques providers are presented. It is hoped the combination of both literature and interview results will depict a complete picture on current status, future opportunities, as well as challenges for final industrial application of the IMs method.

For brevity, Intermetallics (IMs) precipitation and separation method will be named as IMs method hereafter in this sub-chapter.

4.7.1. Literature Results

4.7.1.1. Fundamentals and Principles

The implementation of IMs method consists of two essential steps: 1) precipitation of IM phases in the melt [101]; 2) separation of precipitated IMs [102]. In the following texts, content with respect to IMs precipitation will be introduced first, after which IMs separation methods will be presented per technique category.

Intermetallics Precipitation

Precipitation of IMs plays a critical role in removal of impurities. One needs to make sure that the precipitation occurs ahead of solidification of α-Al. In the meantime, the precipitates must bind richer impurity than the initial impurity content of the melt. Both of the two above requirements limit the alloy series on which the IMs method can be applied, besides they decide which impurity is removable.

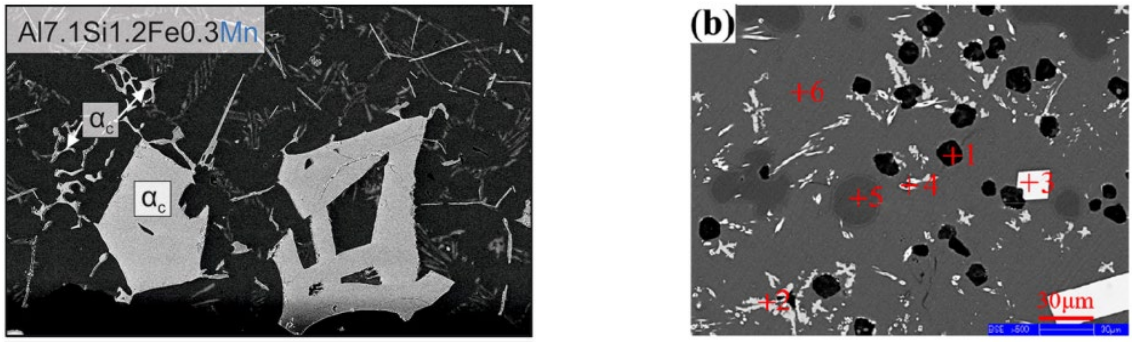

(a) (b)

Figure 42: Morphology of intermetallics: (a) α-Al(FeMn)Si in Al-Si alloy; (b) multiple phases in Al-30Mg alloys, +1: Mg-Si; +2: Fe-Mn-Cr-Cu; +3: Fe-Mn-Al; +4: Mg-Al-Cr-Mn-Fe-Cu-Ni; +5: Al-Mg; +6: Zn-Cu. Reproduced from [101], [103].

Al-Si cast alloys with Si content ranging from 7 to 13 wt. % are among the most researched system, with the articles number accounting for 90 % among assessed literatures for IMs method. In order

MIMI Tech GmbH
Preusweg 98, D-52074 Aachen
friedrich@mimi-tech.com

to precipitate Fe-borne IMs, Mn and Cr are the most common doping elements [102], [104]. Figure 42(a) shows morphology of an α-Al(FeMn)Si phase which is often utilized for Fe removal (vice versa for Mn). The composition of the α-Al(FeMn)Si is given in Table 23, in comparison with the alloy's initial composition. According to mass conservation, by separating such α-Al(FeMn)Si phase from the liquid metal, the Fe and Mn content in the bulk melt can be reduced.

Table 23: Composition of initial melt and precipitated α-Al(FeMn)Si intermetallics in an Al-7Si alloy [101].

Initial Melt Composition (at. %)			Intermetallics Composition (at. %)			
Fe	Mn	Si	Al	Fe	Mn	Si
1.2	0.3	7.1	72.9	9.8	9.7	7.5

Al-Mg alloys are also worth mentioning as another possible system for implementation of IMs method. Two related articles are available with Mg content ranging from 5-30 wt. %. The precipitated intermetallics reported include Φ-$(Al,Si)_{10}(Mn,Fe)$, $Al_6(Mn,Fe)$, Mg-Si, Fe-Mn-Cr-Cu, Mg-Al-Cr-Mn-Fe-Cu-Ni, Zn-Cu phases [103], [105]. Figure 42(b) shows morphology of IMs precipitated in Al-30Mg melt [103].

In exceptional conditions when Fe/Mn content in the melt is well above Al-Fe/Mn binary alloy eutectic point (2-3 wt. %), a highly alloyed melt becomes not necessary for precipitating Fe/Mn-borne IMs [102], [106]. Under such conditions, the precipitation of Fe/Mn-borne phase is relatively easy, and the separation of these phases can lead to Fe/Mn removal as well.

To force intermetallics precipitation, one needs to tailor the melt composition and control the process temperature. For Al-Si alloys, sludge factor (SF) is a useful tool for predicting probability of sludge particle formation. The sludge herein refers to IMs formed before onset of α-Al solidification. Equation 12 gives a well-accepted empirical formula [107], [108]:

$$SF = (\text{wt. \% Fe}) + 2 \times (\text{wt. \% Mn}) + 3 \times (\text{wt. \% Cr}) \qquad \text{Equation 12}$$

A high SF value implies a high probability of IMs formation at a given melt dwelling temperature. According to Equation 12, if formation of Fe-borne IMs is desired at relative high melt process temperature, Mn and Cr elements shall be introduced intentionally. The correlation between sludge factor and temperature (T_l) at which IMs start to precipitate is given in Equation 13 and Equation 14 [107], [108],

$$T_l = (44\ °C \times SF) + 552\ °C \qquad \text{Equation 13}$$

$$T_l = (86.7\ °C \times SF) + 506\ °C \qquad \text{Equation 14}$$

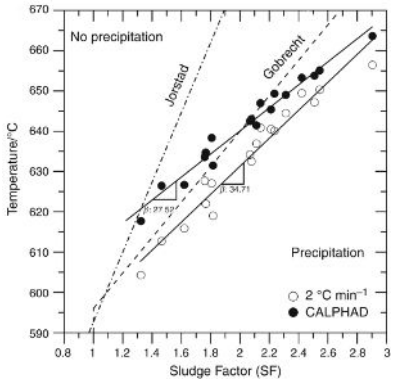

MIMI Tech GmbH
Preusweg 98, D-52074 Aachen
friedrich@mimi-tech.com

Figure 43- Precipitation temperature (T_l) of sludge as a function of a sludge factor. Reproduced from [109].

The plot of above equation is shown in Figure 43 along with results obtained from both calculated phase diagram (CALPHAD) and trials [109].

Figure 43 finds its application in prescribing process window in terms of melt dwelling temperature at a given alloy composition. For instance, in an Al-Si foundry alloy with 1 wt. % Fe and 0.8 wt. % Mn content in the initial melt, the sludge factor is calculated to be 2.6 according to Equation 12. Based on Figure 43 the melt should be held at a temperature lower than ca. 650 °C in order to force precipitation of intermetallics.

Sedimentation

Gravitational sedimentation is one of most easily implemented methods for separating IMs. It works based on density difference between IMs and the melt. Take α-AlFeMnSi phase for example, with a density of 3.58 g/cm^3 [110], [111], once it is formed in a quiescence melt, it will settle downwards, through which way the Fe content in the bulk of the melt is reduced. Figure 44 gives a representative micrograph showing settled α-Al(FeMn)Si phase at based of crucible for an Al-7Si-0.38Fe-0.54Mn melt which was held at 620 °C for 1 hour [112].

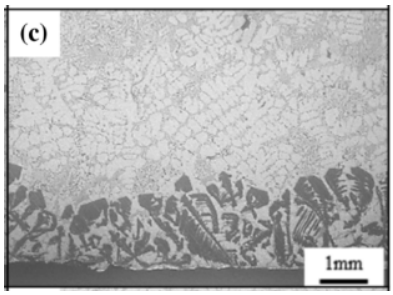

Figure 44: Micrograph showing the settled α-Al(FeMn)Si phase at crucible base. Reproduced from [112].

Centrifugation

Centrifugal separation also works based on density difference between intermetallics (IMs) and melt. IMs with a higher density than aluminium melt are subject to a resultant force directing radially towards the wall region of centrifuge set-up. Because of the high rotation rate, the terminal velocity at which IM move towards the proximity of the wall region can be enhanced significantly with respect to natural gravitation field.

There are three types of centrifugal set-ups which were designed for IM separation. The first one tried to combine centrifugal separation with a solidification process. Given the remelting necessity and low yield of product, this method will not be presented here but the readers are referred to the publication of Matsubara et al. [113] in case of interest. The process more relevant in the context of current study is container-based and rotor-based centrifugal separation equipment, both of which are capable of delivering refined products in melt form.

Figure 45(a) shows snapshots and schematic of a 10 kg-scale container-based centrifuge [103]. On operation, suspended IMs are collected at the periphery region of the container where pores are drilled for melt to pass through. The refined melt expelled from the centrifuge was collected and

MIMI Tech GmbH
Preusweg 98, D-52074 Aachen
friedrich@mimi-tech.com

can be subject to further melt handling process. The other type of centrifugal separation set-up is rotor based and the sketch is shown in Figure 45(b). During high speed rotation, melt with suspended IMs is pumped into the rotor. IMs are collected at the orifice between upper and lower disc. It is worth mentioning that in principle the rotor-based centrifuge can work in a semi-continuous way since it can be lifted and immersed multiple times during batch treatment process.

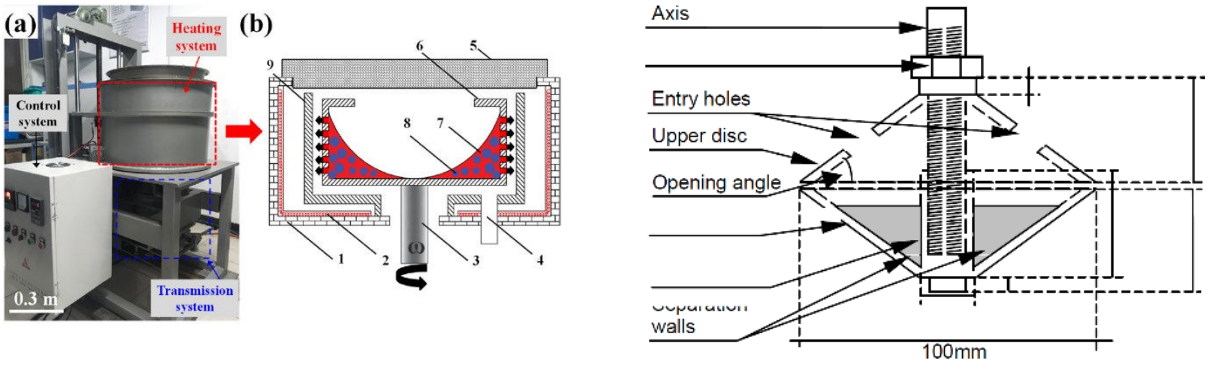

(a) (b)

Figure 45: (a) Container-based centrifugal separation apparatus [103], 1: furnace insulation material; 2: resistance wire; 3: rotation axis; 4: liquid guide pipe; 5: cover; 6: rotary filter cartridge; 7: liquid phase; 8: solid phase; 9: liquid collecting tank. (b) rotor based centrifugal separation unit [102].

Filtration

IMs can also be removed by a filtration process which is usually applied for removal of non-metallic inclusions from aluminium melt. During filtration, IMs which suspend in the melt are captured via deep bed filtration mechanism or a cake filtration mechanism, as is shown in Figure 46 [102].

Figure 46: Polished section of a ceramic foam filter used for collecting intermetallics. Reproduced from [102].

Most of the filtration test was still in laboratory stage, the set-ups constructed were mainly for testing purpose. An example is given in Figure 47 where a ceramic filter was installed in between the two A3 crucibles.

MIMI Tech GmbH
Preusweg 98, D-52074 Aachen
friedrich@mimi-tech.com

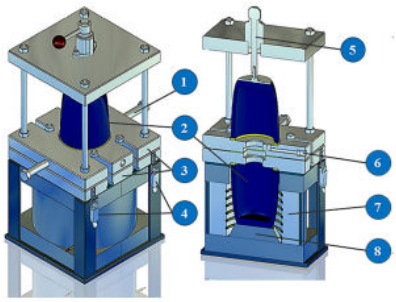

Pos.	Designation of components
1	Pivot bolt: M16 with hexagon head screw (stainless steel)
2	Graphite crucible of form A 3 for 1 kg Aluminum
3	Filter box halves with 240 x 238 x 30 mm (stainless steel)
4	Turnbuckles GN832-55-Ni (stainless steel)
5	Closing lever: Push rod clamp FL-121/45
6	Mounting for screw-in flange M16 DN 16 KF (stainless steel)
7	Heating element: CeraSys™ 1300 with an electric power of 2.1 kW
8	Base-plate of refractory material with dimension of 230 x 228 x 40 mm

Figure 47- Illustration of a laboratory filtration apparatus including component and material designation. Reproduce from [104].

Le Brun et al. [102] conceptualized a forced filtration approach where a mobile filter was driven upside-down to collect IMs. The refined melt was pushed upwards into a SiO_2 tube. As is shown in Figure 48, IMs were pushed towards bottom of the melt upon the forced filtration and hence the impurity partitioning were realized.

Figure 48: laboratory design of forced filtration set-up: (a) snapshot; (b) result of proof-of-concept test. Reproduced from [102].

It should be mentioned that in nearly all filtration trials, the separation process was conducted for melts which have been set dwell for a certain time. The melt holding process allows precipitation of IMs and allows them to settle partially, the latter of which is helpful in terms of reducing the heavy loading of inclusions for filters. However, the pre-conditioning treatment can also increase the overall process time of filtration separation if multi-batches process is not configured.

Electromagnetic (EM) Separation

Electromagnetic (EM) separation works based on the difference of electrical conductivity between intermetallics (IMs) and aluminium melt. When applied or induced EM field is exerted on aluminium melt, IMs having a different electrical conductivity relative to aluminium melt experience a resultant force perpendicular to both of the electrical field and to magnetic field. The resultant force drives the motion of the IMs in such a way that the IMs are enriched (hence the borne impurities) at certain position of the separator/furnace. An illustration of the process principle is shown in Figure 49 [114].

MIMI Tech GmbH
Preusweg 98, D-52074 Aachen
friedrich@mimi-tech.com

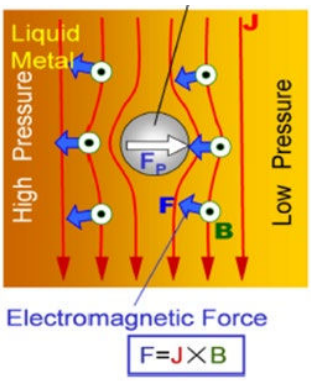

Figure 49: Illustration of intermetallics separation through electromagnetic force. Reproduced based on [114].

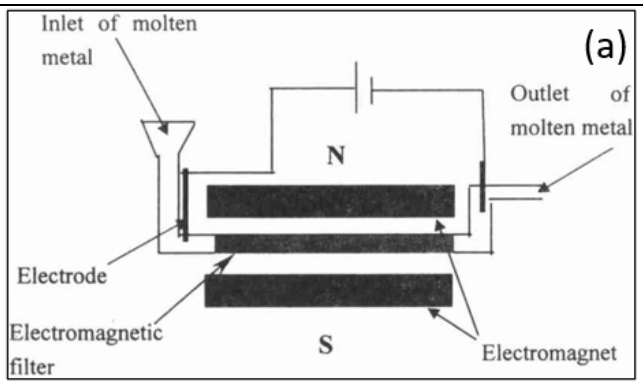

(a)

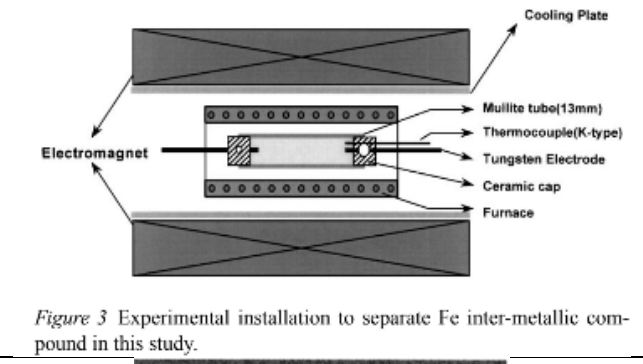

Figure 3 Experimental installation to separate Fe inter-metallic compound in this study.

(b)

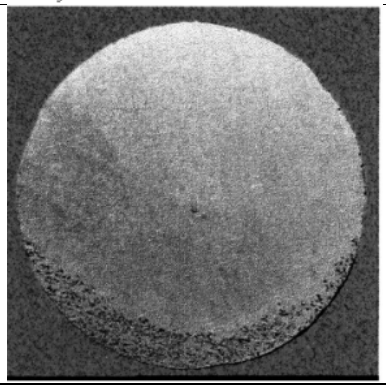

(c)

Figure 50: Electromagnetic separators: (a) in-line set-up [115]; (b) batch-wise set-up [116]; (c) separation results suggested by partitioned IMs, result obtained by using (b) set-up [116].

MIMI Tech GmbH
Preusweg 98, D-52074 Aachen
friedrich@mimi-tech.com

Both batch-wise and in-line EM separators have been tested in laboratories [115], [116]. Figure 50(a) and (b) shows two example separators where applied EM field is utilized for EM separation. Figure 50(c) shows the separation result using the set-up shown in Figure 50(b). It can be seen that IMs phases are partitioned towards lower side of the separator.

Based on proved principles, concepts were proposed for industrial implementation of EM separation [106], [117]. Two of the proposed concepts are given in Figure 51, with the latter one being patented by Cidaut in Spain [117], meaning possibly that a industrial prototype have been developed.

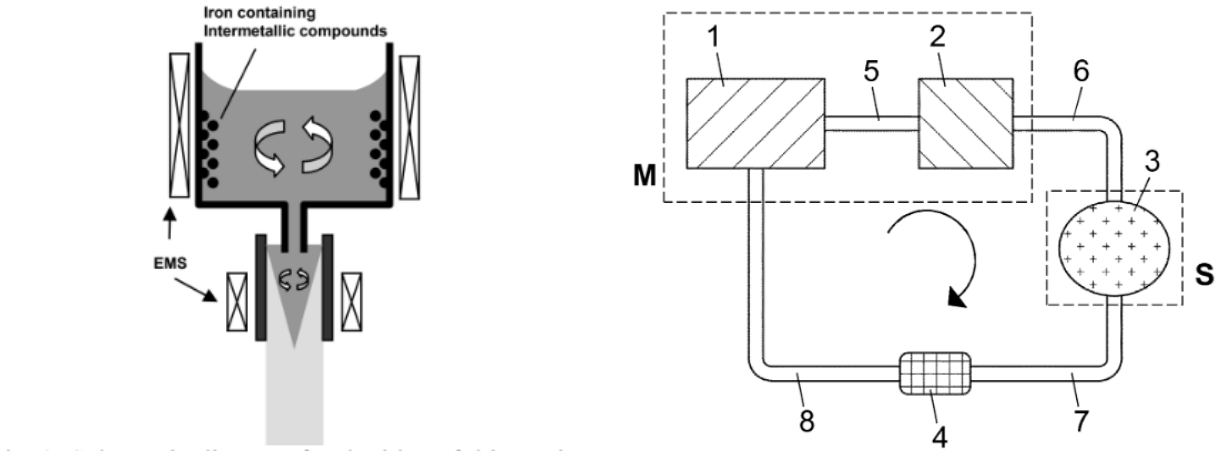

(a) (b)

Figure 51: Concepts were proposed for industrial implementation: (a) inductor induced EM field separation; (b) linear induction pump based separator (3). Reproduced from [106], [117].

Taking a closer look at Figure 51(b), the refining system consists of mainly a holder (2) and an EM separator (3) where the EM field is created by means of linear induction pump. After the melting down of scraps in a melting furnace (1), an independent holding furnace can be used for compositional and temperature control to realize IMs precipitation. The melt discharged from the holding furnace will flow through the EM separator (3), inside which a ceramic reservoir (possibly switchable after certain time) is placed to collect precipitated IMs.

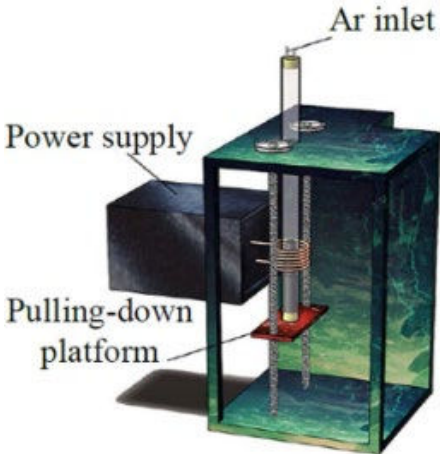

Figure 52: Schematic of intermetallics separation set-up combining electromagnetic separation and directional solidification principles. Reproduced based on [118].

MIMI Tech GmbH
Preusweg 98, D-52074 Aachen
friedrich@mimi-tech.com

Another idea worth mentioning is the combination of EM separation with directional solidification. Bao et al. constructed such a set-up (Figure 52) in their laboratory for a proof of the concept [118]. The main motivation of the investigation was to produce refined Al-Si cast alloys from an Al-55Si-4Fe raw material, (product of carbon electro-thermal reduction). During the process, the pre-conditioned melt was pulled down which allows the cooling and solidification to take place from lower side of the melt. In meantime, induced EM field was applied to provide expulsive force which forced precipitated IMs to move towards bottom of the melt.

Others

Displacement washing concept was proposed by Le Brun et al. for separation and collecting precipitated IMs [102]. A schematic of the washing process is shown in Figure 53. Note that the salt phase is represented by pink color whilst aluminium and IMs phase by blue and black color respectively. Salt compounds (Ba-K-Na based halides) with a higher density relative to aluminium melt were employed as washing liquid. Through intensive agitation at the melt and salt interface where IMs accumulate, the IM precipitates can be collected in the salt phase. The principle of the method has been proved through trials. The method has the advantage of avoiding sludge formation at melt bottom and meanwhile increase aluminium yield.

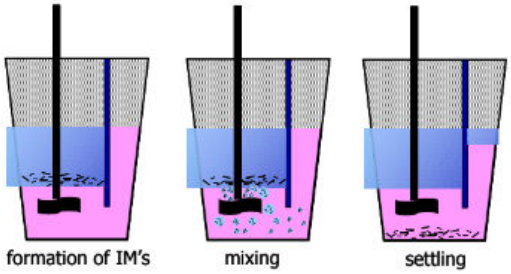

Figure 53: Schematic of intermetallics separation through a displace washing method. Reproduced based on [102].

4.7.1.2. Purification Results

In this section, purification results were grouped by IMs separation methods and introduced separately.

Sedimentation

The scale of sedimentation trials ranges between 0.14-9 kg and the set-up is simply the melting/holding furnace. The treatment temperature was usually controlled at 600-650 °C whilst the process time spans from 30-380 min. Table 24 summarizes the operational parameters for conducting sedimentation separation. In terms of efficiency, the initial concentration of Fe, Mn, Cr varied from 0.56-2.5, 0.29-2.88, 0.014-0.86 wt. % and the removal efficiency varies from 23-83, 48-88, 67-79 %, respectively [101], [102], [112], [119]–[127]. Figure 54 gives a representative result concerning Fe/Mn distribution in the melt after 4 hours of holding time.

MIMI Tech GmbH
Preusweg 98, D-52074 Aachen
friedrich@mimi-tech.com

Table 24: Operational parameters for sedimentation trials [101], [102], [112], [119]–[127].

Alloy	Temperature (°C)	Process Time (min)	Scale (kg)	Set-up
Al-Si Cast alloy, Artificial alloy	600-650	30-380	0.14-9	Melting/Holding Furnace

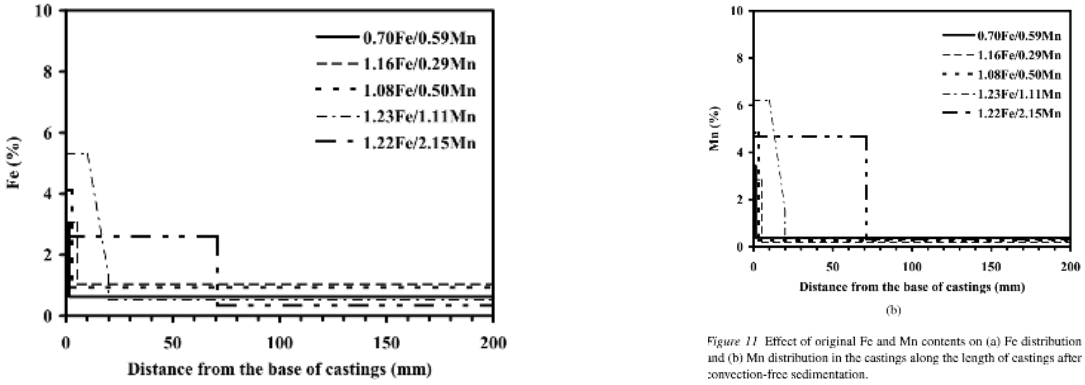

Figure 54: Fe and Mn distribution along the melt depth direction for different Fe and Mn content in an Al-11.5Si melt. Reproduced from [122].

Yield data was not often available from literature. Directly and indirectly, Dhinakar, Zhang, Cao et al. reported 77, 71 and 90 % yield, with correspondingly Fe removal efficiencies of 73.8, 74.5, 57 %, respectively [112], [120], [122] .

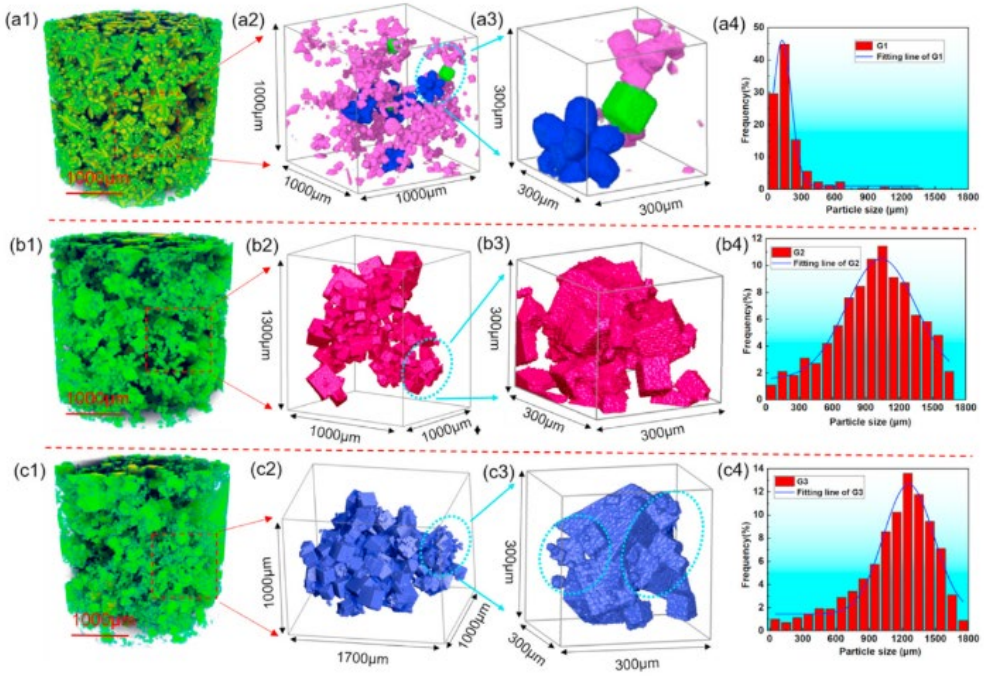

Figure 55: Spatial distribution, local morphology, and size distribution of α-Al(FeMnCr)Si particles and agglomerates under different separation conditions: (a1-4) 80 min holding treatment; (b1-4) 30 min holding-20 min agitation-30 min holding; (c1-4) 30 min holding-20 min agitation&bubbling-30 min holding. Reproduced from [120].

MIMI Tech GmbH
Preusweg 98, D-52074 Aachen
friedrich@mimi-tech.com

During sedimentation separation process, the removal efficiency of certain impurities is influenced by many factors such as initial impurity content, ratio between Fe/Mn or Fe/Cr or Fe/(Mn+Cr) [101], [112], [122]. For a given initial Fe impurity content in the melt, increase Mn/Fe ratio were reported to increase the removal efficiency of Fe, as is already exemplified in Figure 54. Nevertheless the return may diminish at a higher Mn/Fe ratio [122]. Meanwhile higher Mn content may negatively affect the yield (Figure 54). Moreover, if Mn is added externally, excessive Mn remained in the alloy after purification may become an issue [106], [128].

The morphology and size of IMs plays an important role in deciding the separation rate of impurities. In one interesting study from Zhang et al. [120], mechanical stirring and Ar gas purging (6L/min) was conducted as melt conditioning measures to promote the agglomeration of IMs. The effect of melt conditioning on variation of size distribution of IMs is shown in Figure 55. It was found that the removal efficiency of Fe in the conditioned melt was enhanced comparing with reference melt. The purification result is shown in Figure 56,

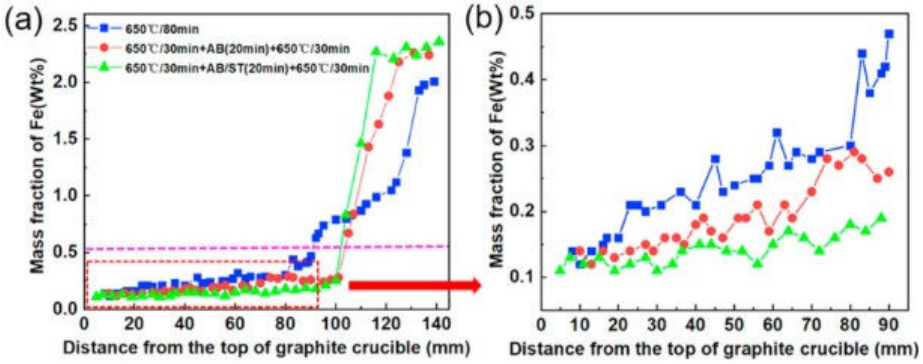

Figure 56: Variation of Fe content along melt depth direction. AB stand for Ar bubbling and ST stands for melt stirring. Reproduced from [120].

Centrifugation

Only two case studies were performed with employment of centrifugal set-ups for impurity removal.

In a series of 50 g-scale trials, Simensen et al. [105] tested Fe and Mn removal in Al-Mg-1Fe-1Mn alloys with Mg content ranging from 0-16 wt. %. The melt was pre-conditioned by holding at 10°C above liquidus of the alloy for 4 hours before centrifugation. The centrifugation was conducted at 1900 rpm. The result is given in Figure 57, showing interestingly that with a 5 wt.% Mg concentration, it is possible to achieve 70 wt.% removal efficiency of Fe and Mn. With further improvement of the Mg content, both Fe and Mn removal efficiency increase. The importance of Mg was attributed by the authors in part to decrease solubility of Fe and Mn in the melt.

MIMI Tech GmbH
Preusweg 98, D-52074 Aachen
friedrich@mimi-tech.com

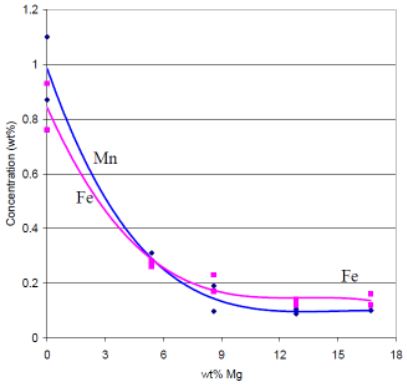

Figure 57: Impurity removal via centrifuge: decrease of Fe and Mn concentration as a function of Mg concentration in the base melt. Melt process temperature 10°C above liquidus of aluminium alloy. Reproduced from [105].

Meng et al. [103] reported another case-study using a 15 g-scale centrifuge where impurities removal from Al-30 wt. Mg alloy melt was tested. The melt was conditioned at from 475-650 °C and subject to centrifugal treatment for one minute with gravity coefficient 600. To minimize melt oxidative loss, protective slag was used to cover the melt. The metallic impurities in the initial melt include Si (1.41 wt.%), Zn (0.297 wt.%), Fe (0.203 wt.%), Mn (0.195 wt.%), Cu (0.114 wt.%), Ni (0.017 wt.%). Figure 58(a) shows the impurities removal efficiency. At 500 °C, the removal efficiency of Fe, Mn, Si, Ni, Cu, Cr, and Zn was respectively 87.4 %, 88.2 %, 73.6 %, 59.1 %, 16.1 %,71.6 %, and 20.6 %. In a 10-kg up-scale trial (set-up shown in Figure 45), the results were reproduced.

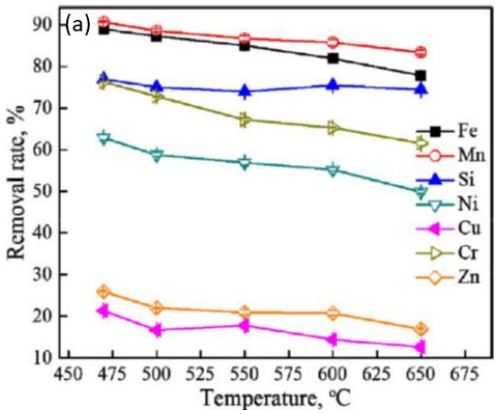

Figure 58: Impurities removal based on intermetallics precipitation method applied in an Al-30 Mg alloy: (a) removal efficiency of different metals; (b) morphology of intermetallics accommodating different impurities, +1: Mg-Si; +2: Fe-Mn-Cr-Cu; +3: Fe-Mn-Al; +4: Mg-Al-Cr-Mn-Fe-Cu-Ni; +5: Al-Mg; +6: Zn-Cu. Reproduced from [103].

Filtration

Filtration separation is often conducted for melt which has been pre-conditioned by a holding process.

The scale of filtration trials ranges between 1.5-100 kg. The treatment temperature was usually controlled at 580-690 °C whilst the process time spans from 30-380 min. Table 25 summarizes the operational parameters for conducting filtration separation. In terms of efficiency, the initial concentration of Fe, Mn, Cr varied from 1-2.5, 1-1.6, 0.28-0.29 wt. % and the removal efficiency

MIMI Tech GmbH
Preusweg 98, D-52074 Aachen
friedrich@mimi-tech.com

varies from 51.3-86.6, 65.5-87.5, 87-88 %, respectively [102], [104], [105], [128]–[130]. Figure 59 gives a representative result from study of Schoss et al. [002] in which a filter box was employed to separate IMs from AlSi9Cu3-Fe(-Mn)(-Cr) alloy. The filtration results in terms of Fe, Mn, Cr, and Cr content reduction is given in Figure 59 [104].

Table 25: Operational parameters for filtration trials [102], [104], [105], [128]–[130].

Alloy	Temperature (°C)	Process Time (min)	Scale (kg)	Set-up
Al-Si Cast Alloy, Al-Mg Alloy	580-690	N.A.	1.5-100	Ceramic Foam Filter, Fabric Filter, etc.

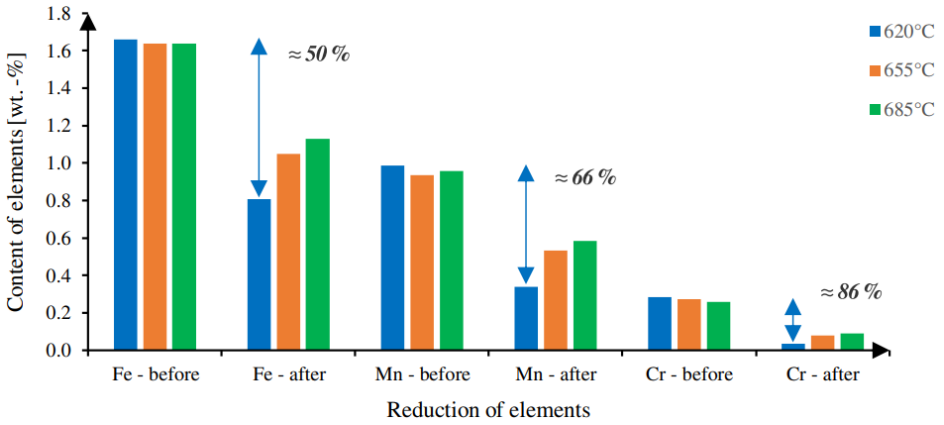

Figure 59: Content of Fe, Mn, Cr in the alloy both at prior- and post-melt filtration status. Reproduce from [104].

The only available yield data was from the 100 kg-scale trial, in which 76 % yield was realized at 78 and 75% removal efficiency of Fe and Mn respectively. The melt was held at 580 °C for 15 min and subject to filtration using a 3*3 mm holes fabric filter.

EM Separation

The scale of EM separation trials ranges between 0.02-5 kg with employment of set-ups including batch-wise type (Figure 50(a)) and in-line EM separator type. The former type set-ups are usually directly a coreless induction furnace. The treatment temperature was usually controlled at 580-690 °C. Table 26 summarizes the operational parameters for conducting filtration separation.

In terms of efficiency, the initial concentration of Fe, Mn varied from 1.1-1.68, 1.2-2.57 wt. %, and the removal efficiency varies from 65.2-76.4, 52.1-85.6 %, respectively [106], [115], [116], [131].

Table 26: Operational parameters for EM separation trials [106], [115], [116], [131].

Alloy	Temperature (°C)	Process Time (min)	Scale (kg)	Set-up
Al-Si Cast Alloy, Al-Mg Alloy	640-690	N.A.	0.02-5	Batch, in-line EM separator

Figure 60 shows purification results with employment of a specially designed EM-involved directional solidification set-up shown Figure 52. Results have suggested that the joint effect of directional solidification and EM separation leads to a successful preparation of Al-11Si-0.4 alloys from an input Al-50Si-4Fe alloy [118].

MIMI Tech GmbH
Preusweg 98, D-52074 Aachen
friedrich@mimi-tech.com

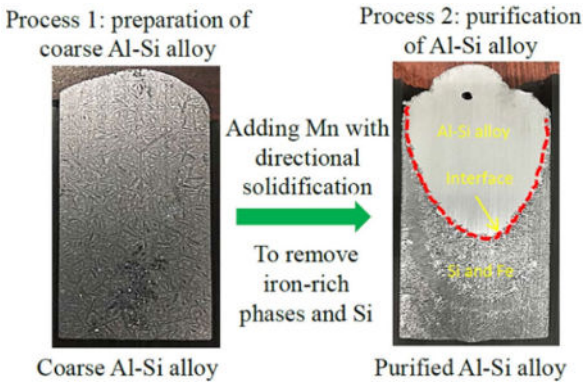

Figure 60: Marco photograph of Al-Si alloy sections: (a) before refining; (b) after EM-assisted directional solidification Refining. Reproduced from [118].

4.7.1.3. Summary of Literature Assessment

Table 27 summarizes the assessments made for all literatures concerning IMs method. Note that for lower removal limit column, results from Al-16/30Mg alloy were excluded. For these two alloys, the lower boundary of Si, Zn, Fe, Mn, Si, Ni, Cu, Cr content achieved via IMs method was respectively 0.3, 2.35, 0.026, 0.023, 0.096, 0.014, 0.007 wt. %.

Table 27: Summary of Literature Assessment Concerning Intermetallics Method.

Category	Impurity Removal Efficiency [Removal rate %][1)]	Lower Removal Limit[2)] (wt. %)	TRL Range within Literature	Max. Treatment Capacity
Intermetallics Method	66.14	Fe-0.14 Mn-0.15 Cr-0.0046	2-6	100 kg

1) averaged value from all assessed literatures.
2) Al-16-30 wt. % Mg purification result not included in the table, given in the above test

4.7.2. Interview Section Analysis

4.7.2.1. Aluminum Companies

Figure 61 compiles all comments collected from interviews with aluminium companies, in a SWOT analysis diagram. In the sections below, the main comments will be presented per two groups, i.e., strength and opportunities group and weakness and threat group.

MIMI Tech GmbH
Preusweg 98, D-52074 Aachen
friedrich@mimi-tech.com

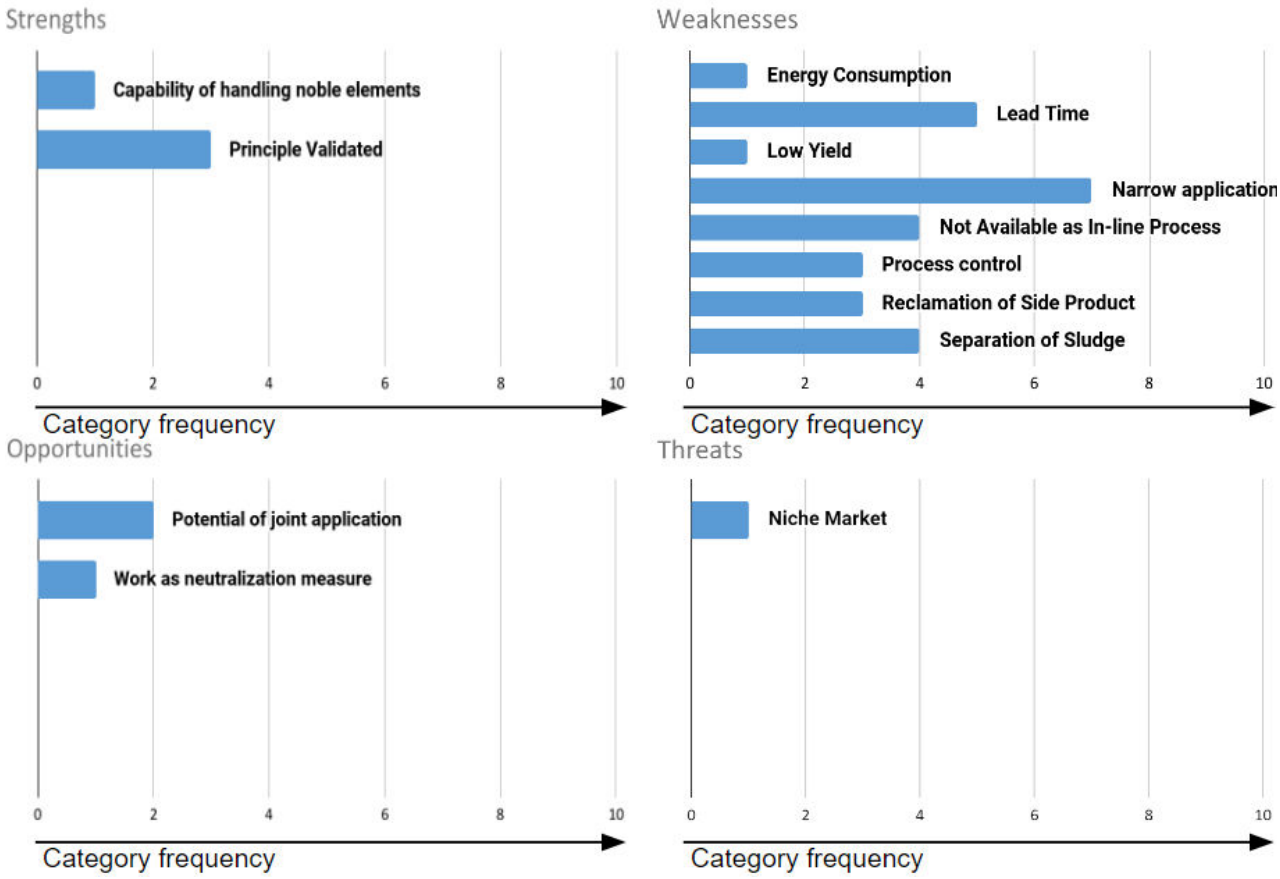

Figure 61: SWOT analysis diagram plotted based on comments from aluminium companies concerning intermetallics method.

Strengths and Opportunities

The main strengths of IMs method were commented as its validated principle and the proved concept for removal of noble elements such as Fe, Mn, and Cr. The opportunities in terms of "potential of joint application" refers to the chances of employing auxiliary set-ups (e.g., electrometric stirrer) to enhances separation kinetics. Another opportunity mentioned was close to the neutralization technique. It was related to trying to precipitate the less harmful type of impurity-borne phases.

Weakness and Threats

The IMs method received many comments falling into weakness category, reflecting the concerns of applying the method in industrial scale. The narrow application range refers to the fact that: 1) currently the removal of Fe/Mn/Cr is only possible for Al-Si/Al-Mg alloy with high content of Si/Mg; 2) the refining test are mainly conducted using melt with high initial content of Fe (0.5-2.5 wt. %), it is not sure lower range of Fe (e.g., 0.15-0.3 wt. %), how well the method will work. Separation of sludge is among another big concerns expressed by the interviewees. To date there has not been any industrial solutions for tackling the IMs which are generated in big amount and size, irrespective of batch-wise and in-line process. The only seemingly "feasible" way is melt holding process (i.e., sedimentation). However, the low melt holding temperature, long lead time and sludge build-up

MIMI Tech GmbH
Preusweg 98, D-52074 Aachen
friedrich@mimi-tech.com

issues hinder application of such separation process in industrial scale furnaces. From economic perspective, the low yield and lack of sound ways for reclaiming values from high amount of IMs additionally retard the industrial-scale implementation.

4.7.2.2. Techniques Providers

Standing from economic perspective, some technique providers are pessimistic on the potential for application of IMs method in the industrial in the near future. The concerns are with regards to low yield, limited value of product, as well as process cost.

However, there are certain number of positive comments received from technique providers during the discussion. Those feedbacks are grouped by IMs separation methods and presented in below. Additionally, during the discussion, neutralization was mentioned in addition to IMs method due to the close relation between the two topics.

Sedimentation

One of the techniques providers mentioned a potential industrial-scale Fe removal process should be able to employ the current equipment. In the best case the process shall be able to be integrated in the current production route. Most of the techniques reported in the literatures, can hardly be industrialized. Sedimentation might be an exception. The said technique provider is now testing the method as a way for IMs separation in up-scaling trials. In their accomplished 3-ton scale trials, Fe was removed from 0.5 to 0.12-0.13 wt. % at an 85 % yield. The process involves steps: 1) addition of Mn elements, 2) conditioning of the melt by intensive stirring, 3) melt holding. After tapping of the refined aluminium, the 15 % sludge was diluted by aluminium (presumably primary) for producing alloys tolerating/favouring high Fe content. It was said the process will in the next step be tested in industrial scale furnaces. Besides, it was conceptualized that melting furnace will be the site where sedimentation separation takes place, and two holding furnaces shall be configured to accept two products namely the refined melt and the high Fe containing melt.

If the sludge can be not directed into production of another alloy as was suggested by above techniques provider, there were solution providers suggesting ways to get rid of IM sediments from floor of the furnace. Siphoning removal is one way worth a try and the other way is related to use of salt flux. By spraying cleaning salt fluxing on the sludge, exothermic reactions can be triggered which turns the IM into ash-like slag. However, in this way the removed IMs may lose their value.

Filtration:

The feasibility of using filters for removal of IMs was also discussed. Some interviewees believed it was not a good idea given the high incoming volume of IMs and their big size, which can easily block the filter. There was also realistic concern if the big size and high-density IM can arrive the filter box without settling during melt transportation in the launder. On the other side, it was brainstormed that chances for a filtration separation process might exist if IM removal can be well distributed within the purification system. In other words, other techniques for IMs removal shall be deployed and orchestrate with filtration. Multi-stage filtration was nominated as a possible way for collect large amount IMs.

MIMI Tech GmbH
Preusweg 98, D-52074 Aachen
friedrich@mimi-tech.com

EM Separation:

EM separation seems not a favorable option according to comments from interviewees given its limited capacity, quick build-up of skull, re-entrainment possibility. However, it was suggested the imposition of external EM field (EM stirring) may play a supportive role in improving the process kinetics (e.g., nucleation, growth of IMs).

Salt-Route and Flotation

Salt-involved route was indicated to be already employed in some plants for IMs removal. The route uses rotary kiln (arc-/gas-driven) as equipment. Salt fluxes including reactive and non-reactive components play dual roles of oxidation avoidance as well as accommodating precipitates.

Degasser was also brainstormed as a possible way to float the IMs out and trap them in the dross layer. The high-density IMs are quoted to have a good potential to be removed in the degasser. The concept has to be tested based on existing knowledge on temperature control and operational parameters of degassing.

Neutralization:

Rapid solidification was mentioned as one of the major approaches for neutralizing the negative effect of Fe. The process works by controlling the Fe-precipitates size and making it a strengthen-phase rather than a harmful one. Processes nominated include high-speed roll casting, 3D printing, and selective laser melting (SLM). Japan was quoted to devote many efforts on high speed roll casting, but it is still very much in research status meanwhile the target Fe level may still be low compared with normal Fe content secondary melt. Both 3D printing and SLM may not consume massive amounts of scrap for market reasons. The interviewees stressed that rapid solidification is not easy to implement particularly in industrial scale.

Development of new alloys which tolerate high Fe content is on the way. Ongoing laboratory research works mentioned include: 1) designing pressure casting aluminium composition which can tolerate more than 0.15 wt. % Fe; 2) development of 6xxx based cross over alloy product with 1-2 wt. % Fe content. It was stressed the alloy development is a comprehensive process hence it may take a long time. It requires design of alloy composition, heat treatment, working process. Property and robustness test will also be indispensable for any commercial alloy product.

Cheap rare earth metals were said to have possibilities to neutralize the harmful IM phases. Conventional heat treatment such as homogenization was commented to help increase the toleration of Fe contamination but only to a limited extent (0.25-0.35 wt. %). It was also commented by one of the interviewees that the control of oxide films in the melt helps reduce negative effect of IMs.

Others

There was one techniques provider planning to look at the properties of sludge via fundamental research and evaluate the possibilities to use sludge as a product. Nevertheless, the research, quote from the interviewee, is quite at the beginning and the specific definition of target is yet to be announced.

MIMI Tech GmbH
Preusweg 98, D-52074 Aachen
friedrich@mimi-tech.com

4.7.3. Challenges towards a Higher TRL Process

Based on assessment of literatures and interview results with aluminium companies, the intermetallics separation methods are evaluated respectively in terms of challenges for Higher TRL. The results are compiled in Table 28.

Table 28- Current TRL level and challenges for higher TRL concerning IMs method.

Method	Current TRL Level	Special Challenges for Higher TRL	Common Challenges for Higher TRL
Sedimentation	3-5	Sludge build-up, lead time	High Si/Mg necessary Low Process Temp. High Amount of IMs;
Centrifugation	4-5	Implementation, cost	
Filtration	4-5	Clogging	
EM Separation	3-6	Capacity, Sludge build-up, cost	

MIMI Tech GmbH
Preusweg 98, D-52074 Aachen
friedrich@mimi-tech.com

4.8. Vacuum distillation (Zn, Mg, Pb, Ca, Na, In, Li)

4.8.1. Fundamentals and Principles

Vacuum distillation technology has a successful history in selectively separating base metals from their impurity elements. Purification of aluminium by vacuum distillation exploits the vapor pressure difference of liquid aluminium and its accompanying impurities. When aluminium is melted at low pressure and high temperature, two distinct phases are formed: a liquid phase and a gas phase. The gas phase obtained is then collected in a condenser inside the furnace chamber. This condenser provides the necessary temperature gradient to deposition the elements directly from the gas phase into liquid or solid form [132], [133].

For binary Al-Me systems (where Me is any impurity element dispersed in the aluminium matrix), the vacuum distillation principle accounts for the difference in concentration of the two elements between the gas phase and the liquid phase. In other words, there is a difference in the amount of aluminium and/or impurities between the gas phase and the liquid phase. When the impurity concentration is higher than the aluminium concentration in the gas phase, the impurities can be collected in the condenser. Due to the conservation of mass in the system, the remaining liquid phase contains less impurities and the melt is purified. On the other hand, if the content of aluminium is higher than that of impurities in the gas phase, more aluminium can be condensed and collected as purified metal fractions, leaving impurities in the residual melt [71].

Combining Raoult's Law with Dalton's Law, for an ideal mixing behavior, and assuming the simultaneous existence of an ideal liquid and an ideal vapor in a vacuum distillation system, the Equation 15 and Equation 16 describe the relationship between the element's concentrations in the gas and liquid phases and the saturated vapor pressure and total system pressure.

$$Y_{Me} \cdot P = P_{M^*e} \cdot x_{Me} \cdot \gamma_{Me} \qquad \text{Equation 15}$$

$$y_{Al} \cdot P = P_{A^*l} \cdot x_{Al} \cdot \gamma_{Al} \qquad \text{Equation 16}$$

where, x is the mole fraction of the components (for Al and for the impurity elements) in the liquid phase; y is the mole fraction of the components in the vapor phase, P is the system pressure, P∗ is the saturated vapor pressure of the components, and γ is the activity coefficient of the components in the liquid phase. By dividing Equation 15 by Equation 16, the system pressure P can be dismissed as seen in Equation 17 below.

$$\frac{\gamma_{Me}}{\gamma_{Al}} = \beta_{Me} * \frac{x_{Me}}{x_{Al}} \qquad \text{Equation 17}$$

The separation coefficients for any individual impurities in aluminium can be calculated using saturated vapor pressure and activity coefficients, which can be found in literature and thermodynamic databases [134]–[136]. Table 29 below shows the beta coefficients at 1000°C for some common impurities present in aluminium, in which the thermodynamic data (γ values for infinitely diluted impurities) are available in the literature.

When the β coefficient is greater than 1 (in bold at Table below), the impurities present in aluminium are preferably concentrated in the gas phase. If the impurities have a coefficient lower than 1, they

MIMI Tech GmbH
Preusweg 98, D-52074 Aachen
friedrich@mimi-tech.com

are preferentially retained in the liquid phase. In some cases, where the impurity has a β coefficient close to 1, they cannot be effectively separated from the aluminium. It is also important to consider the kinetic aspect of this process. In practice, good separation is seen for impurities with β higher than 10^5, such as the case for Mg, Zn, and Pb.

Table 29: Separation coefficients (β) of impurities in aluminium at 1000°C, calculated with the values from the databases in [134]–[136].

Elements	β	Elements	β
Cr	1.45×10^{-4}	Ni	1.79×10^{-7}
Cu	1.04×10^{-2}	Pb	5.99×10^{5}
Fe	7.18×10^{-5}	Si	1.02×10^{-5}
In	1.79×10^{3}	**Sn**	**4.12**
Ga	**5.92**	Th	3.26×10^{-15}
Mg	2.79×10^{5}	V	2.98×10^{-7}
Mn	1.10×10^{1}	Zn	1.30×10^{8}

4.8.2. Results from the literature review

4.8.2.1. Treatment of aluminum scrap

The distillation of volatile elements from a melt by means of vacuum is a widely utilized technique in many metallurgical companies. Yet, its utilization within the aluminum industry is not very common. This is because of the very high temperature and very low pressure needed to promote the volatilization of aluminum main impurities. However, two key elements present in certain aluminum alloys, Mg and Zn, can be easily removed via vacuum distillation. The literature concerned the vacuum distillation of impurities from aluminum covers mostly these two elements, showing the best combination of setup design and process conditions for the efficient separation of Mg and Zn from an aluminium melt [137].

Murphy et al. [138] presented in the 1993 TMS Conference his works on the removal of Mg and Zn from Al scrap. The results from alloy trials were slightly different than the ones obtained from binary synthetic alloys. His finding shows that the interactions between other present elements within the alloy influence the overall effectiveness of the process [138]. In a scenario where heavily contaminated mixed alloy scrap is present, the process of vacuum distillation may be affected by all other competing impurities, as they will inhibit the process kinetics.

Another study made by Ohtaki et al. [139] focuses on the removal of Zn from Al. His work focused on the utilization of melt stirring to achieve an increase in the removal of Zn, requiring less vacuum and temperature to achieve the same result as without stirring. He also stated that higher crucible diameter (surface area) also increases Zn removal. The same applies to lower melt height [139]. All his findings support the fact that, being a Kinect process, the volatilization of an element can only take place in the interface between the melt and the atmosphere. By stirring, creating a large surface area, and reducing the melt height, the likelihood that the targeted impurity reaches the melt surface and goes into the vapor phase increases.

MIMI Tech GmbH
Preusweg 98, D-52074 Aachen
friedrich@mimi-tech.com

Wei et al.[140] investigated, at very low-scale trials, the main process parameters of vacuum distillation (temperature, time, and vacuum level) on the effectiveness of the removal of zinc from aluminum. Starting from a zinc content of over 12 wt.%, they were able to reduce the Zn in aluminum down to 0.3% at a process temperature of 750°C for 30 min, at a vacuum level of around 10^{-1} mbar [140].

Gotenbruck et al. [141] investigated the two-step distillation of aluminum. In the first step, the volatile impurities were distilled from aluminum. At the second step, aluminum was distilled from the Al-melt containing impurities. While both processing steps worked, the second step required a much higher temperature (~1500°C) and 10^{-1} mbar vacuum. This high temperature ultimately caused problems regarding the crucible material (graphite) compatibility with the aluminum melt and vapor high temperatures, causing the undesired formation of carbides [141]. Nevertheless, the distillation was successful, and a small amount of high purity aluminum could be produced from 2N8 aluminum.

All literatures which have been assessed suggest the lower boundary for removal of impurities to be less than 0.1 wt.%. However, this lower limit was achieved only when low-contaminated scrap (around 3 wt.% total initial impurity content) was treated.

Table 30: Summary of Literature Assessment Concerning Vacuum Distillation.

Category	Impurity Removal Efficiency [Removal rate %]	Impacts on process [Energy consumption [1], kWh/kg]	TRL Range within Literature	Max. treatment capacity
Vacuum Distillation – Scrap	94.55%	3.5	TRL 4	Up to 0.7ton/day

[1]when not available, it was estimated based on the additional information available in the source, such as holding time, temperature, etc. The estimations were based on a simplified heat balance using specific heat capacity and latent heat of fusion for Al as well as correction coefficients to compensate for the heat losses occurring during the process through the furnace wall and melt surface.

4.8.3. Interview Section Analysis

4.8.3.1. Aluminum companies

The utilization of vacuum distillation to remove dissolved elements from an aluminum melt is not currently employed within the aluminum industry. However, this technology finds application in a variety of metallurgical industries with a high degree of maturity and know-how. Such expertise can be applied to the aluminum industry, enabling the removal of certain elements from specific scrap input streams. In Figure 62 below, the SWOT analysis made within the interview with the Aluminum companies is shown.

MIMI Tech GmbH
Preusweg 98, D-52074 Aachen
friedrich@mimi-tech.com

SWOT Analysis

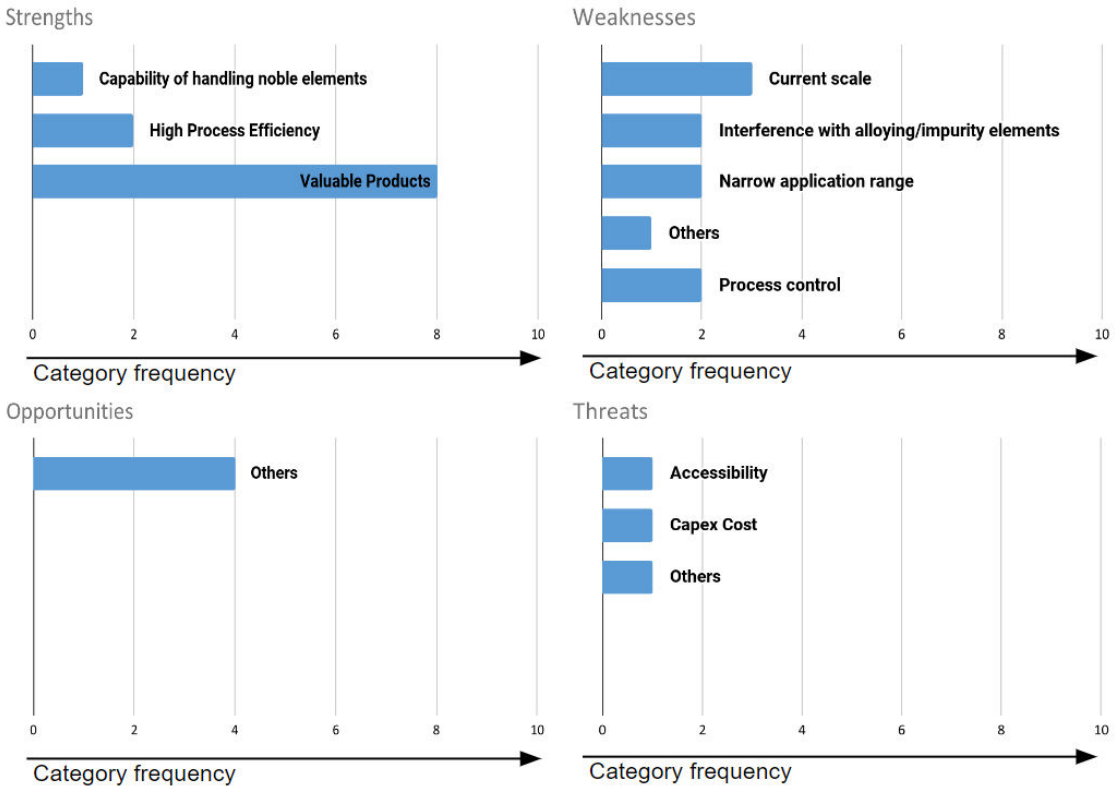

Figure 62:SWOT Analysis for the vacuum distillation process, applied to scrap purification.

Strengths and Opportunities

One of the biggest strengths identified for the usage of vacuum distillation is the conservation of the distilled fraction, i.e., the elements can be extracted in their metallic form, without oxidizing nor losing them at any form. Given that vacuum distillation is suitable for removing magnesium and zinc, the sale or reutilization of both these high value commodities can help to offset the overall cost of the process.

Additionally, the high efficiency of the process and the ability to reach very low levels of impurities from a highly contaminated melt was pointed out as a strong characteristic of this process. This becomes especially important for a class of products that requires very low amounts of a particular element in its alloy composition.

The utilization of vacuum distillation by other metallurgical industries was also identified as a strength, as the process know-how, equipment design and manufacturing experience can be obtained or be inspired from what is available in the market.

Weakness and Threats

The main weakness was the low TRL 4 scale for the application in Al. Furthermore, the shown interference of additional impurities on the process effectiveness was also considered a drawback of this process, making it only suitable for treating specific melt alloys, narrowing its application range. Additionally, the tight process control required to properly distill the impurities is something that was also identified as a weakness.

MIMI Tech GmbH
Preusweg 98, D-52074 Aachen
friedrich@mimi-tech.com

The biggest threat identified is related to the engineering requirements necessary to cool-down the condenser within the vacuum distillation setup. For safety reasons, the use of a water-cooled configuration is ruled out, giving air cooling one of the only options available. This limits the cooling efficiency and may require an elaborate engineering solution. Another issue is the vacuum tightness required from the equipment. This may come as a very problematic point in large-scale applications.

4.8.3.2. Technology providers and industry experts interviewed

Chinese Research Center for Vacuum Metallurgy

This interviewee has a long tradition in the vacuum distillation process within many industries, including aluminum. In the interview section with the head of the research institute and his team, several examples were shown for the distillation of volatiles elements from aluminum.

A large focus of his research group is in recovering valuable elements from Al scrap. Elements such as Mg, Li, and Zn can be economically recovered from selected aluminum scraps containing high amounts of these elements. Since such types of alloys (7075, Al-Li, etc.) consist of a high purity alloy, made mostly with primary grade components, the aluminum fraction obtained from it is very pure as well.

4.8.4. Challenges Towards a higher TRL

The removal of impurities with the utilization of vacuum technology is already mature in many metallurgical industries. From the technical point of view, the application of this technology for the aluminum industry requires an engineering development in the condenser system to comply with the strict safety requirements, and the development of a continuous- or semi-continuous system to allow for its integration within the production chain.

Also, the targeted element limitations of this technology make it only suitable for specific applications, where the specific impurities level need to be very low, and dilution with primary is not a competitive/available solution. Also, the recycling of highly alloyed products containing, for example large, amounts of Mg and Li could be an option to avoid losing too much of these expensive alloying elements during the remelting of scrap. In this example, the recovered metallic Li or Mg could be added back to the alloy at a later stage.

MIMI Tech GmbH
Preusweg 98, D-52074 Aachen
friedrich@mimi-tech.com

4.9. Gross Process

4.9.1. Fundamentals

The Gross process, also known as subchloride process, was developed by Alcan, and extensively studied as a possible replacement for the Hall-Héroult process. In this process, the aluminum chloride (AlCl3) reacts with aluminum metal at high temperatures (1300°C) to form volatile mono- or subchloride of aluminum [142], [143]. When the subchloride is cooled down, the reaction is reversed, and aluminum chloride and aluminum metal is formed in a highly exothermic reaction (see Equation 18) [144].

$AlCl_3 + 2\ Al \leftrightarrow 3\ AlCl$ Equation 18

This process was originally developed to extract aluminum metal from an alloy obtained from the reduction of impure bauxite ore [144]. This reduced metallic alloy consists of aluminium with large portions of silicon, and relatively high amounts of iron and titanium [142], [144].

In the reactor, the aluminum alloy undergoes treatment with gaseous aluminum trichloride at an elevated temperature. During this process, the reaction (Equation 1) predominantly proceeds in the forward direction, resulting in the formation of gaseous aluminum monochloride (AlCl). The produced AlCl, along with some unreacted tri-chloride, then flows into the condenser. Within the condenser, the gas is cooled, leading to the occurrence of the reverse reaction, from right to left. As a result, aluminum metal is deposited, while the tri-chloride vapor is either condensed separately at a lower temperature or recirculated [143].

Under very specific process conditions, the accompanying elements, i.e., impurities present in the alloy like iron, silicon, titanium, manganese, and others do not undergo significant distillation. As a result, it becomes possible to obtain a highly pure aluminum deposit. However, for most conditions, some elements (when present in sufficient amounts in the alloy) may distil and contaminate the product as these elements are in the right conditions, sufficiently strong reducing agents, having significant activity in the crude alloy to partially reduce the aluminum tri-chloride according to the following reaction shown in Equation 19 [143].

$M + AlCl_3 \rightarrow MCl_2 + AlCl$ Equation 19

The impurities chlorides are deposited together with aluminum when the gases are cooled down. To avoid this issue, a temperature gradient can be induced within the cooling chamber, so that the condensation becomes selective as each metal chloride reduces at a specific temperature range [143].

4.9.2. Energy requirements

The energy requirements described in Table 31 were obtained by Little et. Al from Alcan [142], where an energy balance was defined for the Alcan sub-chloride method. It is noted that the refining operations consume only a portion of the total energy requirements, with the majority being required by the carbothermic reduction of the raw materials. The total energy consumption – higher than conventional Hall-Héroult process- were, according to Little et al. [142], the underlying reason Alcan abandoned this process.

MIMI Tech GmbH
Preusweg 98, D-52074 Aachen
friedrich@mimi-tech.com

Table 31: Energy requirements for the Alcan sub-chloride method [142].

Process step	Energy consumption [kWh/kg]
Reduction	-
Sintering	0.09
Coking	0.02
Furnace	14.06
Auxiliary	0.07
Distribution	0.14
Refining	-
Operations & losses	4.71
Total	19.09

4.9.3. Similar applications of sub-chloride method in the Refining and Recycling of Al-containing alloys.

The patent authored by Pedersen et al. [145] details a method for purifying impure aluminum through the utilization of an extractant molten salt. This process involves passing the molten salt over aluminum alloys or mixtures contaminated with other elements. The impure aluminum is exposed to a molten salt mixture containing an aluminum halide, leading to a selective reaction with the aluminum in the impure material. As a result, a soluble aluminum compound is formed within the molten salt mixture. Subsequently, the molten salt mixture, containing the aluminum compound, is separated from the raw material, and its temperature is reduced. This reduction in temperature causes the formation and separation of aluminum metal from the molten salt mixture. An overview of the process is depicted in Figure 63.

This refining process offers the advantage of producing pure aluminum without requiring expensive distillation equipment or high vacuum conditions. It can be carried out under normal atmospheric pressure or even slightly elevated pressure. While aluminum chloride ($AlCl_3$) is the preferred aluminum halide, other options like aluminum fluoride, bromide, or iodide can also be used. The effectiveness of the process relies on two key factors:

1) The molten salt mixture should have a high concentration of aluminum halide to maximize the conversion rate.
2) The salt melt should possess the lowest possible vapor pressure at the operating temperature.

Salt melts composed solely of pure AlF_3, $AlCl_3$, or $AlBr_3$ are unsuitable due to the high pressures required to maintain the aluminum halide in a liquid state at the process temperatures. However, a salt melt consisting of pure AlI_3 can be kept in a liquid state with a relatively moderate overpressure at the process temperature.

Among the various salt melt options, the $AlCl_3$-NaCl system, particularly in a 1:1 molar ratio, has been preferred. This choice is justified by the stability of the complex $(AlCl_4)$-, which leads to a low vapor pressure for the $AlCl_3$.NaCl combination. For instance, while $AlCl_3$ sublimes at 180 °C, the partial pressure of $AlCl_3$ above the $AlCl_3$.NaCl combination is only 150 mmHg at 70 °C.

The specific temperatures employed in the process depend on the choice of halides and the equipment used. As a general guideline, temperatures between 400°C and 1100°C are typically

MIMI Tech GmbH
Preusweg 98, D-52074 Aachen
friedrich@mimi-tech.com

utilized for the formation of aluminum sub-halide from the reaction between aluminum tri-halide in the melt and aluminum metal in the raw material. The temperature for decomposing the formed aluminum sub-halide must be lower than the temperature employed in the initial step.

It has been demonstrated that the reaction proceeds more efficiently when the raw materials are in a molten state. Therefore, it is preferable to melt the raw materials before introducing them into the extraction chamber or lixiviation zone.

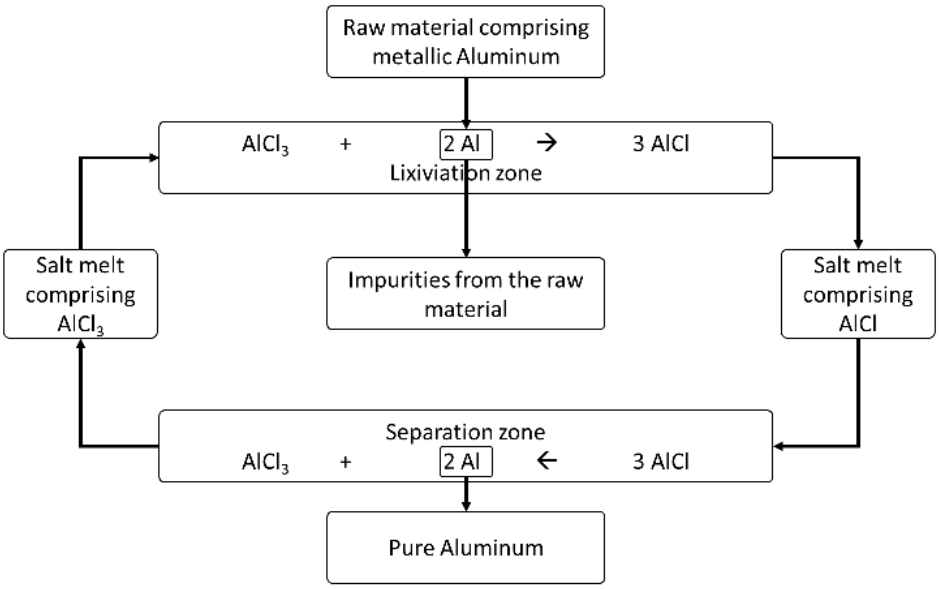

Figure 63: Subchloride method for continuous Aluminum alloy refining according to the Patent from Pedersen et.al [145].

4.10. Other Processes

4.10.1. Pulsed current

Pulsed current method was reported by Sun et al. [146] as a new method being able to remove Fe impurities. The principle of the method is illustrated in Figure 64.

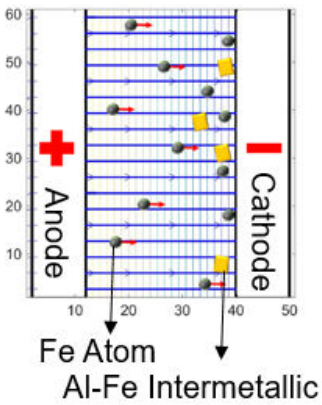

Figure 64: Principles of Fe removal through the pulsed current method. Reproduced from Sun et al. [146].

MIMI Tech GmbH
Preusweg 98, D-52074 Aachen
friedrich@mimi-tech.com

When two electrodes are inserted into aluminium melt with pulsed AC current (200 Hz, 200A) passed through, the Fe atoms were claimed to diffuse and move directionally toward the cathode under the action of electromigration. The partitioning of Fe atom was said to be driven by the difference in the effective charge number between Al and Fe. The trials were run at a 500 g scale with the set-up sketch and sampling procedures provided in Figure 65.

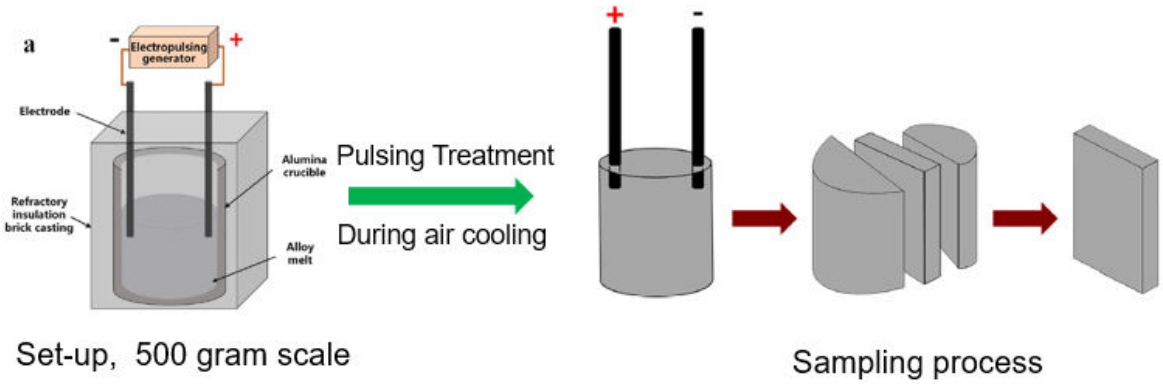

Figure 65: Sketch of set-up and sampling procedures. Reproduced from Sun et al. [146].

The purification effect was evaluated through Scanning Electron Microscopy-Electron Dispersive Spectrum (SEM-EDS) and image analysis, as is shown in Figure 66. It can be seen that at the anode side, Fe was reduced from 2 wt. % to 1.43 wt. %. Many Al-Fe phases can be observed near the cathode. During the pulsed current treatment process, the migration of Fe resulted in a gradual increase in the concentration of iron atoms near the cathode. Upon reaching the solubility limit near the cathode, Al-Fe IMS precipitates.

Before evaluating the potential of the pulsed current method, more studies are needed to validate fundamentally the proposed electromigration principle. Besides, the effectiveness of the method in treating alloys with low Fe content needs also to be assessed.

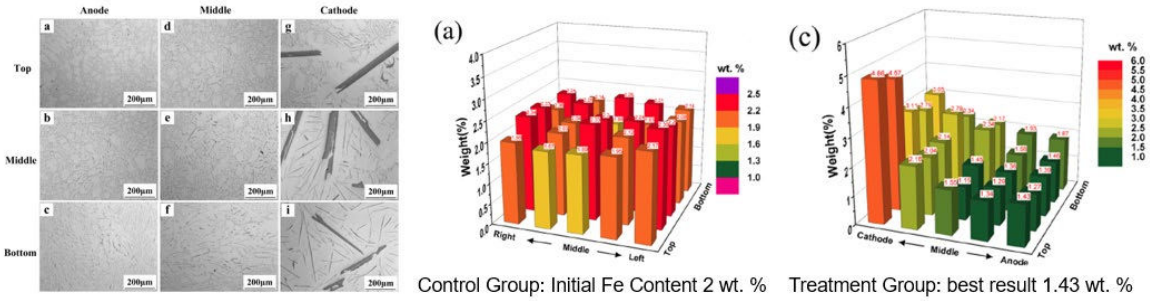

Figure 66: Evaluation of purification results upon application of pulsed current method. Reproduced from Sun et al. [146].

4.10.2. Sulfur Treatment

Fan et al. tested usage of gaseous sulfur for Fe removal. In an 1 kg-scale trials, 30 min purging at melt temperature 750 °C led to an Fe removal from 1.22 to 0.85. The addition rate of sulfur is 3 wt. %. It was proposed FeS formation and flotation are responsible for the Fe removal (Figure 67).

MIMI Tech GmbH
Preusweg 98, D-52074 Aachen
friedrich@mimi-tech.com

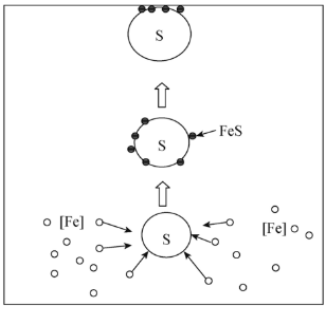

Figure 67: Schematic diagram describing sulfur purification process. Reproduced from Sun et al.[147]

4.10.3. Super Gravity Segregation

Super gravity segregation was reported being capable for removing impurities namely Si, Cu, Mg, Zn, Mn, and Fe. The process is schematically shown in Figure 68. It can be seen that there are two steps for running super gravity segregation. The first step is called semi-solid conditioning, in which the alloy is heated to induce liquification at grain boundary. Through the conditioning, the impurity elements diffused into the intergranular liquid, the inter-dendritic fluid that accumulates a large amount of impurity elements. The second step is the true separation process. By imposing a strong centrifugal field, the liquid migrates along the direction of super gravity field and is collected as filtrate shown in Figure 68(b).

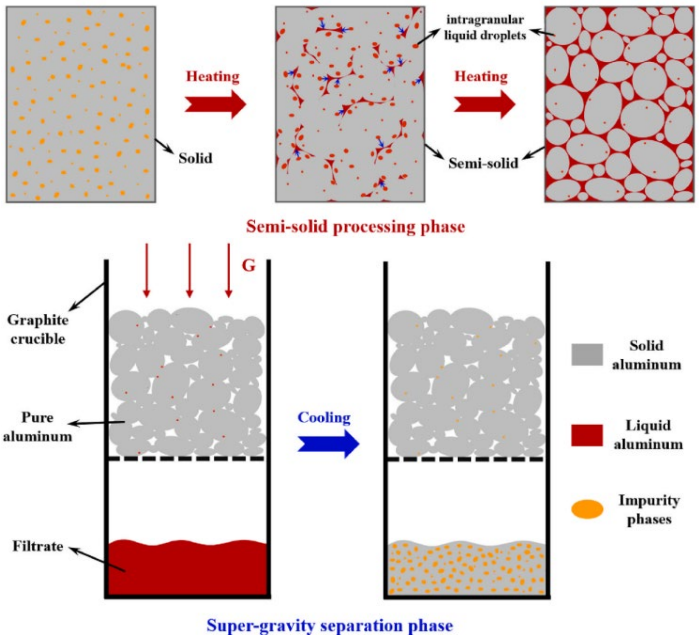

(a)

(b)

Figure 68: Schematic diagram of the super gravity segregation process: (a) semi-solid conditioning; (b) super-gravity separation. Reproduced from Sun et al.[148]

Sun et al. applied super gravity segregation for refining 6061 alloy scraps which contains 0.56 % Si, 0.35 % Cu, 0.88 % Mg, 0.21 % Zn, 0.12 % Mn, 0.95 % Fe. The trials were run at only 30 g-scale. The melt was conditioned at 640 °C for 15 min and then subject to centrifugation. 99.3 % pure aluminium was obtained was obtained as product with a corresponding 82 % yield. The product is shown in Figure 69(a) and (b).

MIMI Tech GmbH
Preusweg 98, D-52074 Aachen
friedrich@mimi-tech.com

(a) (b)

Figure 69: Purified aluminium alloys: (a) polished sections; (b) collected aluminium particles. Reproduced from Sun et al.[148].

In another trial conducted by Zhao et al.[149], the authors studied Fe and Si removal from commercial pure (CP) aluminium. The scale of the trial was 1 kg. The semi-solid conditioning step was skipped and replaced by a simultaneous process of solidification and centrifugation. The collective removal efficiency realized for both elements was reported to be 43%.

MIMI Tech GmbH
Preusweg 98, D-52074 Aachen
friedrich@mimi-tech.com

4.11. Comparison of Identified Removal Technologies and Recommendations

4.11.1. Technology Readiness Level (TRL)

The TRL level identified for each removal technology can be seen in Figure 70 below. In the same figure, information with respect to the largest scale of implementation for each technology was also provided. Technologies identified as TRL 7-9 are the currently employed technologies within most cast-houses such as Gas Purging (TRL 9), Salt fluxing (TRL 9), and Boron Treatment (TRL 9), which performs very well for a limited number of impurities present in the aluminum. The suspension-based Fractional Crystallization and the Three-layer Electrolysis technologies were considered to be at a TRL 7 level for the application of scrap refining, despite being currently used at industrial level within high-purity aluminum production. Hence, their TRL level increase path is mostly business-dependent rather than technological dependent. Nevertheless, to our knowledge, it hasn't been proven in operational environment yet, and the reported studies only demonstrated it in prototype/pilot scale.

Within the range of TRL 4-6, the Layer-based Fractional Crystallization (TRL 6) of aluminum scrap is still in laboratory stages of development, despite being widely used for the industrial production of high purity aluminum. The Selective Oxidation (TRL 6) and Intermetallics method (TRL 6) have reported or claimed to be tested in pilot-scale (3 ton), with certain removal efficiency realized. The Vacuum distillation of aluminum scrap (TRL 4) was only reported to have achieved success in laboratory environment, at very low scale.

Some identified technologies showed promising results but are still in early development stages, hence they were categorized as being within TRL 1-3 level. The Solid-state Electrolysis applied for aluminum scrap (TRL 3) is to-date only reported within a small scale experimental setup, with no detailed results nor performance disclosed to date. The same applies to the Multi-capillary Electrolysis (TRL 3), which showed, even though still in small laboratory scale, a large potential to solve one of the critical aspects of energy cost from the Three-layer electrolysis. Another variant of Fractional Crystallization, so-called Ohno Continuous Crystallizer (TRL 2) has only been reported within a preliminary development stage, mostly simulation based. In an even lower TRL scale, there was a newly method reported be able to remove Fe through application of pulsed electric current to the melt (TRL 1).

The largest scale of technology implementation varies from laboratory to industrial-scale, the changes are in line with TRL evaluation for each technology.

MIMI Tech GmbH
Preusweg 98, D-52074 Aachen
friedrich@mimi-tech.com

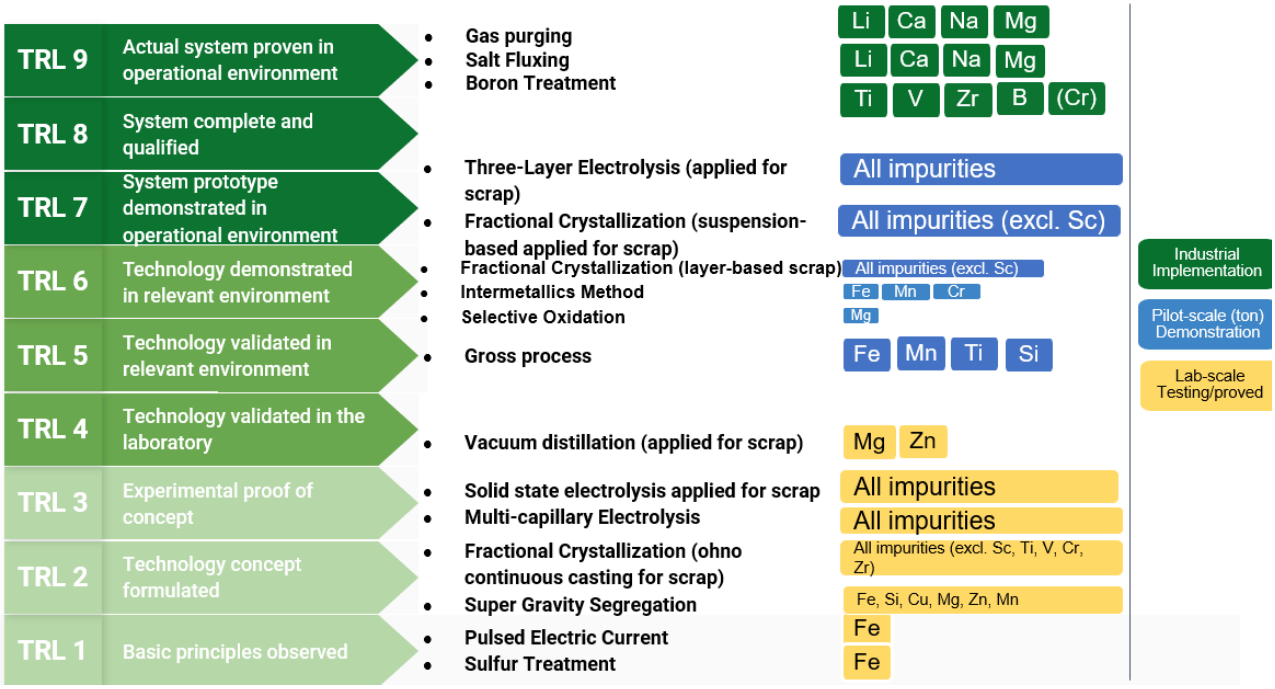

Figure 70: Summary of TRL levels for all assessed removal technologies. When TRL for a technology varies in a range from article to article, the highest level was taken.

4.11.2. Comparison of the Removal Technologies

Figure 71 below shows a qualitative comparison of the identified technologies with at least TRL 4. As there are not enough details to predict its impact on cost, investment, capacity, and performance, only a qualitative estimation was made for most technologies, especially for the ones with low TRL level. In some cases, where even the necessary data for these estimations were not available, this information was not included in the chart below.

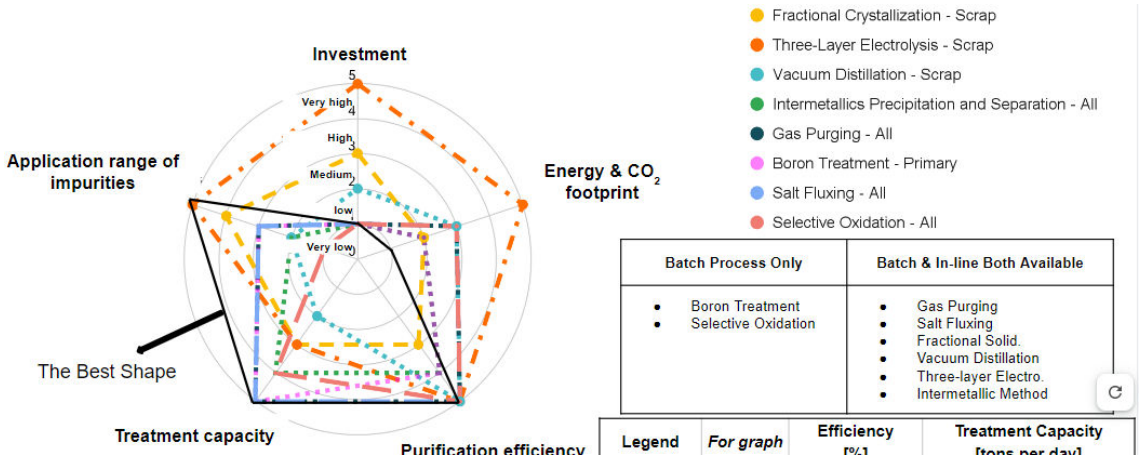

Batch Process Only	Batch & In-line Both Available
• Boron Treatment • Selective Oxidation	• Gas Purging • Salt Fluxing • Fractional Solid. • Vacuum Distillation • Three-layer Electro. • Intermetallic Method

Legend	*For graph*	Efficiency [%]	Treatment Capacity [tons per day]
Very low	1	0 - 10	< 0.1
Low	2	10 - 30	0.1 - 5
Medium	3	31 - 60	5 - 20
High	4	61 - 75	20 - 100
Very High	5	> 75	> 100

Figure 71: Qualitative comparison of the main investigated technologies (TRL 4–9).

MIMI Tech GmbH
Preusweg 98, D-52074 Aachen
friedrich@mimi-tech.com

Energy Consumption (CO_2 footprint)

The heating, melting, and holding time at specific temperatures are the main drivers of energy consumption (related to CO_2 footprint) in all processes. Furthermore, electrolysis processes such as the Three-layer electrolysis have a large additional demand for energy, and it consumes the most among all processes investigated. The main developments and research related to Three-layer Electrolysis is to reduce its energy consumption by decreasing the voltage drop in the electrolyte. However, the current state of this technology still places it as the highest energy consumer. Fractional Crystallization and Vacuum Distillation have much lower energy consumption, mostly associated with the holding time at near melting point for fractional crystallization, and at around 800°C for the vacuum distillation. Given that a very good insulation and temperature control is essential for an efficient segregation of impurities during Fractional Crystallization, it is also expected a lower energy consumption. The energy consumption for intermetallics method is made qualitatively for sedimentation separation process. As only melt holding is necessary, the energy consumption is estimated to be low. The same applies for boron treatment process. With regards to salt fluxing, gas purging, selective oxidation, as melt stirring needs additional mechanical power and leads to heat loss, the energy consumption is estimated to be medium.

Treatment capacity

When comparing the treatment capacity of the identified technologies, Salt Fluxing, Boron Treatment and Gas Purging have the highest proven treatment capacity, as they are currently utilized in most cast-houses. Both the Three-layer Electrolysis and the Fractional Crystallization have a reported capacity of around 20 tons per day. However, any of these technologies can be allocated in parallel, allowing for a much larger capacity. Both Intermetallics Method and Selective Oxidation were reported/claimed to be tested in ton-scale trials. With a lower reported treatment capacity, Vacuum Distillation is very difficult to scale up, as the process requires a large surface-volume ratio, which makes it not feasible for larger batch sizes.

Investment

The investment required for most of the identified technologies is relatively low. As most of them can be implemented within existing equipment in cast houses. Exception to that is the Three-Layer Electrolysis, Fractional Crystallization and Vacuum Distillation. The first requires large infrastructure investments in the electrolysis cells and all related power distribution systems. Fractional Crystallization and Vacuum distillation require specific furnace designs, and vacuum systems for the case of Vacuum distillations.

Application range

The application range of Three-layer electrolysis and Fractional Crystallization is the highest among the identified technologies, making it a very robust process to treat a variety of scrap types. However, unlike the Three-layer electrolysis, Fractional Crystallization has a limitation on the overall quantity of impurities present in the melt, where large amounts of impurities will decrease the process efficiency.

The initial solute concentration has two main effects on the fractional crystallization: The first is the increased likelihood of moving from a planar/cellular growth behavior (seen at low solute

MIMI Tech GmbH
Preusweg 98, D-52074 Aachen
friedrich@mimi-tech.com

concentration) to a dendritic growth at higher concentrations. This is illustrated by Equation 9 describing supercooling in dependence of initial solute concentration (C0). This phenomenon eventually causes the entrapment of solute between the dendritic arms, making it more difficult to be properly expelled into the bulk melt. The second and complementary explanation is based on the stagnant film theory explored by Burton, Prim, and Slichter (BPS) (see Equation 8) where, during the crystallization, a static layer of segregated impurities is formed at the solid-liquid interface and can only move to the bulk melt by diffusion. The effect of forming this layer is that the value of C0 becomes then equal to the solute concentration within layer, directly affecting the purification results. This theory explains the sudden drop in the removal factor at higher initial solute concentrations, where an over-saturation of impurities at the growth front must have occurred, creating a much bigger layer of impurities ahead of the solidification front.

In practice, this could be solved by reducing the growth rate and/or increasing the mass flow (higher rotation rate in the cooled finger) at the growth front. These measures would firstly allow the increase in the available time for the impurities to diffuse before the region solidifies, and secondly, the promoted mixing would contribute to the forced reduction in the diffusion layer thickness and facilitating the move of the impurities to the bulk melt.

The amount of impurities present in the melt is less of a technological issue for the Three-layer electrolysis, in which it was reported to have successfully processed highly contaminated scraps, yielding primary-quality aluminum output. All other technologies are highly selective. The Vacuum distillation is only suitable for a few impurities, such as Mg and Zn. While Boron Treatment can remove impurities such as Ti, V, Cr, B, (Zr). Gas Purging and salt fluxing can effectively remove alkalis and alkaline earth methods such as Mg, Ca, Na, Li. Intermetallics Method, are capable for removal of Fe, Mn, and Cr in alloys containing high content of Si/Mg element. In alloys with extremely high content of Mg (e.g., Al-30 Mg) it is able to remove Si, Zn, Mn, Cu, Cr, Ni in addition.

MIMI Tech GmbH
Preusweg 98, D-52074 Aachen
friedrich@mimi-tech.com

4.11.3. Recommendations

This section aims to provide technical recommendations to the utilization and development of each technology identified for a set of particular scenarios, as described below.

4.11.3.1. Scenario A: Highly contaminated mixed scrap

In this scenario, an input stream of highly contaminated scrap (10 wt. % +), e.g., Zorba, Taint Tabor, or any other heterogeneously sourced mixed scrap is considered.

For this scenario, the most effective and robust technical solutions, among all the technologies identified, are the electrolysis (e.g., Three-layer Electrolysis) and the sub-halide process (E.g., Gross Process). Both of them have been used to treat highly contaminated sources of raw materials, at TRL 7 (Three-layer Electrolysis) and TRL 5 (Gross process).

Within electrolysis, the main constraint is the energy consumption and capex involved. Some activities from industry and from academia have been made to tackle these constraints. From Industry, Alcoa patented a modification to the traditional Three-layer Electrolysis, bringing the electrodes closer to each other inside the electrolyte layer. This has - according to Alcoa's patent – greatly reduced the energy needed to refine the aluminum scrap. From academia, further study needs to be made to improve the electrolysis cell design and process parameters. One example is the approach given by Yasinskiy et. al. (IME Institute / RWTH Aachen University), which holds promising prospects to replace the whole electrolyte layer by a single porous ceramic barrier. This is reported to reduce the energy needed to transport the Al ions from one side to the other of the electrolysis cell.

4.11.3.2. Scenario B: Low contaminated mixed scrap

In this scenario, an input stream of low contaminated source (maximum 3 wt. % total impurity content) is considered.

For this scenario, fractional crystallization may present itself as an optimum solution. Despite not being able to economically remove high amounts of impurities from the initial material, it can remove almost all eutectic impurities present in aluminum, according to the distribution coefficient shown in Table 8 Since most of available Al-based investigations on fractional crystallization relates to the production of ultra-pure aluminum, it is recommended to further investigate the interaction between different impurities at higher concentrations, especially for impurities and/or alloying elements affecting the grain size and morphology of the crystal structure. Any breakdown of the growth structure during solidification will influence the effectiveness of the purification via fractional crystallization.

4.11.3.3. Scenario C: Ultra-low contaminated in scrap

In this scenario, an input stream of dilute-trace contaminated source (maximum 100 ppm) is considered.

-Mg

MIMI Tech GmbH
Preusweg 98, D-52074 Aachen
friedrich@mimi-tech.com

For melt containing dilute concentration of Mg, selective oxidation provides a sound way for removal of Mg. The technical implementation in industrial environment can be readily achieved via adaption of available equipment such as flux injectors. What needs to be tested on research project basis is the melt contamination in terms of Si and oxide particles. Experimental-based research may help to define appropriate addition rate of silica powders and process parameters, both of which is closely related with Mg removal kinetics and will decide the competence of selective oxidation method in comparison to halide-involved methods.

-Ti, V, Zr, Cr

For melt containing dilute concentration of transition metals, boron treatment offers a TRL 9 solution which is established already in the industry. The driven force for future optimization of the process is: 1) to increase removal kinetics; 2) to solve the sludge build-up issues in the furnace bottom. Similarly to IMs method, melt stirring in combination with holding may be worth trying for enhancing removal kinetics. Flotation process on the other hand may provide a possible option which may reduce partitioning of borides particles at bottom of the furnace. Research efforts are certainly needed if process optimization is desired.

-Si

Salt fluxing was mentioned by one of the techniques providers, quote as under serious discussions for removal of Si in dilute concentration. More information is not available for the time being. From research perspective the development of such process may needs combined efforts of thermodynamic definition and experimental validation.

4.11.3.4. Scenario D: Volatile impurities contaminated scrap (Low-medium)

In this scenario, an input stream of low to medium contaminated (around 3 wt.% total Zn, Mg, or any other volatile impurity) is considered.

For this scenario, the vacuum distillation process may be the best alternative, as it can effectively remove volatile impurities from the aluminum melt, while keeping them still recoverable in metallic state. For the impurities Zn and Mg, specifically, the technologies of electrolysis and fractional crystallization have particularly low efficiencies with these impurities. In the case of electrolysis, the Mg is accumulated within the electrolyte layer, and Zn is volatilized by the higher temperature involved in the process. For the fractional crystallization, Zn has one of the highest distribution coefficients among the eutectic impurities, hence its removal efficiency is lower compared to the other elements. These characteristics described above means that for a scenario where Zn and Mg (e.g. 7XXX scrap recycling/contamination occurs), vacuum distillation might be the optimum solution. However, the maturity of this technology for aluminum is still not fully developed, as it is for other metallic systems and industries. Hence, further experimental feasibility studies need to be done, including the further development of equipment design and the corresponding validation to allow for a continuous or semi-continuous distillation process.

4.11.3.5. Scenario E: Noble impurities (against Al) contaminated scrap (Low-medium)

In this scenario, an input stream of low-medium contaminated source (maximum 3 wt. % Fe, Mn, Cr) is considered.

MIMI Tech GmbH
Preusweg 98, D-52074 Aachen
friedrich@mimi-tech.com

Intermetallics (IMs) precipitation and separation, as a TRL 6 technology offers a technically feasible solution for removal of Fe, Mn, Cr without decreasing other alloying elements such as Si, Mg, and Cu etc. Pilot scale-trials in 3 ton-scale suggested a good potential of the method in terms of high yield and removal efficiency. Future research efforts may be casted into identification of IMs separation methods which are robust, efficient, and easily implemented through available equipment in casthouses/foundries. Melt stirring in combination with melt holding is worth trying for enhancing removal kinetics. Flotation and rotary kiln routes from the perspective of IMs separation, are two ways worth exploration to avoid sludge accumulation at furnace bottom.

4.12. Assessment of Interview Results

A bubble plot, also known as a bubble chart, is a visual representation that is used to interpret the results of a SWOT (Strengths, Weaknesses, Opportunities, and Threats) analysis in a more engaging and insightful way. It combines the elements of a scatter plot with the use of bubble size and color to convey information. For the removal techniques evaluated and discussed during the interviews with the aluminum producers, a bubble plot was compiled for this study is shown in the Figure below:

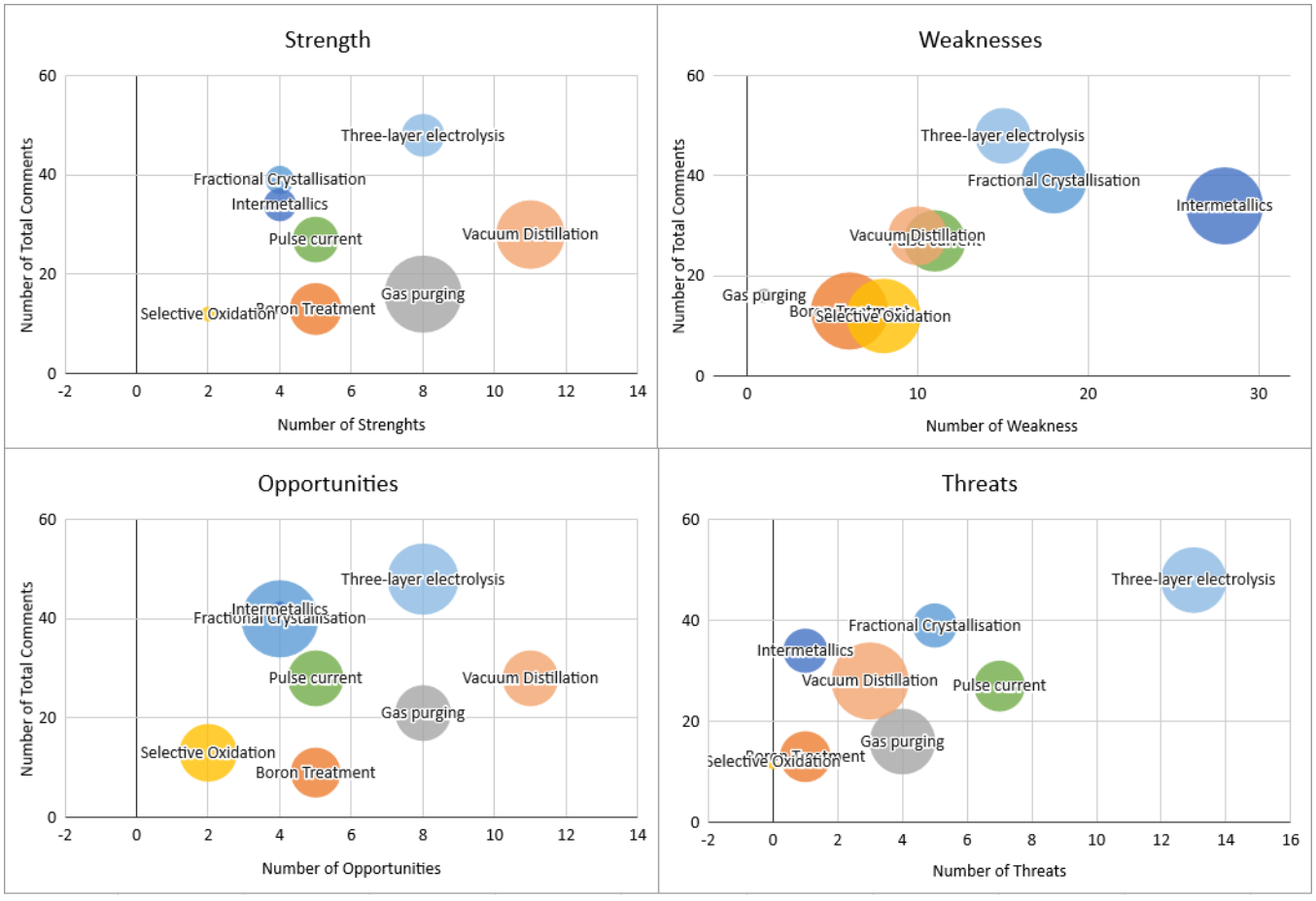

Figure 72 : Bubble Plot with Strength, Weakness, Opportunities and Threats.

For reference to the above bubble plot, there are four quadrants: Strengths, Weaknesses, Opportunities, and Threats. For each of these categories, the data were gathered from the respective interviews with aluminium producers as exemplified in Table 13. According to the comments from the interview, they are classified into several categories as seen in Table 32 below.

MIMI Tech GmbH
Preusweg 98, D-52074 Aachen
friedrich@mimi-tech.com

Table 32 : pre-defined categories for quantifying the comments from the Interview.

Strengths	Weakness	Opportunities	Threats
Currently in use/Well established	Energy Consumption	Others	Legislation
Wide application range	Treatment Capacity	Potential to reach low impurity concentration	Environmental
High Process Efficiency	Process control	Incorporation of additional element	Capex Cost
Valuable Products	Separation of Sludge	Easy industrial implementation	Consumables
Capability of handling noble elements	Reclamation of Side Product	Potential to run in low extent contaminated melt	Energy Cost
Principle Validated	Product Quality	Work as neutralization measure	Accessibility
Others	Loss in Dross	Potential to run as continuous process	Alternatives Available
	Interference with alloying/impurity elements	Environmentally friendly	Others
	Lead Time	Potential of joint application	Niche Market
	low selectivity		
	Melt Contamination		
	Not Available as In-line Process		
	Narrow application range		
	Current scale		
	Others		
	Low Yield		

Based on the number of counts i.e., frequency of the respective category, the comments were quantified and used as variable for the bubble chart. The total number of comments and the comments from the respective quadrant is used to position the data points on the chart.

- X-axis (Number of comments from respective quadrant): This variable measures how significant the respective quadrant is. For example, in the Strengths categories, it can show how much positive interest is shown by companies in the removal techniques.
- Y-axis (Total number of comments): This variable measures the likelihood of a particular technique being discussed. The higher the position of the bubble in the Y-axis, the more interesting is that technique in general.

MIMI Tech GmbH
Preusweg 98, D-52074 Aachen
friedrich@mimi-tech.com

The size of each bubble in the plot can represent another variable, in this case the scale of the identified quadrant. Larger bubbles can indicate that a larger ratio of that quadrant's comments towards the total number of comments i.e. with greater importance.

Each color used in the bubble plot is used to categorize the 8 different removal techniques presented during the interview. This can help visually distinguish between different types of removal technologies along with data labeling.

For interpreting the bubble plot, there are two things to look at:

- Quadrant Analysis: By examining the position of each bubble within the four quadrants (e.g., top-left for Strengths, top-right for Opportunities, bottom-left for Weaknesses, and bottom-right for Threats), key insights and interest can be quickly determined.
- Bubble Size: Larger bubbles in a quadrant indicate high-impact techniques, while smaller bubbles may represent lower-impact techniques

In the Strength quadrant, it can be observed that vacuum distillation and gas purging has the largest bubble size, indicating that interviewees see these two techniques very positively due to its remarkable removal capabilities, while on the other selective oxidation receive much lesser attention. Often discussed together is the opportunities quadrant, where similar trends can be seen. Fractional crystallization and three-layer electrolysis saw a large bubble size due to its successful implementation in primary aluminium production and hence a positive outlook for application in the recycling field.

Intermetallic do receive much attention, but due to its difficulties in implementation i.e., sludge removal and reclamation of materials, it was pushed far right on the weakness quadrant, showing the largest ratio of all bubble size at 0.667. Similarly, at 0.667 was boron treatment, with similar concerns on the sludge removal. It can be seen here that gas purging, a widely used technique in the current industrial production, shows lesser implementation difficulties for the recycling operation. The major concern within the weakness and threats discussion lies with the energy cost of several techniques discussed, including fractional crystallization which requires long holding time and three-layer electrolysis, which in nature requires large amount of energy, hence the distinct position of three-layer electrolysis in the threat's quadrant.

MIMI Tech GmbH
Preusweg 98, D-52074 Aachen
friedrich@mimi-tech.com

5. Part II – Negative Effects and Neutralization techniques

5.1. Effect of Iron (Fe)

5.1.1. Wrought alloys

5.1.1.1. 1XXX

Corrosion

Yu et al. investigated the electrochemical behaviors of different grades of pure aluminum. In their works, he showed that the presence of impurities (Fe, Si, and Cu) accelerates the corrosion rate of aluminum within a 4mol/L KOH solution [150]. The increase of impurity content decreased the transfer resistance values (Rt), resulting in the increase of hydrogen evolution corrosion. According to the author, the presence of impurities in the aluminum generated micro-cathode phases at the grain boundaries. Trace impurities such as Si (-0.445V), Fe(-0.441V), Cu (0.36V), $FeAl_3$ (-0.56V), Al_2Cu (-0.54V) and $Al_6Fe_2Si_3$ (-0.58V) all have higher potential and will produce micro-cells of corrosion, consequently, the electrode potential of aluminum moves to more positive values, and the corrosion rate increases. In addition, the microstructure of aluminum indicated that large grains of second phase impurities at grain boundaries caused point defects in the aluminum substrate, destructing its natural passive film, which led to the rapid increase of self-corrosion [150].

Similarly, Zheng et al. [151] also observed that Al-Fe phase precipitated in the Al can work as a cathode site, in which the formation of microcells between the Al-Fe phase and the Al matrix could promote the self-corrosion process. When the author used a friction stirring process (FSP), it led to the refinement of the grains, breaking the Al-Fe intermetallic particle and at the same time also reducing its amount (see Figure 73). Hence, more Fe was dissolved into the Al matrix, making it less prone to pitting corrosion [151].

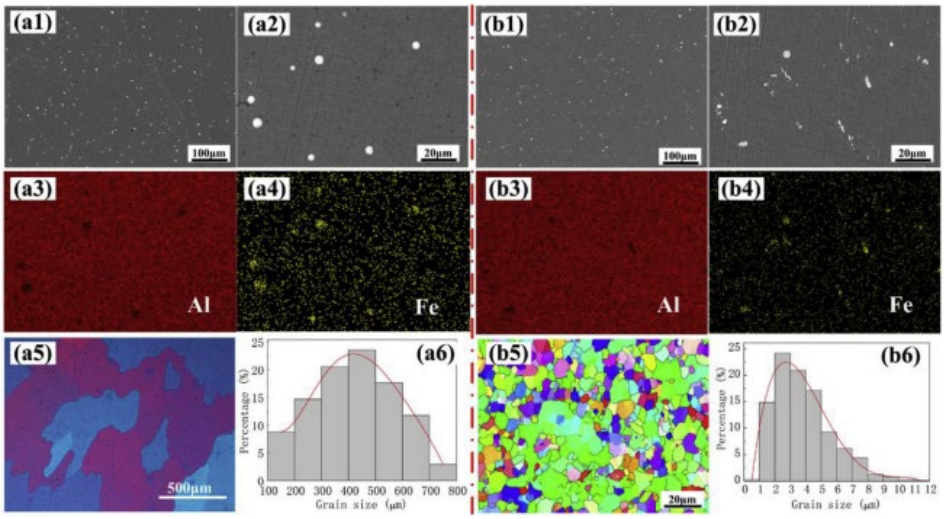

Figure 73: Microstructural features of the C-Al sample☹a1) and (a2) SEM images, (a3) and (a4) EDS mapping analysis, (a5) polarized optical microstructure, (a6) grain size distribution; FSP-Al sample: (b1) and (b2) SEM images, (b3) and (b4) EDS mapping analysis, (b5) EBSD analysis, (b6) grain size distribution [151].

MIMI Tech GmbH
Preusweg 98, D-52074 Aachen
friedrich@mimi-tech.com

In another study from Ren et al. [152], the authors investigated the role of impurities in the Al anode for Al-Air batteries. In their study, it was found that the decrease in contents of Fe and Si impurities in Al anodes can help to alleviate the self-corrosion phenomena (see Figure 74). Both the Fe-rich phases and the Fe-rich precipitates are present unevenly in the microstructure, which can act as corrosion centers that accelerate the corrosion of the material. The authors stated that the surface of 2N8 Al contains two significantly different corrosion morphology features: A deeper and larger short strip corrosion pits and many small corrosion pits. Fe impurities tend to precipitate at grain boundaries, causing large surface potential difference within the matrix, which can lead to galvanic corrosion and accelerate the self-corrosion of Al. Therefore, it was concluded that the 2N8 Al anode with the highest impurity demonstrated the largest self-corrosion rate and the roughest corrosion morphology [152].

sample	Mg	Si	V	Mn	Fe	Ni	Cu	Zn	Ga	Al
2N8	10.4	168.7	322.5	7.2	670.5	32.1	1.1	170.6	148.8	bal
3N6	1.2	52.9	2.8	4.7	144.4	10.8	0.9	78.0	76.7	bal
3N8	15.7	8.3	<0.1	<0.05	18.4	0.7	37.9	0.3	0.3	bal
4N6	3.9	13.6	0.2	<0.1	2.8	0.1	4.5	1.7	0.2	bal
5N	2.3	2.2	<0.1	<0.1	2.0	<0.1	1.6	0.2	<0.05	bal

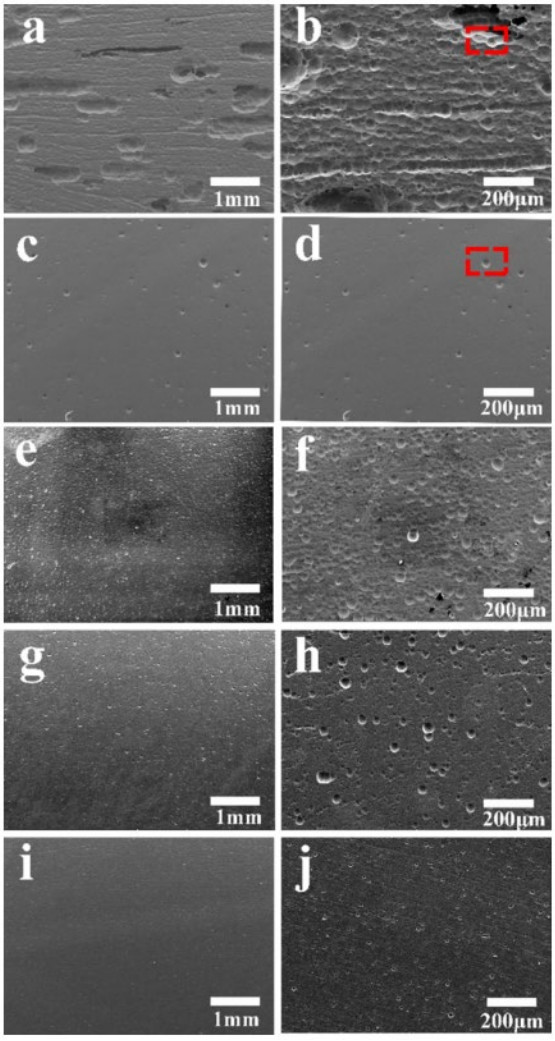

Figure 74: Top: Table with the chemical composition of the tested samples; Left: SEM images of (a, b) 2N8 Al, (c, d) 3N6 Al, (e, f) 3N8 Al, (g, h) 4N6 Al, and (I, j) 5N Al after immersion in 4 M KOH for 60 min [152].

MIMI Tech GmbH
Preusweg 98, D-52074 Aachen
friedrich@mimi-tech.com

5.1.1.2. 2XXX

Mechanical Property

Iron (Fe) has very low solubility in aluminum (Al) and tends to exist predominantly in phases originating from solidification. The morphology of Fe-containing phases significantly influences the mechanical properties of the alloy. Needle-like particles, such as Al_7Cu_2Fe and Al_5FeSi phases, are particularly harmful to the mechanical properties [153]. In the presence of Manganese (Mn), the formed $Al_{15}(Fe,Mn)_2Si_3$ phase, characterized by compact skeleton-like (Chinese script) morphology, is considered preferable for the mechanical properties of the alloy. However, the formation of $Al_{15}(Fe,Mn)_2Si_3$ decreases the "free" manganese (Mn) concentration in the aluminum, resulting in a reduced amount of $Al_{20}Cu_3Mn_2$ dispersoids. Since $Al_{20}Cu_3Mn_2$ dispersoids play a role in affecting the mechanical properties of the alloys, the presence of Fe leads to the loss of manganese and its effect on the strength properties of the alloy [153].

Zhao et al. [154] made a comparison between 2024 and 2124 alloys, in which it was indicated that higher amounts of Fe and Si in the 2024 alloy result in decreased tensile strength and fracture toughness [154]. In a study from Gao et al. [155] on Al-Cu alloys with addition of Sc, Fe, and Si, it is suggested that a Fe content higher than 0.5 wt.% should be generally avoided in Al-based alloys due to its negative impact on ductility and toughness [155]. However, the addition of approximately 0.18 wt.% Fe can be done in this alloy to suppress the formation of the Sc-rich W-phase and instead promote the formation of (Cu,Fe)-rich constituents during solid solution treatment, as this Fe content helps ensure that a higher amount of Sc solutes are dissolved into the matrix, which is desirable for the target properties of the alloy (see Figure 75) [155].

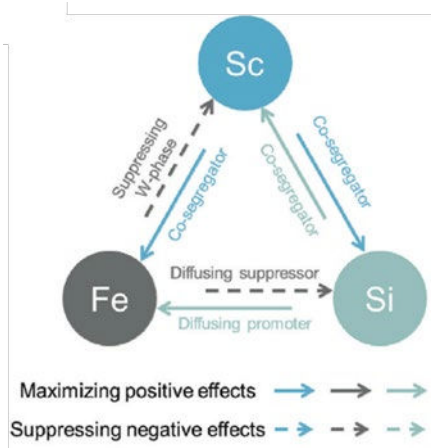

Figure 75: Present the interactions among multiple micro-alloying effects originating from Sc, Fe and Si [155].

In another study from Amer et al. [156], Yttrium (Y) was added to a Al-Cu alloy. Their results showed that the presence of Fe and Si in this alloy resulted in the presence of a larger quantity of well-dispersed intermetallic particles within the alloy structure, which, contrary to expectations, the constant occurrence of iron and silicon impurities did not have a detrimental impact on the mechanical properties of the alloy under study. This was attributed to the formation of a small amount of compact $Al_{11}Cu_2Y_2Si_2$ phase, which exhibits favorable characteristics for maintaining mechanical performance. Furthermore, the author's results showed that when the samples with added Y were annealed up to 300°C, it resulted in a structure with grains elongated along the rolling

MIMI Tech GmbH
Preusweg 98, D-52074 Aachen
friedrich@mimi-tech.com

direction, where the presence of impurities slightly increased the hardness of the alloy. This was attributed to a larger amount of dispersed intermetallic particles in the structure. As the annealing temperature increased, the difference in hardness between the alloys decreased, and above 350°C, recrystallization occurs and the hardness levels out [156].

Their results demonstrated that after annealing the alloy at 100°C and 150°C, It exhibited good strength characteristics with higher conditional yield stress (284-325 Mpa) and conditional ultimate strength (304-369 Mpa) compared to the alloy without impurities. Hence, the presence of both iron and silicon impurities in aluminum did not negatively affect the mechanical properties of the studied alloy [156].

Similar approach was done by Barkov et al. [157]. This time, 0.2 wt. % Gadolinium (Gd) was added in the Al-Cu alloy with the presence of Fe and Si impurities. Gd contributed to an increased hardness compared to the same alloy without impurities (see Figure 76). Iron and silicon impurities did not adversely affected the microstructure and mechanical properties of the new alloy, after rolling and subsequent annealing [157].

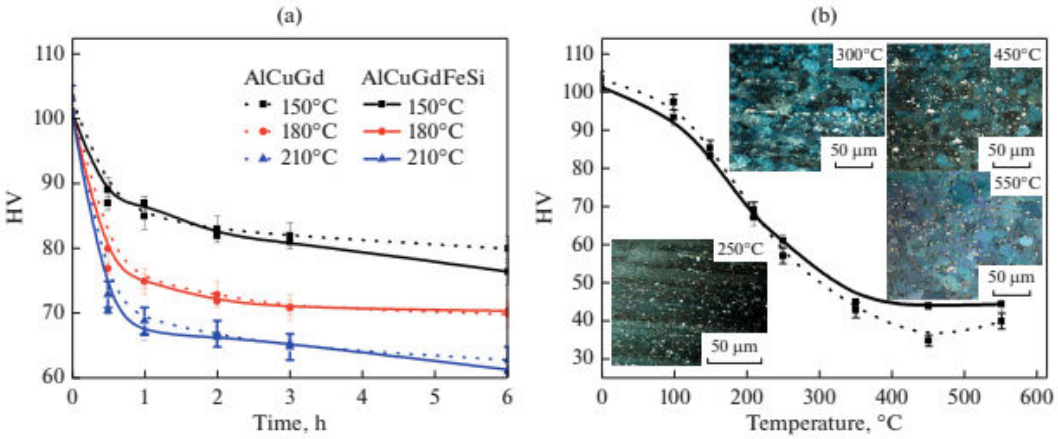

Figure 76: The hardness of the cold-worked alloys as a function of the (a) time of annealing at 100, 180, and 250°C and (b) the temperature of 1-hour annealing (curves for the AlCuGd alloy are indicated by dashed lines, curves for the AlCuGd alloy are indicated by solid lines) [157].

Their results suggest that, by designing the alloy with Gd content of around 0.15 wt. %, Fe impurity in the alloy does not become harmful to its mechanical properties. Around 1 wt. % Fe can be bound as an Al8Cu4Gd eutectic phase instead of precipitating, with the rest being soluble in the Al matrix. Moreover, the Al8Cu4Gd eutectic phase can be spheroidized during heat treatment, further decreasing its impact in the alloy. Another interesting finding was that the presence of Fe and Si, as an Al-Cu-Gd-Fe-Si alloy, promoted better elongation in as-deformed state than the Al-Cu-Gd alloy, which suggests that the Fe is beneficial in the special designed alloy. Presumably, Al-Cu-Gd-Fe-Si alloy shall have also a better elongation than Al-Cu-Fe-Si alloy [157]

5.1.1.3. 5XXX

Mechanical Property

Spencer et al. [158] showed in their research that the presence of angular $FeAl_6$ intermetallic particles (which have a size between 0.5 – 2 µm during casting) are potentially detrimental to the formability and ductility of the alloy, as they promoted the formation of voids when subjected to

MIMI Tech GmbH
Preusweg 98, D-52074 Aachen
friedrich@mimi-tech.com

large plastic strains. Once the void nucleation has occurred, there is a reduction in the strain necessary to attain failure. Therefore, an increase in iron content reduced the alloy ductility in their experiments. Moreover, as seen in Figure 77, in high Fe content alloy, the main mechanism for fracture and low ductility were the localized nucleation, growth, and coalescence of voids along a band of intense shear [158].

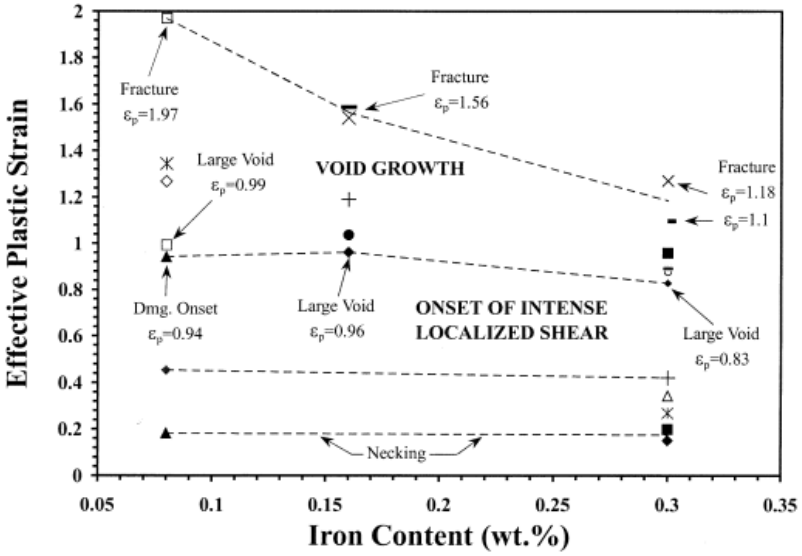

Figure 77: Observed sequence of events and their relative strains leading to fracture as a function of iron content, for the unnotched plane strain geometry, in the rolling direction [158].

Another well-known effect of Fe was further investigated by Liu et al. [159], where he showed that the needle-like or plate-like Fe-containing intermetallic in alloys act as stress concentration points, leading to crack initiation, propagation, and ultimately fracture of the material. These intermetallic are characterized by their brittleness, which further contributes to the reduction in mechanical properties. The author also pointed out that, in Al-Mg alloys, Fe typically precipitates as detrimental Fe-containing intermetallic. This is primarily due to the low solubility of Fe in the solid α-Al matrix. Some of the Fe-containing intermetallic phases that can form during solidification of Al-Mg alloys include θ-$Al1_3Fe_4$, Al_m(FeMn), Al_3(FeMn), Al_6(FeMn), β-Al_5FeSi (β-Fe), and α-Al_{15}(FeMn)$_3Si_2$ (α-Fe). The presence of these intermetallic phases can have adverse effects on the mechanical properties of the alloy [159].

Another outcome from their literature review show that Fe, in the equilibrium form of θ-$Al_{13}Fe_4$ phase, can enhance the mechanical properties of Al alloys containing Mg, and Mn, as the presence of Fe-rich phases blocks slip lines, contributing to the improvement of mechanical properties in these alloys. Fe-containing intermetallic can be alloyed with elements such as Mn, Cr, Si, Ni, and Cu. These alloying elements can not only modify the crystal structure, but also alter the lattice parameters, resulting in changes in overall mechanical characteristics. Elements such as Co, Cr, and Mn are identified as potential candidate elements for mechanical optimization of the θ-$Al_{13}Fe_4$ phase. Simulation studies suggested that Co, Cr, and Mn can simultaneously improve mechanical modulus, hardness, and fracture toughness in $Al_{13}Fe_4$-based alloys, and the addition of these alloying elements can lead to the enhancement of mechanical properties in alloys containing Fe-based intermetallic [159].

MIMI Tech GmbH
Preusweg 98, D-52074 Aachen
friedrich@mimi-tech.com

Corrosion

In a study about the corrosion in an AA5083 alloy, Gao et al. [160] observed that the pitting corrosion attack detected is strongly dependent on the amount and distribution of intermetallic particles. Including cathodic (Mn, Fe)-rich particles. Moreover, he stated that the distribution and number of intermetallic particles were closely related to the anisotropy of the corrosion properties, and local corrosion attack for both "as received" material mainly occurred in the form of pitting at circumferential pits that form a ring of attack around cathodic Al-Mn-Cr-Fe particles. An additional amount of intermetallic phase in the exposed plane led to a higher tendency for pitting corrosion. The author suggested that the strong dependence of stress corrosion susceptibility on orientation appears to be primarily controlled by the amount and distribution of pre-existing intermetallic particles. The corrosion attack was observed to occur primarily around the cathodic Al-Mn-Cr-Fe particles, giving rise to the dissolution of the neighboring oxide layer and matrix as a consequence of the oxygen reduction reaction and the subsequent local alkalinization [160].

5.1.1.4. 6XXX

Mechanical Property

It is well-kwon that the low solubility of Fe in solid solution, typically less than 0.05 wt.%, causes the Fe to form primary phases during the casting process. The effect of Fe in aluminum casting alloys has also been extensively studied due to its significant impact on the alloy's properties [161]. The primary Fe-rich intermetallic phases (IMPs) formed in the alloy are well-known for reducing ductility and having a negative effect on formability, as these IMPs act as detrimental phases, impairing the material's ability to be easily shaped or formed [162], [161]. Therefore, the presence of Fe-rich primary IMPs is an important consideration in the design and processing of aluminum wrought alloys to ensure desired mechanical properties and formability [162].

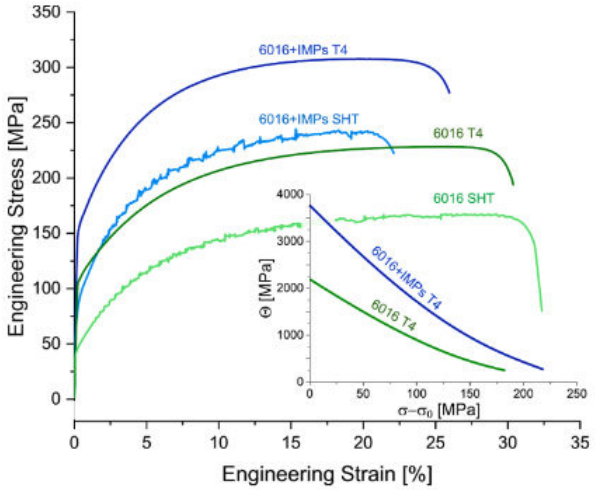

Figure 78: Engineering stress-strain curves for alloy 6016+IMP and reference alloy 6016 in as quenched (SHT) and T4 (16 days of natural aging) condition. The insert shows a "Kocks-Mecking plot" of the data [6016 and 6016+IMP], displaying the hardening rate in dependence on the true stress beginning at the yield point [162].

MIMI Tech GmbH
Preusweg 98, D-52074 Aachen
friedrich@mimi-tech.com

In the research done by Trink et al. [162], a hetero-deformation-induced (HDI) strengthening and HDI strain hardening concepts were used to enhance the mechanical properties of Al-Mg-Si wrought alloys with high Fe-content, hence, a new Al-Mg-Si alloy system with a high fraction of Fe-rich primary intermetallic phases was created, in which this new wrought alloy containing high amounts of Fe-rich phases, greatly exceed current standards (see Figure 78), making the HDI process a potential solution to absorb higher Fe content in the 6XXX alloys [162].

With an aim to analyse the effects of using a larger amount of scrap in the production of the 6060 alloy, Silva et al.[161] studied influence of Fe on mechanical properties of the alloy. The Fe and Si content was adjusted respectively to 0.239 and 0.409 wt. %. Both values are still within the conventional limits of 6060 alloy nevertheless the Si is lower than the amount usually recommended for conventional applications. The reference alloy has 0.176 wt. % Fe and 0.549 wt. %. It was found that through heat treatment in a solution at 560 °C for 1h, followed by water quenching, and then artificial aging at 180 °C for 8h, the difference in UTS, YS, and elongation values between both alloys are less than 10%. The authors concluded from a mechanical performance point of view, there is no serious restriction to the use of higher Fe content than the ones usually adopted for the standard 6060 alloy.

5.1.1.5. 7XXX

Mechanical Property

In their research on the effect of radial-shear rolling in an electromagnetic casted 7XXX Alloy, Gamin et al. states that the performance of this 7XXX series alloys is significantly impacted by the presence of impurities, particularly Fe. These strict purity requirements make it challenging to prepare 7XXX alloys from contaminated recycled materials, as the presence of Fe and other impurities is not permissible. In fact, the presence of Fe and other impurities can negatively affect the mechanical properties and performance of 7XXX alloys, highlighting the often requirements for high purity alloys in the manufacturing process [163].

The author showed that elevated cooling rates during the casting process resulted in the dispersion of the cast structure, including the Fe-containing phases [163]. Moreover, the joint introduction of Fe (iron) and Ca (calcium) into aluminum alloys allowed for the binding of iron into compact particles of the $Al_{10}CaFe_2$ compound, instead of needle-shaped inclusions of the Al_3Fe phase [163].

This change in the morphology of iron-containing phases led to a significant decrease in the negative effect of iron on the mechanical properties of both castings and semifinished products. The incorporation of Ca along with Fe helped to mitigate the detrimental impact of Fe on the mechanical properties of the studied alloys within the Al–Zn–Mg–Ca–Fe system. The observed decrease in the negative effect of Fe suggests that the use of Ca as a neutralizing element can improve the overall performance and mechanical properties of the alloys, both in their cast and deformed states [163].

Corrosion

Zhang et al. studied the effect of intermetallic on the corrosion behavior of 7A52 alloy. Their experimental results indicated that Al-Mn-Fe intermetallic exhibits negative volta potential relative to the Al matrix, indicating an anodic behavior. This intermetallic is also easily dissolved and corroded under the corrosive environment, where it becomes corrosion initiation sites [164].

MIMI Tech GmbH
Preusweg 98, D-52074 Aachen
friedrich@mimi-tech.com

In another study, the electrochemical performance of an 7XXX alloy made using pure constituents was investigated by Moghanni-Bavil-Olyae et al., and it was found that the presence of iron and silicon can lead to a sharp increase in the aluminum corrosion [165]. However, the use of manganese in the composition of commercially pure aluminum anodes was shown by the authors to reduce the corrosion rate of aluminum and reduce the harmful effects of Fe impurity [165]. This effect happens due to the formation of Al6(Mn,Fe) in aluminum, which has an electrochemical potential almost equal to the base Al [165].

5.1.1.6. 8XXX

Mechanical Property

Alloys with higher Fe and Si content generally exhibit reduced ductility, decreased toughness, and an increased occurrence of recrystallization. However, the presence of Fe and Si can enhance the strength of certain alloys, impacting their fatigue life in the long-life region [166]. Impurities, such as Fe and Si, in aluminum alloys can form brittle compound particles that have negative effects on the microstructure [166]. These brittle particles can lead to a breakdown along the interfaces between the particles and the matrix, further deteriorating the material's properties [166].

However, in their research about the role of impurities in Al-Li alloys, Meng et al. [166] stated that, in the case of the 8090 alloy, the fatigue life of the low-purity variant was somewhat higher than that of the high-purity variant. This was attributed to the strengthening effect of Fe and Si in the alloy. The increased strength became the dominant factor influencing the fatigue life of the alloy, especially in the long-life region [166].

In their literature review, Meng et al. illustrates the effects of Cerium (Ce) content in the grain size and mechanical properties of Al-Li and Al-Li-Mg alloys. In a binary Al-Li alloy, increasing Ce content up to 1.1% linearly increases the grain number in a unit area. Also, the Ce addition improves the mechanical properties of Al-Li-Mg alloys and helps control the negative effects of impurity Fe. Ductility is significantly improved by adding 0.05% Ce to 8090 alloy sheets rich in alkali metal impurities or 0.28% Ce to those rich in impurities Fe and Si. The addition of Ce reduces the diffusion coefficient and can delay recrystallization, refine precipitated particles, reduce coarse compounds along grain boundaries, and suppress d'-PFZ (depleted zone) formation. Rare earth elements, like Ce, can also delay impurity segregation to grain boundaries during heat treatment processes, reducing impurity-induced embrittlement of grain boundaries [166].

In an article from Cieslar et al., the author investigated the Portevin-Le Chatelier effect in Al-Fe-Si foils. It is mentioned that the dynamic strain aging (DSA) is a phenomenon observed in certain alloys, where the mechanical properties are affected by the interaction between dislocations and solute atoms [167]. However, the author pointed out that the Fe atoms did not contribute to the Portevin-Le Chatelier effect (a manifestation of DSA) in Al-based alloys with Si addition. This is due to the extremely low solubility limit and low diffusivity of Fe atoms, even at elevated temperatures [167]. This limited solubility and low diffusivity of Fe in Al-based alloys with Si make Fe atoms ineffective in causing DSA or influencing the mechanical properties associated with DSA [167].

Pozdniakov et al. [168] investigated the role of Fe and Si on the Al-Zr-Sc Alloys with and without addition of Y (see Figure 79). The author stated that the presence of Fe and Si impurities in the Al–0.2% Zr–0.1% Sc alloy results in the formation of (Al, Fe, Si, Sc) and (Al, Fe, Sc) phases, leading to the

MIMI Tech GmbH
Preusweg 98, D-52074 Aachen
friedrich@mimi-tech.com

binding of Sc and depletion of Sc from the aluminum solid solution. Due to this binding effect and Sc depletion, the strengthening effect typically observed upon annealing is significantly reduced compared to the same alloy without impurities. However, when Yttrium (Y) was added to the alloys, it improved their thermal stability during annealing at temperatures of 250, 300, and 370°C. The addition of Y counteracted the negative effect of Fe and Sc impurities, suggesting that Y acted as a beneficial element in mitigating their impact [168].

Compositions of the investigated alloys

Alloy	Concentration of alloying elements, wt %				
	Zr	Sc	Y	Fe	Si
Al–0.2% Zr–0.1% Sc (A85)	0.2	0.1	–	0.08	0.07
Al–0.2% Zr–0.1% Sc (A99)	0.2	0.1	–	–	–
Al–0.2% Zr–0.1% Sc–0.2% Y (A85)	0.2	0.1	0.2	0.08	0.07
Al–0.2% Zr–0.1% Sc–0.2% Y (A99)	0.2	0.1	0.2	–	–

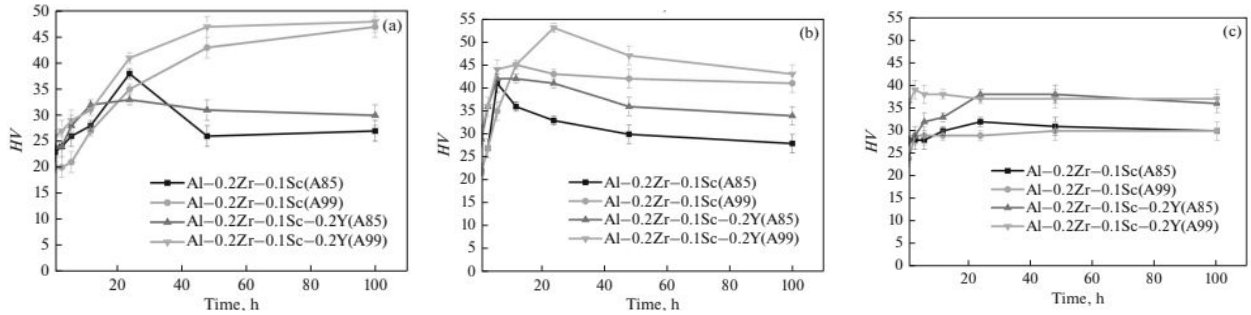

Figure 79: Top: Chemical composition of investigated alloys; Left: Kinetics curves of annealing of the investigated alloys at temperatures of (a) 250, (b) 300, and (c) 370°C [168].

5.1.2. Cast alloys

5.1.2.1. 2XX

Mechanical Property

In Al-Si-Cu type alloys, Fe is widely regarded as the most detrimental element, as it has the ability to form intermetallic phases with various morphologies and lengths when combined with other elements in the alloy. The harmful impact of iron becomes significant when its content exceeds the critical value (Fe_{crit}), representing a threshold beyond which the negative effects of iron on the alloy become more pronounced. The specific morphology and length of the intermetallic phases formed by iron are also contributing factors to its damaging influence on the alloy's properties [169].

In their studies about the influence of remelting cycles on the properties of $AlSi_9Cu_3$ alloy with higher iron content, Kasinska et al. found out that an increase in the weight percentage of Fe caused changes in the morphology of the Fe phases, making it more noticeable, particularly after the fourth remelting trial (see Figure 80) [169].

MIMI Tech GmbH
Preusweg 98, D-52074 Aachen
friedrich@mimi-tech.com

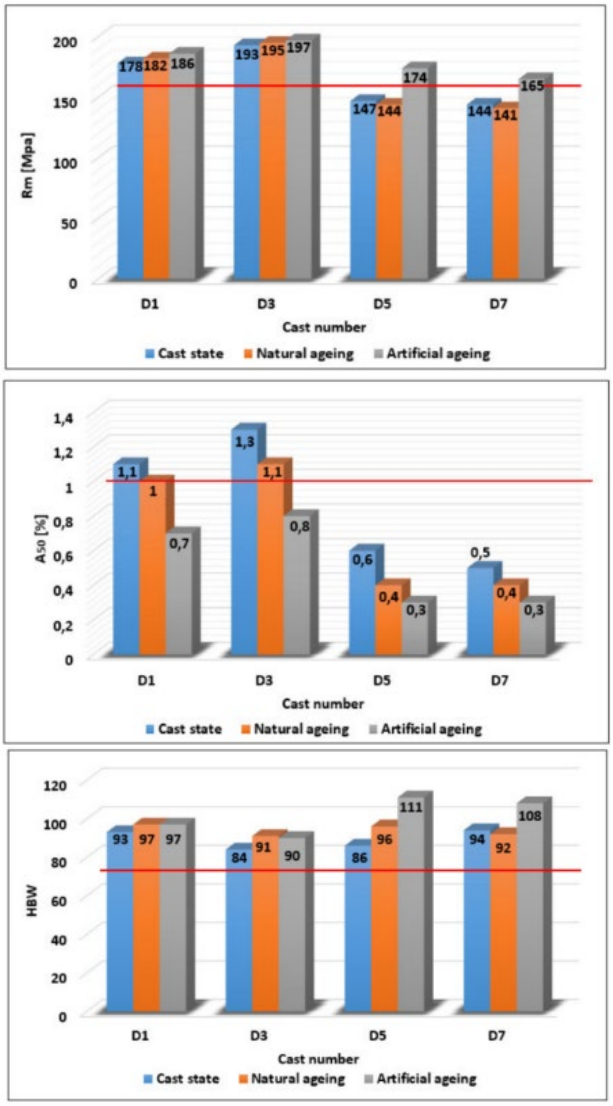

(a)

(b)

(c)

Figure 80: Relationship between (a) tensile strength, (b) elongation, (c) Brinell hardness and melt number and alloy state [169].

The performed elongation tests pointed to the negative effect of the gradual increase in wt.% Fe and a change in the morphology of the iron phases, which began to manifest significantly after the fourth remelting. The presence of the undesirable needle morphology in the alloys subjected to a higher number of remelting cycles resulted in the distortion of the structure by formation of pre-cracks. It was assumed that, with the increasing in Fe concentration, the number, and dimensions of the Al_5FeSi phase also increases. A larger number of these phases degrade the elongation properties of this alloy, as these phases are characterized by higher brittleness and at the tensile load they are more susceptible to fracture than the aluminum matrix [169].

To counteract the negative effects of iron in these alloys, natural aging, as a heat treatment process, showed effectiveness only on alloys with a lower number of remelting cycles. The authors mention that natural aging may not have significant positive effects on alloys that have undergone multiple remelting cycles. In contrast, artificial aging, another heat treatment process, led to improved mechanical properties in all the tested alloys, regardless of the number of remelting cycles [169].

MIMI Tech GmbH
Preusweg 98, D-52074 Aachen
friedrich@mimi-tech.com

5.1.2.2. 3XX

Mechanical Property

The presence of Fe has a detrimental effect on the overall integrity and mechanical properties of the material, increasing the likelihood of porosity, cracks, fatigue cracks, decreased tensile strength, and increased corrosion [170]. Regarding the mechanical properties of the alloys, as the Fe content increased, the presence of the needle-like Al_5FeSi phase increased in the alloys [171]. An increase in their length, as well as thickness, was also observed and poses detrimental effect on the alloy mechanical properties [172], [171].

For 3xx cast alloys, having excessive Fe content often means formation of large size of β-Al_5FeSi phase According to Matejka et al.[173], when Fe content in $AlSi_9Cu_3$ alloy increases from 1.5 to 1.9 wt. %, the size of β-Al_5FeSi phase rises 38 to 90 µm. The large size of β-Al_5FeSi was attributed by the authors to the early-stage formation prior to crystallization of the eutectic phases.

Bjurenstedt et al.[174] studied effect of Fe on ultimate tensile strength (UTS) and elongation of A380 alloys. It was found an increase of Fe from 0.74 to 1.17 wt. % leads to decrease of UTS by 13 % and elongation by 61 %. It was indicated the plate β-Al_5FeSi phase which appears in higher amount and greater size in the alloy with higher Fe content are responsible for the deterioration of the above-mentioned properties. Interestingly, it was found β-Al_5FeSi fractures preferably through cleavage and the particle-matrix de-cohesion was not identified. The crack of β-Al_5FeSi phase taking place during the tensile test was shown in Figure 81. The size of β-Al_5FeSi was suggested by the authors to be a more influencing factor comparing with amount on properties of the alloy. It was found the size of β-Al_5FeSi can be largely influenced by the solidification time. With a more rapid cooling, the size of β-Al_5FeSi were demonstrated to be decreased. As a result, its negative effect can be neutralized.

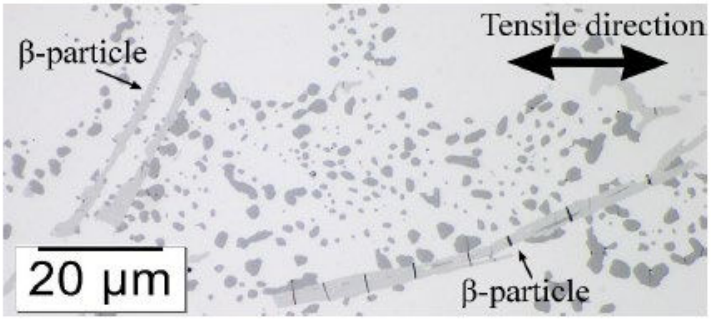

Figure 81: Cracks of β-Al5FeSi phase during tensile test. Reproduced from [174].

Silva et al.[175] studied effect of Fe on elongation and UTS of an artificial Al-7Si alloy, it was found the presence of 1 wt. % Fe in the alloy decreases elongation and increases UTS, as is shown in Figure 82. The precipitated β-Al_5FeSi acts as reinforcement but impacts ductility negatively. Through addition of 0.5 wt. % V and conduct fast cooling (8.5 °C/s), the elongation and UTS values are both enhanced with respect to Al-7Si-1Fe alloy in the same condition, despite not comparable with Al-7Si alloy. The authors attributed the improvement of mechanical properties to the formation of Al_3V phase and α-AlFeSiV phase, both of which help reduce fraction of β-Al_5FeSi phase.

MIMI Tech GmbH
Preusweg 98, D-52074 Aachen
friedrich@mimi-tech.com

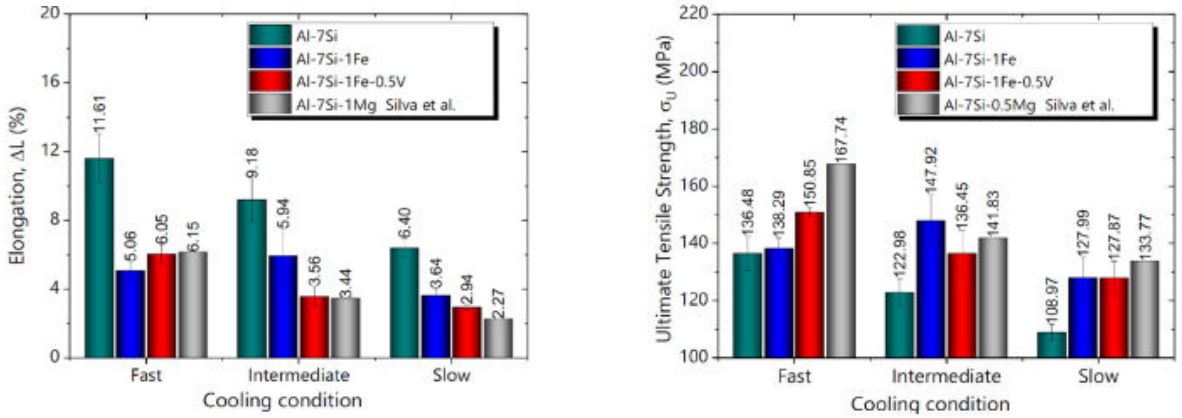

(a) (b)

Figure 82: (a) Elongation; (b) ultimate tensile strength of Al-7Si(-0.5V) alloys. Reproduced from [175].

Eisaabadi B. et al.[170], [176] studied the effect of Fe on the UST and elongation properties of an Al-7Si-0.35Mg cast alloy in T6 state. The effect of Fe was studied at the presence of certain amount of oxides/hydrogen content in the melt. The result suggests that with low content of oxides inclusion present in the melt, an increase of Fe content from 0.09 to 0.85 wt. % leads to 11 % UTS and 74 % elongation decrease. Metallography image analysis suggests a positive relation between Fe content and pore densities. It was proposed high Fe content leads to formation of large amount of platelet β-Al5FeSi phase, which restricts the flow of liquid metal through the inter-dendritic feeding path and favors the formation of shrinkage porosity. The porosities can act as effect stress riser and impair the tensile properties.

Bolibruchova et al. [177] found that an increase of Fe content in the melt leads to decrease of tensile properties of an Al-7Si-0.3Mg alloy. The result is shown in Figure 83(a) and (b). The reference alloy contains 0.1 wt. % Fe and 0.07 wt. % Mn. To counter the negative effect of Fe, Mn was added into the melt. It was found at an optimum Mn content through which Mn/Fe ratio is controlled at 0.64 (Mn: 0.474 wt. %), the alloy, upon T6 heat treatment can arrive at an equivalent tensile property as that of the reference alloy. Microstructure analysis indicates the neutralized is realized through the shortening of β-Al_5FeSi phase size.

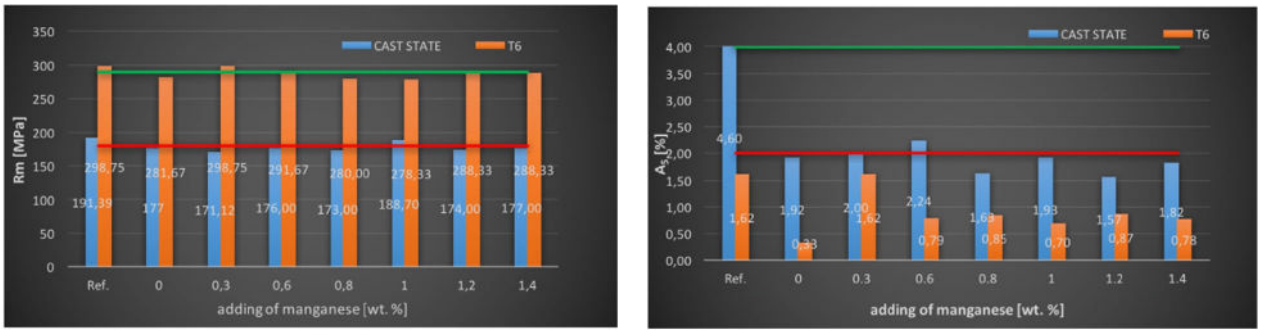

(a) (b)

Figure 83: Dependence of: (a) tensile strength; (b) tensibility of secondary alloy AlSi7Mg0.3 at different Mn content. Blue columns give alloy property in as-cast state whilst yellow in T6 state. Reproduced from [177].

MIMI Tech GmbH
Preusweg 98, D-52074 Aachen
friedrich@mimi-tech.com

Ferraro et al.[178] studied influence of Fe, Mn, and Cr on ductility of Al_7SiCu_3 alloy. At T1 state, it was found the ductility of the alloy decreased with increasing of collective Fe, Mn, and Cr contents. It is suggested the ductility is also sensitive to the presence of primary β-Al_5FeSi phase and meanwhile to the Fe:Mn ratio. A low Fe:Mn ratio, realized by adding Mn, the material's ductility can be improved.

Li et al.[175] studied negative effect of Fe on UTS, YS, and elongation of 319.2 alloy. The detrimental impact of Fe on UTS and elongation is clearly suggested by tensible test using T5 and T6 state alloys solidified at different rates. The reasons are attributed to formation of brittle β-Al_5FeSi phase. With regard to YS property, the positive or negative effect of iron seems to be heat treatment dependent. Quenching modification was demonstrated to be effective on enhancing both UTS and YS properties due to its benefit of microstructure refinement and reduction of porosities. T6 heat treatment was found to be advantageous against T5 heat treatment for improving UST and YS, particularly when coupling with high cooling rate. Sr and P modification was also tested for enhancing UTS and YS. Results indicated the doping of Sr and P shall be carefully coordinated with heat treatment and cooling rate measures, if a modification effect is desired. With respect to neutralization of negative effect of Fe on ductility, the effectiveness of quenching, heat treatment, Sr/P doping appeared to be insignificant.

The effect of T6 heat treatment was investigated by Kucharikova et al. [179] in their research about the microstructure in AlSi7Mg0.3 cast alloy with different content of Fe. The authors stated that a higher amount of iron in the chemical composition tends to result in the formation of Al_5FeSi phase rather than $Al_{15}(FeMg)_2Si_2$ phase, causing detrimental effects on the mechanical properties of the material. In their work, the authors used heat treatment T6, which had an impact on the size of Fe-rich phases, particularly those present in needle form. However, the study did not confirm the increase in the length of Fe-needle intermetallic phases with higher Fe content [179].

Bacaicoa et al. [180] also found out in their research that heat treatments have a positive impact on the mechanical properties of the modified secondary Al-Si-Cu alloy. However, the effectiveness of heat treatments decreases as the Fe content increases [180].

In another research, Zhao et al. [181] stated that, for Al-7Si-0.3Mg casting alloy, the presence of Fe directly reduces the mechanical properties, corrosion resistance, and machinability of the products (see Figure 84). The Fe-rich phases in Al-Si-Mg alloys form hard and brittle intermetallic compounds that serve as crack initiation sites in the material. Additionally, the Fe-rich phases provide additional paths for crack propagation within the alloy [181]. Zihalova et al. [182] also stated that the presence of iron (Fe) in AlSi10MgMn alloy castings leads to increased embrittlement. The presence of Fe causes the formation of intermetallic phases that are harmful to the quality of the casting. In their research, Nickel was added as a Fe modifier, and the optimal amount of nickel addition as the iron corrector is 0.5 wt.%. Their works suggest that the addition of Ni to the alloy serves to modify or correct the presence of Fe, likely by influencing the formation of intermetallic phases. The specific concentration of 0.5 wt. % of nickel was considered optimal for achieving the desired effect on the alloy's properties or microstructure [182].

MIMI Tech GmbH
Preusweg 98, D-52074 Aachen
friedrich@mimi-tech.com

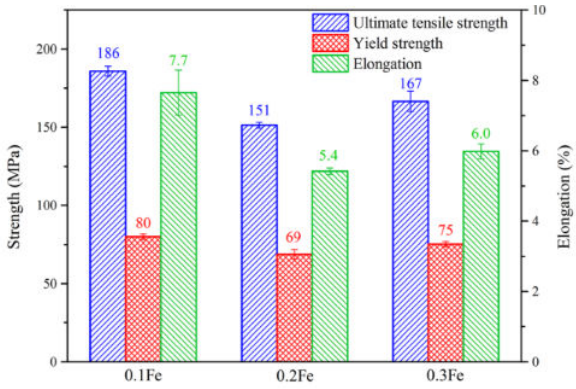

Figure 84: The values of ultimate tensile strength, 0.2 pct proof yield strength, and elongation of the Al–7Si–0.3Mg–xFe alloy [181]

The addition of Nickel was also tested by Bolibruchova et al. [183]. However, the results obtained do not support the conclusion that nickel acts as a segregation corrector for iron-based phases. High nickel content was found to have a negative impact on the microstructure of the material, leading to the formation of thickened and elongated iron-based β-phases in a needle-like shape [183].

To counteract the effects of the Fe-rich phases, Mikolajczak et al. [184] proposed an intensive stirring applied during the casting of the samples (Figure 85). To achieve this, the solidification of the alloy was carried out under an induced magnetic field (11 mT). The induced magnetic field during solidification resulted in the formation of a bulk structure with equiaxed dendrites, and showed to improve the properties of the alloy [184]. Lazaro-Nebreda et al. [175] also studied the effect of intensive melt shearing, noting that it had beneficial effects on the microstructure of the investigated alloys with high Fe content. The intensive melt shearing breaks down oxide bi-films into small particles that act as nucleates for the formation of the ß-phase, resulting in the formation of intermetallic particles with a smaller average size [175]. The fact that the oxide act as nucleates for the Fe-rich phases was also supported in the works of Eisaabadi et al. [176], where he stated that the presence of oxides caused the precipitation of Fe-rich phases in aluminum castings.

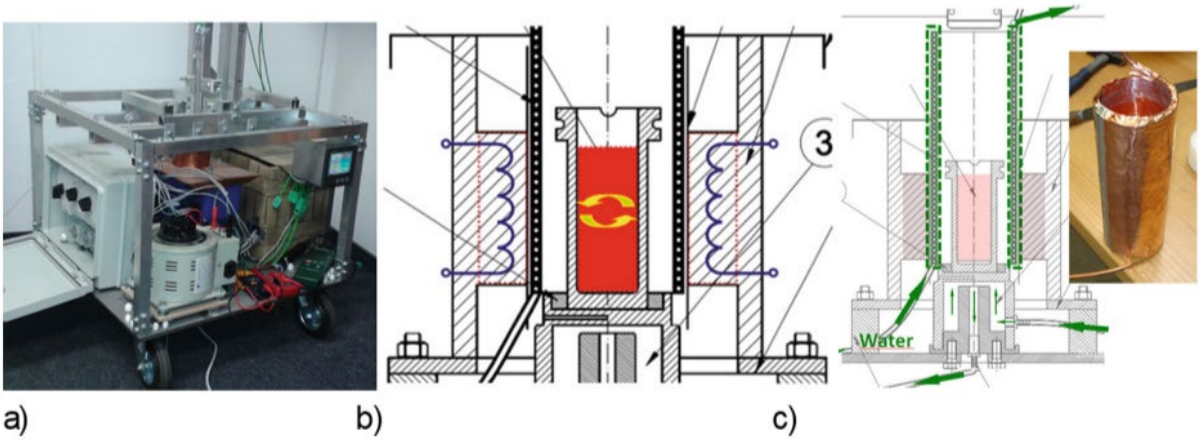

Figure 85: Diagram of the device intended for solidification in the magnetic field: (a) photo with the visible temperature recorder, autotransformer for one-phase power supply and set of switches for three-phase power supply by means of toroidal transformers, (b) diagram of the location of a specimen in the graphite crucible and the field-generating coils, (c) diagram of the location of the copper chiller that separates coils from the crucible with liquid melt [184].

MIMI Tech GmbH
Preusweg 98, D-52074 Aachen
friedrich@mimi-tech.com

In their work on the Influence of returnable material on internal homogeneity of the high-pressure die-cast $AlSi_9Cu_3$(Fe) alloy, Matejka et al. [185] observed a correlation between increased porosity and the increase of recycled content in the material, but the specific reasons for this increase are not explained by the author and it is unclear whether the increase in porosity is directly related to the presence of iron or other additional factors [185].

In similar work, Kasinska et al. [186] studied the effect of returnable material on the hot tearing tendency of the $AlSi_9Cu_3$ Alloy. It was found that large plates of the iron β-phase can impede the flow of the melt into inter-dendritic spaces, preventing proper deposition and promoting the formation and propagation of hot tears. The microstructure of alloys with 50% or higher proportion of returnable material shows a higher amount of iron phases, primarily Al_5FeSi. The sharp ends of these iron phases act as critical regions for hot tearing and subsequent hot tear propagation, significantly increasing the susceptibility to hot tearing [186]. To reduce its influence on hot tearing, the authors tested the increasing in the mold temperature, which generally reduces the hot tearing tendency. The reduction in hot tearing susceptibility was attributed to the ability to replenish the melt to critical regions during solidification, as higher mold temperatures facilitate better flow and filling of the molten material, minimizing the occurrence of hot tearing defects [186].

In another research from Kucharikova et al. [187], the authors investigated the effect of the beta-Al_5FeSi phases in A356.0 cast alloys. The mechanical and fatigue properties of the experimental alloy were correlated with the Fecrit (Mn/Fe) level. It was found that the fatigue properties depend more on porosity size when Fe plate-like phases have a length of up to 50 µm. When the length of Fe needles exceeds 50 µm, the properties are mainly affected by their length [187].

In the works of Bolibruchova et al. [177] in AlSi7Mg0.3 alloys with high Fe content, the authors stated that, even within the permitted range of the experimental alloy (0.5 to 1.2 wt.% Fe), higher iron contents can lead to the formation of phases that greatly reduce tear strength. These phases exhibit higher brittleness and hardness compared to the aluminum matrix. The presence of other elements in the alloy also contributes to the formation of intermetallic compounds. For example, during solidification, intermetallic iron-based phases can form in various morphologies, including β-Al_5FeSi needles, α-$Al_{15}(Fe,Mn)_3Si_2$ Chinese script, polyhedral, or skeleton formations. The β-Al5FeSi phase, in particular, is frequently observed and appears as thin plates or sticks, significantly impacting the properties of the final product [177].

The authors also investigated the role of Manganese (Mn) as an effective element for altering the needle-like intermetallic particles in the alloy [188]. The addition of manganese resulted in the formation of Al(FeMn)Si phases with a cubic crystallographic lattice. These Al(FeMn)Si phases were primarily located in interdendritic regions, forming massive sharp skeleton formations known as "Chinese scripts", which does not initiate cracks as the β-Al_5FeSi phase does, improving the integrity of the material [177], [188]. Therefore, it was observed that increasing the Mn content in the alloy raised the temperature at which the β-Al_5FeSi phase forms, ultimately leading to its elimination. The reduction of β-Al_5FeSi phase in the structure improved the mechanical properties of the alloy. The observed improvement in mechanical properties was at manganese levels ranging from 0.3 to 0.8 wt.% [177], [188].

In similar research from Bjurenstedt et al. [174] who studied the effects of Fe-particles on the tensile properties of Al-Si-Cu alloys, the author stated that it is generally recommended to maintain a Fe:Mn ratio of a maximum 2:1 to convert β-particles into α-particles, specifically Al15(FeMnCr)3Si2 [174].

MIMI Tech GmbH
Preusweg 98, D-52074 Aachen
friedrich@mimi-tech.com

Other research from Song et al. [189] showed that with the addition of Mn, the two-dimensional (2D) morphology of the Fe-rich phase change from interconnected plate-like to separated Chinese-script and star-like. However, excessive Mn addition caused the formation of large primary Fe-rich phases, resulting in a significant reduction in the elongation of the alloys. Therefore, the Mn content required to prevent the formation of β-Al5FeSi was found to be dependent on both the alloy composition and the cooling rate, where the increase of cooling rate led to formation of fine and dispersed α-Fe-IM phase (nucleation promotion), with high number density but low volume fraction (see Figure 86) [189].

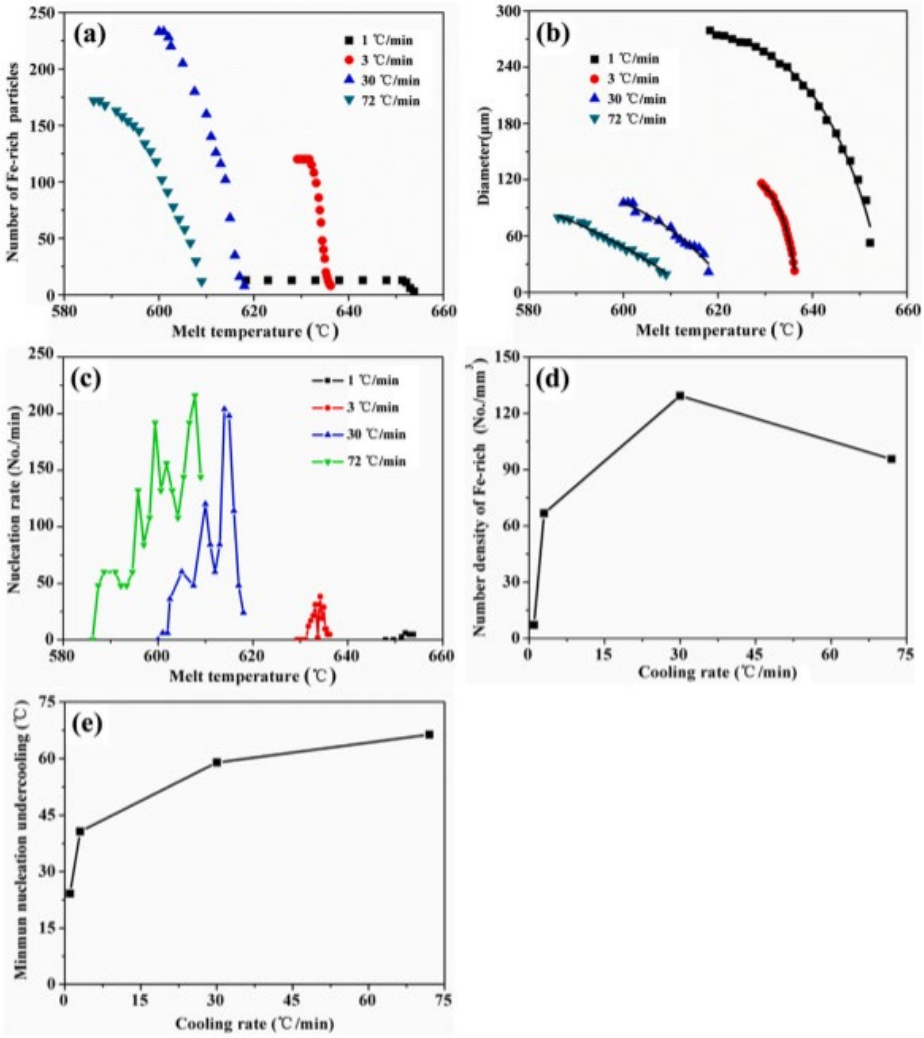

Figure 86: (a) number of primary Fe-rich phases; (b) equivalent diameter of primary Fe-rich phases; (c) nucleation rate of primary Fe-rich phases; (d) number density of primary Fe-rich phases; and (e) minimum nucleation undercooling of primary Fe-rich phases [189].

Another modification of ß-phases was studied by Alkahtani et al. [190] In their work, the addition of Mg to 319 type alloy resulted in the transformation of a significant portion of the β-platelets into the compacted α-Fe script phase ($Al_8Mg_3FeSi_6$). Increasing the Mg content up to 0.45% in the alloy showed a notable positive impact on the alloy's response to heat treatment, particularly in the T5 and T6 tempers. The improved response to heat treatment can be attributed to the combined effect of Cu- and Mg-intermetallic in the 319 alloys. During aging, hardening occurs through the

MIMI Tech GmbH
Preusweg 98, D-52074 Aachen
friedrich@mimi-tech.com

cooperative precipitation of Al_2Cu and Mg_2Si phase particles, and the cooperative precipitation of these phase particles enhances the strength and mechanical properties of the alloy, making it more suitable for the desired applications [190].

In yet another study, Lin et al. [191] investigated the addition of Al–5Ti–B master alloy as a modifier on Fe-rich intermetallic. It was observed that the presence of Al–5Ti–B promoted the formation of α-Fe or refined the existing Fe-rich intermetallic in the alloy [191].

For Al-20Si-1.85Cu-1.05Ni-1.26 Fe alloy, addition of 1.35 wt. % cobalt (Co) leads to formation of plate-like δ-Al4(Fe, Co, Ni)Si2 phase, subsequent solution heat treatment conducted for 7h at 510 °C promotes dissolution of Fe-containing the above mentioned phase [192].

For A380 (Al8.3Si3.5Cu0.15Mg1.9Zn1Fe9.2Mn) alloy, addition of 0.2 wt. % Mn promotes the formation of α-Al15(Fe, Mn)Si phase, in decrement of the β-Al5FeSi phase, the former of which is in bulky shape and believed to be less harmful. When Mn-doped melt was subject to high shear rate melt conditioning technology (HSMC) for 2 min at 3000 rpm, it was found the formed α-Al15(Fe, Mn)Si phase decreases from 137 to 102 µm in dimension. It was proposed melt shearing to molten alloy breaks up oxide films into fine particles in the liquids and disperse them within the melt bath. Those fine particles may act as nuclei for α-Al15(Fe, Mn)Si to form. The more abundant nuclei were found to effectively reduce the undercooling needed to precipitate α-Al15(Fe, Mn)Si phases.

Corrosion

In their research about the Influence of Fe content on corrosion resistance of secondary 3XX cast alloys (Figure 87), Surdova et al. [172] showed that the increased Fe content can lead to a significant reduction in the corrosion resistance of these alloys. From the electrochemical point of view, the Al_5FeSi phase is nobler than the matrix in aqueous media, making the alloy system highly susceptible to localized corrosion [172].

It can be concluded that the critical nucleation sites of the corrosion attack are the Al_5FeSi/silicon needle-like phase interfaces, while the primary Al-matrix remains unaffected. In the eutectic region, corrosion occurs mostly around the Si particles and Fe-phase. Fe and Si are cathodic concerning aluminium and can therefore form a micro galvanic couple together. The silicon and Al_5FeSi needle particles act as local cathodes. The authors also noted that the increase of Fe content also led to a variation of the Si phase size, the latter of which may also have an impact on corrosion resistance of the alloy [172].

The effect of T6 heat treatment was also investigated by the authors. It was found that its effect on the intermetallic phases was manifested as the Fe intermetallic phases were fragmented into smaller formations. The heat treatment, however, did not significantly increased the corrosion resistance of investigated alloys [172].

MIMI Tech GmbH
Preusweg 98, D-52074 Aachen
friedrich@mimi-tech.com

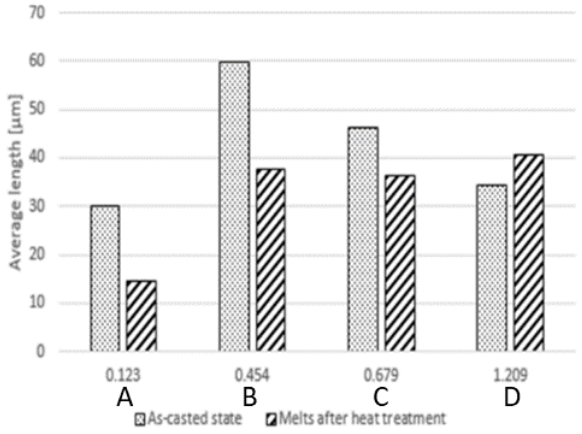

Figure 87: Left: effect of iron content (x-axis) on the average length of Al_5FeSi needles; Bottom: the results of weight changes before and after T6 heat treatment, according to Audi internal PV 11 13 standard (1 dm^3 H_2O + 20g NaCl + 0.1 dm^3 HCl for 2h at 20+-2°C) [172].

Sample	A	A^{T6}	B	B^{T6}	C	C^{T6}	D	D^{T6}
Weight loss	-0.00768	-0.04197	-0.13040	-0.14266	-0.17596	-0.23626	-0.27205	-0.26296

5.1.2.3. 4XX

Mechanical Property

Just like the 3XX series alloys, the presence of Fe-rich intermetallic also negatively impacts the mechanical properties of the 4XX alloys, as the presence of Fe in Al alloys can result in the formation of a long needle-like ß-Al_5FeSi phase, which has a significant impact on the loss of mechanical properties in Al alloys [192], [193]. For example, Silva et at. [194] stated that even a small amount of Fe, such as 0.08 wt.%, can have a detrimental effect on the mechanical behavior of Al-7Si alloy [194].

Sha et al. [192] stated that the transformation of Fe-rich intermetallic into a cuboidal form can negatively affect the mechanical properties of the material, especially when the Fe content is high [192]. In their work, they added Cobalt (Co) to suppress the harmful effect of Fe in Al-Si hypereutectic alloys. Moreover, they investigated the effect of solution heat treatment and found that it had a significant effect on the microstructure and mechanical properties of the alloy[192]. They attributed this improvement due to the fact that as-cast alloys containing coarse plate-like delta-Al_4(Fe, Co, Ni)Si_2 phase exhibit poor mechanical properties, and by increasing the solution heat treatment time up to 7 hours, it led to the replacement and disappearance of this phase, resulting in improved strength and hardness. When the solution heat treatment time is prolonged beyond 7 hours, such as 9 hours, led to the total disappearance of the delta phase, but it also caused the aggregation and coarsening of eutectic silicon particles, resulting in a decrease in ultimate tensile strength (UTS), yield strength, and hardness [192].

In the works of Mikolajczak et al. [195], the role of fluid flow in the formation of the primary Al-phase in AlSi alloys was investigated and it was found that the increase in melt fluid flow has an effect on the length of β-phases in the alloy. It reduces the average length of β phases in the dendritic outer ring of the specimens but increases it in the eutectic center. The fluid flow also affected the primary dendrite stem spacing, reducing its value. However, the secondary dendrite arm spacing remains unaffected by the fluid flow [195].

MIMI Tech GmbH
Preusweg 98, D-52074 Aachen
friedrich@mimi-tech.com

Zhang et al. [196] mentioned that various methods such as rapid solidification, ultrasonic vibration, and the addition of certain elements can suppress the harmful effect of Iron-rich phase. Moreover, elements like Mn, Sc, Be, and Sr have been proven to transform the needle-shaped Fe-rich phase into nodular or Chinese script-like multi-component compounds. Among these elements, Mn is the most effective and extensively studied element for modifying the morphology of the Fe-rich phase and can replace the needle-shaped ß-phase with granular or Chinese script-like alpha-Al(Mn,Fe)Si morphology. In their work, the addition of a 4 wt.% master alloy (Mn/Fe = 0.7) with modified Chinese-script and polyhedral a-Fe phases resulted in the improved mechanical properties, with the ultimate tensile strength (UTS) increasing by 23.8% compared to the Mn-free alloy [196].

In their literature review on the Influence of iron on castability and properties of aluminium silicon alloys, Mbuya et al. [197] identified that there are several paths to neutralize the harmful impacts of Fe in casting alloys. Process Parameters Optimization (cooling rate), Melt Heat Treatment and Solid Solution Heat Treatment, and Iron “Correcting” Elements are among the researched topics [197].

The addition of suitable neutralizing elements like Mn, Cr, Be, Co, Mo, Ni, V, W, Cu, Sr, or rare earth elements have shown mitigating properties on the detrimental effects of Fe in Al-Si alloys. These elements act as iron correctors or neutralizers to modify the nature of Fe-rich intermetallic compounds. The choice of iron-correcting element depends on the specific requirements of the alloy and the desired improvement in properties [197].

Taylor et al. [198] stated in their works that Mn is commonly added to Fe-containing Al-Si alloys to promote the formation of the alpha-phase, reducing the detrimental ß phase. The Mn:Fe ratio is typically at least 0.5, but complete elimination of ß-phase platelets may not always be achieved. Moreover, the addition of Mn can increase the volume fraction of iron intermetallic particles, affecting ductility and causing machining difficulties. Other elements like Co, Mo, Cr, Ni, and Be have been proposed for iron neutralization, but they are not widely used due to cost and health/safety concerns. Strontium, a common eutectic Si modifying element, has a slight refining influence on ß phase size [198].

Silva et al. [194] showed that V (Vanadium) addition promotes a reduction in the area fraction of the ß-AlFeSi phase in aluminum-silicon alloys. The effect of V is more pronounced with faster cooling rates. Also, V plays a role similar to that of Mn in modifying Fe-rich intermetallic and favoring the formation of alpha-Fe phase instead of ß-phase [194]. The addition of 0.5 wt. % V to the Al-7Si-1Fe alloy proved advantageous when combined with fast cooling conditions (Figure 88). Under these conditions, the addition of 0.5 wt.% V improves elongation (ΔL) and ultimate tensile strength (σU), and the hardness of the alloys studied remains practically unaffected by the cooling regime. This method can be a potential alternative for recycling the Al-7Si-1Fe alloy in casting technologies with faster cooling conditions [194].

MIMI Tech GmbH
Preusweg 98, D-52074 Aachen
friedrich@mimi-tech.com

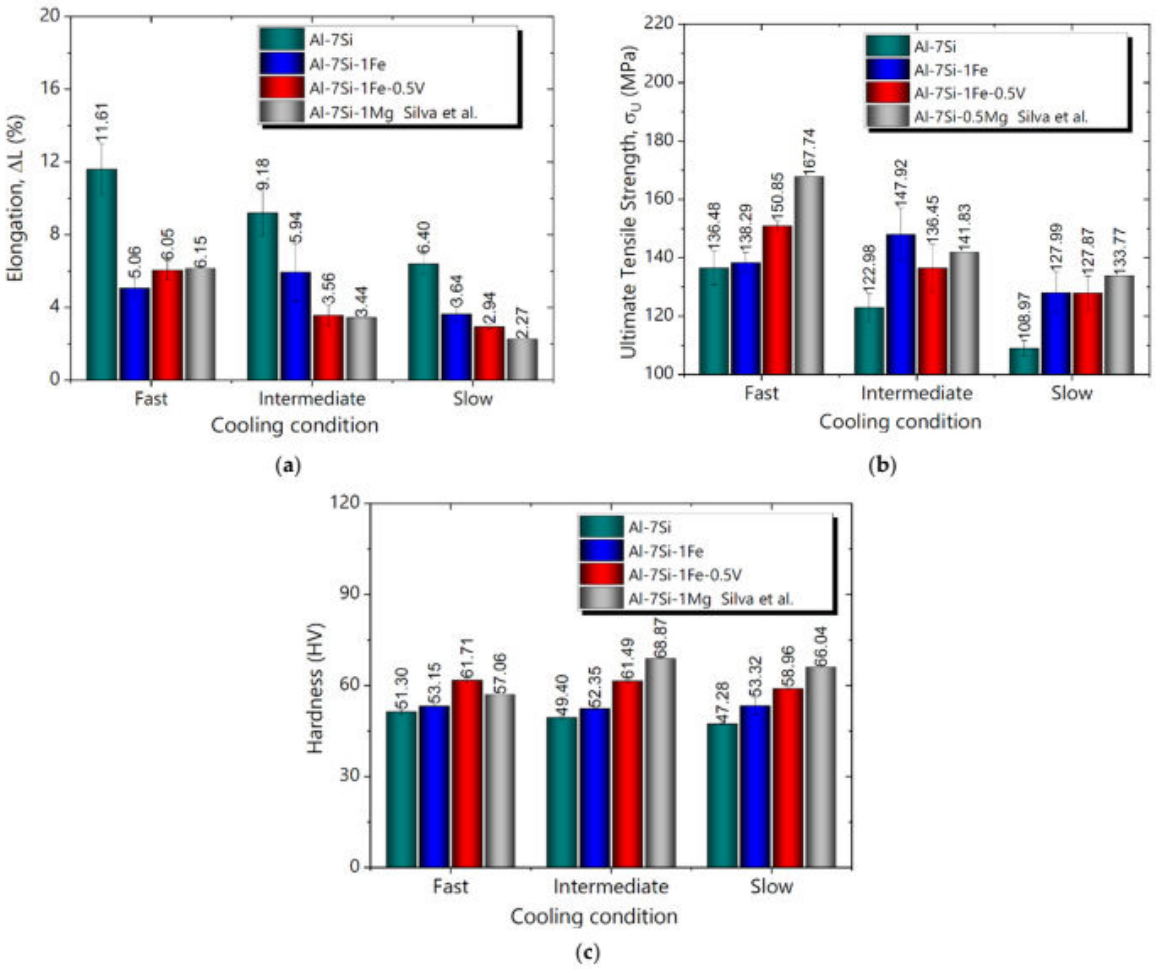

Figure 88: (a) Elongation, (b) ultimate tensile strength and (c) hardness of the Al-7Si-1Fe(-0.5V) alloys considering three different cooling conditions [194].

5.1.2.4. 5XX

Mechanical Property

Mohammed et al. [199] also mentioned that the presence of long needle-shaped β-AlFeSi phases in 5XX alloys has a negative effect on ductility in these alloys. Fe-rich intermetallics, such as Al8Fe2Si with a Chinese script morphology, tend to form at grain boundaries and triple point junctions and acts as stress concentration points, leading to crack initiation and deterioration of ductility and fatigue properties in aluminum alloys [199].

The authors stated that, with the application of heat treatment T6, the ductility and hardening capacity of the alloy increased. However, the yield strength (YS) and ultimate tensile strength (UTS) decreased, showing a typical strength-ductility trade-off relationship. The spheroidization of intermetallic phases, including Mg_2Si and $Al_8(Fe,Mn)_2Si$, was the primary reason for the improved ductility and reduced strength. Overall, the heat-treated condition led to a more desirable microstructure with improved ductility but reduced strength [199].

MIMI Tech GmbH
Preusweg 98, D-52074 Aachen
friedrich@mimi-tech.com

5.1.2.5. 8XX

Mechanical Property

Kong et al. [200] wrote in their research that the presence of coarse and brittle Fe-containing particles in the material serve as crack initiation sites during tensile loading, resulting in deteriorated mechanical properties of the material, leading to reduced lifetime or durability. To neutralize this effect, both Zirconium (Zr) and Erbium (Er) were tested, as they both have an inhibitory effect on the recrystallization process of Al-0.4 wt. % Fe alloy. It was seen that the formation of Al_3Zr or Al_3Er particles contributes to the inhibition of recrystallization [200].

Zr was more effective in inhibiting recrystallization compared to Er due to the preferential precipitation of Al_3Zr. Zr has a significant refining effect on the dendrites of the Al-0.4Fe alloy, leading to smaller dendrite sizes. Er, on the other hand, has a negligible effect on dendrite refining due to the delayed formation of Al3Er during solidification. The low solubility of Er in the alloy is beneficial for enhancing the strength and electrical properties of the Al-0.4Fe alloy. But both Zr and Er showed the ability to modify the morphology of the Al_3Fe particle, transforming it from a needle-like shape to a sphere-like or rod-like shape. This modification of the Al_3Fe phase helps reduce its negative effects on the alloy [200].

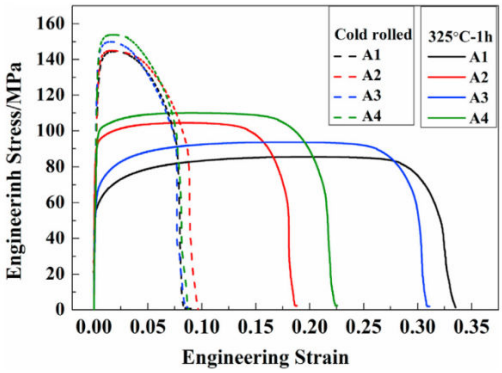

Alloys	Contributions		
	Al_3Fe	Al_3Er	$Al_3(Zr,Er)$
A1	+	–	–
A2	+	–	–
A3	+	+	–
A4	+	+	+

Note: "+" means contribution, and "–" means no contribution.

Figure 89: Left: Tensile properties of investigated alloys in as cold-rolled state and after annealing at 325 C for 1 h; Right: The contributions of secondary particles to strength of cold rolled samples [200].

5.2. Effect of Zinc (Zn)

5.2.1. Wrought alloys

5.2.1.1. 3XXX

Alloy Specification

Kang et al. [201] studied the influence of Zn content on the microstructure of an Al-Mn-Si alloys. It was reported that the presence of Zn in the alloy can decrease ductility. Alloys with high Zn content tend to have a more negative corrosion potential, indicating an increased activity. However, high Zn content can also improve resistance to pitting corrosion. This is because Zn can restrain recrystallization of the alloy, affecting its tensile strength. Tensile test results reveal a significant impact of Zn on the tensile strength of the Al-Mn-Si alloy, with the alloy containing 1.8% Zn having

MIMI Tech GmbH
Preusweg 98, D-52074 Aachen
friedrich@mimi-tech.com

the highest ultimate tensile strength. Zn element has a significant impact on the corrosion potential of the alloy, shifting it in a negative direction when tested with 0.5% NaCl solution. High-density precipitates are also present in the Zn-containing alloys, and the alloy with 1.5% Zn exhibits the most uniform precipitation (compare *Figure 90* below).

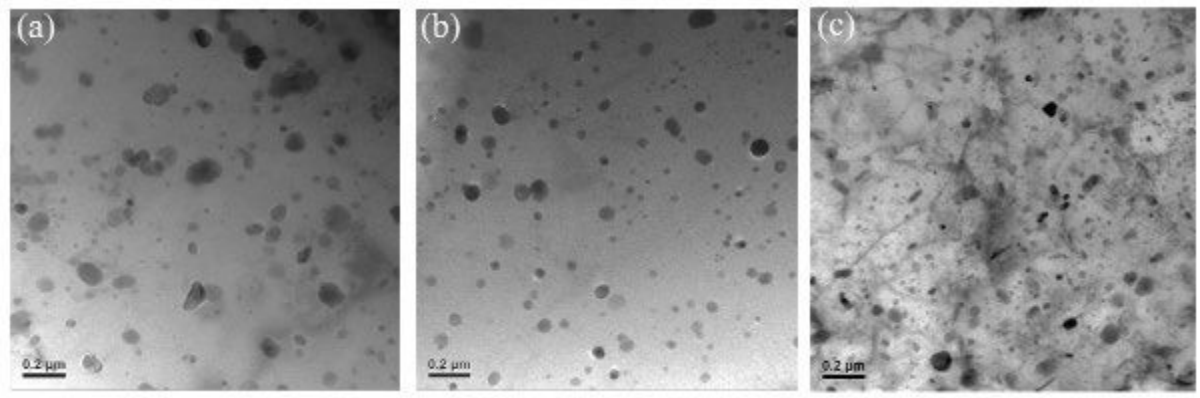

Figure 90: Effect of Zn on the precipitation distribution of the Al-Mn-Si alloy (a) 0% Zn (b) 1.5% Zn, (c) 1.8% Zn

5.2.1.2. 5XXX

Corrosion

Hernandez et al. [202] mentioned in their work on the effect of experimental aging in Al-Mg-Zn alloys that the presence of higher Zn content in the alloy results in increased corrosion behavior, particularly in terms of pitting formation. The heat treatment of these alloys led to the diffusion of elements and the redistribution of phases, which tended to concentrate elements with more negative electrochemical potential in the alloy matrix, leading to an increased reaction area between galvanic couples and ultimately promoting corrosion [202].

Zhang et al. [203] stated in this work that the occurrence of intergranular corrosion (IGC) in 5XXX aluminum alloys is influenced by the continuity of grain boundary precipitates (GBPs), and the addition of zinc (Zn) in Al-Mg alloys can modify the composition of GBPs in these alloys. Modifying the composition of GBPs through the addition of Zn minimizes the electrochemical potential differences between GBPs and the matrix, reducing the likelihood of micro galvanic corrosion and improving the resistance against intergranular corrosion. To achieve that, pre-treatment techniques such as pre-ageing at high temperatures (above 400 °C) have been found to promote the preferential segregation of magnesium (Mg) and zinc (Zn) atoms along grain boundaries in Al-Mg-Zn alloys, significantly improving the intergranular corrosion (IGC) resistance of the alloys [203].

Cold rolling pre-deformation of 20% (expressed as TMP-0 sample) was also performed by the authors on the as-quenched samples, followed by artificial ageing at 150 °C for 0-48 h (TMP-4, TMP-12, TMP-48 represent the alloy aged for 150 C/4 h, 150 C/12 h, 150 C/48 h after pre-deformation, respectively), see Figure 91. In their studies, an as-rolled sample, which underwent pre-deformation without subsequent ageing, showed a significantly lower mass loss of only 2.4 ± 0.43 mg/cm2 compared to the T6 treated alloy with a mass loss of 90.4 ± 0.9 mg/cm2. Furthermore, the yield strength (YS) of the TMP-0 sample was 291.8 MPa, which represents a 94.8% increase compared to the T6 treated alloy. Overall, tailoring the pre-deformation and ageing parameters in Al-Mg-Zn alloys

MIMI Tech GmbH
Preusweg 98, D-52074 Aachen
friedrich@mimi-tech.com

can result in an improved IGC resistance, reduced mass loss, and increased yield strength, providing a high-strength alloy with excellent corrosion resistance [203].

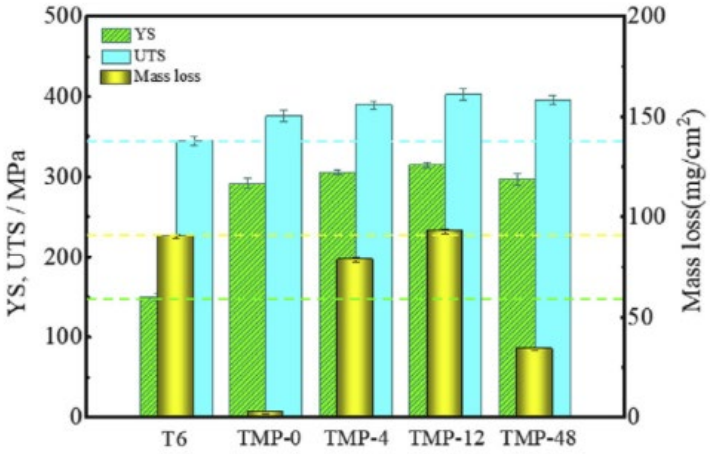

Figure 91: Relevance of mechanical properties and IGC resistance [203].

Workability

Zhu et al. [204] studied the effect of Zn in the microstructure and hot formability of Al-Mg Sheet alloys. They reported that the presence of Zn in solid solution slightly increases the flow stress, making the material harder. However, the addition of Zn decreases the ductility of the material, meaning it becomes less able to deform plastically before fracture. This decrease in ductility is attributed to the anti-recrystallization ability of Zn, which hinders grain boundary migration through the solute drag effect. Overall, the incorporation of Zn in the alloy leads to reduced ductility, indicating a decrease in its ability to undergo plastic deformation.

5.2.1.3. 6XXX

Corrosion

Ma et al. [205], in their work on the aluminum alloy/galvanized steel welded joint, showed that the zinc-rich zone in the welded joint exhibited the highest corrosion sensitivity. In addition, a relatively dense corrosion products film with a thickness of 5 µm was formed on the zinc-rich zone. Despite the corrosion sensitivity, the zinc-rich zone showed a cathodic protective effect on the other parts of the welded joint, but only for a limited immersion period of up to 6 hours. The authors proposed that the corrosion process of dissimilar joints can be categorized into three stages: early corrosion, film rupture, and stable corrosion. As the zinc-rich phases in the zinc-rich zone were consumed, the corrosion pattern of the welded joint shifted from macro-galvanic corrosion to localized corrosion induced by incomplete corrosion products films ($Zn(OH)_2/ZnO$ or $Al(OH)_3/Al_2O_3$) and the presence of second phases (such as Al-Si-Mn-Fe phases, $Al_3Fe_2Si_3$, Al_3Fe_2Si, Fe_2Al_5, and Fe_4Al_{13}) [205].

MIMI Tech GmbH
Preusweg 98, D-52074 Aachen
friedrich@mimi-tech.com

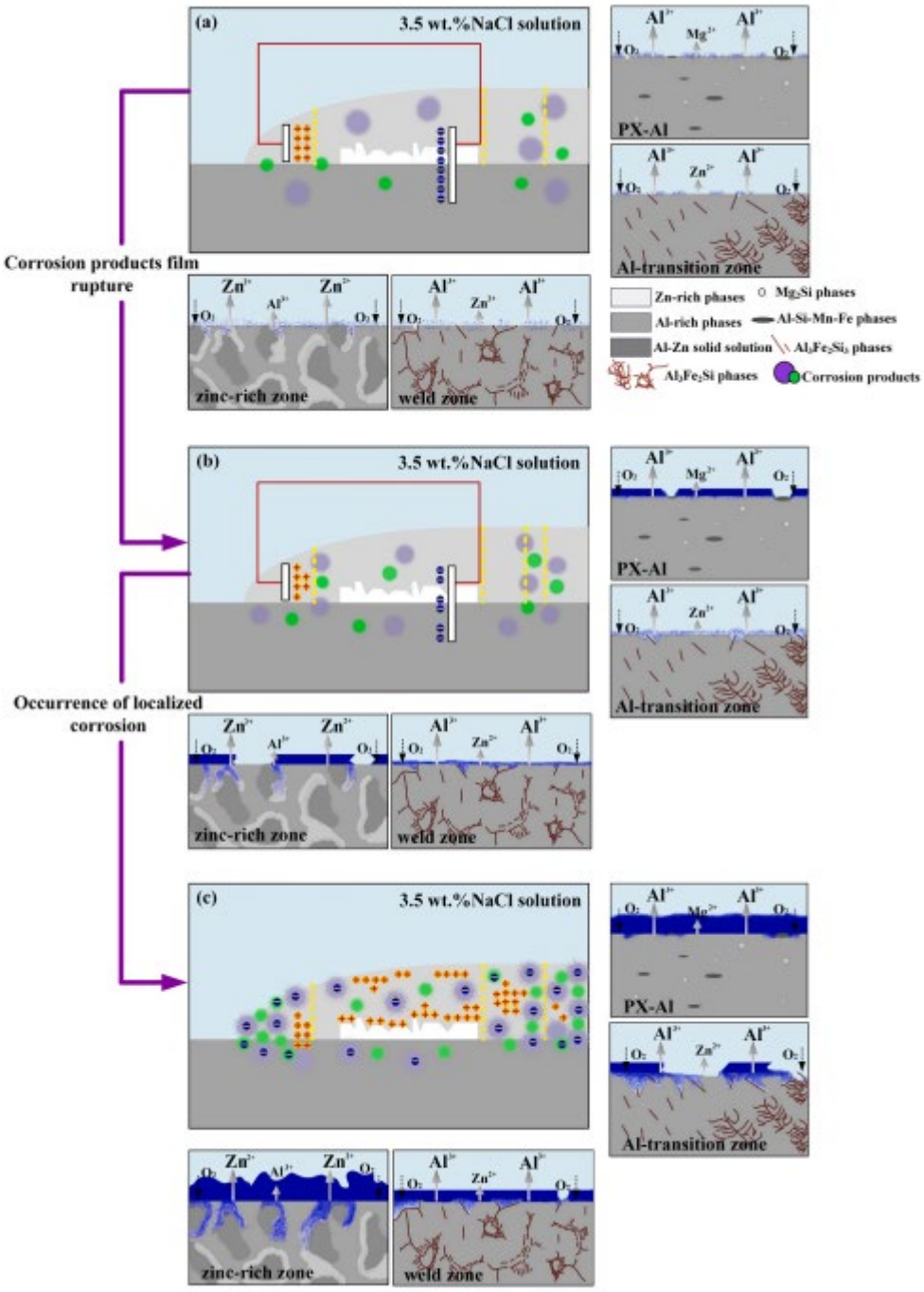

Figure 92: Schematic diagram of corrosion mechanism of aluminium alloy and galvanized steel welded joint after immersion in 3.5 wt.% NaCl solution: (a) at the early stage of corrosion, (b) at the film rupture stage and (c) at the stable stage of corrosion [205].

To enhance the corrosion resistance of the alloy, the authors employed retrogression re-aging (RRA) treatment. The RRA treatment involves the dissolution of some of the precipitates in the alloy and transforming them into discontinuous structures. By making the precipitates discontinuous, the corrosion resistance of the alloy was improved [205].

MIMI Tech GmbH
Preusweg 98, D-52074 Aachen
friedrich@mimi-tech.com

Alloy Specification

Lutz et al.[206] reported the effect of Zn on the grain boundaries in recycled Al-Mg-Si-Cu alloys. In their study, it was found that Zn tends to accumulate in the grain boundary precipitates of the Q phase. The Zn/Cu ratio in the Q phase grain boundary precipitates is significantly higher in the Zn-rich 6063 alloy compared to the Zn-lean 6063 alloy, despite their similar bulk composition in terms of Zn/Cu ratio. In the 6063Z alloy with higher Zn content, there is preferential attack of certain grains, known as preferentially grain etching (PGE). This is attributed to the negligible potential difference between grain boundaries and grains compared to the potential difference between differently oriented grains. Gong et al. [207] on the other hand investigated the pre-aging treatments of similar Al-Mg-Si-Cu alloy with 3wt.% Zn. It was found that the addition of Zn can increase the BHR of the alloys and designed the Al-Mg-Si-Cu-Zn alloys.

Mechanical Properties

Shang et al. [208] focused on the natural ageing behavior and bake hardening of Al-Mg-Si-Cu alloy, from which they reported that The addition of Zn to the alloy does not result in significant partitioning of Zn into clusters or precipitates. During a specific treatment process involving pre-aging (PA), natural aging (NA), and bake hardening (BH), the majority of Zn remains in the Al matrix. This retention of Zn in the Al matrix promotes the transformation of solute clusters into GP (Guinier-Preston) zones and β" phases (compare Figure 93 below). As a result of this transformation and the presence of Zn, the yield strength of the alloy subjected to the PA+NA+BH treatment is higher compared to an alloy without Zn.

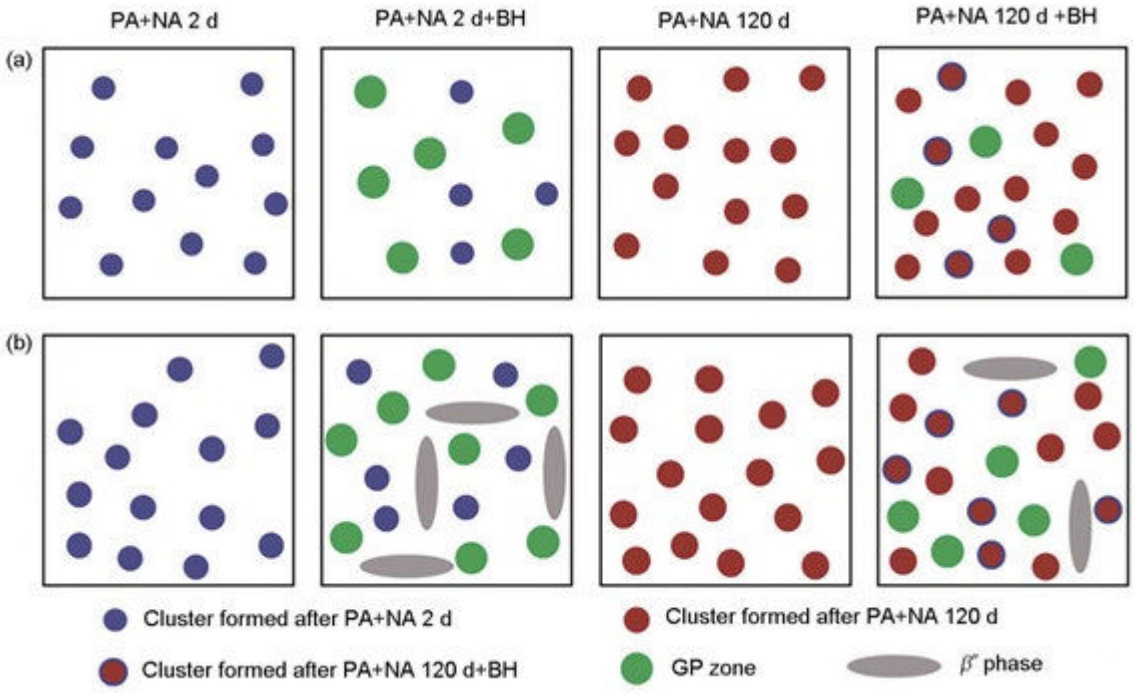

Figure 93 : Illustration of precipitation evolution in the pre-aged (a) Zn free, (b) added Zn, alloys during treatments

5.2.1.4. 7XXX

MIMI Tech GmbH
Preusweg 98, D-52074 Aachen
friedrich@mimi-tech.com

Corrosion

Qiu et al. [209] investigated the Intergranular Corrosion Behavior of 7050 Al Alloys and stated that the intergranular corrosion of 7050 aluminum alloys is strongly influenced by the presence of grain boundary precipitates (GBPs), and the susceptibility to intergranular corrosion is enhanced with the composition of GBPs. During the aging process, the GBPs in the alloy grow through the diffusion of alloying elements. This leads to variations in the size of GBPs and creates a chemical composition heterogeneity in the grain boundary region (see Table 33). The presence of this heterogeneity in chemical components promotes the initiation of corrosion cavities in the grain boundary region [209].

Table 33: Intensity ratio (C_i/C_{Al}) and average potential discrepancy between GBP and matrix in samples with different tempers [209].

Temper	Cu/Al	Mg/Al	Zn/Al	Potential of Matrix (mv)	Potential of GBPs (mv)	Average Potential Discrepancy between GBP and Matrix (mv)
NA	0.04	0.08	0.10	−1330 ± 10	−1490 ± 10	160
PA	0.05	0.10	0.16	−1190 ± 10	−1390 ± 10	200
OA	0.10	0.23	0.41	−1340 ± 10	−1460 ± 10	120

In the study from Ravikumar et al. [210] about corrosion behavior of Al-Zn-Mg-Cu alloy, the authors mentioned that the corrosion rate of this alloy, when subjected to cryo-rolling at -190°C was significantly higher compared to the cast alloy and solutionized alloy tested. The cryo-rolled alloy exhibited a corrosion rate four times higher than the cast alloy and eight times higher than the solutionized alloy [210].

The adverse effect on corrosion resistance was attributed to the synergistic effect of several factors, including the ultra-fine grained structure, the presence of nano/sub-micron size secondary compounds, and enhanced plastic strain induced by cryo-rolling. Cold rolling of this alloy offered a favorable combination of strength (628 MPa) and corrosion resistance (0.512 mm/y) when compared to other processing conditions such as casting, aging, and cryo-rolling (see Table 34) [210].

Table 34: Electrochemical data for Al-12Zn-3Mg-2.5Cu alloy processed under different conditions [210].

Conditions	E_{corr} (V)	I_{corr} (μA)	Corrosion rate (mm/y)
Al-12Zn-3Mg-2.5Cu alloy	−863	11.7	0.785
Cold Rolling	−923	8.68	0.512
Cryorolling (−80°C)	−902	9.28	0.645
Cryorolling (−190°C)	−943	9.62	0.683

The corrosion mechanism in the alloy was predominantly galvanic in nature, indicating that it involved the interaction between different components or phases within the material. The severity of galvanic behavior was influenced by various structural features of the alloy, including the composition of the matrix grains, grain size, presence of secondary compounds, their size and distribution, structural homogeneity, and the presence of structural defects. The solutionized alloy has demonstrated superior corrosion resistance compared to other processing conditions such as cast, aged, and rolled conditions [210].

MIMI Tech GmbH
Preusweg 98, D-52074 Aachen
friedrich@mimi-tech.com

In another study, Liu et al. [211] investigated the corrosion behavior of mechanically polished AA7075-T6 aluminium alloy, and identified that the surface corrosion induced by mechanical polishing was influenced by the formation of continuous zinc- and magnesium-rich segregation bands at grain boundaries in the near-surface layer. These segregation bands have higher zinc and magnesium contents compared to the adjacent matrix regions, creating a micro galvanic coupling between the bands and the matrix, which led to localized corrosion, particularly in the near-surface deformed layer, when the alloy is exposed to aggressive environments like sodium chloride solution [211].

Within the near-surface deformed layer, the typical $MgZn_2$ particles found in the T6 temper were absent. Instead, segregation bands consisting mainly of zinc and magnesium, with a thickness of approximately 10 nm, were developed at the grain boundaries within the near-surface deformed layer, and the presence of these segregation bands promoted localized corrosion along the grain boundaries within the near-surface deformed layer, primarily due to micro galvanic action [211].

To minimize the pitting corrosion, Li et al. [212] proposed a novel two-step PA (pre-aging) treatment, which was developed with the aim of altering the distribution and occurrence state of alloying elements and improving the BH (bake hardening) response. The two-step PA treatment consists of an initial pre-aging step performed at 120 °C for 10 minutes, followed by a subsequent hold at 160 °C for 10 minutes [212].

The effectiveness of this two-step pre-aging treatment was evaluated by comparing it with conventional pre-aging and natural aging (NA) specimens in terms of corrosion resistance. The results showed that the maximum depth of corrosion pit, representing the extent of corrosion, followed the order: two-step pre-aging treatment (33.425 µm) < conventional pre-aging (38.917 µm) < natural aging (49.484 µm). This suggests that the two-step pre-aging treatment resulted in a superior corrosion resistance compared to the conventional pre-aging and natural aging specimens [212].

In their investigation on the corrosion behavior of ultrafine-grained Al-Zn-In alloys for Al-air battery, Linjee et al. [213] found that the presence of high amounts of impurities, such as magnesium (Mg) and zinc (Zn), increases the self-corrosion of aluminum (Al) and reduces the operating voltage of the anode in an Al-air battery. The growth of Al_2ZnO_4 film inhibited the formation of $Al(OH)_3$ film, which resulted in a higher corrosion rate [213].

The use of homogenized heat treatment was effective in reducing micro-segregation of zinc and other trace elements in the Al-Zn-In anodes. This reduced the presence of cathodic regions, leading to increased utilization of the anode. Moreover, the corrosion resistance can be enhanced by refining the grain size through various methods such as grain refiner addition, friction stir processing, and equal channel angular pressing (ECAP). Smaller grain sizes generally result in improved corrosion resistance [213].

Kumar et al. [214] studied the corrosion performance of 7068 aluminum alloy aged using different T6 conditions. The authors stated that the Zn content in 7XXX series alloys affects the aging conditions for achieving peak hardness and SCC (Stress Corrosion Cracking) susceptibility [214].

A Zn/Mg ratio within the range of 2.27% to 2.62% leads to a continuous distribution of second phase precipitates along the grain boundaries in the peak-aged condition, while a ratio of 3.01% to 4.08% results in coarser and intermittent grain boundary precipitates. Alloys with higher zinc content, such

MIMI Tech GmbH
Preusweg 98, D-52074 Aachen
friedrich@mimi-tech.com

as 7068 alloy, exhibit comparable SCC resistance in both peak-aged and over-aged conditions, as they do not have a precipitate free zone (PFZ). Therefore, over-ageing is not necessary for satisfactory SCC performance in these alloys. The T6 specimen, which was aged at 100°C, was most susceptible to SCC due to anodic dissolution of continuous η phase (MgZn2) precipitates along the grain boundaries and embrittlement from hydrogen absorption. In contrast, the specimens that were treated at 120°C and 140°C were less susceptible to SCC because there was an interrupted path for both anodic dissolution and diffusion of hydrogen, thanks to the presence of discontinuous grain boundary precipitates (see Figure 94) [214].

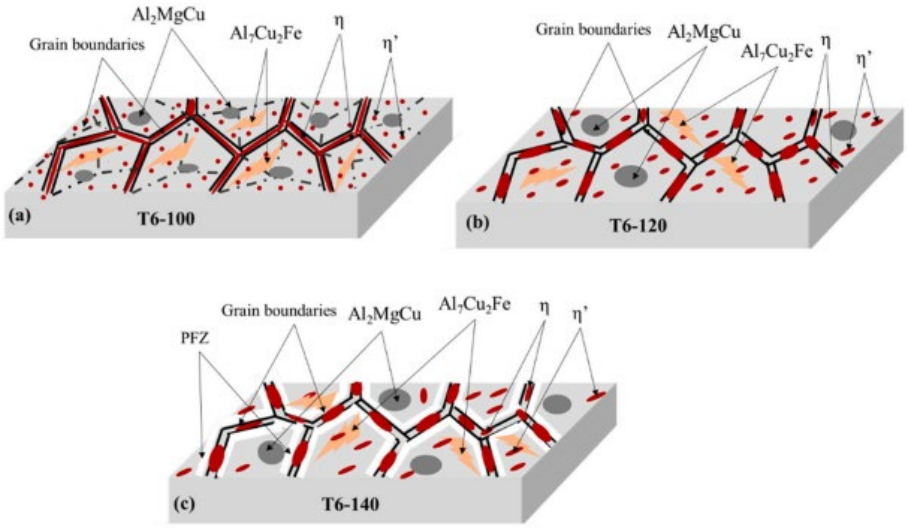

Figure 94: Schematic of the morphology and distribution of second phase precipitates for (a) T6–100, (b) T6–120, and (c) T6–140 condition of 7068 alloy [214].

Dun-Bo et al. [215], in his investigation on the electrochemical corrosion of Al-Zn-Mg aluminum alloy, mentioned that Zn plays a significant role in influencing the corrosion behavior of Al-Zn-Mg alloys, and the presence of zinc can create a potential difference between the precipitates and the matrix, which can lead to localized corrosion phenomena such as pitting corrosion and intergranular corrosion. To enhance the corrosion resistance of Al-Zn-Mg alloys, it is beneficial to reduce the number density and discontinuity of precipitates within the alloy. Forming a grain boundary precipitate-free zone, where there is a lack of precipitates along the grain boundaries, can also contribute to improving the corrosion resistance of the alloy [215].

Guo et al. [216] stated in his study that peak aging treatment can enhance the strength of the alloy [216]. The formation of strengthening phases, specifically η and η' ($MgZn_2$), occurs in both the matrix and along the grain boundaries. However, while these strengthening phases contribute to improved strength, they also increase the susceptibility of the alloy to intergranular corrosion and stress corrosion cracking. The continuous presence of the η phase ($MgZn_2$) along the grain boundaries acts as an anode channel, which further promotes intergranular corrosion. The susceptibility to intergranular corrosion and stress corrosion cracking is a trade-off for achieving higher strength through peak aging treatment [216].

Additionally, Lu et al. [217] observed that increasing the pre-strain from 0% to 3.41% led to an increased susceptibility to exfoliation corrosion (EXCO). However, a slight decrease in susceptibility to EXCO was observed at a higher pre-strain of 7.50%. The coverage ratio of η ($MgZn_2$) phases on high-angle grain boundaries (HAGBs) generally increases with increasing pre-strain, and it may play

MIMI Tech GmbH
Preusweg 98, D-52074 Aachen
friedrich@mimi-tech.com

a dominant role in affecting the resistance to EXCO, rather than the average size of the η phases or the recrystallization fraction. Therefore, the presence and distribution of η ($MgZn_2$) phases on HAGBs have a significant influence on the susceptibility to exfoliation corrosion [217].

Minh Ngo et al. [218] also reinforced that Zn plays a crucial role in the formation of $MgZn_2$ phases, which are responsible for enhancing the mechanical properties of the alloy. However, the authors mentioned that the presence of Zn in the alloy also increases its susceptibility to exfoliation corrosion and intergranular corrosion. The susceptibility to exfoliation and intergranular corrosion limits the application of the alloy in certain contexts where corrosion resistance is critical. Balancing the beneficial effects of Zn on mechanical properties with its negative impact on corrosion resistance is important in the design and application of the alloy. Heat treatment processes such as one-stage and two-stage aging are used to improve the corrosion resistance of the alloy by controlling the size, density and distribution of the Zn-rich phases [218].

Qi et al. [219] also stated in their study that the stress corrosion cracking (SCC) was probably linked to η ($MgZn_2$) phase and alloying elements precipitated on grain boundary. Lower Mg and higher Cu segregation on grain boundary induced by second peak aging treatment were considered to be the reason for better stress corrosion cracking (SCC) behavior [219]. Shen et al. [220] mentioned that the segregation of magnesium (Mg) and zinc (Zn) at the grain boundaries of aluminum alloys can lead to increased susceptibility to stress corrosion cracking (SCC). Moreover, higher contents of Zn and Mg in aluminum alloys, particularly exceeding 7%, can significantly increase the sensitivity of the alloy to SCC [220]. In their work modelling the propertied of Al wrought alloys, Zander et al. [221] demonstrated that the corrosion properties are influenced by the total amount of Zn in the material, including both Zn in solid solution and the presence of the η-phase [221].

As a way to explore the corrosion effect of Zn in Al alloys, Yang et al. [222] mentioned the use of Zn as an alloying element in Al anodes helps to break down the passive Al-oxide film and decrease the potential of these alloys in seawater [222].

Alloy Specification

Chen et al. [223] studied the effect of Zn in super high strength Al-Zn-Mg-Cu alloys. In their study, it was reported that the volume fraction of coarse eutectic-structure increases as the Zn content increases, while the elongation and fracture toughness of alloys decrease as the Zn content increases. The strength of alloys increases as the Zn content increases from 9 wt.% to 10 wt.%, while it does not increase any more as the Zn content increases continuously from 10 wt.% to 11 wt.%. The elongation and fracture toughness of alloys decrease as the Zn content increases in these Al-Zn-Mg-Cu alloys. The SCC (stress-corrosion cracking) resistance decrease as the Zn content increase from 9 wt.% to 10 wt.%, while it changes unobvious as the Zn content increase continuously from 10 wt.% to 11 wt.%. With the increasing Zn content, the amounts of coarse non-equilibrium T (AlZnMgCu) phases increase in the alloy. The T phases hardly dissolve into the matrix during the homogenization and solution treatment, because they are arranging in the grain boundary, align in stringers parallel to the extrusion direction in the quenched state, and exist on the fracture surface of tensile test sample. These T phases are the area of the stress concentration and become the crack source. The T phases may be responsible for the negative effect on properties of high Zn content Al-Zn-Mg-Cu alloys.

MIMI Tech GmbH
Preusweg 98, D-52074 Aachen
friedrich@mimi-tech.com

Workability

Ku et al. [224] investigated the effects of Zn/Mg ratio on the friction stirred process (FSP). In their study, it was found that the presence of higher zinc content in the ZM57 alloy results in a decrease in ductility. This is evidenced by a significant reduction in both ultimate elongation (UE) and total elongation (TE) of the alloy, with values being reduced by approximately 65%.

Tang et al. [225] investigated the effect of Zn content during hot compression deformation. In the study, it was noted that increasing the Zn content in Al–Zn–Mg–Cu alloys enhances their strength but reduces ductility. Hot deformation is commonly used to process ultra-high strength Al–Zn–Mg–Cu alloys with high Zn content to overcome low workability. With higher Zn content, the work hardening rate of Al–Zn–Mg–Cu alloys during early deformation stages accelerates (compare Figure 95 below). This leads to peak stress and hot deformation activation energy initially increase with increasing Zn content and then decrease slightly. Dynamic softening of Al–Zn–Mg–Cu alloys increases gradually at high Z values due to accelerated dynamic precipitation, which primarily causes dynamic softening (compare Figure below).

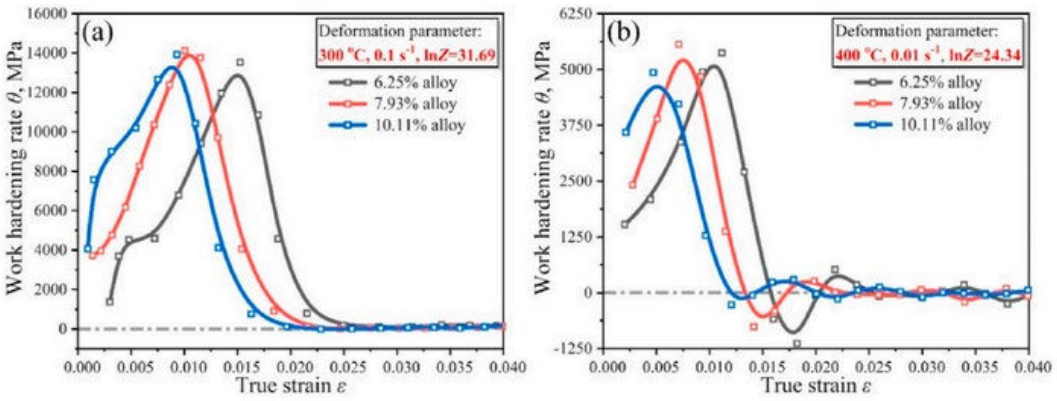

Figure 95 : Work hardening curve of the alloy during hot compression tests, (a) 300°C at 0.1 s^{-1}, (b) 400 °C at 0.01 s^{-1}.

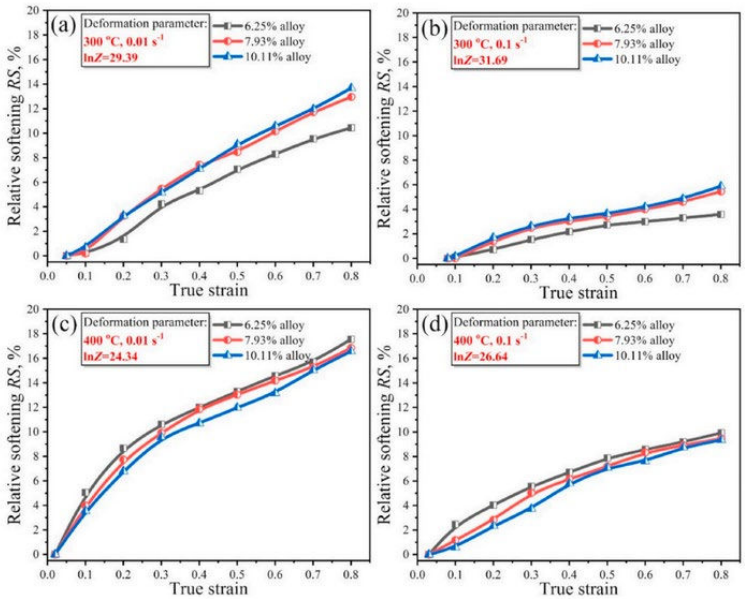

Figure 96 : Relative dynamic softening RS(%) during continuous compression of alloy.

MIMI Tech GmbH
Preusweg 98, D-52074 Aachen
friedrich@mimi-tech.com

5.2.2. Cast alloys

5.2.2.1. 3XX

Alloy Specification

Wang et al. [226] studied the effect of Zn content on the corrosion resistance of Al6Si3Cu alloy, from which they found that the corrosion resistance of the as-cast Al-6Si-3Cu alloy is influenced by the Zn content, initially improving and then deteriorating. The alloy with 0.97 wt.% Zn demonstrates the best corrosion resistance, with a corrosion rate approximately 19.8% lower compared to the Al-6Si-3Cu alloy. The addition of Zn in Al-Si-Cu alloys has two different effects on corrosion resistance. Firstly, Zn addition may form an oxide layer around the Al2Cu phase, enhancing corrosion resistance. Secondly, the addition of 2% Zn alters the morphology of the Al_2Cu phase and promotes Al_2Cu acting as electron transfer channels between Si phases, causing weakened overall corrosion resistance (compare Figure 97 Below). The combination of these two effects results in the optimum corrosion resistance observed in the alloy with approximately 1 wt.% Zn addition.

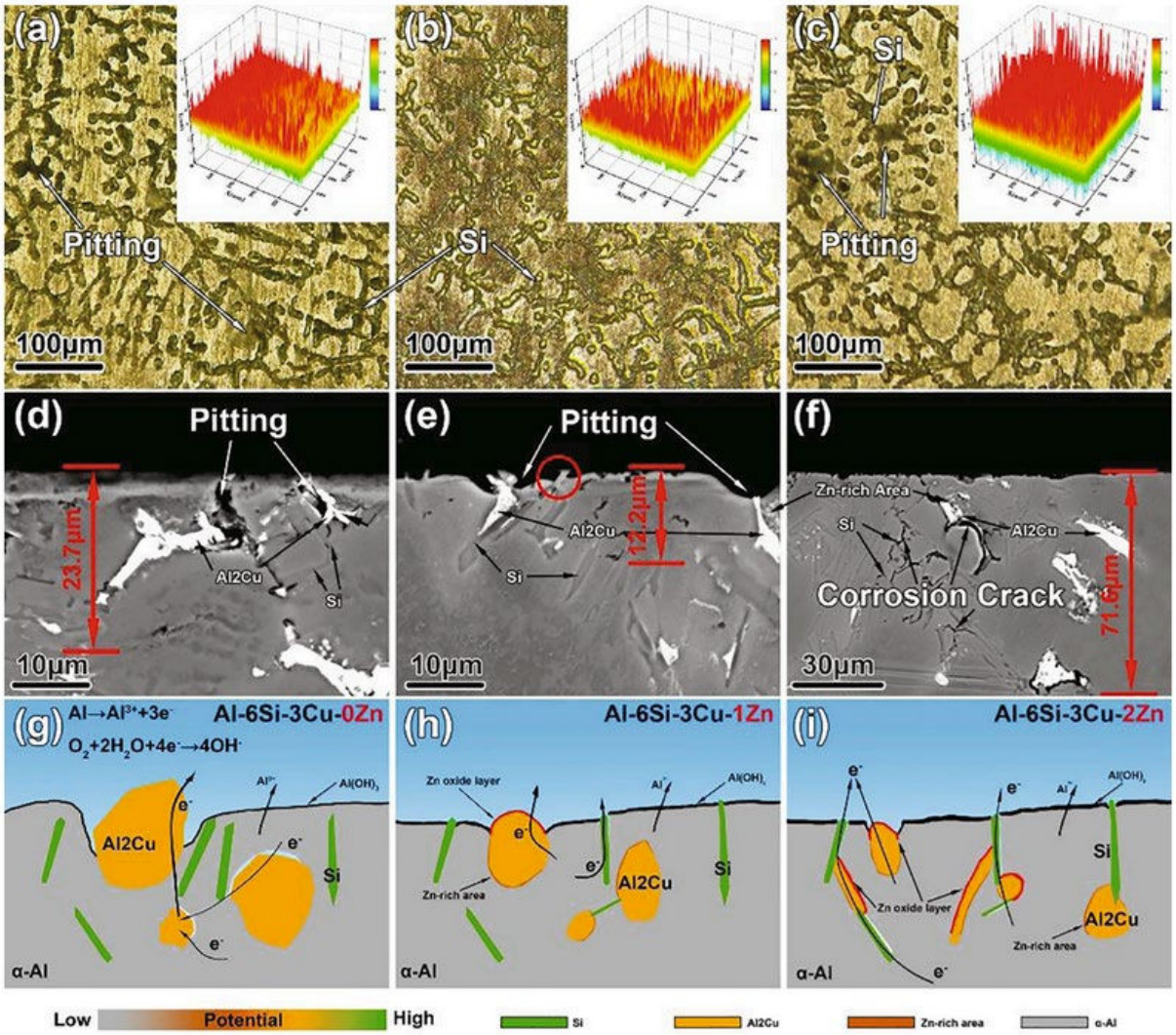

Figure 97 : Microscopic images of the microstructures, (a & d)0.004wt.% Zn, (b & d)0.97 wt.% Zn, (c & f)1.87wt.% Zn, and schematic diagram of corrosion process (g) 0%Zn, (h) 1% Zn, (i) 2% Zn.

MIMI Tech GmbH
Preusweg 98, D-52074 Aachen
friedrich@mimi-tech.com

5.2.2.2. 7XX

Corrosion

Abubakar et al. [227] on their research about the corrosion behavior of recycled Al-Zn-Mg alloy stated that the pitting formation in the alloy was attributed to the presence of second phase $MgZn_2$ (n-phase) particles. These particles have a lower electrode potential than aluminum, causing the aluminum matrix to become more electronegative. As a result, they act as anode sites, promoting localized corrosion and pitting in the alloy [227]. The characterization results indicated that the occurrence of pitting corrosion in the alloy was primarily attributed to the presence of $MgZn_2$ phases. These phases were responsible for initiating and promoting the formation of pits in the alloy's surface. To counteract this effect, the author mentioned that increasing the precipitation hardening time up to 24 hours had a positive effect on both the corrosion rate and anode efficiency in aluminum, as the extended precipitation hardening time leads to the formation of larger and more stable $MgZn_2$ phase particles within the aluminum matrix [227].

Similar results were found by Lameche et al. [228], where he showed that the presence of Zn in aluminum has a significant impact on the propagation and re-passivation of metastable pits. High amounts of Zn enhanced the dissolution kinetics, facilitating the transition to stable pits. Moreover, it was mentioned that Zn influences the behavior of metastable pits in Al-5%Zn alloy, with high amounts of Zn promoting the formation of stable pits. Conversely, low amounts of Zn result in poor activation of aluminum, indicating a reduced tendency for pit formation. The effect of Zn in pitting formation was mainly observed in the kinetics of pit propagation and re-passivation, influencing the transition from metastable to stable pits [228].

Workability

Bayraktar et al.[229] studied the effect of Zn content (5%,15%,25%,35%) on the machinability of Al-Zn alloys. They reported that the decrease in the elongation to fracture in aluminum-zinc (Al-Zn) alloys with increasing zinc content is attributed to the formation of the zinc-rich η phase, which is known to be more brittle than aluminum. The decrease in elongation to fracture indicates a reduction in ductility, suggesting that the alloys become less capable of undergoing plastic deformation before fracture. Increased zinc content in Al(5–35)Zn alloys lead to an increase in hardness and strength. However, this increase in hardness and strength is accompanied by a decrease in elongation to fracture (compare Figure 98 below).

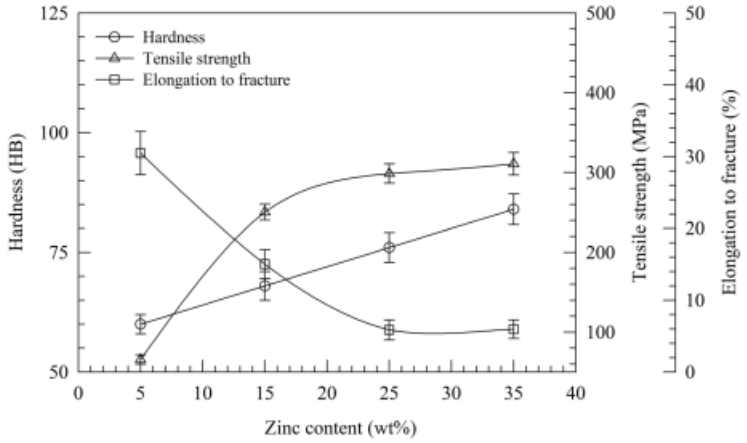

MIMI Tech GmbH
Preusweg 98, D-52074 Aachen
friedrich@mimi-tech.com

Figure 98 : The effect of Zn content on the hardness, tensile strength, and elongation to fracture values.

Quality Impacts

In the same study from Bayraktar et al. [229], they reported that increasing zinc (Zn) content in aluminum alloys leads to a decrease in surface roughness during machining (compare Figure 99 below). Zn-containing Al alloys exhibit superior tribological properties due to their multi-phase microstructures, which consist of both hard and soft phases. The hard phases in the microstructures of zinc-containing alloys bear the load, while the soft phases facilitate sliding, resulting in improved tribological performance. Zinc oxides are formed on the surface of these alloys under the influence of pressure and temperature, particularly in dry friction conditions. The presence of zinc oxides acts as a solid lubricant, facilitating sliding and contributing to the better surface finish of the alloys.

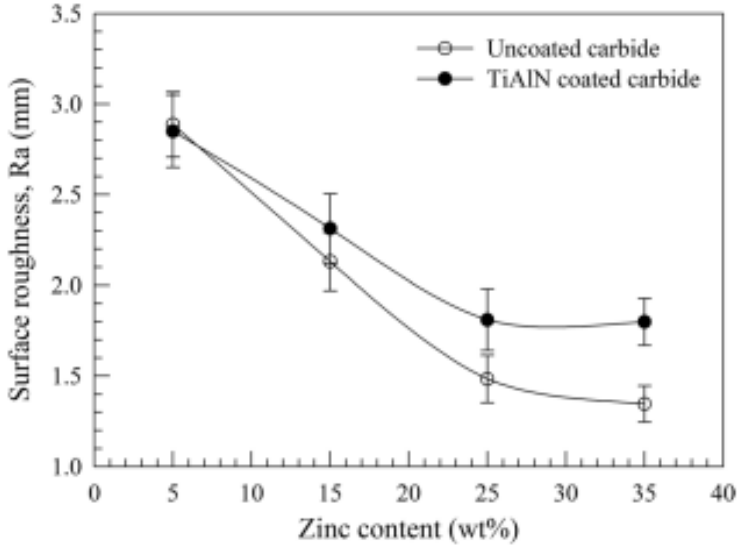

Figure 99 : The effect of Zn content on the surface roughness values.

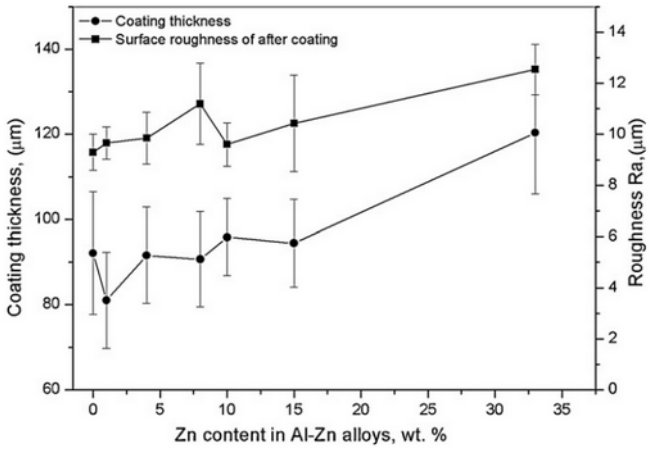

Figure 100 : The effect of Zn content on the coating thickness and surface roughness after coating.

Gencer et al. [230] on the other hand investigated the effect of Zn on the coating behavior of Al-Zn binary alloys. They concluded that the increase in amount of Zn in Al resulted in a rougher surface (compare Figure 100 below). This is due to the alpha-Al_2O_3 phase being observed mainly in the inner

MIMI Tech GmbH
Preusweg 98, D-52074 Aachen
friedrich@mimi-tech.com

region of coating as band of precipitates for low content Zn, these precipitates decrease with increase of Zn and completely disappear with 33 wt.% Zn. Although the coating thickness increased with Zn addition, the formation alpha-Al_2O_3 was suppressed and consequently hardness value of the coatings decreased.

5.3. Effect of Manganese (Mn)

5.3.1. Wrought Alloys

5.3.1.1. 2XXX

Alloy Specification

Zhao et al. [154] studied the precipitation behaviors on the microstructure and fracture toughness of 2024 and 2124 Alloy. The difference between these two alloys lies within the Fe/Mn ratio, with 2024 having 0.24/0.61 and 2124 having 0.08/0.41. Al 2024, characterized by a higher content of impurity elements, exhibited lower tensile strength and fracture toughness compared to Al 2124. The reduced properties in Al 2024 were primarily attributed to the presence of Al7Cu2Fe phases in its matrix. The control of impurity element content is highlighted as a crucial factor in alloy performance. Despite this, the mechanical properties of these alloys can be improved with longer aging times in both alloys. In the peak aging state, the primary precipitations in Al 2124 were S’ and S, while in Al 2024, S’ and S phases were also present, along with the θ phase, which had an impact on mechanical properties.

5.3.1.2. 7XXX

Alloy Specification

Zhang et al. [231] analyzed the intermetallics within a 7A52 Al alloy. The two intermetallics are specifically Al-Mn-Fe and Mg_2Si. Both intermetallic compounds exhibit a negative voltaic potential relative to the matrix, indicating an anodic behavior. This means they are more susceptible to corrosion. Under corrosive conditions, these intermetallic compounds act as corrosion initiation sites, making them prone to dissolution and corrosion. The Al-Mn-Fe intermetallics demonstrate a stronger anodic behavior compared to the Mg2Si intermetallics, indicating that they are more easily corroded. In summary, the study suggests that Al-Mn-Fe intermetallics are particularly vulnerable to corrosion, making them a critical consideration in assessing the overall corrosion behavior of the 7A52 aluminum alloy.

5.3.2. Cast Alloys

5.3.2.1. 3XX

Alloy Specification

Bolibruchova et al. [177] investigated the role of Mn in AlSi7Mg0.3 with high Fe content. They reported that Mn has a positive role in eliminating the negative intermetallic phase β-Al5FeSi. A higher Mn/Fe ratio than traditional recommendations is needed for optimal mechanical

MIMI Tech GmbH
Preusweg 98, D-52074 Aachen
friedrich@mimi-tech.com

characteristics. The best mechanical properties were achieved at a Mn/Fe ratio of >0.64, involving the addition of 0.3 to 0.8 wt. % Mn. Tensile strength and Brinell hardness achieved optimal values for samples with or without heat treatment, despite high iron concentrations. Additionally, the effect of Mn on the crystallization process is reported, where higher manganese content elevated the formation temperature of the β-Al5FeSi phase, causing a change in needle length and morphology with a Mn/Fe ratio > 0.64. The alloy's eutectic silicon formation temperature and solidification temperature were reduced with increased Mn content. The highest Mn content not only influenced iron intermetallic phases but also impacted the morphology of the eutectic silicon.

Bolibruchova et al. [188] studied the role of Mn in mitigating the negative effects of iron in the AlSi7Mg0.3 alloy. The effect of manganese is evaluated across different manganese additions (0.1%, 0.2 %, 0.4 %, and 0.6 % by weight). Higher iron content in the investigated alloys leads to the formation of more intermetallic phases, and this effect becomes more pronounced with higher concentrations of manganese (compare Figure 101 below). The measurements indicate that alloys with the same Mn/Fe ratio can exhibit different structures and characteristics of intermetallic phases which includes but not limited to iron-based, which could have implications for their mechanical properties.

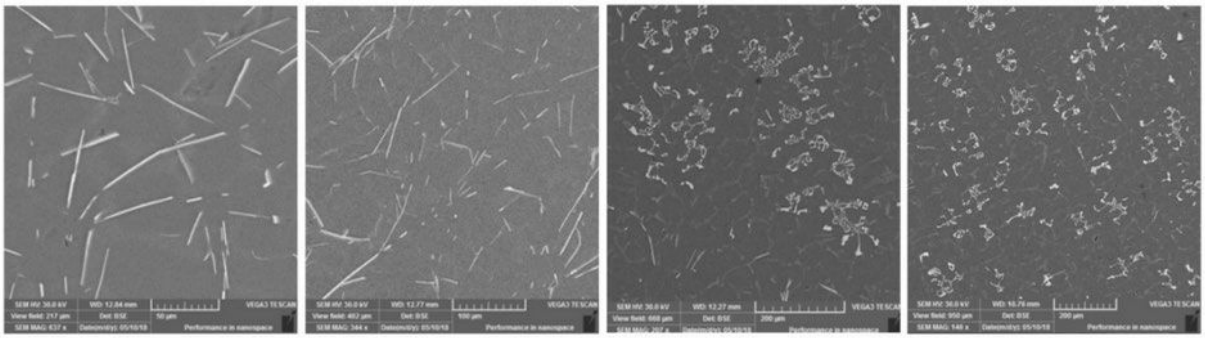

Figure 101 : SEM images of investigated alloys, (a)0.183% Mn, (b) 0.231% Mn, (c) 0.334% Mn, (d) 0.656 % Mn.

5.3.2.2. 4XX

Alloy Specification

Zhang et al. [196] modified an Al17Si2Fe alloy using an Al-Mn-Ti master alloy. The microstructure of the Al–Mn–Ti master alloy consists of a binary quasicrystal matrix and a ternary AlMnTi secondary phase. As the content of the quasicrystal Al–Mn–Ti master alloy increases, the evolution of Fe-rich intermetallic compounds changes: (1) Long needle-shaped b phase for Al–17Si–2Fe alloy, (2) Long plate-shaped ternary d phase with 3 wt.% master alloy addition, (3) Chinese-script and polyhedral a phases with 4 wt.% master alloy addition and (4) Finer plate-shaped quaternary d phase with a phases with 5 wt.% master alloy addition. Adding 4 wt.% master alloy (with a mass ratio of w.Mn/w.Fe ≈ 0.7, compare Figure 102 below) to the Al–17Si–2Fe alloy increases its ultimate tensile strength by 23.8% and reduces the friction coefficient from 0.45 to 0.35 compared to a manganese-free alloy.

5.3.2.3. 5XX

MIMI Tech GmbH
Preusweg 98, D-52074 Aachen
friedrich@mimi-tech.com

Alloy Specification

Mohammed et al. [199] studied the cyclic deformation behavior of a Al4.56Mg1.81Si Alloy. The presence of manganese and other alloying elements influenced the alloy's ductility, hardening capacity, yield stress (YS), and ultimate tensile strength (UTS). The alloy exhibited the Portevin–Le Chatelier effect (serrated flow) during cyclic deformation, attributed to dynamic strain aging caused by interactions between dislocations and precipitates, including those containing manganese. Both the as-cast and heat-treated alloy showed cyclic hardening when the applied total strain amplitude was above 0.4%, with cyclic stabilization below this threshold.

5.3.2.4. 9XX

Alloy Specification

Nadim et al. [232] studied the effect of Mn on the tribological properties of Al15Mg2Si. The behavior of FeMn-rich intermetallics in response to the strains induced by sliding wear plays a significant role in the wear behavior of the composites. In composites with low iron (Fe) content (0.5–1 wt. % Fe), manganese (Mn) promotes the formation of Chinese script a-Al15(Fe,Mn)3Si2 phases instead of harmful b-Al5FeSi platelets. This strengthens the substrate, reduces microcracking, and leads to a more stable tribolayer, resulting in improved wear properties. When the Fe content is higher, Mn modification leads to the formation of primary polyhedral or star-like a-Al15(Fe,Mn)3Si2 compounds in the microstructure. This neutralizes the harmful effect of primary b-Fe crystals on wear behavior. Under friction-induced surface plastic strains, near-surface a-FeMn particles fracture and incorporate into the tribolayer, making it unstable and less protective. Mn modification in composites enhances tribolayer stability, reducing the chances of adhesion between contacting surfaces. This results in a lower average friction coefficient (AFC) and reduced AFC fluctuation under low applied pressures.

MIMI Tech GmbH
Preusweg 98, D-52074 Aachen
friedrich@mimi-tech.com

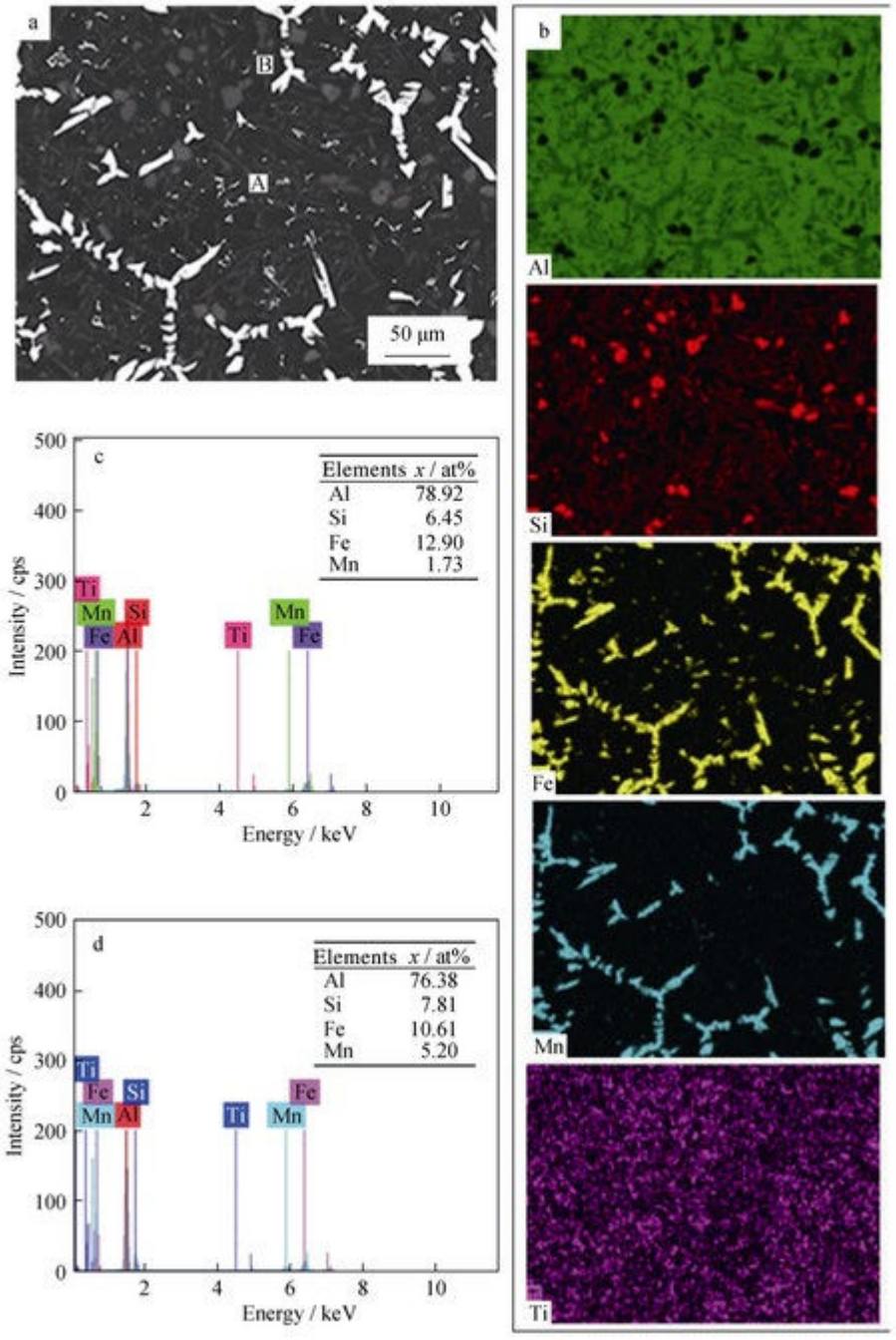

Figure 102 : Microstructure of alloy with 4wt.% Master alloy, (a) SEM image, (b) EDS distribution map (c) &(d) EDS composition of intermetallic compound marked as A and B in (a).

5.4. Effect of Silicon (Si)

5.4.1. Wrought alloys

5.4.1.1. 1XXX

MIMI Tech GmbH
Preusweg 98, D-52074 Aachen
friedrich@mimi-tech.com

Workability

Zhang et al. [233] investigated the effects of Fe and Si on 1235 aluminium sheet with 0.46 wt. % Fe and 0.13 wt. % Si. They reported that Fe and Si from the matrix are crucial microstructural parameters which are found to have marked effects on the formability of aluminium sheets. The fine rod-like phase, β-FeSiAl5, with average size of about 0.2 µm precipitates out from the Al matrix during low temperature additional annealing. The precipitation of this compound could be accelerated by increasing the pre-anneal deformation degree. This type of precipitation, i.e., precipitation of β-FeSiAl5 leads to an increase in the lattice constant of the Al matrix, which is caused by decreased solubility of Si and Fe in the matrix. Annealing at 210 °C is favorable to the precipitation of the compound containing Si and Fe from the matrix. After 15h annealing at 210 °C, the solid solubility of Si is reduced by about 50%. The element Si and Fe staying in aluminium matrix results in a high hardening rate which deteriorates the formability of the sheets. By increasing cold rolling reduction before precipitation annealing, it is possible to provide more nucleation sites for precipitates and therefore accelerates the precipitation process of β-FeSiAl5 phase. As mentioned in the paper, mitigation is possible by pre-annealing. The sheets were produced by direct casting, followed by intermediate annealing at 380 °C for 6h. After that, the sheets were cold rolled to two gauges, 0.35 mm and 0.30 mm, for which the additional annealing was carried on. The gauges for intermediate annealing were 0.6 mm and 1.0 mm, respectively.

5.4.1.2. 5XXX

Workability

Samuel et al. [234] reported that increasing the Si and Fe contents increases the number of coarse intermetallics in the as-cast structure. The main phases observed are Al6(Fe,Mn), Al8(Fe,Mn) Mg2Si in form of Chinese script, with traces of complex ternary eutectic containing Al8Mg5. The increase in the number of coarse intermetallics leads to poor mechanical properties, in particular, the ductility. This limits the alloy formability and amount of applied cold working. Annealing at 520 °C neutralizes negative effect of Si and Fe impurity in terms of elongation, nevertheless it also accelerates spinel formation; The spinel formation starts from outer surface and extends inwards. The addition of Si for a fixed alloy Fe level leads to interaction between Mg2Si and Fe phases, stabilization of the Al15(Fe,Mn)3Si2 phase, and a higher volume fraction of Mg2Si. The effect of heat treatment (8 hours at 520 °C) on the fragmentation and dissolution of intermetallics in CS0 alloy is shown in Figure 103 below. This can be neutralized by homogenization as reported the difference between C alloy (high Fe and Si) as direct casted has elongation of 5 %; while C alloy, 520 °C with 9-hour homogenization, has elongation of 9.5%.

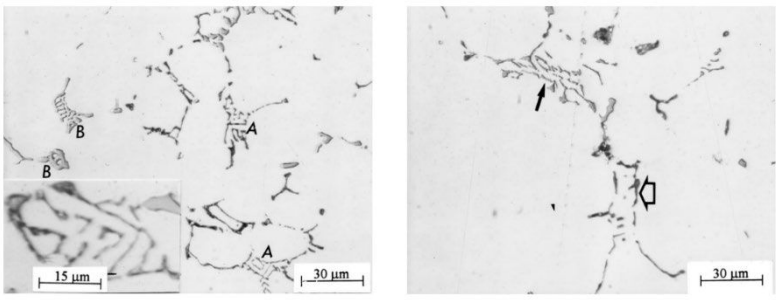

MIMI Tech GmbH
Preusweg 98, D-52074 Aachen
friedrich@mimi-tech.com

Figure 103 : Micrograph showing size and form of intermetallics, (left) before annealing, (right) after annealing.

5.4.1.3. 6XXX

Anodization

Yin et al. [235] studied the effects of Si on the oxidation film in 6061 Al Alloy. They concluded that an excess Si and Mg in the 6061 aluminum alloy have a negative effect on the uniformity of hard anodic oxidation films. The presence of second phases (such as Mg2Si, AlFeMnSi, AlFeSi) in the alloy's basal body contributes to this issue. Aluminum alloys often contain various second phases and elements in solid solution, which can lead to inconsecutive and detached microstructures. During anodizing, the anodic films tend to grow on the second phases, impurities, and basal body rather than on the interface between the alloy and the films. This results in differences in the thickness and hardness of the anodic films, making them uneven across the surface of the alloy.

This effect can be neutralized by controlling the Mg/Si ratio is important for achieving the best uniformity of the anodic film. When the Mg/Si ratio is close to 1.73 and the Mn content is 0.14%, the anodic film exhibits the smallest differences in thickness and hardness. Excessive silicon (Si) content can result in the presence of single Si and (Cu4Mg5Si4Alx) particles in the grain boundaries, leading to rarefactions and discontinuities in the anodic film. The addition of manganese (Mn) can improve the uniformity and consistency of the anodic film by reducing the presence of needle-like Fe-rich and Mg2Si phases and increasing the presence of bone-like Fe-rich phases.

Zhu et al. [236] investigated the effect of Si content and morphology on corrosion resistance of anodized Al-Si alloys. It was found that the corrosion resistance of cast Al-Si alloys after anodizing is influenced by both the Si content and Si particle morphology. The presence of defects such as voids and cracks in regions with lower thicknesses or across the Al dendrite surfaces can provide access of the electrolyte to the substrate, compromising the corrosion protection provided by the oxide layer. Intrinsic stresses and stress gradients inside the anodized layer contribute to the formation of cracks and defects. Higher Si levels in the alloy can decrease corrosion protection due to a higher eutectic fraction on the surface, resulting in a thinner oxide layer and a greater number of defects. The volume expansion of aluminum to aluminum oxide around Si particles that are not fully oxidized introduces localized intrinsic stress, leading to the formation of cracks near the Si particles in the oxide layer (compare Figure 104 below). Si particles in the eutectic region, which are difficult to oxidize during anodizing, can remain embedded as metallic particles in the oxide layer.

Neutralization possibilities are reported as well, where the addition of Sr can change the morphology of Si particles from interconnected flakes to smaller disconnected fibers, leading to improved corrosion protection. The presence of isolated Si fibers within the aluminum oxide results in less stress and fewer cracks during anodizing, contributing to enhanced corrosion resistance. A more compacted oxide layer containing isolated Si particles and fewer cracks leads to improved corrosion resistance in anodized Al-Si alloys.

MIMI Tech GmbH
Preusweg 98, D-52074 Aachen
friedrich@mimi-tech.com

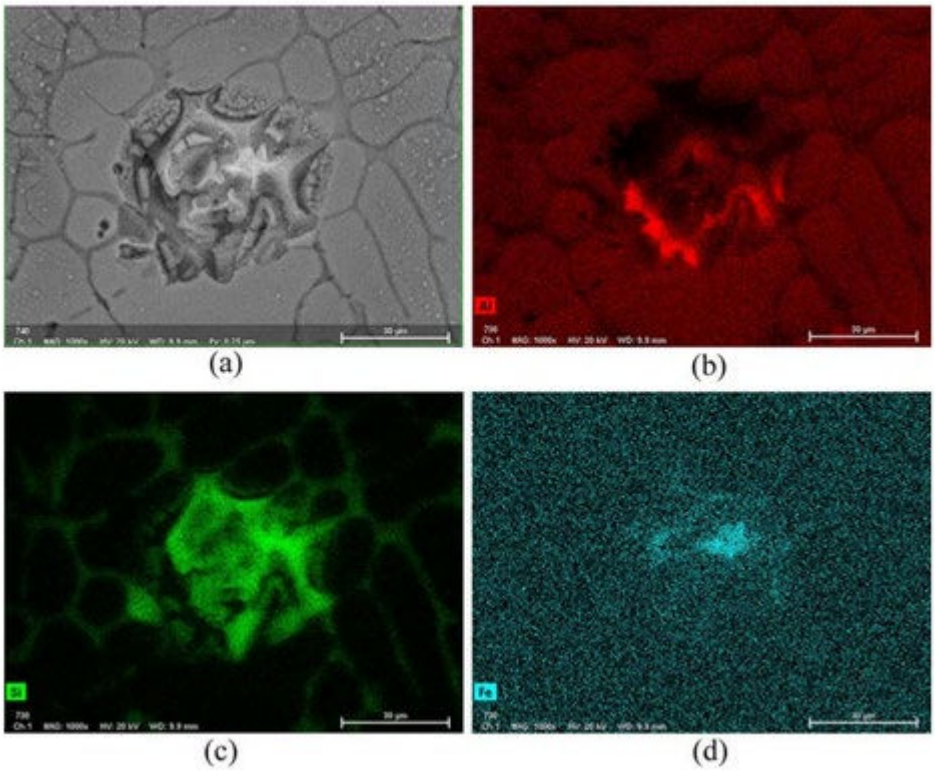

Figure 104 : Corrosion pits in alloy (a) SEM image, (b) Al mapping, (c) Si mapping, (d) Fe mapping.

Further on the corrosion, 3.5 wt. % NaCl was used by Arthanari et al. [237] to evaluate the corrosion resistance of Al-Si-Mg-Zn alloys (compare Table 35 below for composition) . Several key points were reported, firstly, the addition of silicon (Si) in the alloy results in the formation of a pure eutectic phase at the grain boundaries due to its limited solubility in aluminum (Al). This eutectic phase acts as a cathode, promoting the dissolution of aluminum during corrosion. As a result, the formation of a stable anodization layer is inhibited. Secondly, the alloy with lower I_{corr} (corrosion current) values, such as alloy 2, exhibits better corrosion resistance compared to alloys 1 and 3 (compare Figure 105 below). The increase in I_{corr} value in alloys 1 and 3 can be attributed to the presence of cathodic Si and anodic Mg2Si phases. During corrosion, the anodic phase (Mg2Si) dissolves, followed by the dissolution of the Al matrix. This prevents the formation of a stable surface layer. The selective dissolution of magnesium (Mg) from the Mg2Si phase during corrosion leads to the enrichment of the Si phase at the grain boundaries (compare Figure below). This enrichment of Si at the grain boundaries further accelerates the corrosion of alloy 3. The presence of the anodic Mg2Si phase, along with pure Si, is responsible for the poor corrosion resistance of alloy 3. The combined presence of these phases hinders the formation of a protective oxide layer, leading to reduced corrosion resistance

Table 35 : Chemical composition of the investigated alloys

Alloy	Si in wt.%	Mg in wt.%	Zn in wt.%	Al in wt.%
1	8.26	-	0.49	91.3
2	9.49	-	0.96	89.6
3	10.3	0.85	1.36	87.5

MIMI Tech GmbH
Preusweg 98, D-52074 Aachen
friedrich@mimi-tech.com

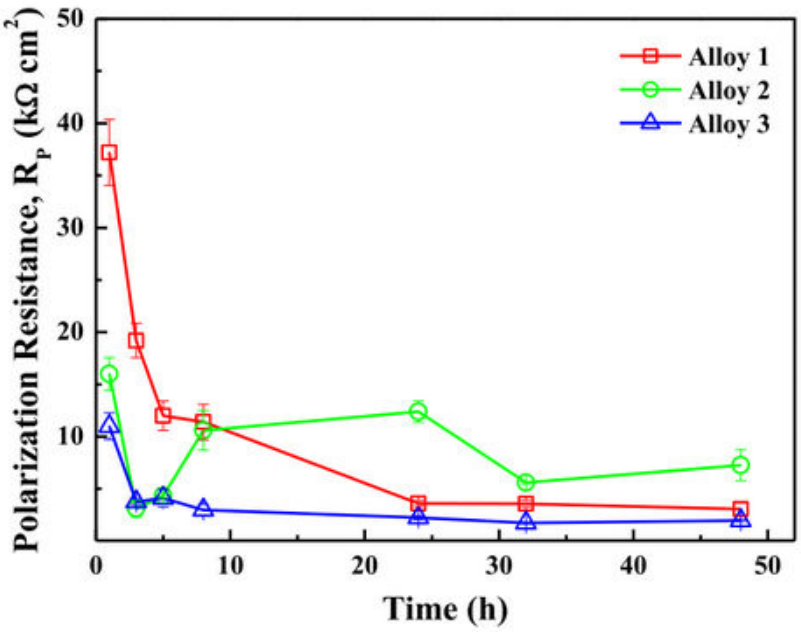

Figure 105 : Change in polarization resistance (R_p) values with different duration in NaCl solution.

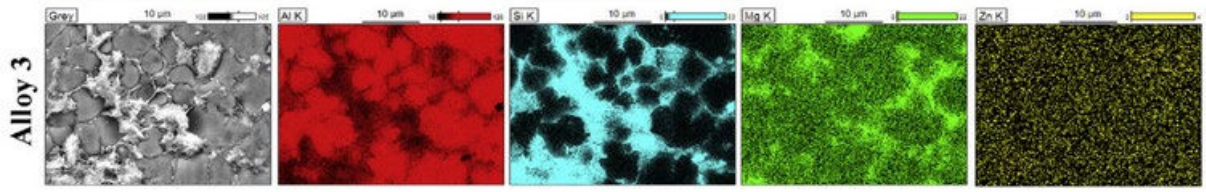

Figure 106 : (a) SEM Image, (b) Al mapping, (c) Si mapping, (d) Mg mapping, (e) Zn mapping.

Regarding anodization, Shi et al. [238] investigated the pretreatment process via alkaline etching on Al-Mg-Si alloy. Alkaline etching as an important step in the anodizing pretreatment for aluminum alloys can effectively remove the dirt and natural oxide film on the matrix surface. Since silicon has the ability to form intermetallic compounds with elements like iron, copper, and magnesium. These intermetallic compounds can be present in the alloy surface and may have an impact on the microstructure and electrochemical properties. During anodization, there is a possibility that these intermetallic particles become embedded in the anodic film, leading to the formation of larger defects or irregularities. Pretreatment via alkaline etching can prevent this from happening. With a 60-second etching time, modifications occur in various microstructures, leading to a faster growth rate (0.39 µm min−1) and improved film integrity. Prolonging etching time to 120 seconds disrupts the regularity of pore order and decreases film growth rate due to excessive corrosion at grain boundaries.

Workability

Bayat et al. [239] studied the phase transformation during homogenization of a 6082 alloy. Reported in the study, intermetallic β-Al5FeSi phase and coarse Mg2Si particles have negative effects on extrudability and workability of 6xxx Al alloy billets. These Mg2Si particle precipitation became visible at the edge and face of beta intermetallic particles at about 250 °C during in-situ heating studies (compare Figure 107 below). At higher temperature some of these Mg2Si particles dissolved while remaining ones became preferred sites for a-Al(FeMn)Si particle nucleation. After nucleation,

MIMI Tech GmbH
Preusweg 98, D-52074 Aachen
friedrich@mimi-tech.com

the a-Al(FeMn)Si particles grow and coarsen via two different modes on the expense of the phase β-Al5FeSi. As-cast billets are homogenized during a heat treatment procedure before extrusion, to neutralize negative effect of intermetallic. It is reported that long homogenization times are required for alloys with a high Si and low Mn content. Generally, the purpose of homogenization include: dissolution of low melting-point Mg2Si and Si particles, which cause tearing during extrusion, to homogenize the alloying concentrations of Mg and Si to decrease the risk of local melting in Mg and Si rich areas during rolling or extrusion; to obtain phase transformation of b-Al5FeSi to a-Al12(Fe,Mn)3Si particles; and spheroidization of a-particles, which will give better extrusion properties. The Mg2Si particles are rather globular and more numerous at the beginning of precipitation (lower temperatures) but become more elongated and fewer at elevated temperatures: while the transformed phases (a-Al(FeMn)Si) become coarser by increasing the temperature, e.g., they can reach to the size of about 1 µm in length at 500 °C. Reported results show that the whole process of homogenization transformation, in the studied samples, is already finished at 450 °C and after less than one hour.

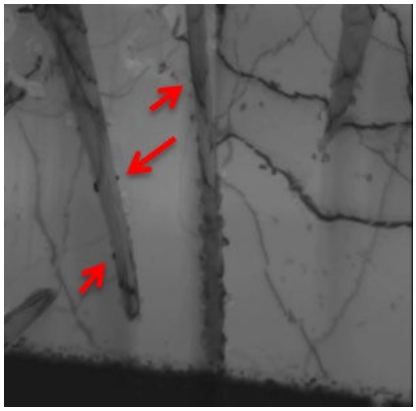

Figure 107 : 6082 alloy phase transformation during heat treatment at 300 °C

Zhong et al. [240] studied the combined effects of alloying elements and heat treatment on the workability of an Al-Mg-Si-Cu alloy. It was reported that increasing Si content and decreasing Mg/Si ratio can raise the tensile ductility and stretch formability of the alloys due to the increased work hardening and strain-rate hardening capability. Particularly, at ~0.43 wt. % Mg, increase of Si from 0.45 to 1.5 wt. % leads to increased flowing limit diagrams (compare Table 2 & Table 3 below), in naturing aging the value is increased from 0.21 to 0.29, for pre-aging it is increased from 0.20 to 0.25.

Table 36 : Tensile properties and FLD0 of alloys after natural ageing for 1 week

Alloy	σ_Y/MPa	σ_{UTS}/MPa	ε_u/%	ε_t/%	FLD_0
A2	136	251	23.6	33.8	0.22
A3	84	183	23.0	33.6	0.21
A4	138	254	25.0	36.7	0.28
A5	147	269	25.2	36.9	0.29
A6	149	264	23.9	35.3	0.25
A7	135	261	24.8	34.3	0.28
A8	157	283	24.8	34.9	0.28
A10	137	262	25.9	37.4	0.28

MIMI Tech GmbH
Preusweg 98, D-52074 Aachen
friedrich@mimi-tech.com

Table 37 :Tensile properties and FLD0 of alloys after pre-ageing for 20 s at 200 °C

Alloy	σ_Y/MPa	σ_{UTS}/MPa	ε_u/%	ε_t/%	FLD_0
A2	132	242	22.0	31.7	0.21
A3	76	168	22.1	31.6	0.20
A4	135	250	24.7	35.6	0.26
A5	140	259	24.8	36.5	0.25
A6	151	264	23.7	35.2	0.24
A7	126	247	24.4	31.3	0.23
A8	150	274	25.0	34.5	0.24
A10	131	255	24.6	34.5	0.24

5.4.1.4. 7xxx

Anodization

On the 7075 alloy as reported by Mukhhophadhyay et la., increased levels of silicon (Si) have a negative impact on the formation of hard anodizing coatings. The presence of Al12(FeMn)3Si-based constituent particles in AA 7075 alloy extrusions hinders the formation and growth of the hard anodic coating. These particles are not affected by the hard anodizing treatment and locally inhibit the growth of the anodic film. The presence of these particles in the anodic film increases electrical resistance, leading to a significant rise in bath voltage during the anodizing process [241]. This can be mitigated by optimizing process parameters, such as Changes in the anodizing electrolyte solution, specifically the addition of hydrochloric acid to the conventional sulphuric acid-oxalic acid system, can result in a stronger electrolyte system. The stronger electrolyte system has the capability to dissolve Al2(FeMn)3Si-based particles during the anodizing treatment. By dissolving these particles, the electrolyte system promotes continuous growth of the anodic film.

Mechanical Properties

Vratnice et al. [242] studied negative impact of Si and Fe impurity on plane-strain fracture toughness of 7xxx aluminium alloys (Al-7Zn-2Mg). The materials were forged to 50 mm thick pancake plate in the T73 condition. It was found the Fe-rich and Si-rich particles play an important role in crack initiation and resultant toughness, although the negative effects of the Fe-rich particles appear strongly. With an increase of Fe+Si level from 0.23 to 0.37, insoluble intermetallic (IM) particles containing Fe and Si increase in amount and size whilst decrease in spacing. As a result, extent of coarse voiding at IM phase sites increases systematically, leading to rupture of the forgings. The identified Si-rich particles include: (Fe, Cr, Mn, Cu)3SiAl12, Mg2Si; (Fe,Cr,Mn,Cu)3SiAl12.

5.4.2. Cast Alloys

5.4.2.1. 3XX

Anodization

Revilla et al.[243] reported that the differences in the cell size of aluminum between casting and additive manufacturing materials result in variations in the uniformity and nanoscale roughness of

MIMI Tech GmbH
Preusweg 98, D-52074 Aachen
friedrich@mimi-tech.com

the anodic oxide layer. Additively manufactured (AM) samples exhibit a smoother oxide layer with a finer cell structure compared to cast alloys. The localized increase in silicon particles, particularly around the melt pool during solidification, has a detrimental effect on the formation of the oxide layer. The presence of these silicon particles leads to a decrease in the quality or thickness of the oxide layer. They find that the AM alloy has a finer and more uniform oxide layer than the cast alloy, but also a lower anodizing efficiency due to the higher oxidation of Si in the AM alloy. They also observe that the melt pool borders in the AM alloy have a slightly thinner oxide layer and a different microstructure than the rest of the surface. They conclude that Si plays a significant role in the anodizing mechanism of Al-Si alloys and that its distribution and phase depend on the manufacturing process.

Labisz et al. [244] investigated the effect of silicon on the anodized Al-Si alloy surface. Comparing the AlSi8 alloy and the AlSi9Cu3 alloy, it is observed that the AlSi8 alloy forms a thicker, more homogeneous, and more porous anodic layer than the AlSi9Cu3 alloy. However, the adhesion of the anodic layer to the substrate is lower in the AlSi8 alloy. The presence of increased silicon in the Al-alloy has a negative effect on the thickness and homogeneity of the anodizing coating. As the silicon content increases, the resulting anodic coating becomes thinner and less uniform.

Lee et al. [245] looked in to a self-sealing anodization approach, and found that Si in the alloy composition can lead to inhomogeneity and the formation of cracks in the anodized oxide film. Anodizing die-cast aluminum alloys with high Si or Cu content at high anodization potentials can be challenging as it is difficult to achieve homogenous films without cracks or defects. This can be neutralized by process optimization. They reported that changes in the anodizing electrolyte solution can have a significant impact on the resulting anodic films. Electrolytes with a high concentration of AlO_2^- anions, derived from $NaAlO_2$, were found to greatly improve the surface morphology and thickness uniformity of the anodic films.

Fom et al. [246] found that hard anodizing of cast aluminum alloys poses challenges in achieving a thick and uniform anodic oxide layer. The presence of silicon in the A357 alloy results in silicon being present in the alloy matrix and as separate elemental silicon particles, which behave differently during anodic film formation compared to the surrounding aluminum matrix. In this study, the anodic oxidation layer on T6 substrates contained spheroidized silicon particles and needle-like β-AlFeSi intermetallics. Once again, neutralization is possible by process optimization. This can be done by performing a solution treatment as part of the T6 treatment on A357 substrates produced by thixocasting can enhance the thickness and uniformity of the anodic oxide layer. Thixocasting, compared to conventional castings, results in reduced porosity and a lower amount of trapped gas in the cast components. The reduction in porosity and trapped gas enables heat treatment of the cast components without blistering. The chemical reactivity of the surface of the cast components also undergoes changes. The study suggests that changes in the casting process, specifically employing thixocasting and subsequent solution treatment, offer the potential for improving the quality and characteristics of the anodic oxide layer.

Fratila-Apachitei et al. [247] tested Vickers micro-hardness of the anodic oxide layer formed in H_2SO_4. The presence of silicon in the aluminum matrix led to a significant drop in the microhardness of the anodic oxide layers compared to pure aluminum. The microhardness decreased from 18HV for pure aluminum to 8HV for AlSi10 alloy. On the other hand, the addition of silicon and copper to the aluminum matrix resulted in an increase in the microhardness of the bulk substrate. However,

MIMI Tech GmbH
Preusweg 98, D-52074 Aachen
friedrich@mimi-tech.com

this beneficial effect did not extend to the microhardness of the oxide layers. In fact, the presence of both silicon and copper as constituent particles in the aluminum matrix had a detrimental effect on the microhardness of the oxide layers.

Mohedano et al.[248] reported that the presence of elemental silicon particles in Al-Si alloys can impede the formation of a continuous anodic film. This is attributed to the generation of oxygen gas that becomes trapped within the coating. In the case of Al-Si alloys, the varying oxidation rates between the silicon-rich phase and the aluminum-rich phase within the alloy matrix negatively affect the structure of conventional plasma electrolytic oxidation (PEO) coatings. Process optimization once again plays a role in mitigating this negative effect. Plasma Electrolytic Oxidation (PEO) coatings can be developed on A356 aluminum alloys with a pre-anodized layer. The PEO coatings exhibit a relatively uniform thickness, with only a slight decrease observed over the eutectic areas of the alloy. X-ray elemental mapping analysis of the PEO coatings revealed two distinct layers: An outer layer rich in Si, an inner layer, denser in nature, primarily composed of Al and O elements.

Caliari et al. [249] investigated the influence of microstructure and surface finishing on the hard anodizing of diecast Al-Si-Cu alloy. Several findings were reported by the authors. Firstly, eutectic Si and intermetallic particles, including Mg2Si, β-Al5FeSi, α-Al(Fe,Mn,Cr)Si, and Al2Cu phases, have a negative impact on the anodizing process. Secondly, surface Si segregation in casting regions can result in non-homogeneous distribution of eutectic Si, with thicknesses ranging from 0.7 to 1.1 mm. Lastly, higher eutectic Si content in the substrate can lead to thinner oxide layers and surface damages during anodizing. These surface damages can manifest as aesthetical defects, such as colored spots, on the casting surface.

5.4.2.2. 4XX

Anodization

Zhu et al. [250] studied the hardness and corrosion behavior of anodized Al-Si alloy. The authors reported that the Al-Si eutectic region can cause localized thinning of the oxide layer formed during anodization. Corrosion attacks often initiate in the area of the Al-Si eutectic region, leading to a thinner oxide layer in that region. Second phase particles, such as silicon (Si) particles and Fe-rich intermetallics, have different effects during anodizing. Si particles tend to remain embedded in the oxide layer, while Fe-rich intermetallics dissolve, leading to the formation of defective regions within the oxide layer.

This can be neutralized by alloying with Sr. The addition of Sr is aimed at modifying the morphology of silicon (Si) particles in the eutectic region. Typically, Si particles in the eutectic region have an interconnected plate-like structure. The addition of Sr helps transform the morphology of Si particles from interconnected plates to more disconnected fibers. This modification in Si particle morphology has been found to be advantageous in enhancing the quality of the anodized layer.

Hazzazi et al. compared the corrosion behavior with and without Si content in the alloys. It was reported that alloying Al with Si enhances its resistance to pitting corrosion in aggressive perchlorate solutions. During localized dissolution, the preferential dissolution of Al leaves the alloy surface enriched in unreactive Si atoms. The enrichment of the alloy surface with unreactive Si atoms hinders the dissolution process by blocking active sites available for Al dissolution. Pitting corrosion ceases when the dissolution is retarded due to the presence of unreactive Si atoms on the surface.

MIMI Tech GmbH
Preusweg 98, D-52074 Aachen
friedrich@mimi-tech.com

To reactivate pitting corrosion, the potential must be further increased (to (E_pit)_alloy) to initiate dissolution at less favorable sites. With an increased Si content, Si atoms appear more frequently on the surface, leading to a further retardation of the dissolution process. Consequently, the (E_pit) alloy, the potential required for pitting to recommence, must increase with higher Si content in the alloy.

5.5. Effect of Vanadium (V)

5.5.1. Wrought alloys

5.5.1.1. 1XXX

Conductivity

In the study from Khaliq et al. [251] about the thermodynamic and kinetic analysis of boride formation in Al alloys, the authors stated that the presence of transition metal impurities, like vanadium (V), dissolved in aluminum (Al), degrades the electrical conductivity of smelter-grade aluminum. This is evident in a 0.28 μΩ·cm increase in electrical resistivity when just 1 % of vanadium is added to the aluminum. According to the authors, these impurities, particularly vanadium, can be eliminated from the solution through boron treatment (Figure 108), during which borides are formed as a result of their in-situ reaction with boron-bearing substances [251].

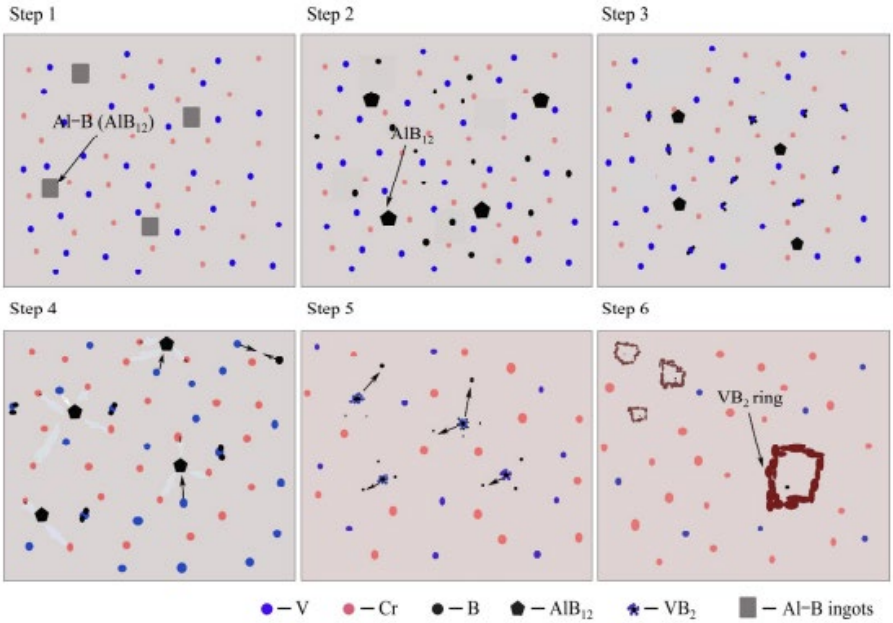

Figure 108: Schematic diagrams of V and Cr interacting with AlB12 master alloy [251].

In industrial operations, it was reported that treating the melt in the launder (Figure 109) using Al-B master alloys is an effective neutralization measure as it helps enhance conductivity of product. It should be pointed out that the treatment operation shown in Figure 109 differs from conventional boron treatment process introduced in Sub-chapter 4.3. As no melt holding was conducted, neither boride agglomeration nor settling will occur. The very fine borides remain in the metal and thus in cast products.

MIMI Tech GmbH
Preusweg 98, D-52074 Aachen
friedrich@mimi-tech.com

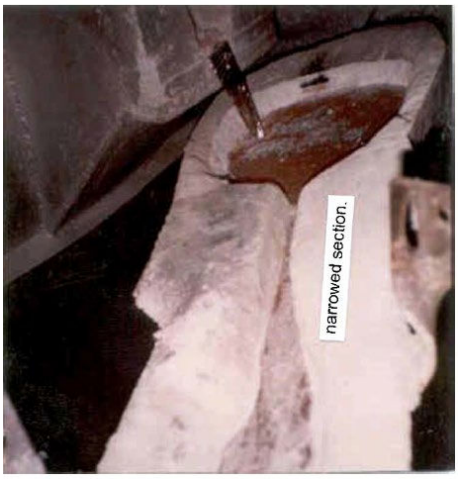

Figure 109: Boron treatment conducted in the launder for neutralizing negative effect of V on conductivity of the product [252].

5.5.1.2. 7XXX

Workability

Shi et al.[253] studied the effect of vanadium on hot workability of 7150 alloy. Three alloys with respectively 0.05, 0.11, and 0.15 wt. % V content were studied, Al21V2 dispersoids were found in the latter two alloys. Two series of hot deformation tests were performed using both V-contained alloy and V-free alloy in the homogenized state. At 450 °C temperature and strain rate 0.01 s^{-1}, it was found increase of V in the alloy leads to decrease of hot workability. At 400 °C-0.001 s^{-1} deformation parameters, even cracking is observed for all V-contained alloys, as is shown in Figure 110. The authors suggested V solute drag and pinning effect of dispersoids on dislocation motion are two of the main reasons responsible for the decrease of hot workability and cracking phenomenon. The optimum hot-working parameters for all 7150 alloys are recommended as 400 °C-0.001 s^{-1}, Deformation is to be avoided at low strain rates between 0.001 and 0.003 s^{-1} in the temperature range of 350-410 °C for the 7150 alloys containing more than 0.05 wt. % V.

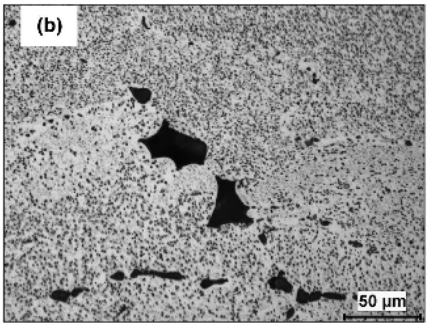

Figure 110: Optical micrograph of 7150 alloy with 0.15 wt. % V, alloy deformed at 400 °C-0.001 s-1 with the true strain of 0.8. Reproduced from [253].

5.5.1.3. 8XXX

MIMI Tech GmbH
Preusweg 98, D-52074 Aachen
friedrich@mimi-tech.com

Quality Impacts

Hao et al. [254] investigated the effect of vanadium addition on a Al0.5Cr0.9FeNi2.5Vx (where x varies from 0 to 1.0) alloy. All of the alloys consisting of different components exhibited a single-phase face-centered cubic structure. The introduction of vanadium led to notable changes in the alloy's microstructure, transitioning from dendrites to equiaxed crystals. Additionally, the formation of a layered CrV phase was observed, contributing to improved alloy properties. Friction-wear testing demonstrated that the addition of vanadium reduced wear debris. The sample with a vanadium content of 0.4 exhibited the best friction and wear performance, resulting in shallower surface grooves, reduced worn debris, and an abrasive wear-dominated wear mechanism.

5.6. Effect of Copper (Cu)

5.6.1. Wrought alloys

5.6.1.1. 2XXX

Corrosion

In their paper about the corrosion-fatigue lifetime of 2050 alloy in chlorine solution, Guerin et al. [255] stated that pitting corrosion occurs mainly as a result of galvanic coupling between second phase particles typically containing copper, such as Al–Cu–Fe–Mn intermetallic particles, and the surrounding matrix. The presence of these particles with a higher electrochemical potential lead to the dissolution of the adjacent matrix. The formed pits are prone to initiate fatigue cracks in aluminum alloys under cyclic loading conditions (Figure 111 and Figure 112) [255].

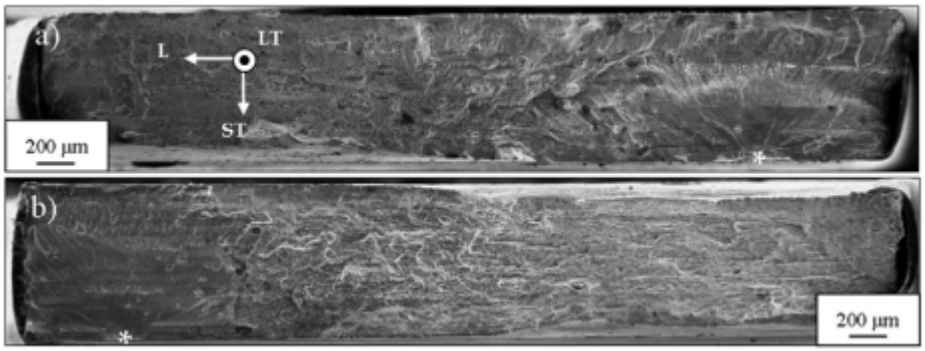

Figure 111: Observations by SEM of the fatigue–corrosion fracture surfaces of AA2050 tested at 20 Hz R = 0.1 for a stress level of 50% YS after a 72 h pre-corrosion treatment: a) T34 state; b) T84 state. White stars indicate the initiation zones [255].

MIMI Tech GmbH
Preusweg 98, D-52074 Aachen
friedrich@mimi-tech.com

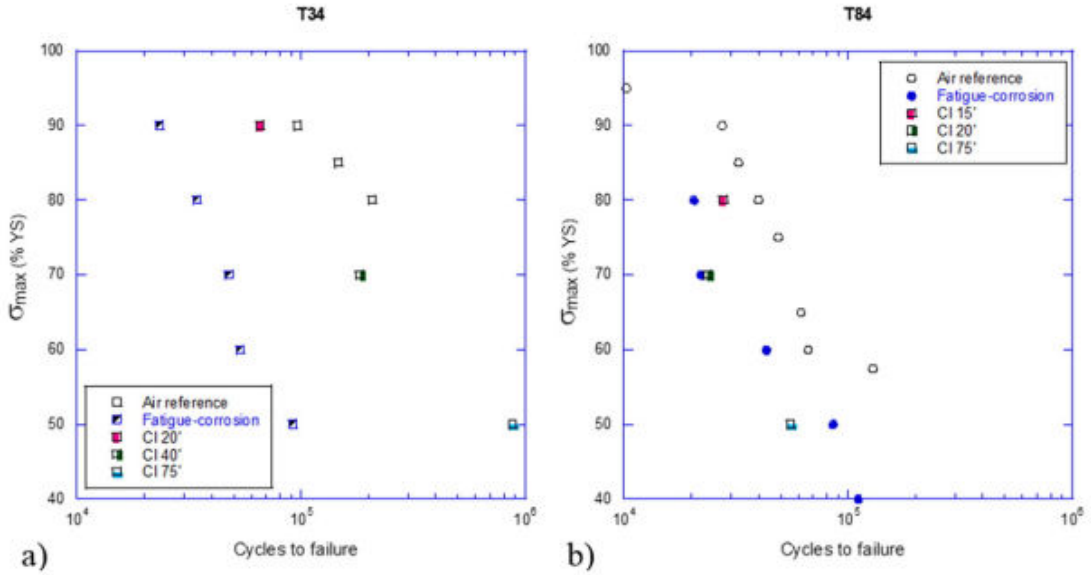

Figure 112: Fatigue–corrosion life curves (σ_{max} (% YS) vs. number of cycles to failure) of a) T34 and b) T84 metallurgical states at 20 Hz R = 0.1. On each graph, results obtained on pre-corroded samples (CI) for short pre-immersion times are given for comparison [255].

It is important to consider the presence and behavior of pits, pitting corrosion, and intergranular corrosion in the design and selection of aluminum alloys to mitigate the initiation and propagation of fatigue cracks and improve overall corrosion resistance. Their findings suggested that the susceptibility to intergranular corrosion was linked to the preferential segregation of alloying elements, primarily copper and/or lithium, at grain boundaries. This segregation creates heterogeneities at the polycrystal scale, making the alloy more prone to intergranular corrosion attack [255].

By changing the heat treatment conditions, it was observed that the corrosion potential of the T84 metallurgical state was significantly lower compared to the T34 state. This decrease in corrosion potential was attributed to the precipitation of the T1 phase within the grains of the T84 state. The T1 phase has a more negative corrosion potential compared to the grains in the T34 state. Additionally, the precipitation of the T1 phase leads to a decrease in the copper content of the solid solution in the heat-treated state, which also contributed to the decrease in corrosion potential of the grains in the T84 metallurgical state. Therefore, the presence and precipitation of the T1 phase in the alloy have a significant impact on its corrosion behavior and potential [255].

Another study made by Fu et al. [256] also reinforced the findings from the previously mentioned research. In their paper, where the corrosion mechanism and fatigue behavior of AA2618-T6 aluminum alloy was studied, and it was also shown that the increased corrosion time and the presence of copper-rich intergranular phases contributed to preferential corrosion of grain boundaries and the formation of erosion pits, primarily concentrated at the grain boundaries. The investigated aluminum alloy matrix and intergranular second-phase particles also showed a tendency to form micro-galvanic couples, which promoted intergranular corrosion [256]. The presence of intergranular second-phase particles affected the diffusion and charge transfer of internal ions during electrochemical corrosion. Moreover, the movement of chloride ions inward

MIMI Tech GmbH
Preusweg 98, D-52074 Aachen
friedrich@mimi-tech.com

was facilitated by the erosion pits, leading to intergranular corrosion. Hence, the existence of a copper-rich phase has an impact on the development of corrosion kinetics [256].

In their paper about the effects of post weld heat treatment on the corrosion behavior of AA2014 alloys, Ramana et al. [257] also stated that, in the annealed (O) condition, the microstructure of the fusion zone consisted of fine grains of $CuAl_2$ eutectics within the dendritic matrix of alpha-solid solution. The eutectics were present within the grains and along the grain boundaries. After applying a post weld heat treatment (PWHT), the author observed that the thickness of the grain boundary eutectics was reduced, and the grains were coarsened in the fusion zone. Furthermore, the pitting corrosion resistance of the partially melted zone (PMZ)/heat-affected zone (HAZ) in PWHT condition was better than that of the annealed condition. This was attributed to copper segregation at the grain boundaries of the PMZ in the annealed condition. The fusion zone also exhibited higher positive E_{pit} (corrosion potential) values compared to the PMZ/HAZ, which was attributed to lower copper enrichment at the dendritic boundaries in the fusion zone compared to the PMZ [257].

5.6.1.2. 7XXX

Corrosion

In their research on the effect of copper content and thermal treatment conditions of fin stock Al alloy (Al-Zn-Mn-Si-Fe-Cu) for heat exchanger, Kang et al. [258] observed that the tensile strength of the alloy sheets increased linearly with an increase in copper content, with an approximate increase of 10-15 MPa per 0.2% copper. This relationship held true regardless of intermediate annealing treatment and final rolling reduction amount. Furthermore, the electrical conductivity of the alloy sheets increased linearly with copper content up to 0.3%. But, beyond 0.3% copper content, there was no significant dependence of electrical conductivity on copper content within the range of 0.3% and 0.5%. There was, however, an increase in corrosion with increasing copper content up to 0.3% in the alloy [258].

When applying a heat treatment involving double annealing, as compared to single annealing, it was observed an impact on the corrosion behavior of the sheets. Single intermediate annealed sheets exhibited significantly lower corrosion potential compared to double intermediate annealed sheets. The corrosion potential value (obtained after the final rolling reduction amount of 30%) for double intermediate annealed sheets after brazing treatment was higher (-537 mV) compared to that of single intermediate annealed sheets (-775 mV) for a 50 µm thick sheet (Figure 113) [258]. The findings suggested that the heat treatment process, specifically the use of double annealing, can influence the corrosion potential and potentially affect the corrosion resistance of the sheets [258].

MIMI Tech GmbH
Preusweg 98, D-52074 Aachen
friedrich@mimi-tech.com

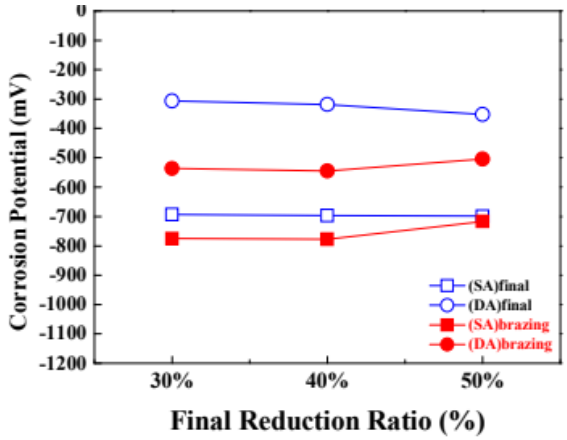

Figure 113: Variation of corrosion potentials with two different intermediate annealing treatments and final rolling amounts for final rolled sheets and brazing treated sheets [258].

Chen et al. [259] studied the corrosion in Al-Zn-Mg-Cu alloy, which are susceptible to localized corrosion, including pitting corrosion, crevice corrosion, intergranular corrosion (IGC), and exfoliation corrosion (EFC). Localized corrosion (LC), particularly in the form of pitting and IGC, is commonly observed in these alloys, especially under under-aged and peak-aged conditions. Pitting and IGC can act as sites for crack initiation, potentially leading to stress corrosion cracking (SCC) or corrosion fatigue failure [259].

The authors identified a two-staged T7x ageing as an effect way in reducing susceptibility to localized corrosion (LC) compared to T6 ageing, although it resulted in a slight reduction in strength (10-30%). The development of T77 ageing provided a method to achieve satisfactory LC resistance without compromising mechanical performance, promoting the use of 7150 and 7055 Al alloys. In their experiments, the improvement in intergranular corrosion (IGC) resistance in the 7085 Al alloy was attributed to larger grain boundary precipitates (GBPs), increased spacing between GBPs, and higher copper (Cu) content within the GBPs. Cu content in GBPs contributes to enhanced IGC resistance [259].

In another research article from Ramgopal et al. [260] on the intergranular corrosion of AA7150 alloy, the author stated that the grain-boundary precipitate $MgZn_2$ (eta phase) present in the alloy is active with respect to the Al matrix. Moreover, the eta phase has solid solubility for both Cu and Al, having a generic composition as Mg(Zn,Cu,Al) [260]. It is known that there is a Cu-depleted zone along the grain boundaries, which is more active than the grain interior. The difference in corrosion potentials between the grain boundary and the grain interiors in the peak-aged temper makes it susceptible to intergranular corrosion (IGC) [260]. In the overaged condition, precipitation of $CuAl_2$ in the matrix eliminates the difference between the grain boundary and the grains in terms of corrosion potential [260].

5.6.1.3. 8XXX

MIMI Tech GmbH
Preusweg 98, D-52074 Aachen
friedrich@mimi-tech.com

Alloy Specification

Mahmood et al. [261] studied the effects on addition of Cu to Al alloy from a range of 1-6% Cu. In the study, the microstructure, hardness, thermal conductivity, and compression were investigated. The effect of adding 6 wt. % Cu resulted in the grain refinement of Al. Other percentages of Cu addition all lead to the formation of Al_2Cu, called coherent particles. Brinell hardness increases linearly with copper addition; max hardness (60 BHN) at 6 wt. % Cu (compare Figure 114 below).

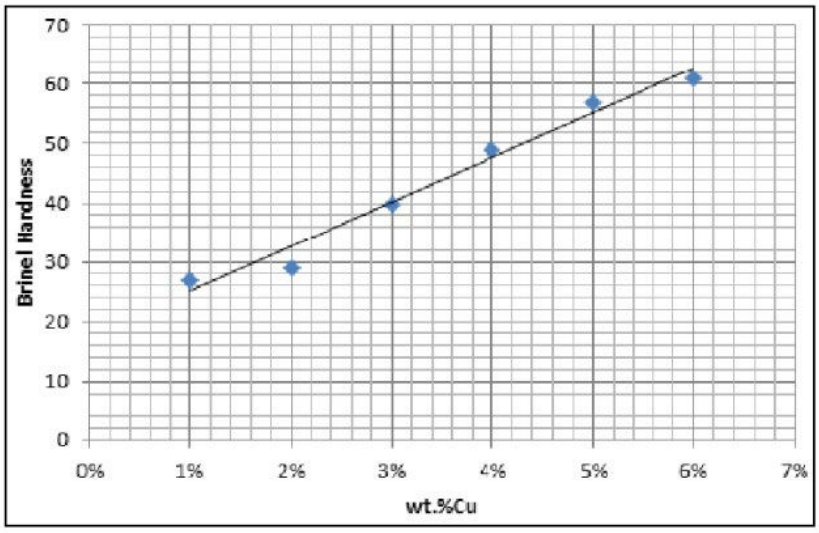

Figure 114 : Relation between Cu content and Brinell hardness test.

Thermal conductivity was reduced by copper addition; highest value at 1 wt. % Cu (166 k). This is due to the formation of Al_2Cu particles, obstructing electron movement at normal temperatures. The relation could be seen in the Figure 115 below:

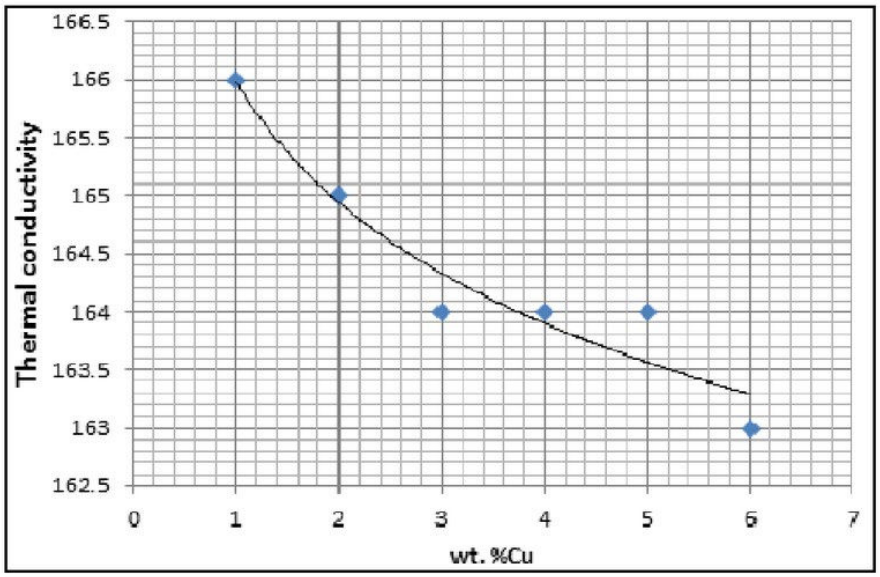

Figure 115 : Relation between Cu content and thermal conductivity.

In the compression test, there is a notable change in the cross-sectional area of the specimens. The diameter increases while the length decreases, which means that lower Cu content i.e., softer Al

MIMI Tech GmbH
Preusweg 98, D-52074 Aachen
friedrich@mimi-tech.com

alloy, can be compressed into thick discs before cracking. Higher Cu content i.e., harder Al alloy, exhibits a clear failure point at 150 MPa, with pronounced cracking observed in 6 wt. % Cu.

5.6.2. Cast alloys

5.6.2.1. 2XX

Corrosion

Stress corrosion is common in aluminum-copper (Al-Cu) based casting alloys such as A206 alloy. The anodic dissolution of grain boundaries is the main mechanism behind stress corrosion in such alloys, where the depletion of copper at grain boundaries during aging leads to grain boundaries acting as anodes and the grains as cathodic sites in the corrosion reaction. Hence, the intergranular corrosion is the main mechanism of corrosion in Al-Cu-based alloys. If was observed that by increasing the number of grain boundaries increases the corrosion rate, indicating that grain boundary attack is the dominant localized corrosion mechanism [262].

In the works from Kordijazi et al. [262], the corrosion resistance improved with increasing solidification time in the alloy. The longer solidification time led to larger grain size in the alloy matrix, and consequently a decrease in the number of grain boundaries observed. Their results (Figure 116) indicated that controlling the solidification time and grain size can be an effective approach to enhance the corrosion resistance of this alloy [262].

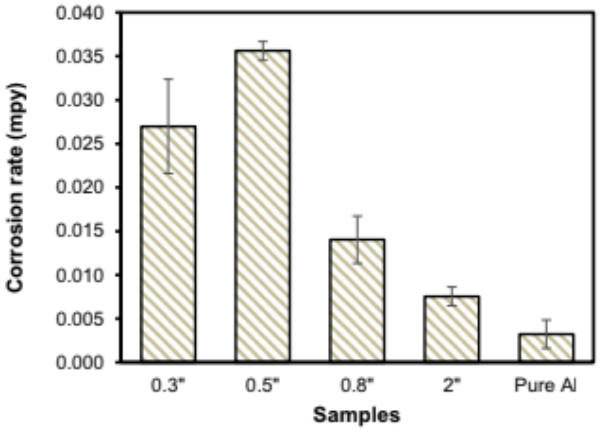

Samples	Corrosion potential (mV)	Corrosion current (μA/cm^2)
0.3″	– 0.69	2.5
0.5″	– 0.68	3.3
0.8″	– 0.66	1.3
2.0″	– 0.64	0.7
Pure Al	– 0.89	0.3

Figure 116: Left: Corrosion rate for A205 samples with different section thicknesses and pure Al; Right: Corrosion current and corrosion potential of A205-T7 Samples and Pure Al [262].

5.6.2.2. 3XX

Corrosion

In the research from Zor et al. [263], the increase in the copper (Cu) content in 3XX alloys was associated with an increase in the rate of intergranular corrosion (IGC). Copper was identified as causing stress corrosion susceptibility in specific compositions, metallurgical conditions, and service environments. The formation of Cu-rich precipitates *Θ*-phase at grain boundaries reduce the intergranular corrosion resistance of the material, and further addition of Cu led to the precipitation of $AlCu_2$ intermetallic phases, which acted as the cathode in a local galvanic cell, causing the

MIMI Tech GmbH
Preusweg 98, D-52074 Aachen
friedrich@mimi-tech.com

initiation of pitting corrosion and dissolution of the metal on the aluminum matrix surrounding the Cu-rich phases. The hydrogen volume evolved by the corroding alloys can be seen in Figure 117 [263]. This effect was also pointed out by Osorio et al. [264], where they stated that the regions affected by Cu segregation showed an increase in current density and a decrease in polarization resistance compared to regions not affected by Cu segregation [264].

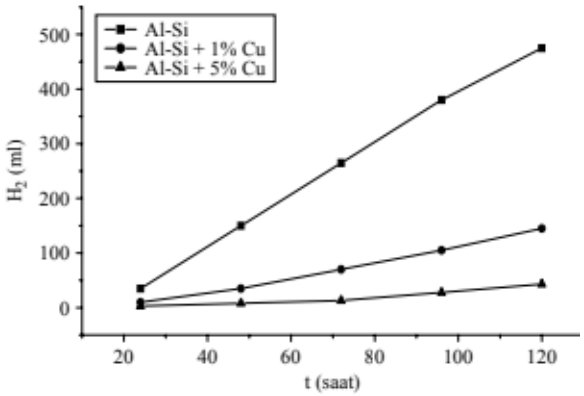

Figure 117: Hydrogen volume evolved by the corroding alloys (Al-Si, Al-Si-1% Cu and Al-Si-5% Cu) in HCl [263] .

Their findings also showed that the corrosion resistance of Al-Si alloys was increased with the addition of Cu, decreasing the corrosion rate. However, the increase in the Cu content was associated with a concurrent increase in the rate of IGC. Their approach to reduce the effect of Cu in the alloy was to subject the material to aging heat treatment, after which, the Cu-containing phases disperse within the grains, contributing to an increase in material strength. The presence of Cu as precipitates at grain boundaries or dispersed in the grains has different effects on the corrosion behavior of the alloy. An increase in Cu content in the alloy is associated with an increase in the rate of intergranular corrosion (IGC) [263].

The results highlight the influence of Cu content on the corrosion behavior and indicate that Cu can play a role in both promoting and inhibiting corrosion, depending on the specific alloy composition and conditions [263]. In the works of Osorio et al. [264], it was also found that in regions with predominant Cu inverse segregation, closer to the casting surface, the Cu content plays a significant role in decreasing the corrosion resistance (increasing current density). The fineness of the dendritic array (with secondary dendrite arm spacings, Gamma2, between 8 and 15 microns) also has a favorable effect on corrosion resistance. However, as the secondary dendrite spacing increases to coarser dendritic arrays, the Si particles become the driving force for corrosion resistance. Coarser microstructures have been shown to improve corrosion resistance in these cases. This improvement is attributed to a decrease in localized deformation sites between Si and Al interfaces for coarser dendritic arrays. Additionally, the presence of needle-like Si particles helps prevent pit coalescence, further contributing to corrosion resistance [264].

In another study, from Lee et al., the addition of Cu to Al–Si–Pb alloys resulted in the formation of the intermetallic phase $CuAl_2$, which enhanced the wear resistance of the alloys. However, the copper addition also led to a higher corrosion rate in the alloys, as the Cu particles formed in the Al–Si alloy lowered the corrosion potential and increases the corrosion current density [265].

5.7. Effect of Gallium (Ga)

MIMI Tech GmbH
Preusweg 98, D-52074 Aachen
friedrich@mimi-tech.com

5.7.1. Wrought alloys

5.7.1.1. 5XXX

Corrosion

Zhang et al. [266] reported in his literature research that the addition of small amount of Ga not only increase the corrosion resistance of the aluminum alloy anodes, but also destroy the passivity of alumina film and improve the electrochemical activity of the alloy [266]. Gallium, in conjunction with Zn, will also induce a higher electrochemical activity in the alloy, as described by Ren et al. [152].

5.7.1.2. 8XXX

Conductivity

Papastaikoudis et al. [267] studied the residual resistivity of Al-Ga alloys and his results shows that it increases linearly with increasing Ga concentration up to 2% [267]. Similar results were obtained in another study [268] from the same authors. In addition, Gunterodt et al. [269] also confirmed in his experimental investigations on liquid Al-Ga alloys a linear relationship of electrical resistance as a function of Ga concentration. Furthermore, Korkmaz et al. [270] carried out analytical investigations, in which the authors reached the same conclusion.

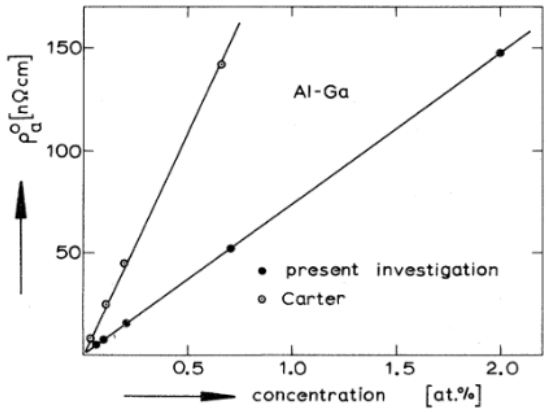

Figure 118: Residual resistivity of Al-Ga alloys as a function of Ga concentration [267].

5.7.2. Cast alloys

5.7.2.1. 7XX

Corrosion

In a study conducted by Hao et al. [271], the impact of Gallium addition on the electrochemical characteristics of Al-Zn-Bi anode alloy was investigated. The incorporation of 0.015% Ga was found to enhance the anodic polarization performance and resistance to pitting corrosion [271].

5.8. Effect of Nickel (Ni)

MIMI Tech GmbH
Preusweg 98, D-52074 Aachen
friedrich@mimi-tech.com

5.8.1. Wrought alloys

5.8.1.1. 8XXX

In a study by Akiyama et al. [272], the impact of severe plastic deformation through equal-channel angular pressing (ECAP) on the corrosion behavior of an Al-5.4%Ni alloy was explored (Figure 119). The findings show that the ECAP process improved the corrosion resistance of the alloy by elevating pitting potentials and lowering passive current densities, indicating enhanced overall resistance to corrosion. This improvement was attributed to the refinement of α-Al crystals, where corrosion initiation mainly occurs. The study also revealed that ECAP led to microstructural changes, where, after two ECAP passes, α-Al crystals were smaller due to plastic deformation, and the α-Al/Al3Ni eutectic region expanded. Six ECAP passes resulted in a more even distribution of the α-Al/Al3Ni eutectic region, with fewer pits in shear band areas [272].

Ultimately, the research proposed that pitting initiation happened in the larger α-Al crystal region, potentially obstructed by the α-Al/Al3Ni eutectic region. ECAP-induced mixing of these regions led to a more uniform microstructure, hence improving corrosion resistance [272].

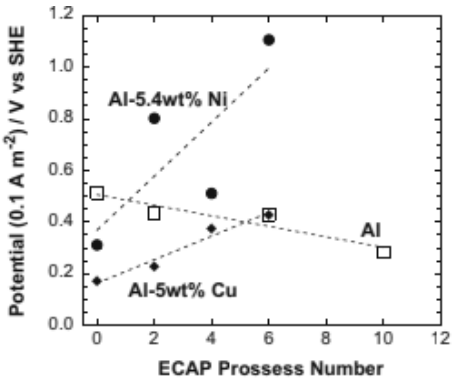

Figure 119: The potential where the current density reaches to 0.1 A m^{-2} in the potentiodynamic polarization curves of Al, the Al–Ni and Al–Cu alloys with/without ECAP.

5.9. Effect of Titanium (Ti)

5.9.1. Wrought alloys

5.9.1.1. 7xxx

Castability

Zeng et al.[273] investigated the effect of Ti on the hot tearing susceptibility (HTS) of AA7050 alloy. Ti was introduced into the alloy through Al-5Ti-1B master alloys. At high cooling rate corresponding to constrained rod mold casting condition, HTS index decreased from the value of 17 (without Ti) to the value of 7 (0.06 wt.% of Ti), further increase of Ti deteriorated castability of the alloys, from the value of 7 (0.06 wt.% of Ti) to the value of 13 (0.24 wt.% of Ti). The HTS index variation trend was found to positively correlated with grain size. It was proposed excessive Ti amount led to larger agglomeration of inoculates which reduce the effective amount grain nucleates. The coarse grains are responsible for the increased HTS index.

MIMI Tech GmbH
Preusweg 98, D-52074 Aachen
friedrich@mimi-tech.com

5.9.2. Cast alloys

5.9.2.1. LM9

Mechanical Properties (Potential Risk)

In the aluminium casting industry, the formation and growth of intermetallics is usually viewed as having only a harmful influence on casting quality and production. Cao et al.[274] studied the precipitation of primary intermetallics (IMs) from LM 9 (Al-11Si-0.38Mg-0.57Fe-0.59Mn) melts with 0.01 and 0.17 wt. % Ti content. There was no Ti-contained IMs found in 0.01 % Ti added alloy. Whereas for 0.17 wt. % Ti, TiAl3 formed as thick plates (with up to 15 % Al replaced by Si), and Ti(AlSi)2 formed as thin platelets. Both phases precipitated ahead of Al solidification. Figure 120 shows morphologies of above-mentioned primary IM phases. Cracks are often observed within IMs and sometimes extend into ductile matrix. The authors proposed that IMs precipitated upon wettable side of bi-films (Al-oxide) and the dry side of the bi-films induce crack. Nevertheless, it should be pointed out that in the article it is not clear whether the cracks are exclusively related with Al-Fe-Si-Mn IM or Al-Ti(-Si) phases.

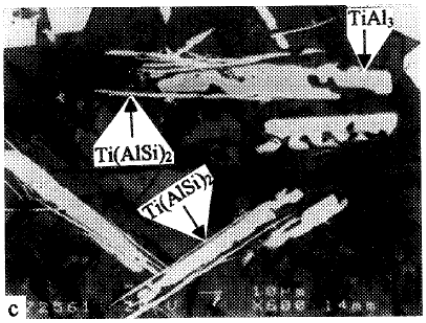

Figure 120: SEM micrographs showing: TiAl3, Ti(AlSi)2 phases. Reproduced from [274].

5.10. Effect of Boron (B)

5.10.1. Wrought alloys

5.10.1.1. 1XXX

Mechanical Properties and Workability (Potential Risk)

Meredith et al.[275] studied effect of B content in intermetallics selection during solidification of 1xxx alloy (0.3 wt. % Fe, 0.15 wt. % Si). B content was controlled by Al3Ti1B grain refiner. Results show that at low levels of B (less than 3 ppm), Al6Fe is the dominant IM. Whilst further increase of B lead to a gradual rise of α-AlFeSi phase formation. At an even higher addition rate, α-AlFeSi ternary phase becomes dominant, but Al_mFe appears under the condition that microstructure is refined (at B more than 8 ppt). It was indicated that B alone is not sufficient enough to cause variation of IMs phase, it influences the IMs formation by interaction with solidification conditions.

5.10.1.2. 6XXX

MIMI Tech GmbH
Preusweg 98, D-52074 Aachen
friedrich@mimi-tech.com

Mechanical Properties and Workability (Potential Risk)

Kumar et al.[276] studied the influence of B on IM phase selection at a pilot-scale billet casting line. B content was controlled at 1 ppm[2] through addition of Al-5Ti-1B grain refiner. Result shown in Table 38 demonstrates that TiB_2 particles promotes β-AlFeSi to form in larger proportions in the alloys. Figure 121 provides microstructure evidence for nucleation of β-AlFeSi on TiB_2 particles. It was proposed the combined availability of favorable solute (Si) rich liquid and potent heterogeneous nucleating particles at inter-dendritic regions are responsible for β-AlFeSi against α-AlFeSi; It was concluded that Al-Ti-B grain refiner controls the Fe-IMC phase selection, and α-Al grain size and morphology affects the Fe-IMCs morphology.

Table 38: Observed features of grain structure and Fe-rich IMs in three different samples. Reproduced from [276].

Melt Condition	Morphology of α-Al	Grain size	Predominant Fe-rich IM	Predominant Fe-rich IM morphology	IM inter-connectivity
No Melt Condition	Columnar feathery dendrites	>10000	α_c-AlFeSi	Skeleton-like, spherical-like,	Less
Intensively Sheared	Mixed equiaxed dendrites and globular	167 ± 8	α_c-AlFeSi	coarse petal, dendrite-like	Nearly High
Al-5Ti-1B	Equiaxed dendrites	100 ± 8	β-AlFeSi	Platelet-like	High

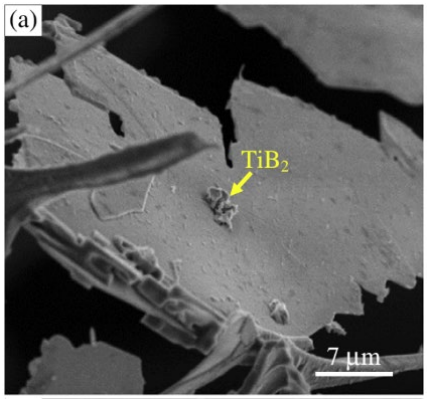

Figure 121: SEM images of the extracted particles showing association between TiB2 and β-AlFeSi. Reproduced from [276].

In the ending remarks of the article, Kumar et al. [276] indicated that high fraction of β-AlFeSi are not to be a concern so long as the fine and dendritic α-Al grain structure can realized. In such cases,

[2] It was indicated in the publication that 1 ppm Al-5Ti-1B grain refiner was added, if so the addition rate of B would be probably too low. Hence it is assumed the 1 ppm refers to B content.

MIMI Tech GmbH
Preusweg 98, D-52074 Aachen
friedrich@mimi-tech.com

the formed β-AlFeSi particles are fine and discrete in distribution can be easily transformed into fine αc-AlFeSi particles at relatively shorter homogenization times and lower temperatures.

5.10.2. Cast alloys

5.10.2.1. Al7SiCu3Mg, 319.2, Al-12.5Si

Mechanical Properties (Potential Risk)

Rakhmonov et al.[277] studied the influence of B on β-AlFeSi' s formation in Al7SiCu3Mg alloy. The Needle-like β-AlFeSi was reported frequently as a stress riser in cast alloys and hence lead to degraded mechanical properties. The studied alloy contains 0.44 wt. %Fe, and B was controlled at 170 ppm through addition of an AlTi5B1 master alloy. As is shown in Figure 122, β-AlFeSi phase only appeared in the microstructure of alloy grain refined with AlTi5B1, no evidence of such β-AlFeSi phase formation was observed in non-grain-refined and AlTi10-grain-refined structures. At higher cooling rates (10 °C/s), the β-AlFeSi phase even becomes the dominating Fe-rich phase in the microstructure. It was proposed during solidification, remaining TiB2 particles which do not nucleate α-Al are pushed towards interdendritic regions, where they act as heterogeneous nucleation sites for β-AlFeSi and for the occurrence of some eutectic reactions.

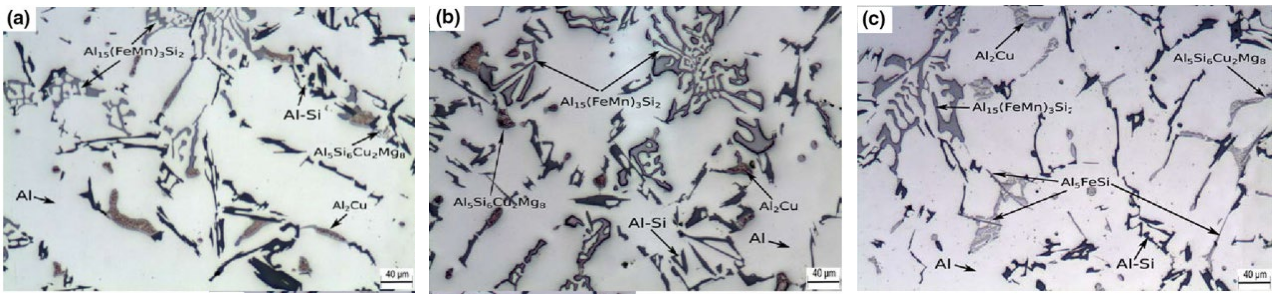

(a) (b) (c)

Figure 122: Typical microstructures of (a) non-grain-refined, (b) AlTi10- and (c) AlTi5B1-grain-refined AlSi7Cu3Mg alloy. Reproduced from [277] .

In another study conducted by Samuel et al.[278] using 319.2 alloy, mmicrostructures obtained from Al-Ti-B refined alloy indicate a tendency for thickening of the β-Al5FeSi phase. Rodriguez et al.[279], on the other hand found addition of Al-Ti-B master alloy to Al-12.5Si alloy reduces size of β-AlFeSi and its aspect ratio. The authors attributed the different findings on influence of B on Fe-rich phases to difference casting conditions and alloy compositions.

5.11. Effect of Sodium (Na)

5.11.1. Wrought alloys

5.11.1.1. 5XXX

Mechanical Property

In the research from Lu et al. [280], the authors investigated the role of trace amounts of Na or Ca impurities in an Al–5% Mg alloy. Their findings showed that these impurities can lead to high-

MIMI Tech GmbH
Preusweg 98, D-52074 Aachen
friedrich@mimi-tech.com

temperature embrittlement. The presence of Na or Ca impurities was reported to cause intergranular fracture and reduce ultimate tensile strength (UTS) during embrittlement. The segregation of Na and Ca weakened the grain boundaries (GB) in the investigate alloy, leading to GB embrittlement [280].

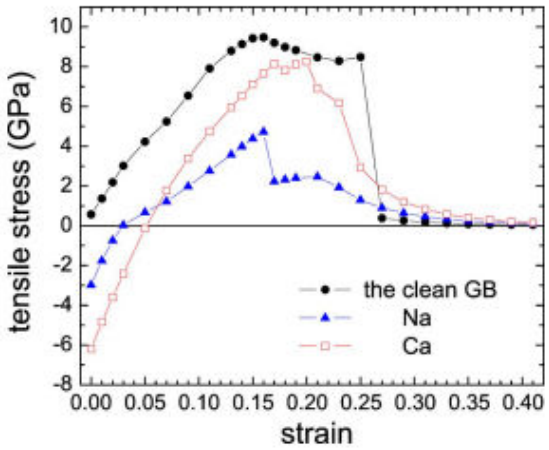

Figure 123: Stress in the tensile direction the GB normal direction as a function of strain. Circles, triangles, and squares represent the clean, Na-segregated, and Ca-segregated GB's, respectively. Positive means tensile, while negative means compressive.

5.12. Effect of Chromium (Cr)

5.12.1. Wrought Alloys

5.12.1.1. 8XXX

Mechanical Property

Banerjee [281] studied the age-hardening behavior of Al-Cr alloys containing 0.63 wt.% - 1.2 wt.% of Cr with several alloyed with Si. His observations reveal that in binary alloys with 0.63 wt.% Cr and 0.78 wt.% Cr, respectively, when the silicon content is relatively low, the aging response is more pronounced in the alloy with 0.78 wt.% Cr, which has a higher chromium content. However, in the case of the alloy containing 0.9 wt.% Cr, which surpasses the primary solubility limit for solutes, there is a distinct delay in the initiation of precipitation hardening until 50 minutes of aging have elapsed. After this point, the hardness value begins to increase.

In binary alloys, increasing the chromium content does not appear to have affected the peak hardness temperature. However, the introduction of higher silicon levels is observed to have shifted the peak hardness temperature to higher values. It's worth noting that, at the same chromium level, alloys with higher silicon content exhibit overall higher hardness values at all aging temperatures.

Figure 124 illustrates the aging behavior of binary alloys, with aging curves derived from micro hardness tests conducted on the matrix. Careful measures were taken to ensure that indentations were placed away from coarse particles. Alloy 0.9 wt.% Cr, which displayed limited aging response during macro hardness testing, exhibits a noticeable aging response when subjected to micro hardness testing of the matrix solid solution. These curves indicate age hardening due to solute rejection within a matrix that is otherwise devoid of interference from coarse insoluble.

MIMI Tech GmbH
Preusweg 98, D-52074 Aachen
friedrich@mimi-tech.com

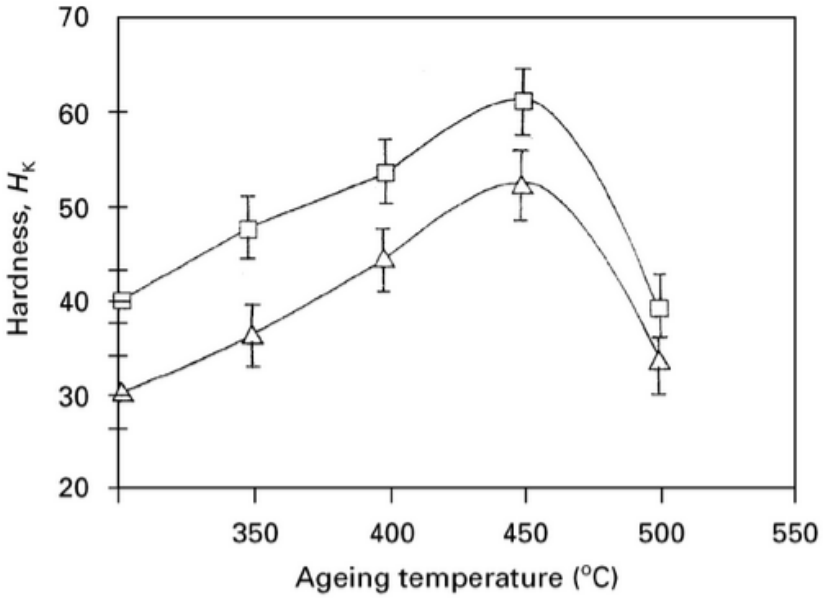

Figure 124: Microhardness-temperature curves for alloys isochronally aged for 1h. Rectangle symbol corresponds to 0.78wt.% Cr, triangle symbol corresponds to 0.9wt.% Cr.

5.13. Effect of Magnesium (Mg)

5.13.1. Wrought Alloy

5.13.1.1. 1XXX

Workability

While commonly used as alloying element to enhances properties in aluminum alloys, negative effects with excessive magnesium content or certain applications are common, revolving around reduced ductility, corrosion issues, weld ability and braze ability.

Miyagi et al. [282] investigated the effect of low boiling temperature elements including Mg, Si, Mn and Zn during laser welding of aluminum alloys. During laser welding, laser irradiation causes immediate metal evaporation, leading to the formation of a keyhole, and then the metal surrounding the keyhole gradually melts due to the heat generated locally. The growth rate of the keyhole depth is positively correlated with the total content of low boiling temperature elements (TCE) in the aluminum alloy. In other words, both the keyhole depth and diameter at the stable stage exhibit a positive linear correlation with the total content of low boiling temperature elements (TCE). The longitudinal view area of the molten pool has a negative linear correlation with the thermal conductivity of the aluminum alloy. The highest absorption rate of 58% is observed in laser welding of aluminum alloy with TCE equal to 2.1%. Aluminum alloys with TCE lower than 2.1% exhibit more stable keyhole shapes, where the surface tension and recoil pressure of metal vapor are balanced.

Karpov et al. [283] reported the temperature (-60°C, 20°C and 85°C) effect on the fracture behavior of laser-welded joints in aluminum alloy containing Mg and Cu. For Mg-containing alloys, heating and cooling cycles have the effect of suppressing the Portevin–Le Chatelier effect, a phenomenon

MIMI Tech GmbH
Preusweg 98, D-52074 Aachen
friedrich@mimi-tech.com

associated with serrated yielding in certain materials. In the case of the 1420 alloy, the ultimate strain is much smaller both at -60°C and 85°C compared to 20°C due to the formation of fixed zones of localized plastic deformation. The welded joint of the 1420 alloy has no significant dependence between ultimate strain and temperature. Deformation is initially localized in a narrow region of the weld, and as the temperature rises, the ultimate relative elongation of the weld-containing region becomes smaller. At 20°C, the ultimate relative elongation of the weld itself is the smallest. The maximum limiting elongation of the welded joint in the Mg-containing alloy is achieved at a negative temperature (i.e., -60°C). despite the formation of secondary cracks begins during the heating process.

5.13.1.2. 5xxx Series

Workability

Yamada et al. [284] evaluated the strain rate dependence of 5xxx series Al alloys, specifically 5005 5021 5082 and 5182. All of them displayed mainly negative strain rate dependence and serration. The behavior depended on the Mg content and strain rate, attributed to the Portevin-Le Chatelier (PLC) effect. Additionally, the flow stress increased at high strain rates in the investigated Al-Mg alloys. At such high strain rates, the thermal activation theory became the dominant mechanism, as Mg atoms couldn't migrate to dislocations effectively. On the solute Mg and strain rate dependence, the solute Mg content in Al phase influenced strain rate dependence. Less solute Mg in the Al phase of the 5182 alloy compared to the 5082 alloy resulted in differing strain rate dependencies due to different precipitation sites for Mg_2Si compounds.

5.14. Effect of Scandium (Sc)

5.14.1. Wrought Alloys

5.14.1.1. 5xxx Series

Mechanical Property

Scandium addition in wrought alloys generally causes grain refinement and a non-dendritic structure. Sidelnikov et al. [285] investigated the mechanical properties of a 5xxx series alloy plate with 0.10-0.11 wt.% of Sc and found that the strength properties of deformed products increased by 20-25%. Annealing has minimal impact on the mechanical properties of plates produced in a hot-deformed state, with ultimate tensile strength in the longitudinal direction ranging from 388–389 MPa, yield strength from 245–247 MPa, and elongation to failure from 18.0–18.8%. After cold rolling, the plates exhibit different mechanical properties, including ultimate tensile strength of 413–414 MPa, yield strength of 386–372 MPa, and elongation to failure of 5.2–6.6%. In addition to reduction of crack formation, an increase in strength of weld joint and fatigue life by 200% was reported. [285]

At 0.12 wt.% Sc, alloys showed persistent dislocation networks, which acted as heterogeneous nucleation sites. These dislocations can be eliminated by a long solution treatment time. The precipitates in the 0.12% Sc alloy exhibited high resistance to coarsening, with size distributions narrower than predicted by classical theory.[286]

MIMI Tech GmbH
Preusweg 98, D-52074 Aachen
friedrich@mimi-tech.com

The grain refinement effects up to 0.1 wt.% were contradicted by Ren et al. [287], where the authors reported insignificant grain refinement for Sc content less than 0.15% despite a slight enhancement in mechanical properties, since the Sc completely dissolves in the alpha-Al matrix (compare Figure below). An optimal Sc content of 0.3 wt.% was mentioned, where the primary Al_3Sc phase precipitates, leading to substantial microstructure changes, significant grain refinement which leads to increases in tensile strength and yield strength along a decrease in elongation. Going above 0.45 wt.% causes aggregation of precipitated phases with coarsened grain boundaries. Mechanical properties remained unimproved compared to 0.3 wt.% and heat treatment could not fully dissolve the agglomerates of the precipitated phases.

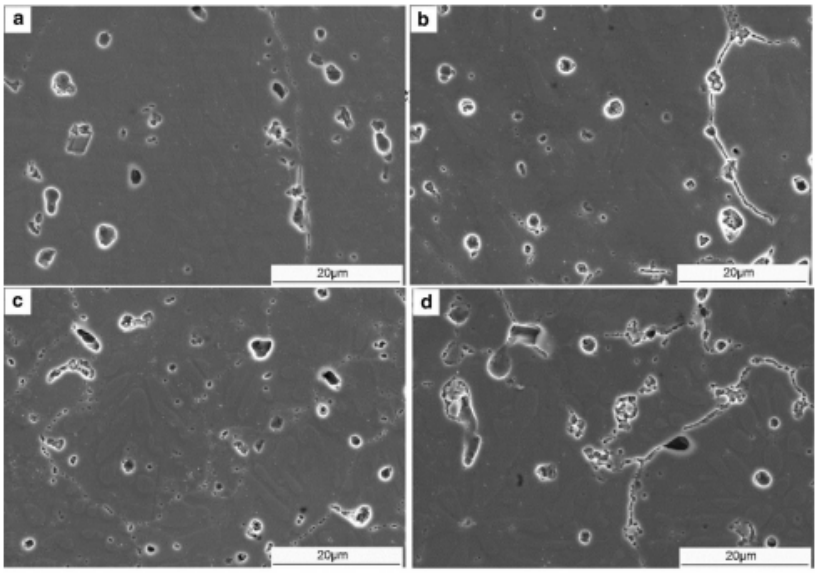

Figure 125 : SEM images of the Al-Mg-Sc alloys with (a) 0% Sc, (b) 0.15%Sc, (c) 0.30%Sc and (d) 0.45% Sc

MIMI Tech GmbH
Preusweg 98, D-52074 Aachen
friedrich@mimi-tech.com

5.15. Summary of Negative Effects of Impurities on Alloy Properties

For summarizing purpose, Table 39 was created to encompass above introduced negative effects and neutralization measures, along with references. It is worth mentioning that for Cd, Hg, Pb, Li, relevant articles were not found.

Table 39: Summary of negative effects of impurities on alloy properties.

Impurity	Product	Effect	Neutralization	References
Fe	1XXX	Corrosion.	Friction stirring process (FSP).	[1], [2], [3]
Fe	2XXX	Formation of Iron-rich phase reduce mechanical properties.	Add Mn, Y, Sc, and Gd as Iron-phase modifiers.	[4], [5], [6], [7], [8]
Fe	5XXX	Reduce formability and ductility, reduction in mechanical properties	Add Co, Cr, and Mn as Iron-phase modifiers.	[9], [10]
Fe	5XXX	Corrosion.	-	[11]
Fe	6XXX	Reduce formability and ductility, reduction in mechanical properties.	hetero-deformation-induced (HDI) strengthening and HDI strain hardening.	[12], [13]
Fe	7XXX	Negatively affect the mechanical properties and performance.	Elevated cooling rates and add Ca as a neutralizing element.	[14]
Fe	7XXX	Corrosion.	Add Mn as Fe modifier.	[15], [16]
Fe	8XXX	Reduced ductility, strength, decreased toughness, increased occurrence of recrystallization, and deteriorate the material's properties.	Add Ce, and Y as Fe modifier.	[17], [19]
Fe	2XX	Decrease alloy's properties.	Heat treatment (artificial aging)	[20]
Fe	3XX	Effect on the overall integrity and mechanical properties, decrease quality of the casting, hot tearing tendency.	T6 heat treatment, Sr, Ni, Mn, Mg, and Al-Ti-B as Iron-phase modifier, intensive stirring, the increasing in the mold temperature.	[21], [22], [23], [24], [25], [26], [27], [29], [30], [33], [34], [35], [36], [37], [38], [39], [40], [41]
Fe	3XX	Increase in the corrosion, UTS, elongation, pore formation	Rapid Cooling, V, Mn Sr, P doping, T7 treatment	[21], [174], [175], [170], [176] [177]
Fe	4XX	Negatively impacts the mechanical properties.	Add Mn, Cr, Be, Co, Mo, Ni, V, W, Cu, Sr, or rare earth elements as Iron-phase modifier, increased fluid flow, rapid	[42], [43], [44], [45], [46], [47], [48]

MIMI Tech GmbH
Preusweg 98, D-52074 Aachen
friedrich@mimi-tech.com

			solidification, ultrasonic vibration, Process Parameters Optimization (cooling rate), Melt Heat Treatment and Solid Solution Heat Treatment.	
Fe	5XX	Deterioration of ductility and fatigue properties.	Heat treatment T6.	[49]
Fe	8XX	Deteriorated mechanical properties of the material, leading to reduced lifetime or durability.	Add Zr, and Er as Fe modifier.	[50]
Zn	5XXX	Corrosion, pitting formation, intergranular corrosion.	pre-ageing at high temperatures (above 400 °C), Cold rolling pre-deformation of 20% followed by artificial ageing at 150 °C.	[51], [52]
Zn	6XXX	Corrosion.	retrogression re-aging (RRA) treatment.	[53]
Zn	7XXX	Intergranular corrosion, pitting corrosion, exfoliation corrosion (EXCO), stress corrosion cracking (SCC).	Addition of Cu, Cold rolling, refining the grain size (grain refiner addition, friction stir processing, and equal channel angular pressing (ECAP)), one or two-step PA (pre-aging) treatment, peak aging treatment.	[54], [55], [56], [57], [58], [59], [60], [61], [62], [63], [64], [65], [66]
Zn	7XX	Pitting corrosion, propagation, and re-passivation of metastable pits.	increasing the precipitation hardening time up to 24 hours.	[68], [69]
V	1XXX	Degrades the electrical conductivity.	Boron treatment	[70] [252]
V	7xxx	Hot workability	Optimum hot working temperature and strain rate	[253]
V	8XXX	Effects on mechanical properties, causes corrosion resistance	-	[254]
Cu	2XXX	Corrosion-fatigue lifetime, pitting corrosion, and intergranular corrosion.	changing the heat treatment conditions.	[71], [72], [73]
Cu	7XXX	General increase in corrosion, localized corrosion, including pitting corrosion, crevice corrosion, intergranular corrosion (IGC), and exfoliation corrosion (EFC). Also stress corrosion cracking (SCC), and corrosion fatigue failure.	Single intermediate annealing treatment, a two-staged T7x ageing.	[74], [75], [76]
Cu	2XX	Stress corrosion.	increasing solidification time.	[77]
Cu	3XX	Intergranular corrosion (IGC), higher corrosion rate.	-	[78], [79], [80]

MIMI Tech GmbH
Preusweg 98, D-52074 Aachen
friedrich@mimi-tech.com

Na	5XXX	High-temperature embrittlement; intergranular fracture and reducing ultimate tensile strength (UTS) during embrittlement	-	[81]
Si	1XXX	Formability	Heat Treatment/ Pre-Annealing	[233]
Si	5XXX	Formability, intermetallic in the as-cast structure	Homogenization, long hours holding time around 500 °C	[234]
Si	6XXX	Anodization: formation of eutectic phase, intermetallic and hard anodic oxidation films, Formability	Controlling Mg/Si ratio and morphology of Si. Formability can be neutralized be homogenization	[235], [239]
Si	7XXX	Anodization, increased Si has negative impact on forming hard anodizing coatings, plane-strain fracture toughness (jointly with Fe)	Changes in anodizing electrolyte solution	[241] [242]
Si	3XX	Anodization, inhomogeneity, and formation of cracks, thinning of oxide layer formed	Process Optimization by changes in anodizing solution, solution treatment, Plasma Electrolytic Oxidation	[243]–[250]
Si	4XX	Anodization	Alloying with Sr to modify structure of Si	
Zn	5XXX	Decreases ductility from increased flow stress	-	[204]
Zn	6XXX	Extrudability, accumulation in grain boundary, decreased ductility	-	[206]–[208]
Zn	7XXX	Extrudability, volume of coarse eutectic structure increases	-	[223]–[225]
Zn	3XX	Influences the corrosion properties	-	[226]
Zn	7XX	Extrudability: affects the elongation. Rougher surface finishing with increasing amount of Zn	-	[229], [230]
Mn	2XXX	Tensile strength and fracture toughness affected by content of Mn	Increasing Ageing time can improve mechanical properties	[154]
Mn	5XXX	Negative strain rate dependence, positive impact on elastic modulus and hardness when combined with Cu and Ni	-	[159], [284]
Mn	6XXX	Dispersoids formation together with V and Cr	-	[288]

MIMI Tech GmbH
Preusweg 98, D-52074 Aachen
friedrich@mimi-tech.com

Mn	3XX	Positive role in eliminating ß phase, impact on morphology of eutectic Silicon. Mechanical and fatigue properties	-	[177], [187]
Mn	4XX	Causes corrosion centers through formation of Mg2Si and MgZn2. Mechanical properties	-	[196], [197]
Mn	5XX	Mechanical properties such as ductility, hardening capacity, YS and UTS	Heat Treatment	[199]
Cr	8XXX	Poor aging response	Alloying with Silicon or alloy below solubility limit	[281]
Sc	1xxx	Grain refinement, effecting nucleation and recrystallization	-	[285]–[287]
Ti	LM9	Coarse IM formation, Hot Tearing Susceptibility	Optimum Al-Ti-B addition rate	[273], [274]
B	1xxx	α-AlFeSi formation	-	[275]
B	6xxx	β-AlFeSi formation (nucleated upon TiB2)	-	[276]
B	Al7SiCu3Mg	β-AlFeSi formation	-	[277]
B	3xx	β-AlFeSi thickening	-	[278]
B	Al-12.5Si	β-AlFeSi refinement	-	[279]

MIMI Tech GmbH
Preusweg 98, D-52074 Aachen
friedrich@mimi-tech.com

6. Conclusion

6.1. Removal Technologies

- **Gas purging** and **salt fluxing** are already industrially deployed processes. Both processes are capable for Na, Li, Ca, Mg removal. The averaged impurity removal efficiency for both processes are over 70 %. The lower boundary for removal of Na, Li, and Ca is in less than 10 ppm, whilst for Mg this value varies between 10-100 ppm (gas purging) and 0.1-1 % (salt fluxing). In most production practices, the impurity removal kinetics follows the first-order model. Removal rate of impurities is influenced by impurity type and content, operational parameters including feeding rate of reactive halides.

  - Strengths & Opportunities: both gas purging and salt fluxing are industrially established processes. A possible opportunity comes from utilizing the already established gas/salt fluxing process for removal of noble impurities, by exchanging the gas/salt compositions.

  - Weaknesses & Threats: it was mentioned that consumables price, particularly concerning salt flux was one of the threats. Depending on countries and regions, legislative issues exist for application of chlorination process.

  - Keynote from Techniques Providers: most interviewees were not optimistic on identifying new substances/compounds which can remove noble elements (e.g., Fe, Mn). However, there was an interviewee mentioned that Si removal through a fluxing process is now in serious discussion. The under-development/developed method is intended to be applied for alloys containing dilute amount of Si.

- **Boron treatment**, as a TRL 9 technique, is effective for removal of V, Ti, Zr. For removal of Chromium (Cr), uncertainty remains. The average impurity removal efficiency is over 60 %. The lower boundary for removal of V, Ti, Zr by application of boron treatment process is respectively less than 10 ppm. Removal rate of impurities is influenced by Al-B master alloy type, melt convection, and addition rate of the master alloy.

  - Strengths & Opportunities: Boron treatment process is already an industrially established process. One of the opportunities is concerning search of innovative ways capable of separating the sludge particles rapidly, without forming large sludge build-up at furnace bottom.

  - Weaknesses & Threats: the holding operation during boron treatment increases process lead time and meanwhile makes frequent furnace hygiene operation necessary. One threat of the boron treatment is related to formation of coarse boride particles which may deteriorate product quality.

  - Keynote from Techniques Providers: both filtration and degasser were nominated as potential alternative sludge separation techniques. For the case of Ti removal, the formed Ti bearing borides particles may be kept in the melt as grain refiner instead of being removed.

- **Selective oxidation** method is demonstrated to be effective for removal of Mg in both laboratory and pilot-scale trials (3 ton). The averaged impurity removal efficiency is over 80 %. Lower boundary for removal of Mg by application of selective oxidation process is less

MIMI Tech GmbH
Preusweg 98, D-52074 Aachen
friedrich@mimi-tech.com

than 10 ppm. Issues which hinder large scale application are metal loss and secondary melt contamination related to dissolved impurities and suspended inclusions.

- Strengths & Opportunities: the pros of selective method is that it can incorporate Si to cast alloys. On the other hand, the method may also find its potential application for removal Mg from alloys which contain dilute amount of Mg impurities.

- Weaknesses & Threats: the amount of dross and melt contamination with respect to spinel particles and Si are among negative aspects associated with selective oxidation process.

- Keynote from Techniques Providers: the potential of applying selective oxidation process for alloys with dilute content of Mg was echoed by one of the techniques providers. Since often the reduction from 40-20 ppm Mg content is difficult for halides-involved process. There was also a suggestion concerning reserving the Mg value by planning production of Al-Mg alloys.

- **Intermetallics (IMs) precipitation and separation method** is capable of removal Fe, Mn, Cr, Si, Zn, Cu, Ni. The technique is with a TRL level of 6. The removal of Fe, Mn, Cr impurity requires high extent of alloying, via Si or Mg. The minimum extent of alloying for Si and Mg is respectively 6.3 wt. % and 5 wt. %. Removal of Si, Cu, Ni, Zn, on the other hand, requires extremely high alloying extent, i.e., 30 wt. % Mg. In normal alloy systems, the collective removal efficiency of Fe, Mn, and Cr are 64 %. The lower boundary for removal of Fe, Mn, Cr from alloys via IMs method is respectively 0.14, 0.15, 0.0046 wt. %.

  - Strengths & Opportunities: the main strengths of IMs method are its validated principle and the proved efficiency for removal of noble elements (against aluminium).

  - Weaknesses & Threats: IMs method has only a narrow application range in terms of requirements on: high-alloying extent (Si or Mg) and high Fe/Mn contamination level. Separation of sludge is another big concern. The only seemingly “feasible” way, melt holding process leads to long waiting time and serious sludge build-up issues. From economic perspective, the low yield and lack of sound ways for reclaiming values from high amount of IMs retard the industrial-scale implementation.

  - Keynote from Techniques Providers:

    - Sedimentation has been tested by one of the solution providers in 3-ton scale trials. Fe was removed from 0.5 to 0.12-0.13 % at an 85 % yield. The process involves steps of: 1) addition of Mn elements, 2) conditioning of the melt by intensive stirring, 3) melt holding. The 15 % sludge was diluted by aluminium (presumably primary) for producing alloys tolerating/favouring high Fe content. It was further conceptualized that in future industrial production, the melting furnace will be the site where sedimentation separation takes place. Two holding furnaces shall be configured to accept two types of products namely the refined melt and the high Fe containing melt.
    - If the sludge can be not directed into production of another alloy, as was suggested by above techniques provider, there were solution providers suggesting siphoning as a removal measure.

MIMI Tech GmbH
Preusweg 98, D-52074 Aachen
friedrich@mimi-tech.com

  - It was brainstormed that chances for a filtration separation process might exist if IMs can be well distributed within the purification system. In other words, other techniques for IMs removal shall be deployed and orchestrated with filtration. Multi-stage filtration was nominated as a possible way for collect the large amount IMs.
  - The imposition of external EM field (EM stirring) may play a supportive role on improving the separation process kinetics (e.g., nucleation, growth of IMs).
  - Salt-involved route was indicated to be already employed in some plants for IMs removal. The route uses rotary kiln (arc-/gas-driven) as equipment.
  - Degasser was proposed as a possible way to float the IMs out and trap them in the dross layer.
  - Rapid solidification was mentioned as one of the major approaches for neutralize the negative effect of Fe. The interviewees had stressed that rapid solidification is not easy to be implemented particularly in industrial scale. Cheap rare earth metals were said to have possibilities to neutralize the harmful IM phases. Conventional heat treatment such as homogenization was commented to help increase the toleration of Fe contamination but only to a limited extent (0.25-0.35 wt. %).
  - Development of new alloys which tolerate high Fe content is on the way. It was also commented by one of the interviewees that the control of oxide films in the melt helps reduce negative effect of IMs. There was one techniques provider planning to look at the properties of sludge via fundamental research and evaluate the possibilities to use sludges as a product.

- Intensive research on **three-layer electrolysis** processes for aluminum refining, similar to those used for primary and high-purity aluminum, has shown that advancements in process control, electrolyte composition, and cell design directly impact energy consumption. Early studies, like Beljajew et al.'s 1957 work, achieved impressive impurity removal efficiency (98.92 %) from heavily contaminated aluminum scrap but had high energy consumption (39 kWh/kg). Pearson et al. in the same year reported an energy consumption of 18-23 kWh/kg for purifying contaminated aluminum sources. De Young et al.'s recent patent for Alcoa introduced an innovative electrode design, claiming to reduce energy requirements to 2-6 kWh/kg, but other embodiments of his patent claim an energy consumption from 1 – 15 kWh/kg. Alternative approaches like solid-state and capillary electrolysis have also shown promise, with Solheim et al. reaching at low TRL lab-scale a 99.75% impurity removal using 7 kWh/kg. Lu et al. and Oya et al. reporting removal efficiencies of 97.83% and 99.00% at 7 and 17 kWh/kg, respectively. Yasinskiy et al. introduced a thin-layer multiple-capillary molten salt electrochemical system for aluminum purification, but no energy consumption data was provided. It's expected to be significantly lower than traditional three-layer electrolysis. All studies suggest achieving a total impurity level below 100 ppm.

  <u>- Strengths & Opportunities:</u> The process is robust, handling various aluminum scrap types with high contamination, yielding a primary grade like aluminum. Opportunities lie in reducing energy costs through recent technological advancements.

MIMI Tech GmbH
Preusweg 98, D-52074 Aachen
friedrich@mimi-tech.com

- Weaknesses & Threats: High energy consumption for upgrading scrap to primary-grade aluminum, comparable to primary aluminum production. The main threat is the residue material, an Al-Cu anode alloy enriched with impurities.

- Keynote from Techniques Providers: The interviews with technology providers and Al companies indicated that the new Alcoa's Astraea process is highly based on the classical three-layer electrolysis. A recent Patent from Alcoa (De Young et al.) also confirms this information.

- **Fractional crystallization** has been employed for upgrading scrap aluminum to primary-grade aluminum in various applications ranging from TRL 2 to TRL 7. In a patent by Kahveci et al. for Alcoa, a suspension-based fractional crystallization process was used to upgrade 5XXX aluminum scrap, achieving, at a yield of 81.6%, a reduction in silicon levels from 290 ppm to 167 ppm and iron levels from 610 ppm to 399 ppm, with other elements similarly reduced based on yield and distribution coefficients. Alcoa's method is a batch process, necessitating the tapping of purified and impure aluminum phases. To make the process continuous, Wouters et al. patented a modification involving the addition of an element like copper to increase initial melt density, allowing purified crystals to float and be separated. It was claimed that when the process ran with an aluminum scrap containing 1 % Fe, 1 % Si, and 1 % Mn, the product was upgraded reaching a removal of 81 % (0.005 % Fe, 0.5 % Si, 0.07 % Mn). Various other research efforts have explored novel techniques to enhance separation efficiency, such as isothermal squeezing and electromagnetic stirring, with promising potential. The literature suggests that the lower boundary for removing major eutectic impurities ($k < 1$) is less than 0.1 wt.%, but this limit was achieved primarily with low-contaminated scrap (less than 3 wt.% initial impurity content).

  - Strengths & Opportunities: It effectively removes common impurities and major alloying elements from aluminum, potentially reducing melt impurity levels significantly. Companies using this technology for high-purity aluminum production highlighted their low energy requirements.

  - Weaknesses & Threats: Interviews mentioned worries about the residual metal fraction post-treatment. The main weakness involves finding a suitable purpose for and economic impact of the impurity-enriched phase on process feasibility. Likewise, the threats are related to the overall process costs, CAPEX, total energy consumption, and consumables.

  - Keynote from Techniques Providers: A Canadian equipment supplier highlighted the readiness of use Fractional Crystallization equipment running in parallel configuration, allowing for a tailored capacity for purification. Moreover, the company reported being implemented their products towards recycling activities in addition to the already established high-purity Al market. A Japanese company also reported that they are running feasibility studies with Fractional Crystallization for removing impurities from Al scrap.

- **Vacuum distillation** has found use in the aluminum industry for the removal of magnesium (Mg) and zinc (Zn) from certain aluminum alloys. The literature primarily focuses on these two elements, detailing setup designs and process conditions for efficient separation. Studies by Murphy et al. demonstrated that interactions between other elements in the alloy can affect the effectiveness of the vacuum distillation process,

MIMI Tech GmbH
Preusweg 98, D-52074 Aachen
friedrich@mimi-tech.com

especially when dealing with heavily contaminated mixed alloy scrap. Ohtaki et al. explored Zn removal by incorporating melt stirring, which increased removal efficiency while reducing vacuum and temperature requirements. Wei et al. conducted low-scale trials and successfully reduced Zn content in aluminum from over 12 % to 0.3 % at a process temperature of 750 °C for 30 minutes and a vacuum level of around 10^{-1} mbar. Gotenbruck et al. investigated two-step distillation, with the second step requiring high temperatures and presenting challenges related to crucible material compatibility. Overall, these studies suggest that vacuum distillation can achieve impurity removal down to 0.1 wt. % but is more effective with low-contaminated scrap (approximately 3 wt. % initial impurity content).

- Strengths & Opportunities: This process is able to maintain the distilled fraction in metallic form, enabling the extraction of elements without oxidation or losses. It features high process efficiency and the capacity to achieve exceptionally low impurity levels in melts highly contaminated with Zn or Mg.

- Weaknesses & Threats: The primary weakness lies in the technology's low TRL 4 scale for aluminum applications. Additionally, the interference of additional impurities on process effectiveness restricts its suitability to specific alloy types, limiting its versatility. The most significant threat revolves around the engineering demands required to cool-down the condenser within the vacuum distillation setup. Due to safety considerations, water-cooled configurations are not feasible, leaving air cooling as one of the limited available options.

- Keynote from Techniques Providers: The interviewed Chinese research institute reported that the continuous technology (CVD) is scaled at 15 ton/day for Sn; Challenges for using for aluminium in a CVD is related to keeping the pressure balance stable, including the scrap input and aluminium output systems. For aluminium, the technology is still in gram scale for CVD and 500 kg for batch process for Al-Zn separation.

- Another identified technology is the **subchloride (a.k.a. Gross) process**. This process was developed by Alcan and investigated as a potential alternative to the Hall-Héroult process for aluminum production. In this method, aluminum chloride ($AlCl_3$) reacts with aluminum metal at elevated temperatures (around 1300°C), resulting in the formation of a volatile subchloride of aluminum. When the subchloride is subsequently cooled, the reaction is reversed, leading to the production of aluminum chloride and aluminum metal.
- **Pulsed current method, Sulfur treatment** (TRL 1) were also reported capable for Fe removal. More studies are needed for validating the proposed fundamental principles.
- **Super gravity segregation method** (TRL 2) was reported capable for removal of Si, Cu, Mg, Zn, Mn, and Fe. The principle was successfully validated via laboratory trials nevertheless the potential for a large scale application needs to be further assessed.
- Figure 126 gives a qualitative comparison of the identified technologies with at least TRL 4. A detailed analysis of each technology in terms of investment, energy efficiency, application range, treatment capacity, and purification efficiency can be found from Part I of the study.

MIMI Tech GmbH
Preusweg 98, D-52074 Aachen
friedrich@mimi-tech.com

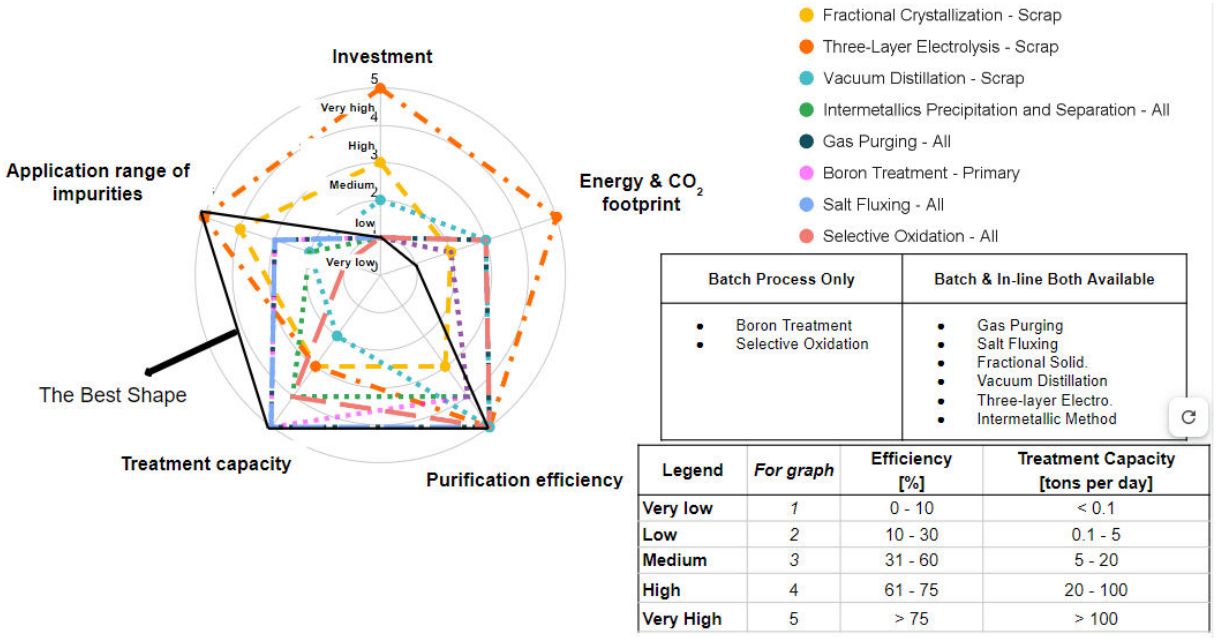

Batch Process Only	Batch & In-line Both Available
• Boron Treatment • Selective Oxidation	• Gas Purging • Salt Fluxing • Fractional Solid. • Vacuum Distillation • Three-layer Electro. • Intermetallic Method

Legend	*For graph*	Efficiency [%]	Treatment Capacity [tons per day]
Very low	*1*	0 - 10	< 0.1
Low	*2*	10 - 30	0.1 - 5
Medium	*3*	31 - 60	5 - 20
High	4	61 - 75	20 - 100
Very High	5	> 75	> 100

Figure 126: Qualitative comparison of the main investigated technologies (TRL 4–9).

- The comments and insights from the interviewees were grouped into respectively strength, weakness, opportunity, and threat. A further comprehensive analysis was made via a bubble plot as seen in the Figure 127 below. Through the bubble plot, the attractiveness and concerns of aluminium producers in implementing the removal technologies for recycling purpose can be clearly seen. Detailed interpretation of the bubble plot is provided in Sub-chapter 4.11.3.

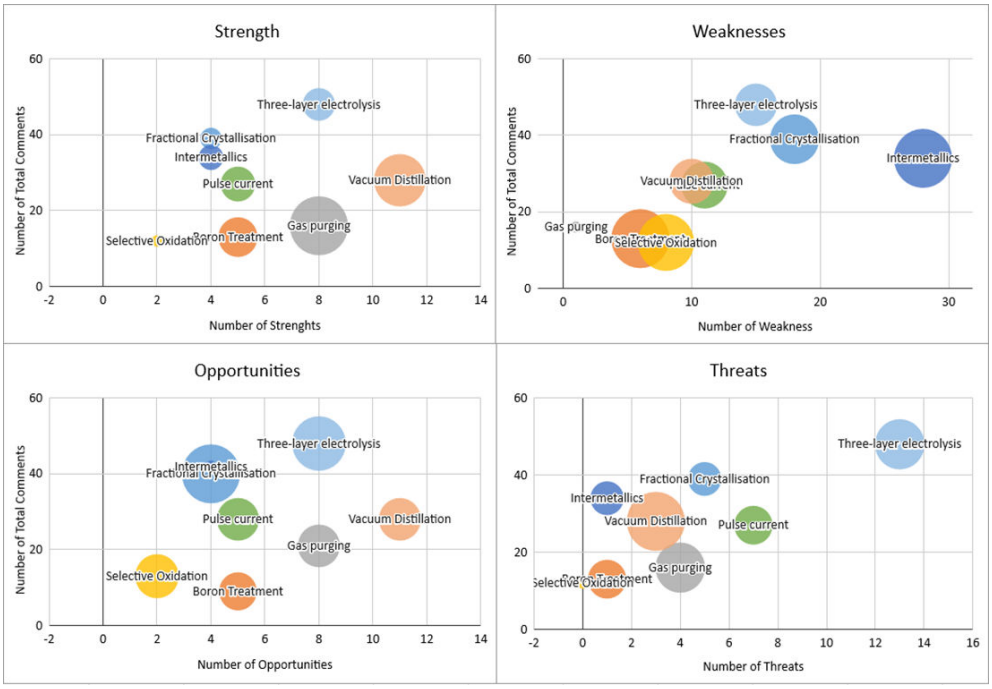

Figure 127: Bubble Plot - A summary and visualization of the interviews with aluminium producers.

MIMI Tech GmbH
Preusweg 98, D-52074 Aachen
friedrich@mimi-tech.com

6.2. Negative Effect and Neutralization Technologies

- The main negative effect of **Iron (Fe)** is the formation of harmful ß-phases, which reduce overall mechanical properties of alloys and have harmful effect of the alloy corrosion resistance. The ß-phases can act as corrosion centers that accelerate the corrosion of the material. The neutralization strategies include modification of iron-rich phases by adding another element (e.g., Mn), reduce the phases' volume fraction, and the break-down of these phases into smaller particles, all of which reduces negative effects of the phase. The approaches for reducing the size or volume fraction of precipitated IMs phases include friction stirring process, fast cooling rates, very high deformation. Moreover, heat treatment has also shown good neutralization results.
- The harmful effect of **Zinc (Zn)** is mostly related to alloy corrosion, particularly pitting formation, intergranular corrosion, exfoliation corrosion, stress corrosion cracking. The occurrence of corrosion was predominantly galvanic in nature, indicating that it involved the interaction between different components or phases within the material. To reduce its effect, heat treatment is the most investigated solution. Others such as grain size refining via mechanical deformation, e.g., cold rolling, also showed positive effect.
- **Copper (Cu)** also affects corrosion behavior of alloys, such as localized corrosion, including pitting corrosion, crevice corrosion, intergranular corrosion, and exfoliation corrosion. Stress corrosion cracking, and corrosion fatigue failure were reported as negative effects of Cu. Heat treatment was found to minimize its harmful effect on the investigated alloys.
- The presence of **Sodium (Na)** was reported to cause high-temperature embrittlement, intergranular fracture, and the reduction of the alloy's ultimate tensile strength.
- **Vanadium (V)** was reported to have an impact on the alloy's electrical conductivity. Boron treatment without actions of borides removal was reported to be helpful in enhancing conductivity of the treated alloy. For 7050 alloy, excessive V content leads to decrease of hot workability and initiate cracking. Deformation at optimum temperature and rate may help to alleviate the negative effect of excessive V.
- The impact of **Titanium (Ti)** and **Boron (B)** are mostly related with usage of Al-Ti-B grain refiners. The inoculated TiB_2 particles were found to influence the precipitation of intermetallics during solidification process, in both cast and wrought alloy systems, which may potentially affect the mechanical properties and workability of alloy. It was also reported excessive amount TiB_2 increased HTS of AA7050 alloy.
- **Silicon (Si)** was report to have impact the workability and anodization. It is one of the most common impurities and often have combined effects with Fe and Mg, where it forms β-FeSiAl5 and Mg_2Si phases. Some also reported the effect of the Si particles morphology, which causes lesser corrosion resistance in certain cases. Neutralization of the effects from Si are mainly controlled by heat treatment as reported by the several authors. The Si particles morphology can be influenced by the addition of Sc, increasing the corrosion resistance by protecting the oxide layer.

MIMI Tech GmbH
Preusweg 98, D-52074 Aachen
friedrich@mimi-tech.com

- **Gallium (Ga)** was reported to have effects on the corrosion and electrical resistivity. The addition of Ga has been shown to improve the electrical activity regardless of being in wrought alloys or cast alloys.
- For Al-Cr alloys containing 0.63-1.2 wt. %, **Chromium (Cr)** itself does not have any obvious effects, but when coupled with Si, it mainly has negative effect on the mechanical properties specifically on the hardness. Additionally, high Cr content (0.9wt.%) causes the delay in the initiation of precipitation hardening.
- **Magnesium (Mg)** affects the weldability the most, where it was said to cause immediate metal evaporation when radiated, leading to the formation of a keyhole. In addition to that, the presence of Mg have the effect of suppressing the Portevin–Le Chatelier effect. This can be neutralized by controlling working temperature.
- The impact of **Scandium (Sc)** are on the increased grain refinement and a direct effect on the grain boundaries and dislocations within the matrix, leading to improvement in the mechanical properties including ultimate tensile strength, yield strength and elongation. When alloyed within 0.12 wt. %, an increased resistance to coarsening can be observed along with dislocation networks. These networks can be eliminated by long solution treatment time. Reported limit was 0.45 wt. %, where from there on precipitation of phases with coarsened grain boundaries are aggregated.
- Neutralization technique for the negative effect of **Nickle (Ni)** on the corrosion was reported such that the process of equal-channel angular pressing (ECAP) managed to elevate pitting potentials and lowering passive current densities.
- The effect of **Manganese (Mn)** is mostly associated with Fe and Si. The element it can be used to eliminate beta phase. However it also forms intermetallics with Fe in the form of Al-Fe-Mn. These intermetallic are particularly vulnerable to corrosion. The ratio of Mn/Fe are widely discussed in intermetallic as well as mechanical properties of the alloy. An alloy with higher ratio (0.41/0.08) exhibited higher tensile strength and fracture toughness compared to a lower ratio (0.61/0.24).

MIMI Tech GmbH
Preusweg 98, D-52074 Aachen
friedrich@mimi-tech.com

7. References

[1] B. K. Reck and T. E. Graedel, "Challenges in metal recycling," *Science*, vol. 337, no. 6095, pp. 690–695, 2012, doi: 10.1126/science.1217501.

[2] T. G. Gutowski, S. Sahni, J. M. Allwood, M. F. Ashby, and E. Worrell, "The energy required to produce materials: Constraints on energy-intensity improvements, parameters of demand," *Philosophical Transactions of the Royal Society A: Mathematical, Physical and Engineering Sciences*, vol. 371, no. 1986, 2013, doi: 10.1098/rsta.2012.0003.

[3] S. K. Das, J. A. S. Green, J. G. Kaufman, D. Emadi, and M. Mahfoud, "Aluminum recycling—An integrated, industrywide approach," *JOM*, vol. 62, no. 2, pp. 23–26, 2010, doi: 10.1007/s11837-010-0026-6.

[4] M. E. Schlesinger, *Aluminum Recycling Economics*. 2013. doi: 10.1201/b16192-7.

[5] "International Aluminium Institute. Global Aluminium Cycle." Accessed: Jan. 10, 2022. [Online]. Available: https://alucycle.international-aluminium.org/public-access/

[6] J. C. Kelly, J. L. Sullivan, A. Burnham, and A. Elgowainy, "Impacts of Vehicle Weight Reduction via Material Substitution on Life-Cycle Greenhouse Gas Emissions," *Environmental Science and Technology*, vol. 49, no. 20, pp. 12535–12542, 2015, doi: 10.1021/acs.est.5b03192.

[7] R. Modaresi and D. B. Müller, "The role of automobiles for the future of aluminum recycling," *Environmental Science and Technology*, vol. 46, no. 16, pp. 8587–8594, 2012, doi: 10.1021/es300648w.

[8] S. K. Das, J. A. S. Green, and J. G. Kaufman, "The development of recycle-friendly automotive aluminum alloys," *Jom*, vol. 59, no. 11, pp. 47–51, 2007, doi: 10.1007/s11837-007-0140-2.

[9] D. V. Hernández, A. F. Valdés, M. A. G. Albarrán, and J. C. E. Bocardo, "A Kinetic Study on the Magnesium Removal from Aluminum Using SF6 Gaseous Mixtures," in *Light Metals*, The Minerals, Metals & Materials Society, 2004.

[10] G. K. Sigworth, E. M. Williams, and D. C. Chesonis, "Gas Fluxing of Molten Aluminum: An Overview," in *Light Metals*, 2008.

[11] Q. Fu, D. Xu, and J. W. Evans, "Chlorine fluxing for removal of magnesium from molten aluminum: Part I. Laboratory-scale measurements of reaction rates and bubble behavior," *Metall Mater Trans B*, vol. 29, no. 5, pp. 971–978, Oct. 1998, doi: 10.1007/s11663-998-0065-3.

[12] T. A. Utigard, "The properties and uses of fluxes in molten aluminum processing," *JOM*, vol. 50, no. 11, pp. 38–43, Nov. 1998, doi: 10.1007/s11837-998-0285-7.

[13] C. Celik and Don Doutre, "THEORETICAL AND EXPERIMENTAL INVESTIGATION OF FURNACE CHLORINE FLUXING," in *Light Metals*, The Minerals, Metals & Materials Society, 1989.

[14] STAS, "Aluminium Compact Degasser." [Online]. Available: https://www.stas.com/en/products/metal-treatment-and-casthouse-technologies/acd-aluminium-compact-degasser-2/

[15] C.R. Boeree, "Zinc Removal from Aircraft Aluminium-alloy scrap," Delft University of Technology, 2011. [Online]. Available: https://repository.tudelft.nl/islandora/object/uuid:9131c40e-df5c-409b-8c60-4fc7ecfb5215

[16] Stein Tore Johansen, Ramin Anvar, and Bjørn Rasch, "Bubble Size and Removal Rate of Sodium in Impeller Stirred Refining Reactors," in *Light Metals*, The Minerals, Metals & Materials Society, 1999.

MIMI Tech GmbH
Preusweg 98, D-52074 Aachen
friedrich@mimi-tech.com

[17] Edward M. Williams, Ron W. McCarthy, Sander A. Levy, and Geoffrey K. Sigworth, "Removal of Alkali Metals from Aluminum," in *Light Metals*, The Minerals, Metals & Materials Society, 2000.

[18] E. M. Williams, "ALKALI REMOVAL AND REDUCED CHLORINE USE DURING FURNACE FLUXING".

[19] M. Badowski, S. Instone, and M. Hagen, "Metallurgical Performance of Salt and Chlorine Fluxing Technologies in Casting Furnaces," in *Light Metals 2014*, J. Grandfield, Ed., Hoboken, NJ, USA: John Wiley & Sons, Inc., 2014, pp. 1031–1036. Accessed: May 04, 2023. [Online]. Available: https://onlinelibrary.wiley.com/doi/10.1002/9781118888438.ch171

[20] J. G. Stevens and H. Yu, "Mechanisms of Sodium, Calcium and Hydrogen Removal from an Aluminum Melt in a Stirred Tank Reactor - The Alcoa 622 Process," in *Light Metals*, The Minerals, Metals & Materials Society, 1988.

[21] B. Kulunk and R. I. L. Guthrie, "On the Removal Kinetics of Calcium from Aluminum and Aluminum-Magnesium Alloys," in *Light Metals*, The Minerals, Metals & Materials Society, 1991.

[22] D. H. DeYoung, "Salt Fluxes for alkali and Alkaline earth element removal from molten aluminum," in *7th Australian Asian Pacific Conference Aluminium Cast House Technology*, The Minerals, Metals & Materials Society, 2001.

[23] G. Dube, "TAC-A NOVEL PROCESS FOR THE REMOVAL LITHIUM AND OTHER ALKALIS IN PRIMARY ALIMINIUM," in *Light Metals*, The Minerals, Metals & Materials Society, 1983.

[24] J. W. Gao, D. Shu, J. Wang, and B. D. Sun, "Study on iron purification from aluminium melt by $Na_2B_4O_7$ flux," *Materials Science and Technology*, vol. 25, no. 5, pp. 619–624, May 2009, doi: 10.1179/174328408X339288.

[25] STAS, "RFI/Rotary Flux Injector." [Online]. Available: https://www.stas.com/en/products/metal-treatment-and-casthouse-technologies/rfi-rotary-flux-injector/

[26] STAS, "The TAC / The Treatment of Aluminium in Crucible."

[27] H. Wang, G. Fu, C. Cheng, and L. Wang, "Highly Efficient and Environmental Process for Removing Alkali Metals from Aluminum Melt," *Met Sci Heat Treat*, vol. 61, no. 1–2, pp. 90–95, May 2019, doi: 10.1007/s11041-019-00381-7.

[28] B. Rasch, "REFINING OF POTROOM METAL USING THE HYDRO RAM CRUCIBLE FLUXING PROCESS," in *Light Metals*, 1998.

[29] S. Leboeuf, C. Dupuis, B. Maltais, M.-A. Thibault, and E. Smarason, "IN-LINE SALT FLUXING PROCESS: THE SOLUTION TO CHLORINE GAS UTILIZATION IN CASTHOUSES," in *Light Metals*, The Minerals, Metals & Materials Society, 2007.

[30] G. Beland, C. Dupuis, and G. Riverin, "ROTARY FLUX INJECTION CHLORINE-FREE TECHNOQUE FOR FURNACE PREPARATION.pdf," in *Light Metals*, The Minerals, Metals & Materials Society, 1998.

[31] G. Riverin, J.-F. Bilodeau, and C. Dupuis, "A NOVEL CRUCIBLE METAL TREATMENT PROCESS FOR IMPURITY REMOVAL IN SECONDARY ALUMINIUM," in *Light Metals*, The Minerals, Metals & Materials Society, 2006.

[32] Z. A.G., N. S.B., and S. A.G., "Choice of Additions to NaCl-KCl Mixture for Aluminum Refining from Alkali and Alkali-Earth Impurities," in *Light metals*, The Minerals, Metals & Materials Society, 2005.

MIMI Tech GmbH
Preusweg 98, D-52074 Aachen
friedrich@mimi-tech.com

[33] B. Maltais, D. Prive, and A. Hashimi, “Operational Experience with a Large Capacity Integrated TAC (Treatment of Aluminium in a Crucible) and a Skimmer,” in *Light Metals*, The Minerals, Metals & Materials Society, 2009.

[34] S. Karabay and I. Uzman, “A STUDY ON THE POSSIBLE USAGE OF CONTINUOUSLY CAST ALUMINIUM 99.6% CONTAINING HIGH Ti, V, AND Cr IMPURITIES AS FEEDSTOCK FOR THE MANUFACTURING OF ELECTRICAL CONDUCTORS,” *Materials and Manufacturing Processes*, vol. 20, no. 2, pp. 231–243, Mar. 2005, doi: 10.1081/AMP-200041884.

[35] P. S. Cooper and M. A. Kearns, “Removal of Transition Metal Impurities in Aluminium Melts by Boron Additives,” *MSF*, vol. 217–222, pp. 141–146, May 1996, doi: 10.4028/www.scientific.net/MSF.217-222.141.

[36] W. C. Setzer and G. W. Boone, “The USE OF ALUMINUM-BORON MASTER ALLOYS TO IMPROVE ELECTRICAL CONDUCTIVITY.pdf,” in *Light Metals*, The Minerals, Metals & Materials Society, 1992.

[37] A. Khaliq, M. Akbar Rhamdhani, G. A. Brooks, and J. Grandfield, “Removal of Vanadium from Molten Aluminum—Part III. Analysis of Industrial Boron Treatment Practice,” *Metall Mater Trans B*, vol. 45, no. 2, pp. 784–794, Apr. 2014, doi: 10.1007/s11663-013-0017-4.

[38] A. Khaliq, M. A. Rhamdhani, G. A. Brooks, and J. Grandfield, “Mechanism of ZrB2 Formation in Molten Al-V-Zr Alloy During Boron Treatment,” *Metall Mater Trans B*, vol. 47, no. 1, pp. 595–607, Feb. 2016, doi: 10.1007/s11663-015-0464-1.

[39] A. Khaliq, M. A. Rhamdhani, G. A. Brooks, and J. Grandfield, “Thermodynamic Analysis of Ti, Zr, V and Cr Impurities in Aluminium Melt,” in *Light Metals 2011*, 1st ed., S. J. Lindsay, Ed., Wiley, 2011, pp. 751–756. Accessed: Sep. 11, 2023. [Online]. Available: https://onlinelibrary.wiley.com/doi/10.1002/9781118061992.ch130

[40] A. Khaliq, M. A. Rhamdhani, G. A. Brooks, and J. F. Grandfield, “Removal of Vanadium from Molten Aluminum—Part II. Kinetic Analysis and Mechanism of VB2 Formation,” *Metall Mater Trans B*, vol. 45, no. 2, pp. 769–783, Apr. 2014, doi: 10.1007/s11663-013-9975-9.

[41] A. Khaliq *et al.*, “Thermodynamic and Kinetic Analyses of the Removal of Impurity Titanium and Vanadium from Molten Aluminum for Electrical Conductor Applications,” *Metall Mater Trans B*, vol. 52, no. 5, pp. 3130–3141, Oct. 2021, doi: 10.1007/s11663-021-02241-3.

[42] A. Khaliq, H. T. Ali, and M. Yusuf, “Thermodynamic and kinetic analysis of CrB2 and VB2 formation in molten Al–Cr–V–B alloy,” *Transactions of Nonferrous Metals Society of China*, vol. 31, no. 10, pp. 3162–3176, Oct. 2021, doi: 10.1016/S1003-6326(21)65723-0.

[43] P. L. Patterson, “The Hoopes Aluminum Refining Process, notarized letter, 17 May 1933.” 1933. [Online]. Available: http://hdl.handle.net/2186/ksl:spcbru01084

[44] H. Hoshikawa, I. Tanaka, and T. Megumi, “Refining Technology and Low Temperature Properties for High Purity Aluminum,” *Sumitomo Kagaku*, pp. 1–12, 2013.

[45] H. Zhao and H. Lu, “The Development of 85kA Three-Layer Electrolysis Cell for Refining of Aluminum,” in *Light metals; proceedings of the technical sessions presented by the TMS Aluminum Committee at the TMS 2008 annual meeting & exhibition*, New Orleans, Louisiana, USA: Warrendale, Pa. : Minerals, Metals and Materials Society, ©2009., 2008, pp. 533–540.

[46] P. Godet, M. Leroy, and J. Thonstad, “Solubility of alumina in three-layer aluminium-refining cell electrolytes,” 1991.

[47] A. I. Beljajew, L. A. Firsanowa, and M. B. Rapoport, *Metallurgie des Aluminiums*, vol. Band II-Die Elektrolytische Aluminiumraffination und die Eletktrothermie. VEB Verlag Technik Berlin, 1957.

MIMI Tech GmbH
Preusweg 98, D-52074 Aachen
friedrich@mimi-tech.com

[48] Y. Plevachuk, V. Sklyarchuk, A. Yakymovych, S. Eckert, B. Willers, and K. Eigenfeld, "Density, Viscosity, and Electrical Conductivity of Hypoeutectic Al-Cu Liquid Alloys," *Metall and Mat Trans A*, vol. 39, no. 12, pp. 3040–3045, Dec. 2008, doi: 10.1007/s11661-008-9659-2.

[49] K. S. Srinivasan *et al.*, "Electro-refining of aluminium," *Bulletin of Electrochemistry*, vol. 2, no. December, pp. 621–623, 1986.

[50] M. E. Samoshina, A. A. Aksenov, A. S. Prosviryakov, P. Y. Bryantsev, and T. B. Sagalova, "Structure and properties of mechanically alloyed composite material from waste of high purity aluminium production," *Powder Metallurgy*, vol. 54, no. 4, pp. 471–473, Sep. 2011, doi: 10.1179/1743290110Y.0000000003.

[51] T. G. Pearson and H. W. L. Phillips, "The production and properties of super-purity aluminum," *Metallurgical reviews*, vol. 2, no. 8, pp. 305–360, 1957.

[52] N. T. Beukes and J. Badenhorst, "Copper electrowinning: theoretical and practical design," p. 28, 2009.

[53] S. S. Vasanc *et al.*, "ELECTRO-REFININGOF ALUMINIUM".

[54] M. Kondo, H. Maeda, and M. Mizuguchi, "The production of high-purity aluminum in Japan," *JOM*, vol. 42, no. 11, pp. 36–37, Nov. 1990, doi: 10.1007/BF03220434.

[55] H. Zhao', "THE DEVELOPMENT OF 85KA THREE-LAYER ELECTROLYSISCELL FOR REFINING OF ALUMINIUM".

[56] D. H. DeYoung, X. Liu, B. L. Mydland, and J. Wiswall, "Systems and methods for purifying aluminum," US11001931

[57] A. Solheim, O. S. Kjos, H. Gudbrandsen, and E. Skybakmoen, "Separation of Aluminum from More Noble Elements in an Electrolysis Cell with Side-by-Side Geometry," *METALLURGICAL AND MATERIALS TRANSACTIONS B-PROCESS METALLURGY AND MATERIALS PROCESSING SCIENCE*, vol. 52, no. 3. SPRINGER, ONE NEW YORK PLAZA, SUITE 4600, NEW YORK, NY, UNITED STATES, pp. 1550–1555, Jun. 2021. doi: 10.1007/s11663-021-02122-9.

[58] X. Lu *et al.*, "A solid-state electrolysis process for upcycling aluminium scrap," *Nature*, vol. 606, no. 7914, pp. 511–515, Jun. 2022, doi: 10.1038/s41586-022-04748-4.

[59] S. Oya, J. Nunomura, H. Matsushima, Y. Kyo, Y. Kojima, and M. Ueda, "Dissolution Characteristics of Al-Si Alloys in AlCl3-NaCl-KCl Molten Salt at 423 K," *ELECTROCHEMISTRY*, vol. 90, no. 12. ELECTROCHEMICAL SOC JAPAN, NIHON-KOUDOUKAI BUILDING 7F, 3-1-6, NISHIKANDA, CHIYODA-KU, TOKYO, 101-0065, JAPAN, 2022. doi: 10.5796/electrochemistry.22-00115.

[60] A. Yasinskiy *et al.*, "Aluminium Recycling in Single- and Multiple-Capillary Laboratory Electrolysis Cells," *Metals*, vol. 11, no. 7, p. 1053, Jun. 2021, doi: 10.3390/met11071053.

[61] L. Wei, P. Li, T. Han, T. Zhang, and X. Zhai, "Study on Purification and Removal of Iron from Alloy Anode," in *CHEMICAL ENGINEERING AND MATERIAL PROPERTIES, PTS 1 AND 2*, H. Zhang and B. Wu, Eds., in Advanced Materials Research, vol. 391–392. KREUZSTRASSE 10, 8635 DURNTEN-ZURICH, SWITZERLAND: TRANS TECH PUBLICATIONS LTD, 2012, p. 883+. doi: 10.4028/www.scientific.net/AMR.391-392.883.

[62] W. G. Pfann, "Zone Melting: This technique offers unique advantages in purification and in control of composition in various substances," *Science*, vol. 135, no. 3509, pp. 1101–1109, Mar. 1962, doi: 10.1126/science.135.3509.1101.

[63] S. Mikubo, "The Latest Refining Technologies of Segregation Process to Produce High Purity Aluminum," in *12th International Conference on Proceedings of the 12th International Conference on AluminiumAlloys*, 2010, pp. 224–228.

MIMI Tech GmbH
Preusweg 98, D-52074 Aachen
friedrich@mimi-tech.com

[64] E. Hashimoto, Y. Ueda, and T. Kino, "Purification of Ultra-High Purity Aluminum," *J. Phys. IV France*, vol. 05, no. C7, pp. C7-153-C7-157, Nov. 1995, doi: 10.1051/jp4:1995715.

[65] J. V. Widiatmo, K. Harada, K. Yamazawa, and M. Arai, "Estimation of impurity effect in aluminium fixed-point cells based on thermal analysis," *Metrologia*, vol. 43, no. 6, pp. 561–572, 2006, doi: 10.1088/0026-1394/43/6/012.

[66] W. D. Hannibal *et al.*, "Entwickling eines technischen Verfahrens zur Herstellung von Reinstaluminum für die Kryoelektrotechnik, speziell für Kryomagnete - Forschungsbericht," Leichtmetall-Forschungsinstitut der Vereingte Aluminum-Werke AG, Bonn, Germany, 1974.

[67] J. Barthel, E. Buhirg, and Et. Al., *Kristallisation aus Schmelzen*. Verlag für Grundstoffindustrie Leipzig, 1982.

[68] J. V. Pearce, "Distribution coefficients of impurities in metals," *International Journal of Thermophysics*, vol. 35, no. 3–4, pp. 628–635, 2014, doi: 10.1007/s10765-014-1585-5.

[69] H. Fredriksson and U. Åkerlind, *Solidification and Crystallization Processing in Metals and Alloys*. 2012. doi: 10.1002/9781119975540.

[70] M. Kondo, H. Maeda, and M. Mizuguchi, "The production of high-purity aluminum in Japan," *Jom*, vol. 42, no. 11, pp. 36–37, 1990, doi: 10.1007/BF03220434.

[71] D. C. Curtolo, N. Xiong, S. Friedrich, and B. Friedrich, "High- and Ultra-High-Purity Aluminum, a Review on Technical Production Methodologies," *Metals*, vol. 11, no. 9, p. 1407, Sep. 2021, doi: 10.3390/met11091407.

[72] P. Rudolph, "A Compressed Approach to the Theory of Crystal Growth . Thermodynamics , Kinetics and Transport," no. February, 2021.

[73] D. T. J. Hurle, "Constitutional During Growth From Stirred Melts - I Theoretical," *Solid-State Electronics*, vol. 3, pp. 37–44, 1961.

[74] D. C. Curtolo, N. Xiong, S. Friedrich, and B. Friedrich, "High- and Ultra-High-Purity Aluminum, a Review on Technical Production Methodologies," *Metals*, vol. 11, no. 9, p. 1407, Sep. 2021, doi: 10.3390/met11091407.

[75] W. Kurz and D. J. Fisher, *Fundamentals of solidification*. Aedermannsdorf: Trans Tech Publ. 1992, 1989.

[76] S. C. Jacobs and L. Burrel, "Purification of Aluminum," 3303019, Feb. 07, 1967

[77] R. K. Dawless, R. L. Troup, D. L. Meier, and A. Rohatgi, "Production of extreme-purity aluminum and silicon by fractional crystallization processing," *Journal of Crystal Growth*, vol. 89, no. 1, pp. 68–74, Jun. 1988, doi: 10.1016/0022-0248(88)90073-5.

[78] S. Mikubo, "The Latest Refining Technologies of Segregation Process to Produce High Purity Aluminum".

[79] P. A. De Vries and H. A. Wouters, "Method for fractional crystallization of a molten metal," WO 2004/005558 A1, Jan. 15, 2004

[80] D. C. Curtolo, S. Friedrich, D. Bellin, G. S. Nayak, and B. Friedrich, "Definition of a First Process Window for Purification of Aluminum via 'Cooled Finger' Crystallization Technique," *METALS*, vol. 7, no. 9, Sep. 2017, doi: 10.3390/met7090341.

[81] D. C. Curtolo, M. J. Rodriguez-Rojas, S. Friedrich, and B. Friedrich, "Alternative fractional crystallization-based methods to produce high-purity aluminum," *JOURNAL OF MATERIALS RESEARCH AND TECHNOLOGY-JMR&T*, vol. 12, pp. 796–806, Jun. 2021, doi: 10.1016/j.jmrt.2021.03.025.

MIMI Tech GmbH
Preusweg 98, D-52074 Aachen
friedrich@mimi-tech.com

[82] X. Zhang, S. Friedrich, and B. Friedrich, "The Influence of Initial Purity Level on the Refining Efficiency of Aluminum via Zone Refining," *METALS*, vol. 11, no. 2, Feb. 2021, doi: 10.3390/met11020201.

[83] M. Gotenbruck, D. C. Curtolo, S. Friedrich, C. J. Mueller, N. Rademacher, and B. Friedrich, "Static Crystallization, an Alternative Methodology for Synthesis of High-Purity Aluminum," *METALS*, vol. 13, no. 2, Feb. 2023, doi: 10.3390/met13020280.

[84] H. Wan *et al.*, "Effect of Silicon Separation on the Preparation of High-Purity Aluminum," *SILICON*, vol. 13, no. 2, pp. 399–407, Feb. 2021, doi: 10.1007/s12633-020-00443-z.

[85] H. Wan, B. Xu, J. Zhao, B. Yang, and Y. Dai, "Analysis of the High-Purity Aluminum Purification Process Using Zone-Refining Technique," in *TMS 2019 148TH ANNUAL MEETING & EXHIBITION SUPPLEMENTAL PROCEEDINGS*, in Minerals Metals & Materials Series. GEWERBESTRASSE 11, CHAM, CH-6330, SWITZERLAND: SPRINGER INTERNATIONAL PUBLISHING AG, 2019, pp. 1697–1706. doi: 10.1007/978-3-030-05861-6_157.

[86] L. Zhao, Z. Guo, Z. Wang, and M. Wang, "Removal of Low-Content Impurities from Al By Super-Gravity," *METALLURGICAL AND MATERIALS TRANSACTIONS B-PROCESS METALLURGY AND MATERIALS PROCESSING SCIENCE*, vol. 41, no. 3, pp. 505–508, Jun. 2010, doi: 10.1007/s11663-010-9376-2.

[87] R. K. Dawless, R. L. Troup, D. L. Meier, and A. Rohatgi, "Production of extreme-purity aluminum and silicon by fractional crystallization processing," *Journal of Crystal Growth*, vol. 89, no. 1, pp. 68–74, Jun. 1988, doi: 10.1016/0022-0248(88)90073-5.

[88] E. Hashimoto, Y. Ueda, and T. Kino, "Purification of Ultra-High Purity Aluminum," *J. Phys. IV France*, vol. 05, no. C7, pp. C7-153-C7-157, Nov. 1995, doi: 10.1051/jp4:1995715.

[89] A. Kahveci and A. Unal, "Refining of a 5XXX series aluminum alloy scrap by Alcoa fractional crystallization process," in *FOURTH INTERNATIONAL SYMPOSIUM ON RECYCLING OF METALS AND ENGINEERED MATERIALS, PROCEEDINGS*, D. Stewart, J. Daley, and R. Stephens, Eds., 184 THORN HILL RD, WARRENDALE, PA 15086-7514 USA: MINERALS, METALS & MATERIALS SOC, 2000, pp. 979–991.

[90] H. A. Wouters *et al.*, "Crystallisation method for the purification of a molten metal, in particular recycled aluminum," US 7892318 B2, Jan. 03, 2008

[91] S. Venditti, D. Eskin, and A. Jacot, "Fractional Solidification for Purification of Recycled Aluminium Alloys," in The Minerals, Metals & Materials Series. Cham: Springer International Publishing, 2020, p. 1110. doi: 10.1007/978-3-030-36408-3.

[92] Y. Murakami and N. Omura, "Reduction of Impurity Elements by Applying Electromagnetic Stirring in Fractional Crystallization," in *LIGHT METALS 2021, 50TH EDITION*, L. Perander, Ed., in Minerals Metals & Materials Series. GEWERBESTRASSE 11, CHAM, CH-6330, SWITZERLAND: SPRINGER INTERNATIONAL PUBLISHING AG, 2021, pp. 818–821. doi: 10.1007/978-3-030-65396-5_107.

[93] X. Xu, J. Li, Z. Dong, L. Zeng, Z. Xu, and J. Li, "Multiphase modelling of the continuous metallurgical purification process for impurity removing of recycled aluminum," *JOURNAL OF MATERIALS RESEARCH AND TECHNOLOGY-JMR&T*, vol. 18, pp. 830–840, Jun. 2022, doi: 10.1016/j.jmrt.2022.03.003.

[94] S. Fashu, Q. Hu, and J. Li, "Purification of an industrial aluminum alloy by melt stirring during Ohno Continuous Casting process," *Materials Letters*, vol. 65, no. 14, pp. 2248–2250, Jul. 2011, doi: 10.1016/j.matlet.2011.04.076.

MIMI Tech GmbH
Preusweg 98, D-52074 Aachen
friedrich@mimi-tech.com

[95] R. Muñoz-Arroyo *et al.*, "Magnesium Removal from an Aluminum A-332 Molten Alloy Using Enriched Zeolite with Nanoparticles of SiO $_2$," *Advances in Materials Science and Engineering*, vol. 2014, pp. 1–7, 2014, doi: 10.1155/2014/747451.

[96] T. Hashiguchi and H. Sueyoshi, "Removal of Magnesium from Molten Aluminum Scrap by Compound-Separation Method with Shirasu," *Mater. Trans.*, vol. 51, no. 5, pp. 838–843, 2010, doi: 10.2320/matertrans.MH200914.

[97] A. FloresV and C. MartinezG, "A kinetic Study of Demagging of Molten Aluminum by the Use of SiO2 Submerged Powder Injection," in *Light Metals*, The Minerals, Metals & Materials Society, 1999.

[98] F. Barrera-Méndez, J. C. Escobedo-Bocardo, D. A. Cortés-Hernández, J. M. Almanza-Robles, R. Muñoz-Arroyo, and H. M. Hernández-García, "Magnesium Removal from Molten Al-Si Alloys Using Zeolite," *Canadian Metallurgical Quarterly*, vol. 49, no. 2, pp. 163–170, Apr. 2010, doi: 10.1179/cmq.2010.49.2.163.

[99] J. C. Escobedo, "Recent Experiences with the Use of SiO2 for Removing of Magnesium from Molten Aluminum Alloys," in *Light Metals*, The Minerals, Metals & Materials Society, 2003.

[100] T. Hashiguchi and H. Sueyoshi, "Removal of Magnesium from Aluminum Scrap by Compound-Separation Method Using Shirasu as an Additive," *Mater. Trans.*, vol. 51, no. 4, pp. 775–780, 2010, doi: 10.2320/matertrans.MBW200919.

[101] H. Becker, A. Thum, B. Distl, M. J. Kriegel, and A. Leineweber, "Effect of Melt Conditioning on Removal of Fe from Secondary Al-Si Alloys Containing Mg, Mn, and Cr," *Metall Mater Trans A*, vol. 49, no. 12, pp. 6375–6389, Dec. 2018, doi: 10.1007/s11661-018-4930-7.

[102] P. Le Brun, C. Kräutlein, G. Rombach, and P. Pouly, "Removal of intermetallic particles for the purification of aluminum alloys," in *Liggt Metals*, The Minerals, Metals & Materials Society, 2007.

[103] L. Meng, Z. Wang, L. Wang, L. Guo, and Z. Guo, "Novel and efficient purification of scrap Al-Mg alloys using supergravity technology," *Waste Management*, vol. 119, pp. 22–29, Jan. 2021, doi: 10.1016/j.wasman.2020.09.027.

[104] J. P. Schoß, H. Becker, A. Keßler, A. Leineweber, and G. Wolf, "Removal of Iron from a Secondary Al–Si Die-Casting Alloy by Metal Melt Filtration in a Laboratory Filtration Apparatus," *Adv Eng Mater*, vol. 24, no. 2, p. 2100695, Feb. 2022, doi: 10.1002/adem.202100695.

[105] C. J. Simensen and P. LeBrun, "REMOVAL OF IRON AND MANGANESE IN ALUMINIUM ALLOYS BY ADDING MAGNESIUM AND SUBSEQUENTLY CENTRIFUGING," in *Light Metals*, The Minerals, Metals & Materials Society, 2009.

[106] G. C. Lee, M. G. Kim, J. P. Park, J. H. Kim, J. H. Jung, and E. R. Baek, "Iron Removal in Aluminum Melts Containing Scrap by Electromagnetic Stirring," *MSF*, vol. 638–642, pp. 267–272, Jan. 2010, doi: 10.4028/www.scientific.net/MSF.638-642.267.

[107] J. Gobrecht, "Settling-out of Fe, Mn and Cr in Al-Si casting alloys," *Giesserei*, vol. 62, no. 10, pp. 263–266, 1975.

[108] J. L. Jorstad, "Understanding Sludge," *Die Cast. Eng.*, vol. 30, no. 6, p. 30, 1986.

[109] G. Timelli, S. Capuzzi, and A. Fabrizi, "Precipitation of primary Fe-rich compounds in secondary AlSi9Cu3(Fe) alloys," *J Therm Anal Calorim*, vol. 123, no. 1, pp. 249–262, Jan. 2016, doi: 10.1007/s10973-015-4952-y.

[110] L. F. Mondolfo, *Aluminium Alloys*. ELSEVIER, 1976.

MIMI Tech GmbH
Preusweg 98, D-52074 Aachen
friedrich@mimi-tech.com

[111] J. Roger, F. Bosselet, and J. C. Viala, “X-rays structural analysis and thermal stability studies of the ternary compound α-AlFeSi,” *Journal of Solid State Chemistry*, vol. 184, no. 5, pp. 1120–1128, May 2011, doi: 10.1016/j.jssc.2011.03.025.

[112] A. Dhinakar, P.-Y. Lu, N.-K. Tang, and J.-K. Chen, “Iron Reduction in 356 Secondary Aluminum Alloy by Mn and Cr Addition for Sediment Separation,” *Inter Metalcast*, vol. 15, no. 1, pp. 182–192, Jan. 2021, doi: 10.1007/s40962-020-00433-2.

[113] H. Matsubara, N. Izawa, and M. Nakanishi, “Macroscopic segregation in Al-11 mass% Si alloy containing 2 mass% Fe solidified under centrifugal force,” *JAPAN INSTITUTE OF LIGHT METALS*, vol. 48, pp. 93–97, 1998.

[114] L. Zhang, S. Wang, A. Dong, J. Gao, and L. N. W. Damoah, “Application of Electromagnetic (EM) Separation Technology to Metal Refining Processes: A Review,” *Metall Mater Trans B*, vol. 45, no. 6, pp. 2153–2185, Dec. 2014, doi: 10.1007/s11663-014-0123-y.

[115] Zhengming XU, Tianxiao Li, and Yaohe Zhou, “Electromagnetic Filtration of Primary Fe-Rich Phases from Al-Si Alloy Melt,” *J. Mater. Sci. Technol.*, vol. 7, no. 3, pp. 306–310, 2001.

[116] J.-H. Kim and E.-P. Yoon, “Elimination of Fe element in A380 aluminum alloy scrap by electromagnetic force”.

[117] MAROTO SOTO, José Antonio *et al.*, “PROCEDURE AND INSTALLATION FOR ELIMINATING IMPURITIES IN A CONTAMINATED”

[118] Y. Bao *et al.*, “Simultaneous Removal of Silicon and Iron-Rich Phases from Coarse Al-Si Alloys Using Manganese Under Electromagnetic Field,” *Metall Mater Trans B*, vol. 49, no. 6, pp. 3413–3423, Dec. 2018, doi: 10.1007/s11663-018-1412-7.

[119] S. G. Shabestari and J. E. Gruzleski, “Gravity segregation of complex intermetallic compounds in liquid aluminum-silicon alloys,” *Metall Mater Trans A*, vol. 26, no. 4, pp. 999–1006, Apr. 1995, doi: 10.1007/BF02649097.

[120] X. Zhang *et al.*, “Highly efficient Fe separation induced by Fe-containing particle agglomeration in Al-7Si-0.3Mg alloy melt,” *Journal of Materials Research and Technology*, vol. 21, pp. 604–616, Nov. 2022, doi: 10.1016/j.jmrt.2022.09.034.

[121] P. Ashtari, K. Tetley-Gerard, and K. Sadayappan, “Removal of iron from recycled aluminium alloys,” *Canadian Metallurgical Quarterly*, vol. 51, no. 1, pp. 75–80, Jan. 2012, doi: 10.1179/1879139511Y.0000000026.

[122] X. Cao, N. Saunders, and J. Campbell, “Effect of iron and manganese contents on convection-free precipitation and sedimentation of primary α-Al(FeMn)Si phase in liquid Al-11.5Si-0.4Mg alloy”.

[123] K. Al-Helal, J. Lazaro-Nebreda, J. B. Patel, and G. M. Scamans, “High-Shear De-Gassing and De-Ironing of an Aluminum Casting Alloy Made Directly from Aluminum End-of-Life Vehicle Scrap,” *Recycling*, vol. 6, no. 4, p. 66, Oct. 2021, doi: 10.3390/recycling6040066.

[124] S. G. Shabestari, M. Keshavarz, and M. M. Hejazi, “Effect of strontium on the kinetics of formation and segregation of intermetallic compounds in A380 aluminum alloy,” *Journal of Alloys and Compounds*, vol. 477, no. 1–2, pp. 892–899, May 2009, doi: 10.1016/j.jallcom.2008.11.037.

[125] A. Flores-V, M. Sukiennik, and A. H. Castillejos-E, “A kinetic study on the nucleation and growth of the AlsFeMnSiz intermetallic compound for aluminum scrap purification”.

[126] D. Song, Y. Jia, Q. Li, Y. Zhao, and W. Zhang, “Effect of Initial Fe Content on Microstructure and Mechanical Properties of Recycled Al-7.0Si-Fe-Mn Alloys with Constant Mn/Fe Ratio,” *Materials*, vol. 15, no. 4, p. 1618, Feb. 2022, doi: 10.3390/ma15041618.

MIMI Tech GmbH
Preusweg 98, D-52074 Aachen
friedrich@mimi-tech.com

[127] W. Yang, F. Gao, and S. Ji, “Formation and sedimentation of Fe-rich intermetallics in Al–Si–Cu–Fe alloy,” *Transactions of Nonferrous Metals Society of China*, vol. 25, no. 5, pp. 1704–1714, May 2015, doi: 10.1016/S1003-6326(15)63776-1.

[128] H. M. van der Donk, G.H. Nijhof, C.A.M. Castelijns, S. Bouvet, and Y. Bertaud, “Purification of Remelted Aluminium Packagings.pdf,” in *Light Metals*, The Minerals, Metals & Materials Society, 1996.

[129] H. L. De Moraes, J. R. De Oliveira, D. C. R. Espinosa, and J. A. S. Tenório, “Removal of Iron from Molten Recycled Aluminum through Intermediate Phase Filtration,” *Mater. Trans.*, vol. 47, no. 7, pp. 1731–1736, 2006, doi: 10.2320/matertrans.47.1731.

[130] F. Wen and A. Ge, “Composite purification technology and mechanism of recycled aluminum alloys”.

[131] X. Zhenming, L. Tianxiao, and Z. Yaohe, “Elimination of Fe in Al-Si cast alloy scrap by electromagnetic filtration”.

[132] R. Harris and W. G. Davenport, “Vacuum distillation of liquid metals: Part I. Theory and experimental study,” *Journal of Electronic Materials*, vol. 21, no. 1, pp. 581–588, 1992, doi: 10.1007/BF02669171.

[133] J. Safarian and M. Tangstad, “Vacuum refining of molten silicon,” *Metallurgical and Materials Transactions B: Process Metallurgy and Materials Processing Science*, vol. 43, no. 6, pp. 1427–1445, 2012, doi: 10.1007/s11663-012-9728-1.

[134] C. J. Smithells, W. F. Gale, and T. C. Totemeier, *Smithells metals reference book*, 8th ed. / edited by W.F. Gale, T.C. Totemeier. Amsterdam ; Boston: Elsevier Butterworth-Heinemann, 2004.

[135] P. D. Desai, “Thermodynamic Properties of Selected Binary Aluminum Alloy Systems,” *Journal of Physical and Chemical Reference Data*, vol. 16, no. 1, pp. 109–124, 1987, doi: 10.1063/1.555788.

[136] R. Hultgren and A. S. for Metals, *Selected Values of the Thermodynamic Properties of Binary Alloys*. American Society for Metals, 1973.

[137] F. Dimayuga and R. Harris, “Removal of Volatile Impurities from Aluminium Melts 1986,” *Light Metals 1986*, 1986.

[138] J. E. Murphy and J. J. Lukasko, “Vacuum distillation of magnesium and zinc from aluminum scrap,” presented at the TMS - Light Metals 1993, pp. 1061–1065.

[139] M. Ohtaki and H. Kudou, “Application of some vacuum distillation process to refine Zn from Al scrap,” presented at the International Conference on Aluminium Alloys 1998, pp. 357–372.

[140] Q. S. Wei, B. Yang, Y. F. Li, and Y. N. Dai, “Zinc Removing from Aluminum Alloy by Vacuum Distillation,” in *Advanced Materials Research*, Nov. 2011, pp. 303–306. doi: 10.4028/www.scientific.net/AMR.402.303.

[141] M. Gotenbruck, D. C. Curtolo, S. Friedrich, and B. Friedrich, “The Effectiveness of Cooled-Finger and Vacuum Distillation Processes in View of the Removal of Fe, Si and Zn from Aluminium,” *METALS*, vol. 12, no. 12, Dec. 2022, doi: 10.3390/met12122027.

[142] A. D. Little, “A Survey of Potential Processes for the Manufacture of Aluminum,” Argonne National Laboratory, Argonne, Ullinois, USA, for U.S. Department of Energy Contract Number 31-109-38-4210, Dec. 1979.

[143] N. W. F. Phillips, B. Rapson, and E. A. Holingshead, “Method of Separating Aluminum from Impurities,” US 2.723.911, Nov. 15, 1955

MIMI Tech GmbH
Preusweg 98, D-52074 Aachen
friedrich@mimi-tech.com

[144] T. Kikuchi, T. Kurosawa, and Yagihashi, "Equilibrium of the 2Al (l) + AlCl3 (g) = 3AlCl (g) Reaction in the Subhalide Process of Aluminium (Study of Extractive Metallurgy of Aluminium (l))," *Trans. JIM*, vol. 5, pp. 122–127, Mar. 1964.

[145] K. H. Pedersen and H. J. Bauck, "Process of Refining Aluminum," US 2.621.120, Dec. 09, 1952

[146] Y. Sun, X. Huang, C. Liu, M. Zhou, and X. Zhang, "Impurity iron separation from molten secondary aluminum by pulsed electric current," *Journal of Alloys and Compounds*, vol. 934, p. 167903, Feb. 2023, doi: 10.1016/j.jallcom.2022.167903.

[147] C. Fan *et al.*, "Reduction of Fe concentration in Al–4Si–1Fe–1Cu–0.5Zn–0.5Mn alloys with S," *Rare Met.*, vol. 35, no. 4, pp. 320–324, Apr. 2016, doi: 10.1007/s12598-014-0347-7.

[148] B. Sun, N. Sun, L. Wang, S. Zhang, and Z. Guo, "A new process for efficient purification of 6061 aluminum alloy scrap under semi-solid and super-gravity conditions," *Journal of Cleaner Production*, vol. 402, p. 136825, May 2023, doi: 10.1016/j.jclepro.2023.136825.

[149] L. Zhao, Z. Guo, Z. Wang, and M. Wang, "Removal of Low-Content Impurities from Al By Super-Gravity," *Metall Mater Trans B*, vol. 41, no. 3, pp. 505–508, Jun. 2010, doi: 10.1007/s11663-010-9376-2.

[150] Z. X. Yu, S. X. Hao, and Q. S. Fu, "Electrochemical Behaviors of Different Gradesof Pure Aluminum in Alkaline Solution," *AMR*, vol. 652–654, pp. 853–859, Jan. 2013, doi: 10.4028/www.scientific.net/AMR.652-654.853.

[151] X. Zheng *et al.*, "Friction stir processing induced elctrochemical performance improvement of commercial Al for Al-air battery," *Electrochimica Acta*, vol. 354, p. 136635, Sep. 2020, doi: 10.1016/j.electacta.2020.136635.

[152] J. Ren *et al.*, "Evaluation of Impurities in Aluminum Anodes for Al-Air Batteries," *ACS Sustainable Chem. Eng.*, vol. 9, no. 5, pp. 2300–2308, Feb. 2021, doi: 10.1021/acssuschemeng.0c08415.

[153] N. A. Belov, S. O. Cherkasov, N. O. Korotkova, A. O. Yakovleva, and K. A. Tsydenov, "Effect of Iron and Silicon on the Phase Composition and Microstructure of the Al-2% Cu-2% Mn (wt %) Cold Rolled Alloy," *PHYSICS OF METALS AND METALLOGRAPHY*, vol. 122, no. 11, pp. 1095–1102, Nov. 2021, doi: 10.1134/S0031918X2111003X.

[154] Y. Zhao *et al.*, "Effects of precipitation behaviors on the microstructure and fracture toughness of Al-Cu-Mg aluminum alloys," *OPTOELECTRONICS AND ADVANCED MATERIALS-RAPID COMMUNICATIONS*, vol. 10, no. 7–8, pp. 583–589, Aug. 2016.

[155] Y. H. Gao *et al.*, "Solute repositioning to tune the multiple microalloying effects in an Al-Cu alloy with minor Sc, Fe and Si addition," *MATERIALS SCIENCE AND ENGINEERING A-STRUCTURAL MATERIALS PROPERTIES MICROSTRUCTURE AND PROCESSING*, vol. 803, Jan. 2021, doi: 10.1016/j.msea.2020.140509.

[156] S. M. Amer, R. Yu. Barkov, and A. V. Pozdniakov, "Effect of Iron and Silicon Impurities on Phase Composition and Mechanical Properties of Al-6.3Cu-3.2Y Alloy," *PHYSICS OF METALS AND METALLOGRAPHY*, vol. 121, no. 10, pp. 1002–1007, Oct. 2020, doi: 10.1134/S0031918X20090021.

[157] M. Barkov V., O. Mamzurina I., M. Glavatskikh V., R. Y. Barkov, and A. Pozdniakov V., "The Effects of Impurities on the Phase Composition and the Properties of the Al-Cu-Gd Alloy," *PHYSICS OF METALS AND METALLOGRAPHY*, vol. 123, no. 6, pp. 604–608, Jun. 2022, doi: 10.1134/S0031918X22060035.

MIMI Tech GmbH
Preusweg 98, D-52074 Aachen
friedrich@mimi-tech.com

[158] K. Spencer, S. F. Corbin, and D. J. Lloyd, "The influence of iron content on the plane strain fracture behaviour of AA 5754 Al–Mg sheet alloys," *Materials Science and Engineering: A*, vol. 325, no. 1–2, pp. 394–404, Feb. 2002, doi: 10.1016/S0921-5093(01)01481-2.

[159] Q. Liu, H. Zhang, P. Jiang, and Y. Lv, "The Alloying Strategy to Tailor the Mechanical Properties of theta-Al13Fe4 Phase in Al-Mg-Fe Alloy by First-Principles Calculations," *METALS*, vol. 12, no. 12, Dec. 2022, doi: 10.3390/met12121999.

[160] W. Gao, D. Wang, M. Seifi, and J. J. Lewandowski, "Anisotropy of corrosion and environmental cracking in AA5083-H128 Al-Mg alloy," *Materials Science and Engineering: A*, vol. 730, pp. 367–379, Jul. 2018, doi: 10.1016/j.msea.2018.06.021.

[161] M. Silva, C. Barbosa, O. Acselrad, and L. Pereira, "Effect of chemical composition variation on microstructure and mechanical properties of a 6060 aluminum alloy," *JOURNAL OF MATERIALS ENGINEERING AND PERFORMANCE*, vol. 13, no. 2, pp. 129–134, Apr. 2004, doi: 10.1361/10599490418307.

[162] B. Trink, I. Weißensteiner, P. J. Uggowitzer, K. Strobel, and S. Pogatscher, "High Fe content in Al-Mg-Si wrought alloys facilitates excellent mechanical properties," *Scripta Materialia*, vol. 215, p. 114701, Jul. 2022, doi: 10.1016/j.scriptamat.2022.114701.

[163] Y. V. Gamin, N. A. Belov, T. K. Akopyan, V. N. Timofeev, S. O. Cherkasov, and M. M. Motkov, "Effect of Radial-Shear Rolling on the Structure and Hardening of an Al-8%Zn-3.3%Mg-0.8%Ca-1.1%Fe Alloy Manufactured by Electromagnetic Casting," *MATERIALS*, vol. 16, no. 2, Jan. 2023, doi: 10.3390/ma16020677.

[164] P. Zhang, Q. Li, J. Zhao, and Z. Cai, "Volta potential analysis of intermetallics in 7A52 aluminum alloy," *J. Wuhan Univ. Technol.-Mat. Sci. Edit.*, vol. 27, no. 2, pp. 227–230, Apr. 2012, doi: 10.1007/s11595-012-0442-2.

[165] H. Moghanni-Bavil-Olyaei and J. Arjomandi, "Enhanced electrochemical performance of Al–0.9Mg–1Zn–0.1Mn–0.05Bi–0.02In fabricated from commercially pure aluminum for use as the anode of alkaline batteries," *RSC Adv.*, vol. 6, no. 33, pp. 28055–28062, 2016, doi: 10.1039/C6RA02113A.

[166] L. Meng and X. Zheng, "Overview of the effects of impurities and rare earth elements in Al-Li alloys," *MATERIALS SCIENCE AND ENGINEERING A-STRUCTURAL MATERIALS PROPERTIES MICROSTRUCTURE AND PROCESSING*, vol. 237, no. 1, pp. 109–118, Sep. 1997, doi: 10.1016/S0921-5093(97)00096-8.

[167] M. Cieslar, C. Fressengeas, A. Karimi, and J. Martin, "Portevin-Le Chatelier effect in biaxially strained Al-Fe-Si foils," *SCRIPTA MATERIALIA*, vol. 48, no. 8, pp. 1105–1110, Apr. 2003, doi: 10.1016/S1359-6462(02)00617-6.

[168] A. V. Pozdniakov, A. R. Aitmagambetov, S. V. Makhov, and V. I. Napalkov, "Effect of impurities of Fe and Si on the structure and strengthening upon annealing of the Al-0.2% Zr-0.1% Sc alloys with and without Y additive," *PHYSICS OF METALS AND METALLOGRAPHY*, vol. 118, no. 5, pp. 479–484, May 2017, doi: 10.1134/S0031918X17050118.

[169] J. Kasinska, D. Bolibruchova, and M. Matejka, "The Influence of Remelting on the Properties of AlSi9Cu3 Alloy with Higher Iron Content," *MATERIALS*, vol. 13, no. 3, Feb. 2020, doi: 10.3390/ma13030575.

[170] G. Eisaabadi B, P. Davami, N. Varahram, and S. K. Kim, "On the effect of hydrogen and Fe on reproducibility of tensile properties in cast Al-Si-Mg alloys," *MATERIALS SCIENCE AND ENGINEERING A-STRUCTURAL MATERIALS PROPERTIES MICROSTRUCTURE AND PROCESSING*, vol. 565, pp. 278–284, Mar. 2013, doi: 10.1016/j.msea.2012.12.022.

MIMI Tech GmbH
Preusweg 98, D-52074 Aachen
friedrich@mimi-tech.com

[171] S. Alkahtani, "Effect of Mg, Sr, Ti and Aging Parameters on the Mechanical Behavior of 319 Alloys in the T5 and T6 Heat Treatment," *AMR*, vol. 482–484, pp. 2275–2288, Feb. 2012, doi: 10.4028/www.scientific.net/AMR.482-484.2275.

[172] Z. Šurdová *et al.*, "The Influence of Fe Content on Corrosion Resistance of secondary AlSi7Mg0.3 Cast Alloy with Increased Fe-content," *Manufacturing Technology*, vol. 22, no. 5, pp. 598–604, Dec. 2022, doi: 10.21062/mft.2022.073.

[173] M. Matejka, D. Bolibruchova, J. Kasinska, and M. Kuris, "Study of AlSi9Cu3 Alloy Crystallization Process with Increased Iron Content at Different Number of Remelts," *ARCHIVES OF FOUNDRY ENGINEERING*, vol. 20, no. 1. POLSKA AKAD NAUK, POLISH ACAD SCIENCES, PL DEFILAD 1, WARSZAWA, 00-901, POLAND, pp. 79–83, 2020. doi: 10.24425/afe.2020.131287.

[174] A. Bjurenstedt, S. Seifeddine, and A. E. W. Jarfors, "The Effects of Fe-Particles on the Tensile Properties of Al-Si-Cu Alloys," *METALS*, vol. 6, no. 12, Dec. 2016, doi: 10.3390/met6120314.

[175] J. Lazaro-Nebreda, J. B. Patel, I. T. H. Chang, I. C. Stone, and Z. Fan, "Solidification processing of scrap Al-alloys containing high levels of Fe," in *JOINT 5TH INTERNATIONAL CONFERENCE ON ADVANCES IN SOLIDIFICATION PROCESSES (ICASP-5) & 5TH INTERNATIONAL SYMPOSIUM ON CUTTING EDGE OF COMPUTER SIMULATION OF SOLIDIFICATION, CASTING AND REFINING (CSSCR-5)*, in IOP Conference Series-Materials Science and Engineering, vol. 529. DIRAC HOUSE, TEMPLE BACK, BRISTOL BS1 6BE, ENGLAND: IOP PUBLISHING LTD, 2019. doi: 10.1088/1757-899X/529/1/012059.

[176] G. B. Eisaabadi, P. Davami, S. K. Kim, N. Varahram, Y. O. Yoon, and G. Y. Yeom, "Effect of oxide films, inclusions and Fe on reproducibility of tensile properties in cast Al-Si-Mg alloys: Statistical and image analysis," *MATERIALS SCIENCE AND ENGINEERING A-STRUCTURAL MATERIALS PROPERTIES MICROSTRUCTURE AND PROCESSING*, vol. 558, pp. 134–143, Dec. 2012, doi: 10.1016/j.msea.2012.07.101.

[177] D. Bolibruchova, R. Podprocka, R. Pastircak, and K. Major-Gabrys, "THE ROLE OF Mn IN ALUMINIUM ALLOYS WITH A HIGHER IRON CONTENT," *ARCHIVES OF METALLURGY AND MATERIALS*, vol. 63, no. 4, pp. 1883–1888, 2018, doi: 10.24425/amm.2018.125119.

[178] S. Ferraro and G. Timelli, "Influence of Sludge Particles on the Tensile Properties of Die-Cast Secondary Aluminum Alloys," *METALLURGICAL AND MATERIALS TRANSACTIONS B-PROCESS METALLURGY AND MATERIALS PROCESSING SCIENCE*, vol. 46, no. 2. SPRINGER, 233 SPRING ST, NEW YORK, NY 10013 USA, pp. 1022–1034, Apr. 2015. doi: 10.1007/s11663-014-0260-3.

[179] L. Kucharikova, E. Tillova, M. Chalupova, M. Mazur, A. Hercko, and R. Cicka, "Analysis of microstructure in AlSi7Mg0.3 cast alloy with different content of Fe," in *13TH INTERNATIONAL SCIENTIFIC CONFERENCE ON SUSTAINABLE, MODERN AND SAFE TRANSPORT (TRANSCOM 2019)*, J. Bujnak and M. Guagliano, Eds., in Transportation Research Procedia, vol. 40. Radarweg 29, PO Box 211, AMSTERDAM, NETHERLANDS: ELSEVIER, 2019, pp. 59–67. doi: 10.1016/j.trpro.2019.07.011.

[180] I. Bacaicoa, "Effect of heat treatment and iron content on the microstructure and mechanical properties of a secondary Al-Si-Cu alloy."

[181] J. Zhao, Y. Guo, B. Xu, C. Gu, Y. Wang, and Q. Tang, "Effect of Microstructure Evolution of Iron-Rich Intermetallic Compounds on Mechanical Property of Al-7Si-0.3Mg Casting Alloy with Low Iron Content," *METALLURGICAL AND MATERIALS TRANSACTIONS B-PROCESS METALLURGY AND MATERIALS PROCESSING SCIENCE*, vol. 53, no. 1, pp. 548–560, Feb. 2022, doi: 10.1007/s11663-021-02390-5.

MIMI Tech GmbH
Preusweg 98, D-52074 Aachen
friedrich@mimi-tech.com

[182] M. Zihalova, D. Bolibruchova, and M. Matejka, “Change in the Microstructure of AlSi10MgMn Alloy with Higher Iron Content Due to an Increase in the Amount of Nickel,” *TEHNICKI VJESNIK-TECHNICAL GAZETTE*, vol. 28, no. 1, pp. 34–37, Feb. 2021, doi: 10.17559/TV-20150513155430.

[183] D. Bolibruchova, J. Macko, and M. Bruna, “ELIMINATION OF NEGATIVE EFFECT OF Fe IN SECONDARY ALLOYS AlSi6Cu4 (EN AC 45 000, A 319) BY NICKEL,” *ARCHIVES OF METALLURGY AND MATERIALS*, vol. 59, no. 2, pp. 717–721, 2014, doi: 10.2478/amm-2014-0118.

[184] P. Mikolajczak, J. Janiszewski, and J. Jackowski, “Construction of the Facility for Aluminium Alloys Electromagnetic Stirring During Casting,” in *ADVANCES IN MANUFACTURING II, VOL 4 - MECHANICAL ENGINEERING*, B. Gapinski, M. Szostak, and V. Ivanov, Eds., in Lecture Notes in Mechanical Engineering. HEIDELBERGER PLATZ 3, D-14197 BERLIN, GERMANY: SPRINGER-VERLAG BERLIN, 2019, pp. 164–175. doi: 10.1007/978-3-030-16943-5_15.

[185] M. Matejka, D. Bolibruchova, and R. Podprocka, “The Influence of Returnable Material on Internal Homogeneity of the High-Pressure Die-Cast AlSi9Cu3(Fe) Alloy,” *METALS*, vol. 11, no. 7, Jul. 2021, doi: 10.3390/met11071084.

[186] J. Kasinska, M. Matejka, D. Bolibruchova, M. Kuris, and L. Siranec, “Effect of Returnable Material in Batch on Hot Tearing Tendency of AlSi9Cu3 Alloy,” *MATERIALS*, vol. 14, no. 7, Apr. 2021, doi: 10.3390/ma14071583.

[187] L. Kucharikova *et al.*, “The Effect of the beta-Al5FeSi Phases on Microstructure, Mechanical and Fatigue Properties in A356.0 Cast Alloys with Higher Fe Content without Additional Alloying of Mn,” *MATERIALS*, vol. 14, no. 8, Apr. 2021, doi: 10.3390/ma14081943.

[188] D. Bolibruchova and R. Podprocka, “The Effect of Different Mn/Fe Ratio on Microstructure Alloy Based on Al-Si-Mg,” *ARCHIVES OF FOUNDRY ENGINEERING*, vol. 19, no. 3, pp. 15–20, 2019, doi: 10.24425/afe.2019.127129.

[189] D. Song *et al.*, “Study of the evolution mechanisms of Fe-rich phases in Al-Si-Fe alloys with Mn modification using synchrotron X-ray imaging,” *Journal of Alloys and Compounds*, vol. 915, p. 165378, Sep. 2022, doi: 10.1016/j.jallcom.2022.165378.

[190] S. Alkahtani, “Effect of Mg, Sr, Ti and Aging Parameters on the Mechanical Behavior of 319 Alloys in the T5 and T6 Heat Treatment.,” in *ADVANCED COMPOSITE MATERIALS, PTS 1-3*, W. Chen, X. Liu, P. Dai, Y. Chen, and Z. Jiang, Eds., in Advanced Materials Research, vol. 482–484. LAUBLSRUTISTR 24, CH-8717 STAFA-ZURICH, SWITZERLAND: TRANS TECH PUBLICATIONS LTD, 2012, pp. 2275–2288. doi: 10.4028/www.scientific.net/AMR.482-484.2275.

[191] B. Lin *et al.*, “Precipitation of iron-rich intermetallics and mechanical properties of Al–Si–Mg–Fe alloys with Al–5Ti–B,” *Materials Science and Technology*, vol. 34, no. 17, pp. 2145–2152, Nov. 2018, doi: 10.1080/02670836.2018.1519945.

[192] M. Sha, S. Wu, L. Wan, and S. Lu, “Effect of Heat Treatment on Morphology of Fe-Rich Intermetallics in Hypereutectic Al-Si-Cu-Ni Alloy with 1.26 pct Fe,” *METALLURGICAL AND MATERIALS TRANSACTIONS A-PHYSICAL METALLURGY AND MATERIALS SCIENCE*, vol. 44A, no. 13, pp. 5642–5652, Dec. 2013, doi: 10.1007/s11661-013-1937-y.

[193] M. Angel Suarez-Rosales, R. Pinto-Segura, E. Guadalupe Palacios-Beas, A. Hernandez-Herrera, and J. F. Chavez-Alcala, “Effect of Rapid Solidification and Addition of Cu3P on the Mechanical Properties of Hypereutectic Al-Si Alloys,” *MATERIALS RESEARCH-IBERO-AMERICAN JOURNAL OF MATERIALS*, vol. 19, no. 1, pp. 67–73, Dec. 2016, doi: 10.1590/1980-5373-MR-2016-0126.

MIMI Tech GmbH
Preusweg 98, D-52074 Aachen
friedrich@mimi-tech.com

[194] C. Silva *et al.*, "Microstructure and Tensile Strength of an Al-Si-Fe-V Alloy: Vanadium and Solidification Thermal Parameters as Recycling Strategies," *SUSTAINABILITY*, vol. 14, no. 21, Nov. 2022, doi: 10.3390/su142113859.

[195] P. Mikolajczak and L. Ratke, "The role of fluid flow and intermetallic phases in the formation of the primary Al-phase in AlSi alloys," in *3RD INTERNATIONAL CONFERENCE ON ADVANCES IN SOLIDIFICATION PROCESSES*, in IOP Conference Series-Materials Science and Engineering, vol. 27. DIRAC HOUSE, TEMPLE BACK, BRISTOL BS1 6BE, ENGLAND: IOP PUBLISHING LTD, 2012. doi: 10.1088/1757-899X/27/1/012024.

[196] J. Zhang *et al.*, "Microstructure and properties evolution of Al-17Si-2Fe alloys with addition of quasicrystal Al-Mn-Ti master alloy," *RARE METALS*, vol. 39, no. 10, pp. 1210–1221, Oct. 2020, doi: 10.1007/s12598-020-01449-7.

[197] T. Mbuya, B. Odera, and S. Ng'ang'a, "Influence of iron on castability and properties of aluminium silicon alloys: literature review," *INTERNATIONAL JOURNAL OF CAST METALS RESEARCH*, vol. 16, no. 5, pp. 451–465, 2003, doi: 10.1080/13640461.2003.11819622.

[198] J. A. Taylor, "Iron-containing intermetallic phases in Al-Si based casting alloys," in *11TH INTERNATIONAL CONGRESS ON METALLURGY & MATERIALS SAM/CONAMET 2011*, A. Armas, Ed., in Procedia Materials Science, vol. 1. SARA BURGERHARTSTRAAT 25, PO BOX 211, 1000 AE AMSTERDAM, NETHERLANDS: ELSEVIER SCIENCE BV, 2012, pp. 19–33. doi: 10.1016/j.mspro.2012.06.004.

[199] S. Mohammed, S. Gupta, D. Li, X. Zeng, and D. Chen, "Cyclic Deformation Behavior of A Heat-Treated Die-Cast Al-Mg-Si-Based Aluminum Alloy," *MATERIALS*, vol. 13, no. 18, Sep. 2020, doi: 10.3390/ma13184115.

[200] Y. Kong, Z. Jia, Z. Liu, M. Liu, H. J. Roven, and Q. Liu, "Effect of Zr and Er on the microstructure, mechanical and electrical properties of Al-0.4Fe alloy," *JOURNAL OF ALLOYS AND COMPOUNDS*, vol. 857, Mar. 2021, doi: 10.1016/j.jallcom.2020.157611.

[201] S. Kang, D. Ding, and Y. Gao, "Influence of Zn Content on the Microstructure and Properties of As-annealed Al-Mn-Si Alloys," *MATERIAL SCIENCES AND TECHNOLOGY, PTS 1 & 2*, vol. 560–561. in Advanced Materials Research, vol. 560–561. TRANS TECH PUBLICATIONS LTD, KREUZSTRASSE 10, 8635 DURNTEN-ZURICH, SWITZERLAND, pp. 937–942, 2012. doi: 10.4028/www.scientific.net/AMR.560-561.937.

[202] A. Hernandez, A. Torres, S. Serna, J. Mayen, and B. Campillo, "Effect of Experimental Aging on the Performance of Al-7.9Mg-13.3Zn and Al-10.5Mg-8.6Zn Alloys as Sacrificial Anodes," *METALS*, vol. 9, no. 8, Aug. 2019, doi: 10.3390/met9080863.

[203] H. Zhang, C. Guo, S. Li, B. Li, and H. Nagaumi, "Influence of cold pre-deformation on the microstructure, mechanical properties and corrosion resistance of Zn-bearing 5xxx aluminum alloy," *JOURNAL OF MATERIALS RESEARCH AND TECHNOLOGY-JMR&T*, vol. 16, pp. 1202–1212, Feb. 2022, doi: 10.1016/j.jmrt.2021.12.080.

[204] H. Zhu, A. K. Dahle, and A. K. Ghosh, "Effect of Sc and Zn Additions on Microstructure and Hot Formability of Al-Mg Sheet Alloys," *METALLURGICAL AND MATERIALS TRANSACTIONS A-PHYSICAL METALLURGY AND MATERIALS SCIENCE*, vol. 40A, no. 3, pp. 598–608, Mar. 2009, doi: 10.1007/s11661-008-9728-6.

[205] Y. Ma *et al.*, "A novel corrosion transformation process in aluminum alloy/galvanized steel welded joint," *CORROSION SCIENCE*, vol. 194, Jan. 2022, doi: 10.1016/j.corsci.2021.109936.

MIMI Tech GmbH
Preusweg 98, D-52074 Aachen
friedrich@mimi-tech.com

[206] A. Lutz *et al.*, "Effect of Zn on the grain boundary precipitates and resulting alkaline etching of recycled Al-Mg-Si-Cu alloys," *JOURNAL OF ALLOYS AND COMPOUNDS*, vol. 794, pp. 435–442, Jul. 2019, doi: 10.1016/j.jallcom.2019.04.259.

[207] W. Gong, M. Xie, and J. Zhang, "Giant bake hardening response of multi-scale precipitation strengthened Al-Mg-Si-Cu-Zn alloy via pre-aging treatments," *MATERIALS CHARACTERIZATION*, vol. 181, Nov. 2021, doi: 10.1016/j.matchar.2021.111464.

[208] Z. Shang, L. Zhihui, Y. Lizhen, L. Xiwu, Z. Yongan, and X. Buiqing, "Effects of Zn Addition on the Natural Ageing Behavior and Bake Hardening Response of a Pre-Aged Al-Mg-Si-Cu Alloy," *ACTA METALLURGICA SINICA*, vol. 55, no. 11, pp. 1395–1406, Nov. 2019, doi: 10.11900/0412.1961.2018.00555.

[209] Y. Qiu *et al.*, "Influence of Grain Boundary Precipitates on Intergranular Corrosion Behavior of 7050 Al Alloys," *COATINGS*, vol. 12, no. 2, Feb. 2022, doi: 10.3390/coatings12020249.

[210] V. V. Ravikumar and S. Kumaran, "Microstructure and corrosion behaviour of precipitation hardened and thermo-mechanical treated high strength Al-12Zn-3Mg-2.5Cu alloy," *ANTI-CORROSION METHODS AND MATERIALS*, vol. 65, no. 1, pp. 79–86, 2018, doi: 10.1108/ACMM-04-2017-1780.

[211] Y. Liu *et al.*, "Corrosion behaviour of mechanically polished AA7075-T6 aluminium alloy," *SURFACE AND INTERFACE ANALYSIS*, vol. 42, no. 4, SI, pp. 185–188, Apr. 2010, doi: 10.1002/sia.3136.

[212] H. Li, X.-T. Liu, and J.-Y. Wang, "Influence of Preaging Treatment on Bake-Hardening Response and Electrochemical Corrosion Behavior of High Strength Al-Zn-Mg-Cu-Zr Alloy," *METALS*, vol. 9, no. 8, Aug. 2019, doi: 10.3390/met9080895.

[213] S. Linjee, S. Moonngam, P. Klomjit, N. S. Palsson, and C. Banjongprasert, "Corrosion behaviour improvement from the ultrafine-grained Al-Zn-In alloys in Al-air battery," *ENERGY REPORTS*, vol. 8, pp. 5117–5128, Nov. 2022, doi: 10.1016/j.egyr.2022.03.132.

[214] A. Kumar, G. P. Chaudhari, and S. K. Nath, "Correlation of microstructure with corrosion performance in high zinc 7068 aluminum alloy aged using different T6 conditions," *MATERIALS CHARACTERIZATION*, vol. 191, Sep. 2022, doi: 10.1016/j.matchar.2022.112133.

[215] T. Dun-Bo *et al.*, "Microstructure evolution and electrochemical corrosion behavior of Al-Zn-Mg aluminum alloy," *MATERIALS RESEARCH EXPRESS*, vol. 9, no. 4, Apr. 2022, doi: 10.1088/2053-1591/ac6731.

[216] F. Guo, S. Duan, D. Wu, K. Matsuda, T. Wang, and Y. Zou, "Effect of retrogression re-aging treatment on corrosion behavior of 7055 Al-Zn-Mg alloy," *MATERIALS RESEARCH EXPRESS*, vol. 7, no. 10, Oct. 2020, doi: 10.1088/2053-1591/abc191.

[217] X. Lu *et al.*, "Effect of pre-strain on precipitation and exfoliation corrosion resistance in an Al-Zn-Mg alloy," *1ST INTERNATIONAL CONFERENCE ON FRONTIERS OF MATERIALS SYNTHESIS AND PROCESSING (FMSP 2017)*, vol. 274, 2017, doi: 10.1088/1757-899X/274/1/012007.

[218] T. Minh Ngo, T. Thi Van Nguyen, H. Thi To Phung, B. T. Le, H. P. Nguyen Thi, and D. Duc La, "Nanostructured phases, mechanical properties, exfoliation and intergranular corrosion behaviours of 7075 Al-Zn-Mg-Cu alloy-Effect of one-stage and two-stage aging processes," *ADVANCES IN NATURAL SCIENCES-NANOSCIENCE AND NANOTECHNOLOGY*, vol. 11, no. 4, Dec. 2020, doi: 10.1088/2043-6254/abb93c.

[219] X. Qi, X. M. Chen, and R. G. Song, "Study on double peaks aging strengthening and stress corrosion cracking behaviour of 7075 aluminium alloy," *CORROSION ENGINEERING SCIENCE*

MIMI Tech GmbH
Preusweg 98, D-52074 Aachen
friedrich@mimi-tech.com

AND TECHNOLOGY, vol. 56, no. 7, pp. 668–677, Oct. 2021, doi: 10.1080/1478422X.2021.1937452.

[220] L. Shen, H. Chen, L.-D. Xu, X.-L. Che, and Y. Chen, "Stress corrosion cracking and corrosion fatigue cracking behavior of A7N01P-T4 aluminum alloy," *MATERIALS AND CORROSION-WERKSTOFFE UND KORROSION*, vol. 69, no. 2, pp. 207–214, Feb. 2018, doi: 10.1002/maco.201709527.

[221] J. Zander and R. Sandstrom, "Modelling technological properties of commercial wrought aluminium alloys," *MATERIALS & DESIGN*, vol. 30, no. 9, pp. 3752–3759, Oct. 2009, doi: 10.1016/j.matdes.2009.02.004.

[222] M. Yang, Y. Liu, Z. Shi, X. Lv, B. Liu, and L. Sun, "Study on the Electrochemical Behavior of Al-6Zn-0.02In-1 Mg-0.03Ti Sacrificial Anodes for Long-Term Corrosion Protection in the Ocean," *CORROSION*, vol. 76, no. 4, pp. 366–372, Apr. 2020, doi: 10.5006/3404.

[223] Z. Chen, Y. Mo, and Z. Nie, "Effect of Zn Content on the Microstructure and Properties of Super-High Strength Al-Zn-Mg-Cu Alloys," *METALLURGICAL AND MATERIALS TRANSACTIONS A-PHYSICAL METALLURGY AND MATERIALS SCIENCE*, vol. 44A, no. 8, pp. 3910–3920, Aug. 2013, doi: 10.1007/s11661-013-1731-x.

[224] M.-H. Ku, F.-Y. Hung, T.-S. Lui, L.-H. Chen, and W.-T. Chiang, "Microstructural Effects of Zn/Mg Ratio and Post Heat Treatment on Tensile Properties of Friction Stirred Process (FSP) Al-xZn-yMg Alloys," *MATERIALS TRANSACTIONS*, vol. 53, no. 5, pp. 995–1001, May 2012, doi: 10.2320/matertrans.M2012003.

[225] J. Tang *et al.*, "Effect of Zn content on the dynamic softening of Al-Zn-Mg-Cu alloys during hot compression deformation," *VACUUM*, vol. 184, Feb. 2021, doi: 10.1016/j.vacuum.2020.109941.

[226] R. Wang, D. Wang, H. Nagaumi, Z. Wu, X. Zhang, and X. Li, "Effect of Zn content on corrosion resistance of as-cast Al-6Si-3Cu alloy," *MATERIALS LETTERS*, vol. 312, Apr. 2022, doi: 10.1016/j.matlet.2022.131658.

[227] M. Abubakar and M. A. Onimisi, "Effect of Precipitation Hardening Treatment on Corrosion Behavior and Anodic Efficiency of Sacrificial Anode Produced from Recycled Al-Zn-Mg Alloy," *JOURNAL OF FAILURE ANALYSIS AND PREVENTION*, vol. 21, no. 4, pp. 1212–1219, Aug. 2021, doi: 10.1007/s11668-021-01150-6.

[228] S. Lameche-Djeghaba, A. Benchettara, F. Kellou, and V. Ji, "Electrochemical Behaviour of Pure Aluminium and Al-5%Zn Alloy in 3% NaCl Solution," *ARABIAN JOURNAL FOR SCIENCE AND ENGINEERING*, vol. 39, no. 1, pp. 113–122, Jan. 2014, doi: 10.1007/s13369-013-0876-7.

[229] S. Bayraktar and A. P. Hekimoglu, "Effect of Zinc Content and Cutting Tool Coating on the Machinability of the Al-(5-35) Zn Alloys," *METALS AND MATERIALS INTERNATIONAL*, vol. 26, no. 4, pp. 477–490, Apr. 2020, doi: 10.1007/s12540-019-00582-y.

[230] Y. Gencer and A. E. Gulec, "The effect of Zn on the microarc oxidation coating behavior of synthetic Al-Zn binary alloys," *JOURNAL OF ALLOYS AND COMPOUNDS*, vol. 525, pp. 159–165, Jun. 2012, doi: 10.1016/j.jallcom.2012.02.094.

[231] Z. Ping, L. Qi, Z. Junjun, and C. Zhihai, "Volta Potential Analysis of Intermetallies in 7A52 Aluminum Alloy," *JOURNAL OF WUHAN UNIVERSITY OF TECHNOLOGY-MATERIALS SCIENCE EDITION*, vol. 27, no. 2. WUHAN UNIV TECHNOLOGY, 122, LUOSHI RD, WUHAN, HUBEI 430070, PEOPLES R CHINA, pp. 227–230, Apr. 2012. doi: 10.1007/s11595-012-0442-2.

[232] A. Nadim, R. Taghiabadi, and A. Razaghian, "Effect of Mn Modification on the Tribological Properties of In Situ Al-15Mg(2)Si Composites Containing Fe as an Impurity," *JOURNAL OF*

MIMI Tech GmbH
Preusweg 98, D-52074 Aachen
friedrich@mimi-tech.com

TRIBOLOGY-TRANSACTIONS OF THE ASME, vol. 140, no. 6. ASME, TWO PARK AVE, NEW YORK, NY 10016-5990 USA, Nov. 2018. doi: 10.1115/1.4040384.

[233] J. Zhang, F. Pan, R. Zuo, and C. Bai, "The low temperature precipitation in commercial-purity aluminium sheets for foils," *JOURNAL OF MATERIALS PROCESSING TECHNOLOGY*, vol. 206, no. 1–3. ELSEVIER SCIENCE SA, PO BOX 564, 1001 LAUSANNE, SWITZERLAND, pp. 382–387, Sep. 12, 2008. doi: 10.1016/j.jmatprotec.2007.12.042.

[234] F. Samuel, A. Samuel, H. Doty, and S. Valtierra, "Influence of composition, Sr modification, and annealing treatment on the structure and properties of cast Al-4 pct Mg alloys," *METALLURGICAL AND MATERIALS TRANSACTIONS A-PHYSICAL METALLURGY AND MATERIALS SCIENCE*, vol. 34, no. 1. MINERALS METALS MATERIALS SOC, 184 THORN HILL RD, WARRENDALE, PA 15086 USA, pp. 115–129, Jan. 2003. doi: 10.1007/s11661-003-0213-y.

[235] Y. Yin, S. Jian, Y. Xiaodong, X. Xiaojing, L. Junpeng, and J. Tao, "Effect of Alloying Elements on the Quality of Hard Anodic Oxidation Film in Aluminum Alloy 6061," *RARE METAL MATERIALS AND ENGINEERING*, vol. 40, no. 3, pp. 59–62, Oct. 2011.

[236] B. Zhu, M. Fedel, N.-E. Andersson, P. Leisner, F. Deflorian, and C. Zanellaa, "Effect of Si Content and Morphology on Corrosion Resistance of Anodized Cast Al-Si Alloys," *JOURNAL OF THE ELECTROCHEMICAL SOCIETY*, vol. 164, no. 7, pp. C435–C441, 2017, doi: 10.1149/2.1631707jes.

[237] S. Arthanari, J. C. Jang, and K. S. Shin, "Corrosion performance of high pressure die-cast Al-Si-Mg-Zn alloys in 3.5 wt% NaCl solution," *JOURNAL OF ALLOYS AND COMPOUNDS*, vol. 783, pp. 494–502, Apr. 2019, doi: 10.1016/j.jallcom.2018.12.313.

[238] H. Shi *et al.*, "Effect of alkaline etching on microstructure and anticorrosion performance of anodic film on Al-Mg-Si alloy," *CORROSION SCIENCE*, vol. 169, Jun. 2020, doi: 10.1016/j.corsci.2020.108642.

[239] N. Bayat, T. Carlberg, and M. Cieslar, "In-situ study of phase transformations during homogenization of 6005 and 6082 Al alloys," *JOURNAL OF ALLOYS AND COMPOUNDS*, vol. 725. ELSEVIER SCIENCE SA, PO BOX 564, 1001 LAUSANNE, SWITZERLAND, pp. 504–509, Nov. 25, 2017. doi: 10.1016/j.jallcom.2017.07.149.

[240] H. Zhong, P. Rometsch, and Y. Estrin, "Effect of alloy composition and heat treatment on mechanical performance of 6xxx aluminum alloys," *TRANSACTIONS OF NONFERROUS METALS SOCIETY OF CHINA*, vol. 24, no. 7. ELSEVIER SCIENCE BV, PO BOX 211, 1000 AE AMSTERDAM, NETHERLANDS, pp. 2174–2178, Jul. 2014. doi: 10.1016/S1003-6326(14)63329-X.

[241] A. Mukhopadhyay and A. Sharma, "Influence of Fe-bearing particles and nature of electrolyte on the hard anodizing behaviour of AA 7075 extrusion products," *SURFACE & COATINGS TECHNOLOGY*, vol. 92, no. 3, pp. 212–220, Jul. 1997, doi: 10.1016/S0257-8972(97)00102-3.

[242] M. Vratnica, Z. Cvijović, H. P. Degischer, and G. C. Requena, "The effect of coarse intermetallic particles on the fracture process in forged 7000 alloys," *J Microsc*, vol. 224, no. 1, pp. 117–120, Oct. 2006, doi: 10.1111/j.1365-2818.2006.01683.x.

[243] R. I. Revilla, H. Terryn, and I. De Graeve, "Role of Si in the Anodizing Behavior of Al-Si Alloys: Additive Manufactured and Cast Al-Si10-Mg," *JOURNAL OF THE ELECTROCHEMICAL SOCIETY*, vol. 165, no. 9, pp. C532–C541, 2018, doi: 10.1149/2.1301809jes.

[244] K. Labisz, J. Konieczny, L. Wierzbicki, J. Cwiek, and J. Mlynczak, "Silicon Addition Influence on Properties of Anodised Al-Si Alloy Surface," *ACTA PHYSICA POLONICA A*, vol. 135, no. 2, pp. 143–146, Feb. 2019, doi: 10.12693/APhysPolA.135.143.

MIMI Tech GmbH
Preusweg 98, D-52074 Aachen
friedrich@mimi-tech.com

[245] C. Lee *et al.*, "Self-sealing anodization approach to enhance micro-Vickers hardness and corrosion protection of a die cast Al alloy," *JOURNAL OF PHYSICS AND CHEMISTRY OF SOLIDS*, vol. 103, pp. 87–94, Apr. 2017, doi: 10.1016/j.jpcs.2016.12.005.

[246] A. Fom, J. A. Picas, M. T. Baile, E. Martin, and V. G. Garcia, "Microstructure and tribological properties of anodic oxide layer formed on Al-Si alloy produced by semisolid processing," *SURFACE & COATINGS TECHNOLOGY*, vol. 202, no. 4–7, pp. 1139–1148, Dec. 2007, doi: 10.1016/j.surfcoat.2007.07.070.

[247] L. Fratila-Apachitei, J. Duszczyk, and L. Katgerman, "Vickers microhardness of AlSi(Cu) anodic oxide layers formed in H2SO4 at low temperature," *SURFACE & COATINGS TECHNOLOGY*, vol. 165, no. 3, pp. 309–315, Feb. 2003, doi: 10.1016/S0257-8972(02)00750-8.

[248] M. Mohedano, E. Matykina, R. Arrabal, B. Mingo, and A. Pardo, "PEO of pre-anodized Al-Si alloys: Corrosion properties and influence of sealings," *APPLIED SURFACE SCIENCE*, vol. 346, pp. 57–67, Aug. 2015, doi: 10.1016/j.apsusc.2015.03.206.

[249] D. Caliari, G. Timelli, T. Salata, G. Cavagnini, S. Maestri, and A. Manfredini, "Influence of microstructure and surface finishing on the hard anodizing of diecast Al-Si-Cu alloys," *METALLURGIA ITALIANA*, no. 4, pp. 23–31, Apr. 2019.

[250] B. Zhu and C. Zanella, "Hardness and corrosion behaviour of anodised Al-Si produced by rheocasting," *MATERIALS & DESIGN*, vol. 173, Jul. 2019, doi: 10.1016/j.matdes.2019.107764.

[251] A. Khaliq, H. T. Ali, and M. Yusuf, "Thermodynamic and kinetic analysis of CrB2 and VB2 formation in molten Al-Cr-V-B alloy," *TRANSACTIONS OF NONFERROUS METALS SOCIETY OF CHINA*, vol. 31, no. 10. ELSEVIER, RADARWEG 29, 1043 NX AMSTERDAM, NETHERLANDS, pp. 3162–3176, Oct. 2021. doi: 10.1016/S1003-6326(21)65723-0.

[252] S. Karabay and I. Uzman, "Inoculation of transition elements by addition of AlB2 and AlB12 to decrease detrimental effect on the conductivity of 99.6% aluminium in CCL for manufacturing of conductor," *Journal of Materials Processing Technology*, vol. 160, no. 2, pp. 174–182, Mar. 2005, doi: 10.1016/j.jmatprotec.2004.06.015.

[253] C. Shi and X.-G. Chen, "Hot Workability and Processing Maps of 7150 Aluminum Alloys with Zr and V Additions," *JOURNAL OF MATERIALS ENGINEERING AND PERFORMANCE*, vol. 24, no. 5, pp. 2126–2139, May 2015, doi: 10.1007/s11665-015-1478-1.

[254] D. Hao, N. Zhang, Y. Zhang, and D. Li, "Effect of vanadium addition on microstructure and properties of Al(0.5)Cr(0.9)FeNi(2.5)multi-principal alloys," *JOURNAL OF IRON AND STEEL RESEARCH INTERNATIONAL*, vol. 28, no. 5. SPRINGER, ONE NEW YORK PLAZA, SUITE 4600, NEW YORK, NY, UNITED STATES, pp. 586–596, May 2021. doi: 10.1007/s42243-020-00466-1.

[255] M. Guerin, J. Alexis, E. Andrieu, C. Blanc, and G. Odemer, "Corrosion-fatigue lifetime of Aluminium-Copper-Lithium alloy 2050 in chloride solution," *MATERIALS & DESIGN*, vol. 87, pp. 681–692, Dec. 2015, doi: 10.1016/j.matdes.2015.08.003.

[256] L. Fu *et al.*, "Corrosion mechanism and fatigue behavior of 2A70-T6 aluminum alloy under alternating corrosion and fatigue," *ANTI-CORROSION METHODS AND MATERIALS*, vol. 68, no. 5, pp. 422–437, Sep. 2021, doi: 10.1108/ACMM-02-2020-2265.

[257] V. S. N. V. Ramana, R. Mohammed, G. M. Reddy, and K. S. Rao, "Effect of Post Weld Heat Treatment on Corrosion Behavior of AA2014 Aluminum - Copper Alloy Electron Beam Welds," *INTERNATIONAL CONFERENCE ON RECENT ADVANCES IN MATERIALS, MECHANICAL AND CIVIL ENGINEERING*, vol. 330, 2018, doi: 10.1088/1757-899X/330/1/012052.

[258] S. B. Kang, D. B. Kim, and J. Choi, "Effect of Copper Variation and Thermomechanical Treatment on Microstructure and Properties in Aluminum Alloy Fin Stock for Heat Exchanger,"

MIMI Tech GmbH
Preusweg 98, D-52074 Aachen
friedrich@mimi-tech.com

in *THERMEC 2011, PTS 1-4*, T. Chandra, M. Ionescu, and D. Mantovani, Eds., in Materials Science Forum, vol. 706–709. Minerals, Metals & Mat Soc, 2012, pp. 311–316. doi: 10.4028/www.scientific.net/MSF.706-709.311.

[259] J.-Z. Chen *et al.*, "Microstructure Evolution and the Resulted Influence on Localized Corrosion in Al-Zn-Mg-Cu Alloy during Non-Isothermal Ageing," *MATERIALS*, vol. 11, no. 5, May 2018, doi: 10.3390/ma11050720.

[260] T. Ramgopal, P. Gouma, and G. Frankel, "Role of grain-boundary precipitates and solute-depleted zone on the intergranular corrosion of aluminum alloy 7150," *CORROSION*, vol. 58, no. 8, pp. 687–697, Aug. 2002, doi: 10.5006/1.3287699.

[261] N. J. Mahmood, A. S. Hassan, and N. F. Soliman, "Studying the Effect of Adding Alloying Elements to Aluminum on its Thermal Conductivity and Mechanical Properties," *European Journal of Scientific Research*, vol. 118, no. 3, pp. 409–415, Feb. 2014.

[262] A. Kordijazi, D. Weiss, S. Das, S. Behera, H. M. Roshan, and P. Rohatgi, "Effect of Solidification Time on Microstructure, Wettability, and Corrosion Properties of A205-T7 Aluminum Alloys," *INTERNATIONAL JOURNAL OF METALCASTING*, vol. 15, no. 1, pp. 2–12, Jan. 2021, doi: 10.1007/s40962-020-00457-8.

[263] S. Zor, M. Zeren, H. Ozkazanc, and E. Karakulak, "Effect of Cu content on the corrosion of Al-Si eutectic alloys in acidic solutions," *ANTI-CORROSION METHODS AND MATERIALS*, vol. 57, no. 4, pp. 185–191, 2010, doi: 10.1108/00035591011058192.

[264] W. R. Osorio, D. J. Moutinho, L. C. Peixoto, I. L. Ferreira, and A. Garcia, "Macrosegregation and microstructure dendritic array affecting the electrochemical behaviour of ternary Al-Cu-Si alloys," *ELECTROCHIMICA ACTA*, vol. 56, no. 24, pp. 8412–8421, Oct. 2011, doi: 10.1016/j.electacta.2011.07.028.

[265] C. K. Lee, "Effects of Pb and Cu additives on microstructure and wear corrosion resistance behaviour of PM Al-Si alloys," *CORROSION ENGINEERING SCIENCE AND TECHNOLOGY*, vol. 41, no. 4, pp. 342–352, Dec. 2006, doi: 10.1179/174327806X120874.

[266] Y. Zhang, S. Liang, A. Javed, and D. Guan, "Effect of pass deformation on microstructure, corrosion and electrochemical properties of aluminum alloy anodes for alkaline aluminum fuel cell applications," *METALS AND MATERIALS INTERNATIONAL*, vol. 19, no. 3, pp. 555–561, May 2013, doi: 10.1007/s12540-013-3025-7.

[267] C. PAPASTAIKOUDIS, N. KONTOLEON, K. PAPATHANASOPOULOS, and P. ANDRONIKOS, "PHONON RESISTIVITY IN AL-GA ALLOYS," *PHYSICAL REVIEW B*, vol. 11, no. 6, pp. 2077–2081, 1975, doi: 10.1103/PhysRevB.11.2077.

[268] C. PAPASTAIKOUDIS and K. PAPATHANASOPOULOS, "DEPENDENCE OF PHONON-RESISTIVITY ON RESIDUAL RESISTIVITY IN AL-GE AND AL-GA ALLOYS," *SOLID STATE COMMUNICATIONS*, vol. 16, no. 9, pp. 1083–1084, 1975, doi: 10.1016/0038-1098(75)90009-5.

[269] H. GUNTHERODT and H. KUNZI, "HALL COEFFICIENT AND ELECTRICAL RESISTIVITY OF LIQUID AL-GA ALLOYS," *PHYSIK DER KONDENSITERTEN MATERIE*, vol. 10, no. 3, p. 285+, 1969, doi: 10.1007/BF02422648.

[270] S. Korkmaz and S. D. Korkmaz, "Structure and Electrical Resistivities of Liquid Al and Ga Metals and Their Binary Alloys," *INTERNATIONAL JOURNAL OF THERMOPHYSICS*, vol. 33, no. 5, pp. 831–842, May 2012, doi: 10.1007/s10765-012-1186-0.

[271] Q. Hao, J. Wen, J. He, and J. Ma, "Effects of Gallium Addition on the Microstructure and Electrochemical Properties of Al-Zn-Bi Series Alloy Anode," in *ADVANCED STRUCTURAL MATERIALS*, Y. Han, F. Pan, J. Tang, and C. Zhou, Eds., in Materials Science Forum, vol. 686. Int

MIMI Tech GmbH
Preusweg 98, D-52074 Aachen
friedrich@mimi-tech.com

Union Mat Res Soc (IUMRS); Chinese Mat Res Soc; Mat Res Soc Taiwan; Mat Res Soc Japan; Govt Qingdao City, 2011, pp. 107–112. doi: 10.4028/www.scientific.net/MSF.686.107.

[272] E. Akiyama, Z. Zhang, Y. Watanabe, and K. Tsuzaki, "Effects of severe plastic deformation on the corrosion behavior of aluminum alloys," *JOURNAL OF SOLID STATE ELECTROCHEMISTRY*, vol. 13, no. 2, pp. 277–282, Feb. 2009, doi: 10.1007/s10008-007-0496-9.

[273] X. Zeng, C. Ferguson, K. Sadayappan, and S. Shankar, "Effect of Titanium Levels on the Hot Tearing Sensitivity and Abnormal Grain Growth After T4 Heat Treatment of Al–Zn–Mg–Cu Alloys," *Inter Metalcast*, vol. 12, no. 3, pp. 457–468, Jul. 2018, doi: 10.1007/s40962-018-0227-2.

[274] X. Cao and J. Campbell, "Precipitation of primary intermetallic compounds in liquid Al 11.5Si 0.4Mg alloy," *International Journal of Cast Metals Research*, vol. 13, no. 3, pp. 175–184, Nov. 2000, doi: 10.1080/13640461.2000.11819400.

[275] M. W. Meredith, A. L. Greer, P. V. Evans, R. G. Hamerton, "THE GENERATION OF AlmFe IN DILUTE," in *Light Metals*, The Minerals, Metals & Materials Society: TMS, 1999.

[276] S. Kumar and K. A. Q. O'Reilly, "Influence of Al grain structure on Fe bearing intermetallics during DC casting of an Al-Mg-Si alloy," *Materials Characterization*, vol. 120, pp. 311–322, Oct. 2016, doi: 10.1016/j.matchar.2016.09.017.

[277] J. Rakhmonov, G. Timelli, F. Bonollo, and L. Arnberg, "Influence of Grain Refiner Addition on the Precipitation of Fe-Rich Phases in Secondary AlSi7Cu3Mg Alloys," *Inter Metalcast*, vol. 11, no. 2, pp. 294–304, Apr. 2017, doi: 10.1007/s40962-016-0076-9.

[278] A. M. SAMUEL, F. H. SAMUEL, "Observation on the formation of beta-Al5FeSi Phase in 319 type Al-Si Alloys," *JOURNAL OF METERIALS SCIENCE*, vol. 31, pp. 5529–5539, 1996.

[279] S. H. Rodríguez, R. E. Goytia Reyes, D. K. Dwivedi, O. A. González, and V. H. Baltazar Hernández, "The Effect of Al-5Ti-1B on Microstructure and Mechanical Properties of Al-12Si-xFe Alloy," *Materials and Manufacturing Processes*, vol. 27, no. 6, pp. 599–604, Jun. 2012, doi: 10.1080/10426914.2011.560230.

[280] G.-H. Lu *et al.*, "Origin of intergranular embrittlement of Al alloys induced by Na and Ca segregation: Grain boundary weakening," *PHYSICAL REVIEW B*, vol. 73, no. 22, Jun. 2006, doi: 10.1103/PhysRevB.73.224115.

[281] M. Banerjee, "Age-hardening characteristics of aluminium-chromium alloys," *JOURNAL OF MATERIALS SCIENCE*, vol. 32, no. 24. CHAPMAN HALL LTD, 2-6 BOUNDARY ROW, LONDON, ENGLAND SE1 8HN, pp. 6645–6651, Dec. 15, 1997. doi: 10.1023/A:1018652420101.

[282] M. Miyagi, H. Wang, R. Yoshida, Y. Kawahito, H. Kawakami, and T. Shoubu, "Effect of alloy element on weld pool dynamics in laser welding of aluminum alloys," *SCIENTIFIC REPORTS*, vol. 8. NATURE PUBLISHING GROUP, MACMILLAN BUILDING, 4 CRINAN ST, LONDON N1 9XW, ENGLAND, Aug. 28, 2018. doi: 10.1038/s41598-018-31350-4.

[283] E. V. Karpov, A. G. Malikov, A. M. Orishich, and B. D. Annin, "TEMPERATURE EFFECT ON THE FRACTURE OF LASER WELDED JOINTS OF AVIATION ALUMINUM ALLOYS," *JOURNAL OF APPLIED MECHANICS AND TECHNICAL PHYSICS*, vol. 59, no. 5. MAIK NAUKA/INTERPERIODICA/SPRINGER, 233 SPRING ST, NEW YORK, NY 10013-1578 USA, pp. 934–940, Sep. 2018. doi: 10.1134/S002189441805022X.

[284] H. Yamada, T. Kami, R. Mori, T. Kudo, and M. Okada, "Strain Rate Dependence of Material Strength in AA5xxx Series Aluminum Alloys and Evaluation of Their Constitutive Equation," *METALS*, vol. 8, no. 8. MDPI, ST ALBAN-ANLAGE 66, CH-4052 BASEL, SWITZERLAND, Aug. 2018. doi: 10.3390/met8080576.

MIMI Tech GmbH
Preusweg 98, D-52074 Aachen
friedrich@mimi-tech.com

[285] S. B. Sidelnikov *et al.*, "Investigation of rolling modes, structure, and properties of aluminum-magnesium alloy plates with a reduced scandium content," *INTERNATIONAL JOURNAL OF ADVANCED MANUFACTURING TECHNOLOGY*, vol. 121, no. 1–2. SPRINGER LONDON LTD, 236 GRAYS INN RD, 6TH FLOOR, LONDON WC1X 8HL, ENGLAND, pp. 1373–1384, Jul. 2022. doi: 10.1007/s00170-022-09403-w.

[286] G. Novotny and A. Ardell, "Precipitation of Al3Sc in binary Al-Sc alloys," *MATERIALS SCIENCE AND ENGINEERING A-STRUCTURAL MATERIALS PROPERTIES MICROSTRUCTURE AND PROCESSING*, vol. 318, no. 1–2. ELSEVIER SCIENCE SA, PO BOX 564, 1001 LAUSANNE, SWITZERLAND, pp. 144–154, Nov. 2001. doi: 10.1016/S0921-5093(01)01326-0.

[287] L. Ren *et al.*, "Effect of Sc Content on the Microstructure and Properties of Al-Mg-Sc Alloys Deposited by Wire Arc Additive Manufacturing," *METALS AND MATERIALS INTERNATIONAL*, vol. 27, no. 1. KOREAN INST METALS MATERIALS, KIM BLDG 6TH FLOOR, SEOCHO-DAERO 56 GIL 38, SEOCHO-GU, SEOUL 137-881, SOUTH KOREA, pp. 68–77, Jan. 2021. doi: 10.1007/s12540-020-00763-0.

[288] E. M. Elgallad, K. Liu, Z. Zhang, and X.-G. Chen, "Effect of transition elements on dispersoid formation and elevated-temperature mechanical properties in 6082 aluminum alloy," *PHILOSOPHICAL MAGAZINE*, vol. 101, no. 1. TAYLOR & FRANCIS LTD, 2-4 PARK SQUARE, MILTON PARK, ABINGDON OR14 4RN, OXON, ENGLAND, pp. 96–116, Jan. 02, 2021. doi: 10.1080/14786435.2020.1826592.

MIMI Tech GmbH, Preusweg 98, D-52074 Aachen
www.mimi-tech.com, friedrich@mimi-tech.com